STUDY OF INFLUENCE OF POLY-ADP-RIBOSYLATION AND REGRESSION OF CHEMICALLY INDUCED CARCINOGENESIS *IN VIVO*

ABSTRACT

BY

BRAHMACHARIMAYUM JAYLATA DEVI

DEPARTMENT OF BIOCHEMISTRY

SUBMITTED

IN FULFILMENT OF THE REQUIREMENT OF THE DEGREE OF

DOCTOR OF PHILOSOPHY

IN

BIOCHEMISTRY

NORTH-EASTERN HILL UNIVERSITY

SHILLONG, INDIA

OCTOBER 2001

Thesis

Several macromolecules, especially proteins, undergo some modifications subsequent to their biosynthesis. These events are necessary to determine their functions. The modifications, particularly of nuclear origin, are important in terms of their degree of association with the fundamental structure of life i. e. DNA. poly-ADP-ribosylation (PAR) is one such post-translational modification widely studied and yet, enigmatic about its implications in several molecular processes including carcinogenesis. This post-translational modification involves addition of ADP-ribose moieties from endogenous NAD^+ substrates to target proteins forming linear and branched chains of ADP-ribose polymers. The reaction is catalyzed by chromatin associated enzyme poly ADP-ribose polymerase (PARP). The protein bound polymers are simultaneously degraded by enzyme poly ADP-ribose glycohydrolase (PARG). These two enzymes are physiological counterparts to each other. Therefore, poly-ADP-ribosylation reaction condition of a physiological system is determined by the equilibrium state between the activities of the two main enzymes involved. It is now known that normal cells escape chain of sequential control mechanisms at molecular level when they become progressively transformed to cancer cells or malignancy. The causes include interactions with exogenous agents such as ionizing radiation, UV radiation and chemical carcinogens. The earlier events during the process include alterations in gene expression pattern, expression of neogenes, shut down of differentiation genes, etc. Carcinogenesis begins with initiation stage in which genome is irreversibly altered. It usually takes a long intervening period before these initial events manifest themselves as detectable cancers. The reaction of PAR, which modifies primarily DNA bound histones, brings about changes in chromatin superstructure by essentially modifying charge interactions between histones and DNA. Therefore, this modification would have implications in carcinogenesis. In this perspective, the work envisaged to monitor level of PAR of total cellular proteins as well as histone proteins during experimentally established two biological systems in Swiss albino mice. In the first model, carcinogenesis was induced by a hepatocarcinogen compound, dimethylnitrosamine (DMN) at a chronic dose rate of 10 mg/ kg. b. wt. The study was restricted to the initial phase in multistage carcinogenesis. Bi-weekly observations were made in the study. The effect of 3-aminobenzamide (3-AB), an inhibitor of poly-ADP-ribose synthesizing enzyme, PARP, was examined at a dose of 2 mM either alone or during simultaneous exposure of the mice to DMN. In the second system tumerogenesis was induced by Dalton's lymphoma ascites. Ten million ascites cells were used for the initial intraperironeal injection in mice abdomen. The observation for the study was limited to 15

days after transplantation of ascites cells. In both experimental model level of PAR was monitored from different tissues along with simultaneous examination of physiological changes. The work also aimed to develop a suitable, sensitive, convenient and optimized method to monitor the endogenous level of PAR. For this purpose, polyclonal ADP-ribose polymer antibody was raised in the laboratory. The specificity of the poly ADP-ribose was confirmed using snake venom phosphodiesterase (SVP), a degradative enzyme which cleaves pyrophosphate bonds in poly ADP-ribose, besides checking with standard Ouchterlony immunodiffusion assay. The techniques of slot- and Western blots were used for monitoring level of PAR of total cellular proteins and individual histone proteins, respectively. Another focus of the work was to correlate chromatin structural organization and PAR from the results. The work brings out the following main points.

- A polyclonal antibody against heterogenous ADP-ribose polymer antigen isolated from normal mouse spleen cells has been raised in the laboratory. An ELISA based immunoprobing method employing the polyclonal antibody has been established and optimized. The method specifically detects PAR of proteins by immune interaction between the raised polyclonal antibody and ADP-ribose polymer antigens.

- In the assay developed and optimized in this work, level of PAR of total cellular proteins and individual histones have been monitored by slot blot immunoprobing for total cellular protein while Western blot immunodetection for individual histone proteins. The novel assay developed has been found to be simple, sensitive and the assay can be applied to varied tissue without involving tedious sample preparations like those in isotopic assay. Thus, the assay provides an advantageous step ahead of the conventional method.

- In DMN induced carcinogenesis, the physiological parameters such as body weight, cell number in spleen and BMC, protein content in liver and spleen, and histone content in spleen remained essentially unaffected during the treatment period. Similar was the case in 3-AB treatment, so also in combined regime of DMN + 3-AB. However, in ascites Dalton's lymphoma induced tumorogenesis, the growth of tumor cells was proportional to the increase in body weights of mice. Protein contents in liver and spleen showed declining tendencies.

- The slot blot immunoassay reveals that the method is limited obscuring a clear insight. However, general lowering of PAR in liver and spleen under DMN influence was observed in the later part of treatment. Level of PAR generally declined for histones. During carcinogenesis and tumorogenesis, the extent of PAR of total cellular proteins of liver, spleen and bone marrow cells were relatively higher than histones isolated from spleen and ascites suggesting ribosylation of other proteins besides histones.

- Under the influence of DMN, the protein expression pattern did not change markedly in liver and spleen homogenates and isolated histones from spleen cells except for slight over- and under expression of some proteins. Influence of Dalton's lymphoma showed similar results during tumorogenesis.

- Histones were primary targets of poly-ADP-ribosylation as revealed by Western blot assay. Most non-histone proteins were not ADP-ribosylated in liver. Polyclonal anti ADP-ribose polymer antibody also detects higher molecular weight proteins particularly in spleen in both the systems suggesting that proteins other than histones were ribosylated in spleen.

- The general lowering of PAR, especially of histones H1 and some core histones is accompanied by relaxation of chromatin superstructure as revealedby DNase I fragmentation. The result suggests that a negative correlation exists between level of PAR and cellular transformation by DMN.

- Lowering of level of PAR was evident in histones H1, H2b + H3 and H4 under DMN influence especially in liver as shown by the Western blot analysis. 3-aminobenzamide (3-AB), an inhibitor of PARP enzyme, potentiated the effect of inhibition of PAR in the combined regime of DMN and 3-AB. In spleen, inhibition was observed in H1 only in the later part of DMN exposure. The inhibition of PAR was extensive and significant, especially for H1, H2a and H2b + H3 in liver under 3-AB influence. In spleen, the inhibition of PAR of histones was not so pronounced. However, the lowering of PAR by combined treatment was usually less pronounced than that caused by 3-AB exposure. During tumorogenesis, general lowering of PAR in most histones in liver, spleen, histones isolated from spleen and ascites cells were more evident. Therefore, the extent of PAR in different histones varied.

- The results obtained from the work undertaken in this investigation suggest that lowering of PAR is a hallmark during both initiation phase of carcinogenesis induced by DMN as well as tumorigenesis induced by Dalton's lymphoma ascites. Therefore, it can be proposed that employing Western blot immunoprobing assay for measuring endogenous poly-ADP-ribose, lowering of level of PAR can be used as predictive assay for detecting carcinogenesis and tumorigenesis.

STUDY OF CHEMICAL CARCINOGEN INDUCED GENOMIC INSTABILITY

BY

CHAITALI BHATTACHARJEE

DEPARTMENT OF BIOCHEMISTRY

SUBMITTED
IN PARTIAL FULFILMENT OF THE REQUIREMENT
OF THE DEGREE OF
DOCTOR OF PHILOSOPHY
IN
BIOCHEMISTRY

NORTH EASTERN HILL UNIVERSITY
SHILLONG, INDIA
SEPTEMBER, 2007

The North-Eastern Hill University

September, 2007

I, **Chaitali Bhattacharjee**, hereby declare that the subject matter of this thesis is of the record done by me, that the content of this thesis did not form basis of the award of any previous degree to me or to the best of my knowledge to anybody else, and that the thesis has not been submitted by me for any research degree in any other University/ Institute.

This is being submitted to the North-Eastern Hill University for the degree of **Doctor of Philosophy** in **Biochemistry**.

Chaitali Bhattacharjee

(CHAITALI BHATTACHARJEE)

Candidate

R. Lalthantluanga 20/9/7

(PROF. R. LALTHANTLUANGA)

Head

Department of Biochemistry

18/9/07

(PROF. R. N. SHARAN)

Supervisor

CONTENTS

ACKNOWLEDGEMENT

First of all, I would like to thank my mentor and supervisor, Prof. R. N. Sharan for the wonderful experience that I had as a research scholar in his laboratory. His excellent perception of ideas and encouraging words have always been qualities that I have admired. Under his able guidance, I have been able to delve into the world of genomic instability and discover the wonders therein. The support that I received from him in order to pursue my line of thought was truly inspirational.

I take this opportunity to thank the faculty of the Department of Biochemistry for their support during the entire course of my study. I extend my sincere gratitude to Prof. R. Lalthantluanga, the Head of the Biochemistry, for allowing me to use the facilities of the department. I would also like to thank Prof. Sharma, for his timely help in anything that I needed. Thanks are also due to Prof. A. N. Rai, Prof. A. Alam, Dr. A. K. Singh, Dr. D. Syiem, Dr. M. B. Syiem, Dr. L. Kma, Dr. P. K. Ambasht, for their help whenever required. Special thanks also goes to the non-teaching staff of the department, Mani Baboo Singh, Pushpa, Kong Yen, Bah Ponderly.

I will always remember with gratitude the help that I received from Manish (BIC, NEHU) and Pynkup whenever I needed any help with softwares. The help received from Jos for the transmission electron microscopy work is duly acknowledged.

My tenure in the lab has been made memorable by my labmates, who have been nothing less than wonderful. Special mention goes to Meriyani, who became my sister and friend. Rennie, Yashmin, Pathaw, Banri, Khet, Dannis, Saiba and Dr. Sanghamitra all started out as labmates but have become life long friends whom I shall cherish knowing all my life. Life in the lab was always full of fun and there has never been a dull moment thanks to these wonderful people.

Help received from within the department and also the departments of Botany and Chemistry are also duly acknowledged. In this respect, I would specially like to thank Cressida,

Chumbeni, David, Manik, Snigdha, Thomas, Ashima, Khup, James, RK, Dr. Nonibala, Lalngura, Pramod, Shairi, Mitali, Nakhuru, Soma and Jenny.

This acknowledgement would be incomplete if I did not mention my friends who made valuable contributions to my research directly or indirectly. I shall remain indebted forever for the help received in collection of literature by numerous friends, among whom, Dr. Arnaud Boissiere (UCSF, Berkeley) played a major role. Literature collection was also helped by Dr. Manish (University of Virginia, USA). Timely help received from Supriya (Rutgers University, USA) is also gratefully acknowledged.

There have been friends who have been with me throughout the course of my study. They have been by me through thick and thin. Among them, Dipanjali finds a special place. Her absence will always be felt. Also, the support received from Jhinai (Rajeshwari) and Jhanakda (Dr. Shyamananda Bhattacharjee) will be remembered forever. I take this opportunity to specially thank Vikram, who has helped me in ways too numerous to count. Also, the support received from Arijit, Parmita, Debashish, Bibek, Anju, for their support through the years will always be cherished.

A special mention must go to my parents and family members have given me the necessary support and strength that was required to get to this stage. They have been patient and understanding and their constant presence gave me the courage to continue with my endeavors.

I would also like to thank the Department of Biotechnology/ Biochemistry, St. Anthony's College for giving me the opportunity to work and complete my Ph.D.

The financial support received from CSIR-UGC as JRF and SRF is gratefully acknowledged.

Chaitali Bhattacharjee

Chaitali Bhattacharjee

ABBREVIATIONS

°C	Degree Centigrade
6-4 PP	pyrimidine (6-4) pyrimidone photoproducts
A	Adenine
AEBN	Aqueous extract of betel nut
Amp	Ampicillin
AT	Ataxia telangiectasia
ATLD	AT like disorder
BER	Base Excision Repair
BN	Betel nut
bp	Base pair
C	Cytosine
CA	Chromosomal Aberrations
$CaCl_2$	Calcium chloride
CHO	Chinese Hamster Ovary
CPD	Cyclobutane pyrimidine dimers
CS	Cockayne's Syndrome
CTAB	Cetyltrimethylammonium bromide
DNA	Deoxyribonucleic acid
DNaseI	Deoxyribonuclease I
DSB	Double strand break
DTT	Dithiothreitol
E. coli	*Escherichia coli*
EDTA	Ethylene diamine tetra acetic acid
ER	Excision repair
FA	Fanconi Anemia
Fig.	Figure
g	Centrifugal force
G	Guanine

Gy	Gray
HNPCC	Hereditary Nonpolyposis Colorectal Cancer
IR	Ionizing radiation
J	Joules
LB	Luria Bertani medium
LET	Linear energy transfer
M	Molar
min^{-1}	Per minute
mM	Millimolar
MMR	Mismatch Repair
MNPA	3-(methyl nitrosamino)-propionaldehyde
MNPN	3-(methyl nitrosamino)-propionitrile
NaOH	Sodium hydroxide
NER	Nucleotide Excision Repair
NIR	Non-ionizing radiation
NOC	Nitroso compounds
NT	Nucleotide
O/N	Overnight
PP	Pyrimidine photoproducts
PRE	Photoreactivating enzymes
RNA	Ribonucleic acid
RNase	Ribonuclease
ROS	Reactive oxygen species
rpm	Revolutions per minute
RR	Recombination Repair
RT	Room temperature
s^{-1}	per second
SCE	Sister Chromatid Exchange
SDS-PAGE	Sodium dodecyl sulphate Polyacrylamide Gel Electrophoresis

SD	**Standard deviation**
SEM	**Standard error of the mean**
SSB	**Single strand break**
T	**Thymine**
TEMED	**NNN'N-Tetramethylethylene diamine**
TTD	**Trichothiodystrophy**
UDS	**Unscheduled DNA synthesis**
UV-C	**Ultraviolet-C**
V	**Volts**
XP	**Xeroderma Pigmentosum**
γ	**Gamma**
µl	**Microlitre**
µm	**Micron**

Introduction

Genomic instability is the increased tendency of the genome to acquire mutations when the mechanism of maintaining the genome is either damaged or destroyed. The study of the phenomenon of induction of genomic instability has gained importance ever since its role in aging and cancer has been discovered. Genomic instability may also, and most commonly, results from gross chromosomal changes, such as translocations or amplifications, which lead to chromosomal instability. In fact, genomic instability has also been implicated in a number of diseases like Ataxia telangiectasia (AT) and related disorders, AT like disorder (ATLD), Nijmegen breakage syndrome, Werner's syndrome , Bloom's syndrome, Fanconi's Anemia (FA), Cockayne's Syndrome (CS), Xeroderma pigmentosum (XP) (Venema *et al.*, 1990; Crabbe *et al.*, 2007). These diseases also lead the patient to have a high predisposition to cancer. This is particularly true in case of FA patients who have been seen to have a significant predisposition to acute myeloid leukaemia (Auerbach, 1992; Lui *et al.*, 1993). That genomic instability predisposes a cell to cancer was known ever since Boveri observed aneuploidy in cancers (Boveri *et al.*, 1929). Today, genomic instability is known as a hallmark of many kinds of solid tumors and leukemias. This and other studies have only reiterated the importance of understanding genomic instability to tackle the problem of cancer.

Even in normal circumstances, cells undergo mutations spontaneously. However, the rate of mutation in normal cells is insufficient to account for the large numbers of mutations observed in cancer cells. Therefore, cells are said to undergo genomic instability which leads the tumor cells to manifest a mutator phenotype (Loeb, 1991; 1994). The mutator phenotype hypothesis postulates that an initial mutator mutation generates further mutations, including mutations in additional genetic stability genes, resulting in a cascade of mutations throughout the genome (Loeb, 2001). The concept of a mutator phenotype has been supported by the demonstration of microsatellite instability in tumor cell DNA (Peinado *et al.*, 1992; Aaltonen *et al.*, 1993; Perucho *et al.*, 1996). Thus, the importance and need of study of genomic instability is very relevant to human welfare.

The agents that induce genomic instability are numerous. Environmental genotoxins including mutagens and carcinogens have repeatedly been shown to affect the genetic

material of host cells, leading to uncontrolled growth and ultimately malignant tumors (Ames *et al.*, 1995; Stoner and Gupta, 2001). A report by Li *et al.* (2001) has shown that a variety of DNA damaging and non-damaging stress leads to heritable genomic instability in a minority but significant number of cells.

Such stress includes exposure to free radicals, reactive oxygen species (ROS), ionizing radiation (IR) and non-ionizing radiation (NIR) and a variety of chemical carcinogens. Normal cellular metabolism generates a variety of free radical species capable of causing oxidative damage to DNA. But genome integrity is usually maintained by the complex interplay of various defense mechanisms and repair processes. Free radical overload causes gross cellular damage resulting in depletion of nucleotide coenzymes, disturbance of sulfur-containing enzymes and saturation and attenuation of the defense systems (Slater, 1987). When such an antioxidant/ pro-oxidant imbalance occur, the cell becomes oxidatively stressed, thus becoming prone to genomic instability.

Another species that causes genomic instability are superoxide ROS. Cells exposed to superoxide from extracellular sources display high levels of cytogenetic aberrations (Emerit and Cerutti, 1981), in particular, chromatid aberrations (Duell *et al.*, 1995). ROS, another by-product of normal cellular metabolism generates 10,000 residues of 8-oxo-deoxyguanosine per cell per day that has been implicated in having a role in the induction of genomic instability by damaging the cellular DNA (Ames *et al.*, 1995).

Apart from these agents that the cell encounters during its normal process of development, it is also exposed to various agents in the environment (eg. radiation and chemical carcinogens) that induce genomic instability. In particular, cells can be exposed to radiation of varying kinds, viz., IR and NIR. Various qualities of IR have been studied. γ- radiation, one of the most biologically relevant IR, is known to induce genomic instability. In addition, other weaker varieties of radiation are also known to induce genomic instability. For example, environmentally relevant doses of plutonium 238 α-particles have been reported to induce a transmissible chromosomal instability in bone marrow (Kadhim *et al.*, 1992). NIR,

i.e., UV also have serious implications on the genome and are able to induce genomic instability.

Genomic instability has been shown to have serious implications on the cellular metabolism. The effects observed when the cells are exposed to radiation also appear to be the result of destabilization of the genome. The end results include delayed cell death (Seymour, *et al.,* 1986), delayed mutations (Gorgojo and Little, 1989) and delayed cell differentiation (Nicoletti *et al.,* 1992; Clutton *et al.,* 1995). All these effects lead the cell to be more prone to becoming cancerous. In fact, cancer is seen by many as a well-defined linear process very similar to normal, stepwise biological differentiation, except for the fact that it is accelerated in its steps due to acquired genomic instability (Loeb and Loeb, 2000). This view is supported by findings such as one that shows instability at repetitive loci scattered throughout the genome are found in colorectal cancers (Aaltonen *et al.,* 1993; Thibodeau *et al,* 1993; Ionov *et al.,* 1993). In fact, such instability is shown to be present in numerous other cancers.

It has been proposed that genetic instability in human cancers can be divided into two types: microsatellite instability (MIN), which is usually equated with DNA polymerase errors, and chromosomal instability (CIN), which can result from errors in chromosome partitioning (Lengauer, 1998; Grady, 2006).

The genome is particularly vulnerable during its replication and segregating chromosomes to daughter cells provides a further opportunity for large losses of genetic information. Damage repair deals with single events through base excision repair (BER), nucleotide excision repair (NER), or mismatch repair (MMR). Specialized genes exist for various forms of repair optimized for the particular damage, such as large or small chemical adducts, replication fork errors, or UV-generated cytobutane pyrimidine dimers (CPD). XP and hereditary nonpolyposis colorectal cancer (HNPCC) provide clear examples of how defects in these genes can contribute to genomic instability and malignancy (Lindahl and Wood, 1999; Peltomaki, 2001).

In the current investigation, two genomic instability inducing agents were chosen to study the induction of genomic instability. UV-C radiation was chosen as this fraction of UV light is the prime causative factor for skin cancer. Despite considerable information about the mechanism of action of this fraction of UV spectrum, more information needs to be gained. In our laboratory, extensive studies have been made on γ-radiation (Humtsoe and Sharan, 2004). Hence a comparison of the effects of this radiation with UV-C would shed more information. The other agent chosen was betel nut (BN) as it is a commonly used masticatory in this part of the world (Wary and Sharan, 1988). It is known to be carcinogenic and hence, study of the process by which genomic instability is induced is relevant. Despite considerable information gained about the mechanism of carcinogenesis by this agent, the exact mechanism of interaction is not known (Sharan, 1996).

1.1. Radiation induced genomic instability

Radiation is known to cause genomic instability (Kronenberg, 1994). The genomic instability induced by radiation depends on the type of radiation causing damage the DNA. Qualitatively, the IR and NIR are very different. Hence, the types of damages that these two qualities of radiation induce on the DNA are also significantly different. While IR proceeds with the induction of SSB and DSB on the DNA (Goodhead, 1994; Klungland *et al.*, 1999; Blaisdell and Wallace, 2001; Budworth *et al.*, 2002), NIR proceeds with the formation of pyrimidine photoproducts (PP) (Haseltine, 1986; Ravanat *et al.*, 2001, Douki *et al.*, 2003). Generally, it is the unrepaired and misrepaired DNA damages that are the principal lesions of importance in the induction of chromosomal abnormalities and gene mutations (Hoeijmakers, 2001).

In case of eukaryotes, genotoxic stress caused by environmental or endogenous genotoxic agents such as IR, NIR and various chemicals and reactive cellular metabolites cause the activation of cell cycle checkpoints which slow down or arrest cell cycle progression. This allows the cell to repair or prevent the transmission of damaged or incompletely replicated chromosomes (Ishikawa *et al.*, 2006). Inability to repair the damages can lead to gross defects in the genome which can lead to cell death or in some cases, the induction of cancer.

1.2. Induction of genomic instability by UV-C radiation

One of the agents that a cell has to encounter in its environment is the ultraviolet (UV) component of light. UV radiation induces deleterious effects in all living organisms ranging from prokaryotic bacteria to eukaryotic lower and higher plants, animals and humans. UV rays are mutagenic and are known to induce skin lesions and cancer (Cadet *et al.*, 2001). Therefore, a lot of studies have been focused on understanding the mechanism of interaction of this radiation with DNA. Based on the energy of the radiation, UV (100-400 nm) can be divided into three types, viz. UV-A (320-400 nm), UV-B (290-320 nm) and UV-C (100-290 nm). Of the three components, UV-A, having the longest wavelength has the least energy. UV-B radiation has a shorter wavelength and, therefore, possess higher energy. UV-C radiation has the shortest wavelength and, hence, the highest energy. Due to their differences in energy content, these waves interact with cellular components inducing varying effects on the cellular components including DNA. A relation of high pyrimidine absorption to high quantum yield is expected, since pyrimidines are the most UV-sensitive components of DNA (Shugar, 1960; Wacker, 1963). Thus, UV-A interacts with DNA to form various kinds of products like oxidized purine and pyrimidine bases (Bohr and Dianov, 1999; Ravanat *et al.* 2001, Douki *et al.* 2003b). UV-B interacts with DNA to form products like CPD (Snellman *et al.*, 2003), which were the first type of UV-induced damage to be recognized (Beukers and Berends, 1960), pyrimidine (6-4) pyrimidone photoproducts (6-4 PP) and the related Dewar valence isomers (Taylor *et al.*, 1987; Cadet *et al.*, 1992; Taylor, 1994) and cytosine photoproducts (Weirzchowski and Shugar, 1961). UV-C radiation, on the other hand, is more efficient in terms of photoproduct formation, (Mitchell *et al.*, 1991; Perdiz *et al.*, 2000; Douki *et al.* 2003a), and small number of single strand breaks (SSB) in DNA (Miguel and Tyrrell 1986, WHO 1994). The CPD are the most abundant and probably most cytotoxic lesions produced as a result of UV radiation, but the 6–4 PP may have more serious, potentially lethal, mutagenic effects. Dewar isomers are formed by the photoisomerization of 6-4 PP by wavelengths longer than 290 nm (Mitchell *et al.*, 1987; Matsunaga *et al.*, 1993). CPD have been reported to inhibit the progress of DNA polymerases. Mammalian RNA polymerase II has been reported to stall at both CPD and 6–4 PP (Protic-Sabljic and Kraemer, 1986; Mitchell *et al.*, 1989). Pyrimidine dimers have been found to serve as blocks to the transcription machinery (Giorno and Sauerbier 1976). Every

CPD acts as a block to transcription and replication and only a small fraction of dimers results in a mutation (Britt, 1995; 1996). Therefore, these DNA lesions, if left unrepaired, may interfere with DNA transcription and replication and can lead to misreading of the genetic code and cause mutations and death. In higher organisms, such damages can lead to induction of cancers.

UV light owes its powerful mutagenic effect in *E. coli* primarily to misrepair of radiation damage to the bacterial chromosome (Bridges, 1969; Witkin, 1969; Kondo, 1973). The damages that UV causes are known to induce apoptosis in a variety of organisms (Zhou and Streffer, 2003). The presence of UV-induced lesions inhibits the normal replication of DNA and, therefore, results in the inactivation of microorganisms (Harm, 1980; Friedberg *et al.*, 1995). The effect of UV has been seen to be enhanced as a result of the presence of ROS (He and Hader, 2002; Alam and Oligaki, 2002; Muela *et al.*, 2002). UV-C induced DNA damage is repaired in many organisms (Hartman *et al.*, 1989). However, in repair deficient *E. coli* cells, the damages are not repaired and hence, the induced damages can be seen from their protein expression profiles (Courcelle *et al.*, 2001).

Despite the wide amount of information already available about the mechanism of interaction of UV radiation with DNA, there are still a lot of unanswered questions. UV is a low-energy radiation. However, its interaction with DNA is known to cause the formation of SSB. Unlike IR, which can interact with DNA directly by the formation of SSB and DSB, UV is a NIR. Therefore, its mechanism of induction of SSB probably takes an indirect pathway that is still not very clear. This process needs to be studied as SSB have highly deleterious effects on the DNA such damages being potentially lethal, or at least highly mutagenic for the cell.

1.3. Induction of genomic instability by ionizing radiation

In contrast to NIR, IR is known to induce a high number of lesions in DNA. These lesions can give rise to genomic instability. The damages inflicted upon cells by IR are implicated in the biological consequences of radiation (Painter, 1979; Ward, 1988; Makrigiorgas *et al.*, 1990). All these damages may potentially lead to induction of genomic instability. The final

results of the radiation induced damage are the biological endpoints such as mutation, chromosomal aberration, oncogenic transformation and cell death (Kiefer, 1990; Sharan, 1998; Blakeley and Kronenberg, 1998). DNA damage by radiation may be the result of either direct or indirect effects (Scholes *et al.*, 1969; Roots *et al.*, 1985; O'Neill and Fielden, 1993). DNA lesions induced by radiation include strand breaks, base damage, sugar-phosphate damage, multiple lesions, etc (Humtsoe and Sharan, 2004). The extent of energy and oxidative radical attack required for such damages, however, depend on the nature and concentration of scavengers as well as the physical parameters of the incident radiation such as linear energy transfer (LET). The damage induced on DNA is also found to be a function of the nucleotide (NT) sequence of the DNA (Ward, 1985; Sy *et al.*, 1997; Humtsoe *et al.*, 1998). DNA damage by IR has been seen to occur in clusters (Ward, 1994). Damage in clusters has now been recognized as a characteristic feature of radiation damage that is deposited stochastically. Holley *et al.* (1998) have defined "cluster" as a group of closely damaged sites separated by undamaged regions of about 20 NT on each side.

The cell, being exposed to endo- and exogenously generated assaulted by various agents all the time need to have very efficient repair machinery. In fact, very efficient repair machineries exist in cells to either reverse or repair the damages induced by various agents. It will be important to look into the agents involved in repair of damages induced by the IR and NIR.

1.4. Repair of damages induced by UV and gamma radiation

1.4.1. *Role of RecF protein*

Pyrimidine dimers are the major aberrations induced by UV. In *E. coli*, these dimers can be repaired by different mechanisms. They can be repaired in the presence of light by a process called photoreactivation repair system (Kelner, 1949). This is accomplished by photoreactivating enzymes (PRE), also called DNA-photolyases. By photoreactivation, UV-induced pyrimidine dimers are restored to their native base form in a light-dependent (wavelengths mainly between 310 and 400 nm), error-free and economic manner (Rupert *et al.*, 1973; Rupert, 1975). The process is mediated by the action of DNA-photolyases, which

are structurally and functionally conserved across species (Yasui & Eker 1998). The DNA-photolyases work by monomerizing the dimers in a light dependent manner.

However, majority of the damages induced by UV are repaired by a dark repair pathways, which are post-replicative repair pathways whereby the pyrimidine dimers formed are removed by a multienzymatic excision repair (ER) system, primarily the nucleotide excision repair (NER) (Sancar, 1996), base excision repair (BER) (Britt, 1996), and recombinational repair (RR) (Courcelle and Hanawalt, 2001) systems. Under severe stress produced by replication arrest by UV-induced DNA damage, many bacteria mount a productive response which involves the new synthesis of a large number of specific gene products (Little and Mount, 1982; Walker, 1985). The response has been named SOS (Radman, 1974) response. It is triggered by the activation of preexisting RecA protein and its increased synthesis, probably due to the interaction of RecA protein with single stranded regions of DNA. RecA has been recently found to be involved in ER (Bichara *et al.*, 2007).

In *E. coli* cells exposed to UV radiation (10 J/m^2) repair of active genes was very rapid with 40% of pyrimidine dimers being removed within 4 h. Repair is almost complete (80%) within 24 h. Although NER is not essential for viability, defects in repair genes may result in three distinct sun-sensitive, cancer-prone genetic disorders such as XP, CS and trichothiodystrophy (TTD) in humans (Friedberg, *et al.*, 1995; Lehmann, 1995; Lindahl and Wood, 1999; Thoma, 1999). The UV sensitivity of XP has been correlated with the inability to excise UV-induced DNA damage or to seal daughter-strand gaps left after DNA synthesis on a damaged template (Lehman, 1982).

RR takes place with the help of the *rec* genes. Various *rec* genes, viz., *recA, recB, recC, recF, recO, recJ and recQ* play crucial roles in the recombination pathways of *E. coli* (Clark, 1991; Courcelle and Hanawalt, 2001). The RecA and RecF proteins have been found to be important for the repair of strand break type of damages. However, RecA proteins are found to be more critical than the RecF proteins for the repair of the strand break types of damages (Sharan *et al.*, 2007). UV induced damages are repaired by the RecF protein (Clark *et al.*, 1979), which repairs damages in the DNA by the recFOR pathway (Kuzminov, 2001).

The RecF protein is found to be structurally homologous to Rad50 in eukaryotes, which implies a conserved mechanism of DNA binding and recognition of the boundaries of double-stranded DNA regions. It is known that RecF protein forms a complex with the RecO and RecR proteins and together this RecFOR complex takes part in RR of UV-damaged DNA. In addition, it is also thought to have a role in replisome assembly (Courcelle *et al.,* 1997). Therefore, mutations in *recF*, *recO*, or *recR* conferred recombination-deficient and extremely UV-sensitive phenotypes (Horii and Clark, 1973; Kolodner *et al.,* 1985). The mechanism of function of the RecF protein indicates that it binds to single-stranded DNA (ssDNA) and, in the presence of ATP or ATP-γ S to double-stranded DNA (dsDNA) (Madiraju and Clark, 1991, 1992). RecF does not appear to have any positive effect on RecA-catalyzed reactions *in vitro* (Madiraju and Clark, 1991; Umezu *et al.,* 1993). Mutations in the *recF*, *recO*, and *recR* genes delay the induction of several SOS-regulated genes (Thoms and Wackernagel, 1987; Whitby and Lloyd, 1995).

1.4.2. ***Role of RecA protein***

Strand breaks are a major type of damage that a cell has to repair in order to survive. Strand breaks can be SSB or DSB types of damages. DSB pose a serious threat to the survival of the cell and, hence, their repair becomes crucial. Conventionally, DSB are repaired by nonhomologous end joining or homologous recombination repair pathways (Takahashi and Kobayashi, 1990). Defects in either pathway leads to failure in repairing damaged DNA properly. This is found to contribute to chromosome unstable phenotypes (Mills *et al.*, 2003).

In eukaryotes, homologous recombination is carried out by a homologue of the *recA* gene, the RAD51 recombination/repair family (Pastink *et al.*, 2001; Dronkert and Kanaar, 2001). In human cancers, defects in expression or mutations in *RAD51* genes are associated with chromosome rearrangements in human cancers (Thompson and Schild; 2002; Rodriguez-Lopez *et al.*, 2004). In fact, defects in the *RAD51* paralogs are thought to contribute to the formation of breast, uterine, skin, or bladder cancer (Thompson and Schild 2002; Rodriguez-Lopez *et al.*, 2004).

In *E. coli*, the RecA protein has been shown to be responsible for two main steps of recombination process: the search for homology and for strand exchange between two DNA molecules (Clark, 1965; Kowalczykowski and Eggelston, 1994). Purified RecA protein can catalyze a number of reactions, which includes the hydrolysis of ATP in the presence of single stranded (SS) DNA (Ogawa, *et. al.,* 1978), the ATP- dependent uptake of single stranded DNA by duplex DNA (Shibata, *et. al.,* 1979; McEntee, *et. al.,* 1979) and the ATP-dependent hybridization of homologous SS DNA (Weinstock, *et. al.,* 1979). RecA performs homologous recombination by recruiting the RecBCD proteins, which have helicase and nuclease functions. The RecBCD unwinds and degrades one strand leaving an ssDNA overhang (Kuzminov 1999; Lusetti and Cox, 2002). The RecA proteins coat the DNA strand, which pairs with undamaged homologous DNA strand and initiate strand exchange. IR is known to induce strand breaks, therefore, impairment of the *recA* gene impairs RR pathway, and thereby affects the repair of the IR induced damages. The expression of the recA gene is regulated within the SOS response. The activity of the RecA protein itself is autoregulated by its own C-terminus. RecA is also regulated by the action of other proteins. To date, these include the RecF, RecO, RecR, DinI, RecX, RdgC, PsiB, and UvrD proteins. The SSB protein also indirectly affects RecA function by competing for ssDNA binding sites. The RecO and RecR, and possibly the RecF proteins, all facilitate RecA loading onto SSB-coated ssDNA (Cox, 2007). RecA proteins have also recently been found to play a role in NER (Bichara *et al.*, 2007). Not surprisingly, therefore, the *recA* genes are implicated in the induction of genomic instability (Volff and Altenbuchner, 1997).

1.5. Chemical carcinogens induced genomic instability

In addition to the damages that a cell has to encounter due to its exposure to radiation, the cells are exposed to genotoxic stress by chemicals. Several chemicals are known to be capable of inducing carcinogenesis. For most chemicals, however, pharmacokinetic variables complicate the relation between exposure and effect on the target cells. Therefore, of thousands of chemicals that have been found to induce carcinogenesis in the laboratory, definite evidence of human carcinogenicity exists only for a handful of them (IARC, 1982). Studies have revealed that tobacco smoking, betel quid chewing, and alcohol consumption are major known risk factors for esophageal cancer (Lee *et al.*, 2005).

BN chewing in form of a quid, a common habit in Southeast Asia, has been found to increase the risk of developing cancer (IARC, 1985; 2004), in particular, esophageal cancer by 4.7-13.3 fold, although other exogenous risk factors may also be involved (Lee *et al.*, 2005). This assumes importance since using fermented BN with any form of tobacco is a common habit of people in Assam and other north-eastern states and has been reported to be a potential risk factor of esophageal cancer in this region (Sharan, 1996; Phukan *et al.*, 2001).

1.6. Genomic instability induced by betel nut

Betel nut (*Aceca catechu*, L.) or BN is widely used as a masticator in various forms by an estimated over 600 million strong human population across the globe despite its reported association with carcinogenesis in humans (reviewed in Sharan, 1996; IARC, 1985; 2004; Nelson and Heischober, 1999; Trivedi *et al.*, 2002). BN chewing has been thought to be one of the high risk habits leading to enhanced incidence of cancer in several parts of the world, particularly in south-east Asia, particularly in India, Taiwan and China (IARC, 1987; Sharan, 1996; Hsieh *et al.*, 2001; He *et al.*, 2002; Zhang *et al.*, 2007). Its chewing has been associated with oral squamous fubrosis and leukoplakia (Jeng *et al.*, 1999; Ariawardana *et al.*, 2006).

As the major part of the betel quid, BN has been the main suspect for delivering carcinogenic chemicals to the masticators (Mather *et al.*, 1994). A number of reports on the constituents of betel nuts show considerable variations in their contents due to geographical and climatic conditions of growth of the plant and also because of the special treatments (processing, curing, ripening) that are applied to the BN before they are consumed (Sharan, 1996). When mice were fed with aqueous extracts of betel nut (AEBN) *ad libitum*, gastrointestinal tumors were seen to be produced (Bhide *et al.*, 1979). Detailed studies of the components of the BN extract have been made (Kumpawat *et al.* 2003).

As BN is chewed, its components get extracted in saliva, an aqueous medium. Hence, in our laboratory, the effect of betel nut has been studied with AEBN, which will mimic the normal environment of the interaction of BN with the cellular components. AEBN has been shown to be a potent carcinogen without any tissue specificity (IARC, 1987; Sharan, 1996). The potential carcinogenic component of BN is water soluble alkaloids, which predominantly consist of arecoline and arecaidine, and small amounts of guvacine (methyl ester of arecaidine), guvacoline (methyl ester of guvacine) and arecolinidine besides some polyphenols and tannins (IARC, 1985; 1987; Sharan, 1996). Arecoline (1, 2, 4, 5-tetrahydro-1-methyl-3-pyridine carboxylic acid; MW 155.19 Da) is the most abundant alkaloid of BN and is the main carcinogenic component of BN. Arecaidine is reported to be more toxic than arecoline and both have similar pharmacokinetic behaviour (Panigrahi and Rao, 1984; Wary and Sharan, 1998). However, it is the abundance of arecoline that makes it the most important of all the components in the induction of the carcinogenic effects. The derivatives of arecoline have been seen to show a strong evidence of carcinogenicity (Saikia *et al.,* 1995, 1999). Arecoline, upon nitrosation, produces at least four types of betel nut specific nitrosamines (BNSA) with high affinities towards DNA (IARC, 1985; Sharan, 1996). Due to this, they readily interact with DNA and potentially produce adducts (Pérez-Cabré *et al.*, 2004). Such adducts on genomic DNA is one known cause of initiation of mutagenesis and eventual carcinogenesis (Gaskell, 2004).

Arecoline as well as various extracts of BN, especially AEBN, have been shown to be cytostatic and cytotoxic to human *hep2* cell line (Wary and Sharan, 1991). They also induced strand breaks in DNA and enhanced cell cycle (Wary and Sharan, 1988) besides causing different types of chromosomal aberrations including sister chromatid exchanges (Kumpawat *et al.*, 2003) and unscheduled DNA synthesis (UDS) (Sharan and Wary, 1992). The metabolic activation of arecoline via nitrosation in *hep2* cell line has been shown (Wary and Sharan, 1991). AEBN is known to induce damages in the DNA in a dose dependent manner in the buccal cavity (Murti *et al.*, 1985; Sundqvist *et al.*, 1989; Sundqvist *et al.*, 1992; Jeng *et al.*, 1999).

BN also has polyphenols like catechins, flavanoids, flavin-3:4-diols, leucocyanidins and hexahydroxyflavins. The predominant tannin of BN is gallotannic acid. In addition, minor amounts of gallic acid, D-catechols and phiobatannins are also present (Sharan, 1996).

Incubation of BN extract or arecoline with primary oral keratinocytes has been reported to promote cell survival and an inflammatory response by induction of prostaglandin E_2, interleukin-6 (IL-6) and cyclooxygenase-2 (COX-2) production *via* activation of MEK1/ERK/c-Fos pathway (Chang *et al.*, 2004). A recent study has shown that there is a down-regulation of genes involved in structural constituents of ribosome and upregulation of genes involved in cation transporter activity (Chattopadhyay *et al.*, 2007).

When AEBN interacts with DNA, it has been found to induce more strand breads as compared with the interaction of arecoline alone with DNA. This indicates that other constituents of betel quid may contribute synergistically to the geno-and cytotoxic effects (Wary and Sharan, 1988; Sundqvist *et al.*, 1991; Jeng *et al.*, 1994). Cell proliferation was also enhanced under these conditions (Wary and Sharan, 1988). It has been observed that arecoline, AEBN, as well as other extracts of BN, induced variable levels of dose dependent unscheduled DNA synthesis (UDS) in *hep*-2 cells *in vitro* (Sharan and Wary, 1992) pointing to genomic damages caused by these treatments. Arecoline has been shown to inhibit DNA and protein synthesis in a dose dependent manner (Wary and Sharan, 1991).

Study of mutations induced by BN extracts showed that AEBN was weakly mutagenic in Ames test (Balachandran and Sharan, 1995). Sister chromatid exchange (SCE) frequency was elevated in BN chewers (Sharan, 1996). Chinese hamster ovary (CHO) cells subjected to a 3 h exposure to urine of BN and tobacco chewers showed significant elevations of 11 or more SCE metaphase cells (Trivedi *et al.*, 1995), indicating that it caused genomic damage of systems and tissues other than oral cavity and oropharyngeal tract. Significant increase in oral cancer has also been reported (Thomas *et al.*, 2006). Chromosomal aberrations (CA) represent several types of DNA damage (eg. Gaps, breaks, acentric fragments, interchange, ring chromosomes and dicentric chromosomes) and unrepaired or misrepaired damaged sites. The most prevalent type of CA associated with betel quid was chromatid type (Dave *et*

al., 1992). Urine samples of BN and tobacco chewers induced significantly high levels of different types of CA, particularly chromatid type, in CHO cells (Trivedi *et al.*, 1995).

The BN alkaloids are chemically transformed upon metabolic activation to nitroso compounds (NOC) of arecoline, containing a 3-ethylenic bond at the 3-4 position on the pyridinium ring. This reaction results in the production of a variety of BNSA and their metabolites. The BNSA may interact with the DNA, proteins or other targets forming adducts to exert its carcinogenic activity. BN chewers have been found to have the presence of three major NOC of arecoline, N-nitrosoguvacoline, 3-(methyl nitrosamino)-propionitrile (MNPN) and 3-(methyl nitrosamino)-propionaldehyde (MNPA) (Wenke *et al.*, 1984). The interaction of BNSA or their metabolites with cellular targets may initiate carcinogenesis. One of the most important targets is DNA. The interaction of BNSA or its metabolites with DNA is likely to be weak and non-covalent in nature since the interaction was reversible (Wary and Sharan, 1991). It is evident that the first point in BN associatied carcinogenesis is at the level of metabolic activation of the carcinogen's interaction with macromolecular targets. Interaction with DNA being one of the targets, leads to a variety of damage, ultimately leading to altered gene expression. Targets other than DNA have not been clearly identified. However, their existence has been shown by a few biochemical parameters. One such target could be proteins, because β-alkylation adduct formation on cysteine has been observed (Wary and Sharan, 1988). These two interaction pathways finally may culminate in pre-neoplastic changes and cancer. It is again possible that extreme damages due to the two pathways of interaction could result in metabolic disorders leading to cell death (Sharan, 1996).

Till now, however, no detailed study of the interaction of AEBN or its components with DNA and its effect on genomic instability has been studied. The kinetics of the interaction of the AEBN or its components with the DNA is also not known. The exact mechanism of interaction of the AEBN with the DNA, therefore, remains obscure.

Study of genomic instabiltity can be done using a variety of organisms including prokaryotes like *E. coli*, *Campylobacter jejuni*, eukaryotes like *Saccharomyces cerevisiae*

mice and so on. However, each organism has its own advantages and disadvantages. Therefore, for an investigation, the choice of organism depends on the aspects that are targeted for the study.

1.7. Use of *E. coli* to study genomic instability:

In many respects, *E. coli* serves as an excellent model organism to study DNA damage. This is partly due to the fact that the availability of different repair deficient mutants makes it an attractive agent to study the role of the respective repair mechanisms. *E. coli* is an organism that is widely used in the study of DNA damages. The popularity of *E. coli* stems from the ease with which one can propagate this organism in the study damages induced by a variety of agents. The genome of *E. coli* is known to have microsatellite regions, which serve as excellent target regions for the study of genomic instability.

Microsatellite regions in the genome are sequences showing tandem repeats (Weissenbach *et al.*, 1992), which make them prone to accumulating damages and mutations due to a variety of processes, mainly that of replication slippage (Levinson and Gutman, 1987; Schlotterer and Tautz, 1992). The microsatellite regions have been shown to be hypervariable in eukaryotes, yeast and bacteria. Native mononucleotide runs have been shown to be unstable in coding regions of mismatch repair (MMR) deficient strains of *E. coli* (Schaaper and Dunn, 1987; Longerich *et al.*, 1995). Eukaryotes contain a huge amount of microsatellite regions (Hancock, 1995; Pupko and Graur, 1999) in contrast to prokaryotes, which contain lesser amounts of these repetitive DNA (Hancock, 1995). Prokaryotes have been found to be rich in mono- and tri- nucleotide repeats (Field and Wills, 1998). The length of the microsatellite regions in prokaryotes is again slightly smaller than that in eukaryotes. Microsatellite instability was correlated with cancer when it was first reported in hereditary non-polyposis colorectal cancer (HPNCC) (Aaltonen *et al.*, 1993, Peltomaki *et al.*, 1993). Since then, it was found that defects in mismatch repair systems could be responsible for the induction of microsatellite instability and also a strong predisposition to cancer (Jiricny, 1998). Microsatellite instability can also be caused by ROS and oxidative damage (Jackson *et al.*, 1998). Microsatellite instability has also been implicated in other cancerous tumors.

The non-dysplastic mucosa of patients with dysplastic ulcerative colitis have also been found to harbor microsatellite instability (Brentnall *et al.*, 1996).

For our studies, the *E. coli* strains used were two *rec* mutants of *E. coli* (Clark, 1991; Cox, 1999), viz., the *recA* mutant and the *recF* mutant. The use of *recA* mutants has been extensive in the study of damages induced by various kinds of mutagens, primarily damages induced by ionizing radiations (Horii *et al.*, 1980; Sancar et al., 1980). The RecA proteins also play important roles in the processes of mitosis and meiosis (Gaisor *et al.*, 2001). Besides *recA* mutations, other kinds of mutants have also been used for the study of DNA damage (Thomas and MacPhee, 1986). The DNA that has been damaged can be repaired by various mechanisms (Mol *et al.*, 1999). The *recF* mutant has been used to study the damages induced by the UV-C radiation.

1.8. Aims and objectives

With the background information that was available, therefore, an attempt was made to study the effect of these two agents, viz., UV-C radiation and AEBN in the induction of genomic instability. The model organism used was *E. coli.* In particular, the *E. coli* strains were transformed with a plasmid, pMTa4, which has served as an excellent model for the study of ionizing radiation induced damages in our laboratory (Humtsoe and Sharan, 2004).

The following objectives were set forth:

1. To study the mechanism of interaction of UV-C with pMTa4 DNA and to study the reason for the observed changes by employing various tools of molecular biology; *in vitro* as well as *in vivo* approaches.

2. To study the mechanism of interaction of AEBN with pMTa4 DNA and to study the reason for the observed changes by employing various tools of molecular biology; *in vitro* as well as *in vivo* approaches.

3. To study the synergistic effect of UV-C radiation on AEBN induced addcut formation on DNA.

Materials & Methods

2.1. Chemicals

2.1.1. ***General chemicals:*** The chemicals used were all of analytical grade and were obtained from various suppliers. Acrylamide, Ammonium persulfate (APS), Bisacrylamide, Calcium chloride ($CaCl_2$), Diethyl pyrocarbonate (DEPC), Dithiothreitol (DTT), DNA (Sperm Whale), Ethylenediaminetetraacetic acid (EDTA), Guanidium thiocyanate (GTC), Hexadecyltrimethylammonium bromide (cetyltrimethylammonium bromide) (CTAB), β-mercaptoethanol, Phenylmethylsulfonyl fluoride (PMSF), N,N,N',N'-Tetramethylethylenediamine (TEMED) were obtained from Sigma, USA; low EEO agarose was obtained from Bangalore Genei Ltd., India; Ethidium bromide (EB) (1 % solution) was obtained from Merck, Germany; Bromophenol blue, Coomassie Brilliant Blue R-250 (CBB R-250), Coomassie Brilliant Blue G-250 (CBB G-250)Glacial acetic acid, Isoamyl alcohol, Methanol, Sodium acetate was obtained from SRL, Mumbai, India; Chloroform, Glacial acetic acid, Glycerol, Orthophosphoric acid, Phenol, Sodium chloride (NaCl), Sodium dodecyl sulphate (SDS), Sodium hydroxide (NaOH), Sucrose, conc. Sulphuric acid and Tris[hydroxymethylamine]-aminomethane (Tris) were obtained from Qualigens, India; Diphenylamine was obtained from Glaxo, India; Ammonium isothiocyanide from Merck, India and ethanol from Bengal Chemicals, India.

2.1.2. ***Antibiotic:*** Ampicillin was obtained from Duchefa, The Netherlands.

2.1.3. ***Enzymes and markers:*** Deoxyribonuclease (DNase) free Ribonuclease (RNase) was obtained from Bangalore Genei, India; Lysozyme (from chicken egg white) was obtained as a lyophilized powder from Sigma, USA; the restriction endonucleases, *AccI, DraI,* and *SspI* were obtained from Bangalore Genei, India; and the restriction endonucleases *HaeII* and *NciI* were obtained from Boehringer Mannheim, Germany. The DNA molecular weight markers, 100 kb ladder, Lambda DNA *HindIII* digest and Lambda DNA *EcoRI Hind III* double digests were obtained from Bangalore Genei, India and the primers were obtained from Hysel, India.

2.1.4. ***Media:*** Luria Bertani (LB) broth and LB agar media were obtained from Himedia, India.

2.1.5. ***Kits:*** DNA amplification kit was purchased from Bangalore Genei Ltd., India.

2.2. Radiation sources

2.2.1. ***UV-C radiation:*** The source of UV-C radiation was a germicidal UV-C tube placed approximately 46 cm above the irradiation table in a sterile chamber delivering 0.04 $J.m^{-2}.s^{-1}$ as measured by UV 340 dosimeter (Biostep, Germany). Lower doses of UV-C radiation were obtained by placing a cardboard in the path of the UV-C radiation, which was found to reduce the dose to 0.01 $J. m^{-2}.s^{-1}$.

2.2.2. ***Gamma radiation:*** The source of gamma radiation was the Gamma Chamber 900 (Isotope Group, BARC, India) delivering γ-rays at a dose rate of ~ 0.05 $Gy.s^{-1}$ from a cobalt-60 source.

2.3. Preparation of aqueous extract of betel nut (AEBN)

The main carcinogenic component of betel nut is known to be the alkaloids which are soluble in water (Sharan, 1996). In this study, AEBN was used as a carcinogen. AEBN was prepared by method standardized in the laboratory (Pariat and Sharan, 1995; Yonekura *et al.*, 1992), which is briefly described below.

2.3.1. ***Materials required:***

[a] *Betel nut*: Locally available raw and wet variety of betel nut, commonly known as *kwai im*, was used for the study. This nut is an unprocessed form of the betel nut that is consumed widely in the Khasi Hills of North-east India.

[b] Mortar and pestle, sterile sieve, Whatman No. 1 filter paper.

2.3.2. ***Methodology:*** Betel nuts (100 g) were dehusked, coarsely ground with the help of a mortar and pestle and suspended in 250 ml of autoclaved Millipore water at (room temperature) RT for 24 h for extraction. The suspension was filtered through a sterile sieve to separate the particulate matter from the filtrate. This coarse filtrate was now filtered

through Whatman Filter paper No. 1, whereby a clear yellow filtrate was obtained. This filtrate was lyophilized to a fine powder. This lyophilized powder will henceforth be called AEBN. The AEBN thus obtained was stored refrigerated and dissolved in sterile water at required dose for experiments.

2.4. Bacterial strains and plasmid pMTa4

2.4.1. ***Strains of E. coli used for the study:*** For the studies related to the effect of the various agents inducing genomic instability, three isogenic variants of *E. coli* K12 strains have been used. These strains of *E. coli* included one repair proficient strain, AB1157 (DeWitt, 1962), which harbors 21 mutations. However, this strain is wild with respect to the *recA* and *recF* genes. Hence, this strain is also referred to as wild type strain. The other two strains of *E. coli* used are isogenic with AB1157 with the exception that JC9239 carries an additional mutation in the *recF* gene (Horii Z. *et al.*, 1973), making it deficient in repair of damages induced by UV-C radiation and XL1 Blue carries an additional mutation in the *recA* gene (Bullock et al, 1987), making it deficient in repair of damages induced by ionizing radiation. The mutations in the genotypes of the strains are shown in table 1:

Table 1: Details of *E. coli* strains used with relevant genotypes

Strain (Common name)	Genotype
AB1157 (wild type)	*thr-1, araC14, leuB6(Am), DE(gpt-proA)62, lacY1, tsx-33, qsr'-0, glnV44(AS), galK2(Oc), LAM-, Rac-0, hisG4(Oc), rfbC1, mgl-51, rpoS396(Am), rpsL31(strR), kdgK51, xylA5, mtl-1, argE3(Oc), thi-1*
JC9239 (*recF* mutant)	*thr-1, araC14, leuB6(Am), DE(gpt-proA)62, lacY1, tsx-33, qsr'-0, glnV44(AS), galK2(Oc), LAM-, Rac-0, hisG4(Oc), rfbC1, mgl-51, rpoS396(Am), rpsL31(strR), kdgK51, xylA5, mtl-1, argE3(Oc), thi-1, recF143*
XL1 Blue (*recA* mutant)	*thr-1, araC14, leuB6(Am), DE(gpt-proA)62, lacY1, tsx-33, qsr'-0, glnV44(AS), galK2(Oc), LAM-, Rac-0, hisG4(Oc), rfbC1, mgl-51, rpoS396(Am), rpsL31(strR), kdgK51, xylA5, mtl-1, argE3(Oc), thi-1, $recA_1$*

2.4.2. ***Plasmid pMTa4:*** The pBluescript (pBS) II SK is a 2958 bp phagemid derived from pUC19. It has an Ampicillin resistance gene at 1975-2832 bp and a multiple cloning site (MCS) at 657-759 bp. A replication competent hepatitis B virus genome sequence, with a

preX open reading frame (hpvprex), comprising 3215 bp, has been integrated ay MCS [*Xho I* restriction site] (Rakotomahanina *et al.*, 1994). This plasmid construct of 6173 bp has been designated as pMTa4 and was a kind gift from Prof. C. H. Schroeder (DKFZ, Heidelberg, FRG) and has also been described earlier (Humstoe *et al.*, 1998; 2003; Odyuo and Sharan, 2005). Figure 2.1 shows the pMTa4 schematic profile with relevant origins of replication and the site encoding for the Ampicillin resistance. The complete NT sequence of the + stand of pMTa4 is provided in table **1**.

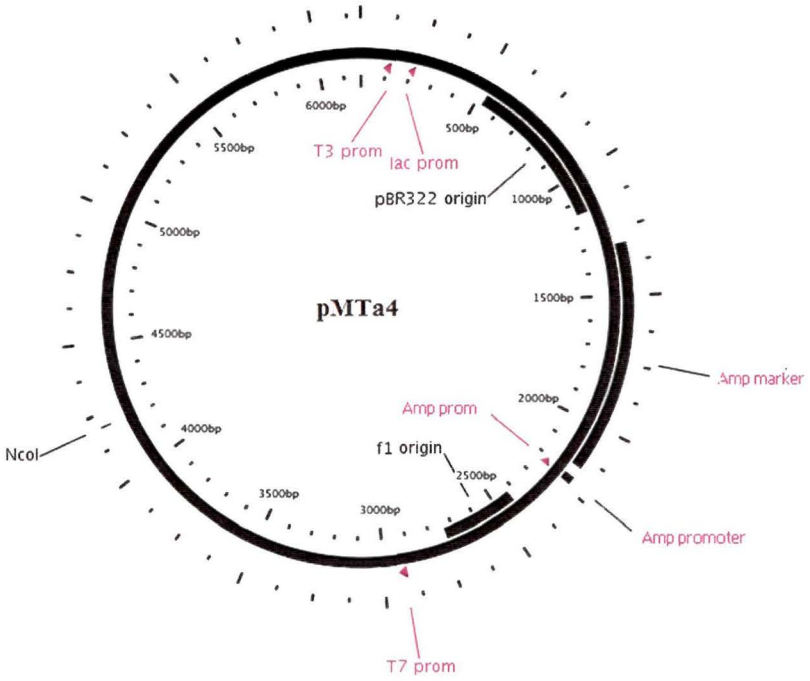

Figure 2.1: Diagrammatic representation of the pMTa4 DNA showing some features of the plasmid.

2.5. Medium preparation and culture of *E. coli*

2.5.1. ***Preparation of LB broth:*** LB broth was prepared by dissolving 25 g of the LB broth in 1000 ml of Millipore quality water. This medium was autoclaved at 15 psi for 20 min to sterilize it and stored refrigerated.

2.5.2. ***Growing of bacterial cultures:*** For growing the desired strains of *E. coli*, either a CFU from a master plate or very pure form of the strain was inoculated into fresh LB broth in a culture flask. The flask was incubated overnight (O/N) with rigorous shaking in a Remi

make (India) RS-24 rotary shaker maintained at 37 °C till it reached an OD of ~ 1 at 600 nm.

2.5.3. ***Preparation of master plates:*** Separate master plates were prepared for each of the three strains of *E. coli* used in this study. To prepare this, pure bacterial culture of interest was grown as described (§ 2.5.2.). From this, 1 µl of *E. coli* culture was diluted 10^{-9} times with sterile medium and plated on the LB agar plate in sterile conditions. After allowing the plates to stand at RT for 30 min for adsorption, the plate was sealed, inverted and incubated O/N at 37 °C in an incubator. CFU of medium size were formed by the next day. This plate containing ~ 40 CFU of the desired strain is called the master plate. Master plates were usually stored refrigerated and used up to one month.

2.6. Transmission electron microscopic (TEM) analysis

The *E. coli* cells were grown in the absence or presence of saturating concentrations of AEBN (2000 µg), following which the cells were processed and transmission electron micrographs were taken in the Sophisticated Analytical Instrumentation Facility (SAIF), NEHU, Shillong. The TEM studies were done using JEOL electron microscope 100CXII. The samples were processed as described below:

(i) Primary fixation: This was done with modified Karnovsky's fixative - containing 0.2 M sodium cacodylate buffer, 10% para formaldehyde and 25% glutaraldehyde at 4 °C.

(ii) Secondary fixation: This was done with 0.1 M cacodylate buffer, post fixed with 1 % osmium tetroxide for 2 h at 4 °C.

(iii) Washing: Following this, the samples were washed with 0.1 M cacodylate buffer, serially dehydrated with 30 %, 50 %, 70 %, 80 %, 90 % and 95 % acetone for 15 min each (2 changes at 4 °C) followed by 100 % acetone and dry acetone for 15 min each at room temperature (RT), cleared with propylene oxide (2 changes, 30 min each at RT).

(iv) Infiltration and embedding: After washing, the samples were infiltrated and embedded in embedding medium and propylene oxide in the ratio 1:3 O/N at RT, 1:1 for 1 h at RT, 3:1 for 1 h at RT in vacuum, and 1 change in pure embedding medium at 50 °C

Table 2: The NT sequence of the pMTa4 DNA used for the study

The nucleotide (NT) sequence of pMTa4, + strand (total number of NT = 6173):

TCGAGGTCGACGGTATCGATAAGCTTGATATCGAATTCCTGCAGCCCGGGGGATCCACTAGTTCTAGAGCGGCCGCCACCGCGGT
GGAGCTCCAGCTTTTGTTCCCTTTAGTGAGGGTTAATTTCGAGCTTGGCGTAATCATGGTCATAGCTGTTTCCTGTGTGAAATTGT
TATCCGCTCACAATTCCACACAACATACGAGCCGGAAGCATAAAGTGTAAAGCCTGGGGTGCCTAATGAGTGAGCTAACTCACA
TTAATTGCGTTGCGCTCACTGCCCGCTTTCCAGTCGGGAAACCTGTCGTGCCAGCTGCATTAATGAATCGGCCAACGCGCGGGGA
GAGGCGGTTTGCGTATTGGGCGCTCTTCCGCTTCCTCGCTCACTGACTCGCTGCGCTCGGTCGTTCGGCTGCGGCGAGCGGTATCA
GCTCACTCAAAGGCGGTAATACGGTTATCCACAGAATCAGGGGATAACGCAGGAAAGAACATGTGAGCAAAAGGCCAGCAAAA
GGCCAGGAACCGTAAAAAGGCCGCGTTGCTGGCGTTTTTCCATAGGCTCCGCCCCCCTGACGAGCATCACAAAAATCGACGCTCA
AGTCAGAGGTGGCGAAACCCGACAGGACTATAAAGATACCAGGCGTTTCCCCCTGGAAGCTCCCTCGTGCGCTCTCCTGTTCCGA
CCCTGCCGCTTACCGGATACCTGTCCGCCTTTCTCCCTTCGGGAAGCGTGGCGCTTTCTCATAGCTCACGCTGTAGGTATCTCAGT
TCGGTGTAGGTCGTTCGCTCCAAGCTGGGCTGTGTGCACGAACCCCCCGTTCAGCCCGACCGCTGCGCCTTATCCGGTAACTATC
GTCTTGAGTCCAACCCGGTAAGACACGACTTATCGCCACTGGCAGCAGCCACTGGTAACAGGATTAGCAGAGCGAGGTATGTAG
GCGGTGCTACAGAGTTCTTGAAGTGGTGGCCTAACTACGGCTACACTAGAAGGACAGTATTTGGTATCTGCGCTCTGCTGAAGCC
AGTTACCTTCGGAAAAAGAGTTGGTAGCTCTTGATCCGGCAAACAAACCACCGCTGGTAGCGGTGGTTTTTTTGTTTGCAAGCAG
CAGATTACGCGCAGAAAAAAAGGATCTCAAGAAGATCCTTTGATCTTTTCTACGGGGTCTGACGCTCAGTGGAACGAAAACTCA
CGTTAAGGGATTTTGGTCATGAGATTATCAAAAAGGATCTTCACCTAGATCCTTTTAAATTAAAAATGAAGTTTTAAATCAATCTA
AAGTATATATGAGTAAACTTGGTCTGACAGTTACCAATGCTTAATCAGTGAGGCACCTATCTCAGCGATCTGTCTATTTCGTTCAT
CCATAGTTGCCTGACTCCCCGTCGTGTAGATAACTACGATACGGGAGGGCTTACCATCTGGCCCCAGTGCTGCAATGATACCGCG
AGACCCACGCTCACCGGCTCCAGATTTATCAGCAATAAACCAGCCAGCCGGAAGGGCCGAGCGCAGAAGTGGTCCTGCAACTTT
ATCCGCCTCCATCCAGTCTATTAATTGTTGCCGGGAAGCTAGAGTAAGTAGTTCGCCAGTTAATAGTTTGCGCAACGTTGTTGCCA
TTGCTACAGGCATCGTGGTGTCACGCTCGTCGTTTGGTATGGCTTCATTCAGCTCCGGTTCCCAACGATCAAGGCGAGTTACATGA
TCCCCCATGTTGTGCAAAAAAGCGGTTAGCTCCTTCGGTCCTCCGATCGTTGTCAGAAGTAAGTTGGCCGCAGTGTTATCACTCAT
GGTTATGGCAGCACTGCATAATTCTCTTACTGTCATGCCATCCGTAAGATGCTTTTCTGTGACTGGTGAGTACTCAACCAAGTCAT
TCTGAGAATAGTGTATGCGGCGACCGAGTTGCTCTTGCCCGGCGTCAATACGGGATAATACCGCGCCACATAGCAGAACTTTAAA
AGTGCTCATCATTGGAAAACGTTCTTCGGGGCGAAAACTCTCAAGGATCTTACCGCTGTTGAGATCCAGTTCGATGTAACCCACT
CGTGCACCCAACTGATCTTCAGCATCTTTTACTTTCACCAGCGTTTCTGGGTGAGCAAAAACAGGAAGGCAAAATGCCGCAAAAA
AGGGAATAAGGGCGACACGGAAATGTTGAATACTCATACTCTTCCTTTTCAATATTATTGAAGCATTTATCAGGGTTATTGTCTC
ATGAGCGGATACATATTTGAATGTATTTAGAAAAATAAACAAATAGGGGTTCCGCGCACATTTCCCCGAAAAGTGCCACCTAAAT
TGTAAGCGTTAATATTTTGTTAAAATTCGCGTTAAATTTTTGTTAAATCAGCTCATTTTTTAACCAATAGGCCGAAATCGGCAAAA
TCCCTTATAAATCAAAAGAATAGACCGAGATAGGGTTGAGTGTTGTTCCAGTTTGGAACAAGAGTCCACTATTAAAGAACGTGG
ACTCCAACGTCAAAGGGCGAAAAACCGTCTATCAGGGCGATGGCCCACTACGTGAACCATCACCCTAATCAAGTTTTTTGGGGTC
GAGGTGCCGTAAAGCACTAAATCGGAACCCTAAAGGGAGCCCCCGATTTAGAGCTTGACGGGGAAAGCCGGCGAACGTGGCGA
GAAAGGAAGGGAAGAAAGCGAAAGGAGCGGGCGCTAGGGCGCTGGCAAGTGTAGCGGTCACGCTGCGCGTAACCACCACACCC
GCCGCGCTTAATGCGCCGCTACAGGGCGCGTCCCATTCGCCATTCAGGCTGCGCAACTGTTGGGAAGGGCGATCGGTGCGGGCCT
CTTCGCTATTACGCCAGCTGGCGAAAGGGGGATGTGCTGCAAGGCGATTAAGTTGGGTAACGCCAGGGTTTTCCCAGTCACGACG
TTGTAAAACGACGGCCAGTGAATTGTAATACGACTCACTATAGGGCGAATTGGGTACCGGGCCCCCCCTCGAGGACTGGGGACC
CTGCACCGAACATGGAGAGCACAACATCAGGATTCCTAGGACCCCTGCTCGTGTTACAGGCGGGGTTTTTCTTGTTGACAAGAAT
CCTCACAATACCACAGAGTCTAGACTCGTGGTTGACTTCTCTCAATTTTCTAGGGGGAACACCCAAGTGTCCTGGCCAAAATTCG
CAGTCCCCAACCTCCAATCACTCACCAACCTCTTGTCCTCCAACTTGTCCTGGGTATCGCTGGATGTGTCTGCGGCGTTTTATCAT
ATTCCTCTTCATCCTGCTGCTATGCCTCATCTTCTTGTTGGTTCTTCTGGACTACAAAGGTATGTTGCCCGTTTGTCCTCTACTTCCA
GGAACATCAACTACCAGCACGGGACCATGCAAGACCTGCACGATTCCTGCTCAAAACACCTCTATGTTTCCCTCTTGTTGCTGTA
CAAAACCTTCGGACGGAAACTGCACTTGTATTCCCATCCCATCATCCTGGGCTTTCGCAAGATTCCTATGGGAGTGGGCCTCAGT
CCGTTTCTCCTGGCTCAGTTTACTAGTGCCATTTGTTCAGTGGTCTGCAGGGCTTTCCCCCACTGTTTGGCTTTCAGTTATATGGAC
GATGTGGTATTGGGGGCCAAGTCTGTACAACATCTTGAGTCCCTTTTTACCTCTATTACCAATTTTATGTTGTCTTTGGGCATACAT
TTGAACCCTAATAAAACCAAGCGTTGGGGCTACTCCCTTAACTTCATGGGATATGTAATTGGAAGTTGGGGTACTTTACCACAAG
AACATATTGTACAAAAACTCAAGCAATGTTTTCGAAAACTGCCTGTCAATAGACCTATTGATTGGAAAGTATGTCAGAGAATTGT
GGGTCTTTTAGGCTTTGCTGCCCCTTTTACACAATGTGGCTATCCTGCCTTGATGCCTTTATATGCCTGTATACAATCTAAGCAGGC
TTTCACTTTCTCGCCAACTTACAAGGCCTTTCTGTGTAAACAATATCTGAACCTTTACCCCGTTGCCCGGCAACGGTCAGGCCTCT
GCCAAGTGTTTGCTGATGCAACCCCCACTGGATGGGGCTTGGCCATTGGCCATCAGCGCATGCGTGGAACCTTTGTGGCTCCTCT
GCCGATCCATACTGCGGAACTCCTAGCAGCTTGTTTTGCTCGCAGCCGGTCTGGAGCGACACTTATCGGAACCGACAACTCTGTT
GTCCTCTCTCGGAAATACACCTCCTTTCCATGGCTGCTAGGGTGTGCTGCCAACTGGATCCTGCGCGGGACGTCCTTGTCTACGT
CCCGTCGGCGCTGAATCCCGCGGACGACCCGTCTCGGGGCCGTTTGGGCCTCTATCGTCCCCTTCTTCGTCTGTCGTTCCGGCCGA
CCACGGGGCGCACCTCTCTTTACGCGGTCTCCCCGTCTGTGCCTTCTCATCTGCCGGACCGTGTGCACTTCGCTTCACCTCTGCAC
GTCGCATGGAGACCACCGTGAACGCCCACCAGGTCTTGCCCAAGGTCTTATATAAGAGGACTCTTGGACTCTCAGCAATGTCAAC
GACCGACCTTGAGGCATACTTCAAAGACTGTTTGTTTAAAGACTGGGAGGAGTTGGGGGAGGAGATTAGGTTAATGATCTTTGTA
CTAGGAGGCTGTAGGCATAAATTGGTCTGTTCACCAGCACCATGCAACTTTTTCACCTCTGCCTAATCATCTCATGTTCATGTCCT
ACTGTTCAAGCCTCCAAGCTGTGCCTTGGGTGGCTTTAGGGCATGGACATTGACCCGTATAAAGAATTTGGAGCTTCTGTGGAGT
TACTCTCTTTTTTGCCTTCTGACTTCTTTCCGTCTGTTCGAGATCTCCTCGACACCGCCTCTGCTCTCTATCGGGAGGCCTTAGAGT
CTCCGGAACATTGTTCACCTCACCATACAGCACTCAGGCAAGCTATTCTGTGTTGGGTTGAGTTGATGAATCTGGCCACCTGGGT
GGGAAGTAATTTGGAAGACCCAGCATCCAGGGAATTAGTAGTCAGCTATGTCAATGTTAATATGGGCCTAAAAATCAGACAACT
ATTGTGGTTTCACATTTCCTGTCTTACTTTTGGAAGAGAAACTGTTTTAGAGTATTTGGTGTCTTTTGGAGTGTGGATTCGCACTCC
TCTCGCTTACAGACCACCAAATGCCCCTATCTTATCAACACTTCCGGAAACTACTGTTGTTAGACAACGAGGCAGGTCCCCTAGA
AGAAGAACTCCCTCGCCTCGCAGACGAAGATCTCAATCGCCGCGTCGCAGAAGATCTAAATCTCGGGAATCTCAATGTTAGTATC
CCTTGGACTCATAAGGTGGGAAACTTTACTGGACTTTATTCTTCTACTGTACCTGTCTTTAATCCTGAGTGGAAAACTCCCTCTTTT
CCTAACATTCATTTACAGGAGGACATTATTGATAGATGTCAACAATATGTGGGCCCTCTTACAGTGAATGAAAAAAGGAGATTAA
AATTAATTATGCCTGCTAGGTTCTATCCTAACCTTACCAAGTATTTACCCTTGGATAAAGGCATTAAACCTTATTATCCTGAACAT
GCAGTTAATCATTACTTCCAAACTAGGCATTATTTACATACTCTGTGGAAGGCTGGCATTCTATATAAGAGAGAAACTACACGCA
GTGCCTCATTTTGTGGGTCACCATATTCTTGGGAACAAGAGCTACAGCATGGGAGGTTGGTCTTCCAAACCTCGACAAGGCATGG
GGACGAATCTTTCTGTTCCCAATCCTCTGGGATTCTTTCCCGATCACCAGTTGGACCCTGCGTTCGGAGCCAACTCAAACAATCCA
GATTGGGACTTCAACCCCAACAAGGATCACTGGCCAGAGGCAAAGCAGGTAGGAGCGGGAGCATTCGGGCCAGGGTTCACCCCA
CCACACGGCGGCCTTTTGGGGTGGAGCCCTCAGGCTCAGGGCACATTGACAACAGTGCCAGCAGCGCCTCCTCCTGCTTCCACCA
ATCGGCAGTCAGGAAGACAGCCTACTCCCATCTCTCCACCTCTAAGAGACAGTCATCCTCAGGCCATGCAGTGGAACTCCACAAC
ATTCCACCAAGCTCTGCTAGATCCAAGAGTGAGGGGCCTCTATTTCCCTGCTGGTGGCTCCAGTTCCGGAACAGTAAACCCTGTT
CCGACTACTGCCTCACCCATATCGTCAATCTTC

(embedding medium contains Araldite CY212, dodecenyl succinic anhydride, tri (dimethylaminomethyl) phenol and di-butyl phthalate).

(v) Embedding: After infiltration, the specimens are embedded in medium using BEEM capsules as mould (24 h at 50 °C), following which the temperature was raised to 60 °C for 24 h.

(vi) Ultramicrotomy was then performed producing section sizes ~60 nm in thickness.

(v) Staining: The sections were stained with uranyl acetate for 30-120 min at RT. Following this, the changes observed in the size and morphology of the cells was studied and the results analyzed (Terzakis, 1968).

2.7. Preparation of cell free extract

In order to study the effect of gamma irradiation on pMTa4 DNA, a cell free extract of the cell was prepared as per the protocol given by Sambrook and Russel (2001). The methodology is described below.

2.7.1. ***Buffers and solutions:*** The compositions of the buffers and solutions required are described below.

[a] *Lysozyme:* A solution of concentration 5 $\mu g.\mu l^{-1}$ was prepared.

[b] *Lysis buffer:* This buffer had the following composition:

Tris-Cl, pH 7.5	50 mM
NaCl	50 mM
DTT	1 mM
PMSF	1 mM
Glycerol (v/v)	15 %

[c] *PMSF stock solution*: This was a 100 mM solution in isopropanol.

2.7.2. ***Methodology:*** From an *E. coli* culture grown as described (§ 2.5.2.), 1.5 ml of the culture was centrifuged. The cell pellet obtained was resuspended in lysis buffer in a ratio of 1 mg cell wet weight to 1 ml lysis buffer. Following this, 10 µl of the stock PMSF solution was

added. Lysozyme was added to a final concentration of 300 $\mu g.ml^{-1}$ and the cell suspension was incubated at 4 °C for 4 h. The cell debris was removed by centrifugation at 40,000 x g. The resulting supernatant was the cell-free-extract of *E. coli*.

2.8. Transformation of pMTa4 DNA

Standard transformation protocol (Sambrook and Russel, 2001) was used with some modifications for the transformation of pMTa4 DNA into the various strains of *E. coli* used for the study (Sharan *et al.*, 2007). The methodology used for the study is as follows:

2.8.1. ***Materials required***: The requirements are described below.

[a]	LB agar plates with and without Ampicillin	
[b]	*E. coli* cultures grown till it reached OD of ~ 1 at 600 nm	
[c]	$CaCl_2$	0.1 M
[d]	pMTa4 DNA	100 ng ml^{-1}

2.8.2. ***Methodology***: Freshly sterilized LB broth (5 ml) was inoculated with 500 µl *E. coli* culture grown as described (§ 2.5.2.) till it reached an OD of 0.5 at 600 nm. This culture was cooled on ice for 15 min. From this culture, which consisted primarily of competent cells in the mid-log phase, 1.5 ml of culture was centrifuged. The cell pellet obtained was resuspended in 600 µl of ice cold 0.1 M $CaCl_2$ and stored on ice for 30 min. It was then centrifuged and the cell pellet so obtained was resuspended in 200 µl of ice-cold 0.1 M $CaCl_2$. To this, 75 µl of pMTa4 (75 ng DNA) was added, gently mixed and kept on ice for 20 min. The tube was then incubated, in sequence, at 42 °C for 30 s and on ice for 180 s. LB medium (500 µl, pre-warmed to 37 °C) was added into the tube, gently mixed and incubated at 37 °C for 60 min. The content (200 µl) was then plated on LB agar plates containing 100 $\mu g.ml^{-1}$ Ampicillin at dilutions of 10^{-3} and 10^{-5} and incubated O/N at 37 °C. Control was LB agar plate without Ampicillin. The following day, some colony forming units (CFU) were observed on the Amp^+-LB agar plates. These CFU were the *E. coli* cells which had been transformed with the pMTa4 DNA, as confirmed by isolating pMTa4 DNA from cultures grown from single CFU. The control plates showed confluent growth (lawn). The cultures grown from the CFU of pMTa4 transformed *E. coli* were used for further studies.

2.9. Growth of the different strains of *E. coli*

For determining the growth characteristics of the *E. coli* strains, three different flasks were inoculated with single CFU of the three strains of *E. coli*, viz., AB1157, XL1 Blue and the cultures grown (§ 2.5.2.) in the presence of 100 $\mu g.ml^{-1}$ Ampicillin.

To determine the growth characteristics, the OD of the culture at 600 nm was recorded every 2 h and plotted.

2.10. Clonogenic survival assay

The clonogenic assay is a measure of an organism's reproductive ability following some injury (Pacelli *et al.*, 1995, Birrell *et al.*, 2001). This assay has been used to monitor the effect of UV-C radiation induced injury to *E. coli* as different strains of *E. coli* used in the study had varying susceptibilities to UV-C radiation induced injuries (Sharan, *et al.*, 2007). The methodology used for the study is as follows:

2.10.1. ***Requirements:*** The compositions of the buffers and solutions required are described below.

[a] LB agar plates

[b] The desired *E. coli* culture grown as described (§ 2.5.2.).

[c] Source of UV-C radiation (§ 2.2.1)

2.10.2. ***Methodology:*** The *E. coli* cultures were plated on LB agar plates containing 100 $\mu g.ml^{-1}$ Ampicillin, at dilutions of 10^{-7}, 10^{-8} and 10^{-9}. The plates, after an incubation of 30 min at RT, were shifted to an incubator (37 °C). The following day, the CFU formed were counted and the values recorded. These results were converted to percentage of control and plotted on a semi-log graph paper as percent of controls to represent the survival of the *E. coli* strain.

2.11. Preparation of plasmid DNA

Plasmid DNA was isolated from the *E. coli* cells essentially following the method of Sambrook and Russel (2001) with modification as adapted in the laboratory (Odyuo and Sharan, 2005).

2.11.1. ***Buffers and solutions***: The compositions of the buffers and solutions required are described below.

[a] Suspension buffer: This had the following composition:

Tris-HCl, pH 8.0	10 mM
EDTA, pH 8.0	1 mM

[b] DNase free RNase solution: DNase free RNase solution (100 μg ml^{-1}) was prepared in sterile Millipore quality water.

[c] Lysis solution: This solution was freshly prepared and had the following composition:

NaOH	0.2 M
SDS	1 %

[d] Renaturation buffer: A 3 M solution of Sodium acetate served as the renaturation buffer. The pH was adjusted at 5.2 with acetic acid.

[e] Phenol:Chloroform solution was prepared by mixing phenol and chloroform in a ratio of 1:1.

[f] Ethanol: Two dilutions (95 % and 70 %) of ethanol were prepared by appropriate dilution of absolute alcohol with water.

2.11.2. ***Methodology*:** Fresh LB medium was inoculated with a single CFU of *E. coli* and grown at 37°C O/N (§ 2.5.2.). In a microfuge tube 1.5 ml of the culture was taken. It was subjected to centrifugation at 10,500 xg in a Sigma centrifuge for 1 min. After discarding the

supernatant, the cell pellet was resuspended in 20 µl of the suspension buffer. To this, 7 µl of DNase free RNase was added and mixed. To this suspension, 200 µl of the lysis buffer was added, mixed gently and allowed to stand for 3 min at RT, which rendered the suspension of cells translucent, indicating lysis of the cells. Following this, 150 µl of the renaturation buffer was added, the suspension gently mixed and left on ice for 5 min. This suspension was now centrifuged at 10,500 xg for 5 min and the supernatant collected in a fresh tube. An equal volume of phenol:chloroform solution was added and mixed well by vortexing for 10 s. The resulting suspension was centrifuged for 2 min at 10,500 xg and the upper aqueous phase collected in a fresh tube. To this, 900 µl of 95 % ethanol was added, allowed to stand in cold for 10 min and centrifuged for 10 min at 10,500 xg. The plasmid DNA, which collected at the bottom of the tube as a white pellet, was washed with 400 µl of 75 % ethanol. After pouring off the ethanol, traces of the remaining ethanol were evaporated in a 37 °C incubator. The dried pellet was dissolved in sterile water or TE buffer as required and stored refrigerated for further analysis. The average yield of the pMTa4 DNA obtained was 2 $\mu g.\mu l^{-1}$.

2.12. Preparation of genomic DNA

Genomic DNA was isolated from the *E. coli* by the method described by Ausubel *et al.* (1995) with minor modifications.

2.12.1. ***Buffers and solutions:*** The compositions of the buffers and solutions required are described below.

[a] TE buffer: This had the following composition:

Tris-HCl, pH 8.0	10 mM
EDTA, pH 8.0	1 mM

[b] Proteinase K solution: A 20 mg ml^{-1} solution of Proteinase K was prepared in sterile Millipore water.

[c] SDS solution: This was prepared by dissolving 10 g of SDS in 100 ml of sterile Millipore water making a 10 % solution.

[d] CTAB/NaCl solution: This has the following composition:

CTAB	10 %
NaCl	0.7 M

NaCl was first dissolved in sterile Millipore water and then the CTAB was slowly added to the solution with slow heating and stirring.

[e] Chloroform:Isoamyl alcohol mix was prepared by mixing chloroform and isoamyl alcohol in the ratio 24:1.

[f] NaCl: A 5 M solution was prepared and stored at RT.

[g] Phenol:Chloroform:Isoamyl alcohol mix was prepared by mixing phenol, chloroform and isoamyl alcohol in the ratio 25:24:1.

2.12.2. ***Methodology:*** In a microfuge tube, 1.5 ml of O/N bacterial culture was centrifuged for 1 min at 10,000 xg in a Sigma centrifuge. The supernatant was discarded and the cell pellet resuspended in 367 µl of TE buffer. After adding 3 µl of proteinase K and 30 µl of SDS solution, the suspension was mixed well and incubated at 37 °C in a water bath for 60 min. To this, 100 µl of 5 M NaCl was added and mixed well. Following this, 80 µl of CTAB-NaCl solution was added. After mixing, the solution was incubated in a water bath at 65 °C for 10 min. Following this, an equal volume of chloroform:isoamyl alcohol mix was added, mixed well and centrifuged for 5 min at 10,000 xg. The upper aqueous phase was carefully pipetted out, collected into a fresh tube and an equal volume of phenol:chloroform:isoamyl alcohol mix was added. The mixture was centrifuged at 10,000 xg for 5 min. The upper clear aqueous phase was collected in a fresh tube and the genomic DNA precipitated out by mixing it with 0.6 ml isopropanol at RT. The precipitate was spun down by centrifugation at 10,000 xg for 5 min. The pellet of genomic DNA was washed with 70 % ethanol, dried in a 37 °C incubator and dissolved in sterile Millipore water or TE buffer as required.

2.13. Preparation of total RNA from *E. coli*

Total RNA was isolated from the cells using the trizol method (Sambrook and Russel, 2001) with minor modifications. The materials required and method employed are described below:

2.13.1. ***Buffers and solutions:*** The buffers and solutions required for the extraction are listed below:

[a] Trizol reagent: This had the following composition:

GTC	0.8 M
Ammonium thiocyanate	0.4 M
Sodium acetate, pH 5	0.1 M
Glycerol	5 %
Phenol	38 %

DEPC treated water to make the final volume to 100 ml.

DEPC treated water was prepared by mixing by stirring O/N, 2 ml of DEPC in 1000 ml water.

[b] TE buffer: This had the following composition:

Tris-HCl, pH 8.0	10 mM
EDTA, pH 8.0	1 mM

[c] Chloroform: This was used directly from the bottle.

[d] Isopropanol: This was used directly from the bottle.

[e] Ethanol: A 75 % solution was prepared using absolute alcohol by appropriate dilution.

2.13.2. ***Methodology***: The entire isolation protocol was performed in a sterile room with restricted entry. Only sterile, RNase free glassware and plasticware were used, which were prepared by treating the plasticware and glassware with DEPC water, following which they were autoclaved. Fresh gloves were also used for the isolation process. These precautions were

taken in order to mimimize the possibilities of comtamination as success of isolation of RNA is largely dependent on contamination free isolation conditions.

From an *E. coli* culture grown as described (§ 2.5.2.), 1.5 ml of culture was taken in a microfuge tube and spun at 10,000 xg. The resulting cell pellet was resuspended in 1 ml trizol reagent and allowed to stand at RT for 5 min. To this, 0.4 ml of chloroform was added, shaken for 15 s and again allowed to stand at RT for 3 min. The suspension was centrifuged for 5 min at 13,000 x g. The upper 90 % of the supernatant was carefully collected and 0.5 ml of isopropanol was added to it. It was left to stand at RT for 30 min and spun in a Sigma centrifuge for 10 min at 13,000 xg. The supernatant was discarded. The pellet, which primarily contained the total cellular RNA, was washed with 75 % ethanol and dried. The dried pellet was dissolved in TE buffer. Quantification of the isolate was done spectophotometrically (§ 2.14.2). The isolated RNA was subjected to 2 % AGE (§ 2.18).

2.14. Quantification of nucleic acid

2.14.1. ***Quantification of DNA by chemical method:*** DNA was quantified by the diphenylamine assay of DNA estimation (Burton, 1968) with minor modifications. The methodology is briefly described below.

2.14.1.1. *Solution required:* Diphenylamine reagent: The reagent was prepared using the following ingredients:

Diphenylamine	1.5 g
Glacial acetic acid	100 ml
Concentrated sulfuric acid	1.5 ml.

The above reagents were mixed in the specified quantities carefully. The resulting reagent was stored at RT.

2.14.1.2. *Methodology:* DNA was estimated by adding 2 ml of diphenylamine reagent to 0.1 ml of the DNA sample and boiling the mixture in a water bath for 10 min. The absorbance of the blue colored solution was read at 595 nm after the solution had cooled down to RT. Sperm whale DNA served as a standard.

2.14.2. ***Quantification of DNA and RNA by spectrophotometric absorbance method:*** DNA or RNA samples were also quantified by measuring the absorbance of the appropriately diluted sample at 260 nm in a DU-530 Beckman spectrophotometer. The DNA and RNA contents were calculated using the relationship of one unit absorbance at A_{260} being equivalent to 50 $\mu g.ml^{-1}$ DNA and 40 $\mu g.ml^{-1}$ RNA, respectively (Sambrook and Russel, 2001). The purity of DNA or RNA was also determined by the absorption ratio A_{260}:A_{280} (Sambrook and Russel, 2001).

2.15. UV-C irradiation protocols

The effect of UV-C on the pMTa4 DNA profiles was studied *in vitro* and *in vivo*. The irradiation protocols followed are described below.

2.15.1. ***Irradiation of pMTa4 DNA in vitro*:** For irradiation of pMTa4 *in vitro*, aqueous solution of pMTa4 DNA (4 µg DNA in 2 µl) was irradiated in a UV chamber (§ 2.2.1) in dark and on ice for varying intervals of time.

2.15.1.1. *Low dose studies:* For the low dose studies, the irradiation was done for 30, 60, 90, 120 and 150 s which delivered UV-C doses of 1.2, 2.4, 3.6, 4.8 and 6 $J.m^{-2}$, respectively, to pMTa4 DNA.

2.15.1.2. *High dose studies:* For the high dose studies, the irradiation was done for 120, 240, 480 and 960 s, which delivered UV-C doses of 4.8, 9.6, 19.2 and 38.4 $J.m^{-2}$ respectively to pMTa4 DNA.

Immediately after irradiation, non-irradiated control and irradiated pMTa4 DNA were subjected to AGE (§ 2.18.) for analysis. From the captured image the band intensities of the CC and OC forms of pMTa4 were calculated using the KDS 1D software.

2.15.2. ***Irradiation in vivo:*** For *in vivo* irradiation with UV-C, 1.5 ml of pre-cooled mid-log *E. coli* cultures grown as described (§ 2.5.2.) were irradiated on ice in a dark UV-C chamber (§

2.2.1.) at low dose conditions (§ 2.15.1.1.). Plasmid DNA was isolated from these irradiated cells following one of the two protocols listed below. Isolated plasmid DNA from non-irradiated control and the irradiated cells (§ 2.11.) were subjected to AGE (§ 2.18.) for analysis. From the captured image the band intensities of the CC and OC forms of pMTa4 were calculated using the KDS 1D software.

2.15.3. ***Irradiation of E. coli cells:*** AB1157 and JC9239 cells of *E. coli*, precooled for 30 min, were irradiated for 120, 240, 480 and 960 s, which delivered UV-C doses of 4.8, 9.6, 19.2 and 38.4 $J.m^{-2}$. Following this, RNA was isolated (§ 2.13.) in repair permissive, (i.e., after incubation at 37 °C for 60 min in the presence of light) and repair non-permissive (i.e., immediately after irradiaton) conditions, AGE performed (§ 2.18.) and the results analyzed (§ 2.26.). The total proteins were also analyzed (§ 2.34.).

2.15.3.1. Plasmid isolation under repair non-permissive (R^-) conditions: For isolation of pMTa4 under R^- conditions, pMTa4 DNA was isolated immediately after UV-C irradiation (§ 2.11.) in dark.

2.15.3.2. Plasmid isolation under repair permissive (R^+) conditions: For isolation of pMTa4 under R^+ conditions, the UV-C irradiated *E. coli* cultures were first incubated in a 37 °C water bath for 60 min and then plasmid DNA was isolated (§ 2.11.). In order to study the kinetics of the repair, the UV-C irradiated *E. coli* cultures were also subjected to variable periods of post-irradiation repair incubation (15, 30 or 60 min) and then the pMTa4 DNA isolated.

2.16. Gamma irradiation protocol

Cultures of AB1157 and XL1 Blue strains of *E. coli* (§ 2.4.1.) were subjected to gamma irradiation.

2.16.1. ***Irradiation in vivo:*** Cells grown in an LB medium (§ 2.5.2.) (1.5 ml) were pre-cooled on ice in microfuge tubes for 30 min before placing the tubes in gamma chamber for 30, 60 and 120 min of exposure to gamma radiation accumulating doses of 100, 200 and 400 Gy,

respectively, under *in vivo* condition. The plasmid DNA was isolated for analysis following either of the two protocols listed below.

2.16.1.1. Plasmid isolation under repair non-permissive (R^-) conditions: pMTa4 DNA was isolated (§ 2.11.) from cells immediately after irradiation in the dark. Isolated plasmid was dissolved in 20 µl of sterile Millipore water and kept refrigerated for analysis.

2.16.1.2. Plasmid isolation under repair-permissive (R^+) conditions: After irradiation, the cells were subjected to post-irradiation repair incubation in a water bath at 37 °C for 60 min in the presence of light. After this incubation, pMTa4 DNA was isolated (§ 2.11.), dissolved in 20 µl of sterile Millipore water and stored refrigerated for analysis. In an experiment designed to study the effect of repair system reconstitution on the repair kinetics (§ 2.26.), the reconstituted XL1 Blue culture was incubation under repair permissive condition for 30 min only.

2.17. AEBN exposure protocols

The effect of exposure of pMTa4 to AEBN was studied *in vitro* and *in vivo*. The exposure protocols followed are described below:

*2.17.1.**AEBN exposure of pMTa4 DNA in vitro:*** Aliquots of whole or linearized (with *NcoI*) pMTa4 DNA (2µl containing 4 µg DNA) were exposed to 0.5, 1, 1.5, 2 or 2.5 µl of AEBN (100 $\mu g.\mu l^{-1}$) subjecting the pMTa4 to increasing concentrations of AEBN (50, 100, 150, 200 or 250 µg) at 37 °C for 30 min or to 2.5 µl AEBN (100 $\mu g.\mu l^{-1}$) subjecting the pMTa4 to 250 µg AEBN for increasing time intervals (5, 10, 15, 20, 25, 30, 35, 40 or 45 min).

*2.17.2.**AEBN exposure of pMTa4 DNA in vivo:*** AB1157 cells were grown as described (§ 2.5.2.) in the presence of 50, 100, 150, 200 or 250 µl AEBN (100 $\mu g.\mu l^{-1}$) per 10 ml culture, essentially exposing the cells to 500, 1000, 1500 or 2000 µg AEBN per ml culture O/N at 37 °C in a shaker.

2.18. Agarose gel electrophoresis (AGE)

Standard AGE protocol was followed (Ausubel *et al.*, 1995) as adapted in the laboratory (Odyuo and Sharan, 2005). The methodology is briefly described below.

2.18.1. ***Buffers and solutions:*** The compositions of the buffers and solutions required are described below.

[a] TAE buffer, pH 8.0 (1 x): This had the following composition:

Tris-acetate, pH 8.0	40 mM
EDTA, pH 8.0	1 mM

[b] Sample loading solution: This had the following composition:

Sucrose	40 %
Bromophenol blue	0.2 %

[c] EB staining solution was used as supplied.

2.18.2. ***Gel preparation:*** In 100 ml of TAE buffer in a beaker, 1, 1.2 or 2 g of agarose was added to prepare 1, 1.2 or 2 % agarose gel, respectively. The agarose was dissolved by slowly heating the beaker to about 90 °C in a microwave with repeated swirling. The clear agarose solution was cooled to about 40 °C, slowly poured into gel casting chambers and a comb inserted into the molten gel. The gel usually solidified in ~ 20 min at RT. The comb was removed and the gel was placed into the electrophoresis tank containing 1 X TAE buffer.

2.18.3. ***Sample loading:*** After mixing the DNA or RNA samples (usually containing ~ 4 µg of the nucleic acid) with $1/10^{th}$ volume of the sample loading solution, the mixture was loaded into the wells of the agarose gel with the help of microtips.

2.18.4. ***Electrophoresis:*** The samples in the submerged agarose gels were subjected to electrophoresis at constant voltage for specific periods of time, as shown below, in a Mupid gel electrophoresis apparatus (Japan). The electrophoresis conditions for the various samples used are described in table 3.

Table 3: Agarose gel electrophoresis details

Sample for electrophoresis	Gel percentage	Voltage (V)	Time (min)
pMTa4 DNA	1 %	100	60
RNA	1.2 %	100	60
PCR amplicon	2 %	100	30
Restriction digests of pMTa4 DNA	1 %	50	60

2.18.5. ***Staining and documentation:*** Gels were stained in 0.3 $\mu g.ml^{-1}$ EB in TAE buffer for 10 min on a rocker, following which the gels were destained in TAE buffer for 30 min. The gels were visualized on a UV transilluminator. The fluorescence emancipating from the EB intercalated in the nucleic acid was captured and digitized using a Kodak DC120 camera.

2.19. Alkaline agarose gel electrophoresis (AAGE)

AAGE was performed after exposing the pMTa4 DNA to varying doses of AEBN *in vitro* (2.17.1.). The method followed was that of Sambrook and Russel (2001) with minor modifications. Briefly, it is described below.

2.19.1. ***Buffers and solutions:*** The compositions of the buffers and solutions required are described below.

[a] *Alkaline agarose gel electrophoresis buffer (10 x)*: This had the following composition:

NaOH	500 mM
EDTA, pH 8.0	10 mM

The stock buffer was stored refrigerated. For use, it was diluted to 1 x concentration with water. The resulting pH was found to be ~ 9 when checked with a pH strip.

[b] *Gel loading buffer (6 x)*: This comprised the following:

NaOH	300 mM
EDTA, pH 8.0	6 mM
Bromophenol blue	0.2 %

The buffer was stored refrigerated and used for up to 2 months.

[c] *Neutralizing solution*: This solution had the following composition:

Tris-Cl, pH 7.6	1 M
NaCl	5 M

[d] *EB*: It was used as supplied.

*2.19.2.**Methodology**:* The agarose gel solution was prepared by melting 1 g of agarose in 80 ml of Millipore water by heating it in the microwave to ~ 90 °C. It was cooled to ~ 55 °C and 10 ml of the 10 x AAGE buffer was added. This gel usually solidified in 20 min at RT. The DNA samples (which consisted of pMTa4 DNA exposed to varying concentrations of AEBN (§ 2.17.1.) and untreated control pMTa4 DNA) were mixed with 1/6 volumes of 6 x gel loading buffer and loaded. Electrophoresis was performed at 3.5 $V.cm^{-1}$ for 16 h in 1 X AAGE buffer. After electrophoresis, the gel was neutralized using the neutralizing solution for 1 h, stained in EB (§ 2.18.5.), photographed and the results analyzed by comparing the mobility of the bands with the mobility of a lambda DNA *HindIII* digest DNA marker.

2.20. Recovery of CC and OC forms of the DNA from the agarose gel

The pMTa4 isolate upon electrophoresis (§ 2.18.) gives two major bands on an agarose gel. These bands are the OC and the CC topological forms of plasmid DNA (Humstoe *et al.*, 1998; 2003). To isolate pure OC and CC forms of pMTa4 from the plasmid isolate, the plasmid was prepared in bulk and subjected to a preparative AGE. In one of the lanes of this gel a small amount of the pMTa4 isolate was loaded to serve as a marker. After electrophoresis the marker lane of the gel was carefully cut out using a sterile scalpel and stained with EB (§ 2.18.5) in order to determine the location of the OC and CC forms of the plasmid on the gel. Placing this stained marker gel next to the unstained portion of the preparative gel on a UV-transilluminator and using the stained section of the gel as a guide, the portion of the preparative gel containing the CC and OC forms of the plasmid were carefully excised out. The desired piece of gel was crushed and placed over tightly packed sterile glass wool in a column. This column was placed in a microfuge tube and centrifuged at 10,000 x g for 45 s. The eluent containing the desired conformational form of the pMTa4 DNA was collected in a fresh tube and concentrated by speed vacuum. The A_{260} of the eluent was recorded to calculate the quantity of the recovered topological form of pMTa4.

2.21. Gel mobility shift assay

To study the effect of AEBN exposure on pMTa4 DNA, gel mobility shift assay was employed. The AEBN unexposed and exposed pMTa4 DNA (§ 2.17.1.) was subjected to AGE (§ 2.18.). The mobilities of CC and OC forms of pMTa4 DNA were analyzed using KDS 1D software and the shift in mobilities, if any, were calculated from the data (§ 2.26.2.).

2.21.1. ***Gel mobility shift in vitro as a function of concentration of AEBN:*** pMTa4 DNA samples in microfuge tubes were exposed to increasing concentrations of AEBN (§ 2.17.1.). The control tube had pMTa4 DNA without AEBN. Following this, samples were subjected to 1 % AGE (§ 2.18.) and shift in mobilities determined (§ 2.26.2.).

2.21.2. ***Gel mobility shift in vivo as a function of concentration of AEBN***: AB1157 cells were grown O/N in LB broth (§ 2.5.2.) in the absence or presence of increasing doses of AEBN (§ 2.17.2.). The following day, pMTa4 DNA was isolated from the flasks (§ 2.11.) subjected to AGE (§ 2.18.) and the mobilities of the OC and CC forms of the pMTa4 DNA were determined (§ 2.26.2.).

2.21.3. ***Gel mobility shift assay in vitro as a function of time of incubation at 37 °C***: pMTa4 DNA isolates in microfuge tubes were mixed with 250 µg of AEBN. The tubes were incubated at 37 °C for varying intervals of time (5, 10, 15, 20, 25, 30, 35, 40 or 45 min). After incubation, the plasmid samples were subjected to AGE (§ 2.18.) and change in mobilities of CC and OC bands determined (§ 2.26.2.).

2.22. Study of the effect of AEBN on the molecular mass of pMTa4 DNA

To study the effect of AEBN on the molecular mass of pMTa4 DNA, the pMTa4 DNA was linearized with the restriction endonuclease *NcoI* (§ 2.25.) and this linearized plasmid was exposed to increasing concentrations of AEBN (§ 2.17.1.). The samples were subjected to AGE (§ 2.18.) and the results analyzed by comparing the mobilities of the treated and untreated DNA against a Lambda DNA *HindIII* digest marker.

2.23. Dissociation kinetic analysis of AEBN adduct from the pMTa4

To study the stability of the AEBN adduct on pMTa4 DNA, AB1157 cells were grown as described (§ 2.5.2.) in 20 ml of LB broth in the presence of 2000 µg of AEBN per ml culture. In thirteen separate microfuge tubes each with 1.5 ml culture medium, pMTa4 was isolated from the AEBN exposed culture the following day essentially following the standard method (§ 2.11.) with one modification, that is, the ethanol precipitate of plasmid DNA was not immediately dissolved in water. The plasmid pellets in the thirteen separate microfuge tubes could be sequentially dissolved in sterile water every 2 h, essentially allowing AEBN exposed pMTa4 isolates to remain in solution for precisely 0, 2, 4, 6, 8, 10, 12, 14, 16, 18, 20, 22 and 24 h. Following this, the samples were subjected to AGE (§ 2.18) and stained (§ 2.18.5.) as described.

2.24. Effects of pH, and K^+ & Na^+ ions on the stability of AEBN adduct:

To study the factors affecting stability of the AEBN induced adducts on pMTa4 DNA, AB1157 cells were grown as described (§ 2.5.2.) in the presence of 2000 µg AEBN. pMTa4 was isolated from this culture the following day (§ 2.11.) and effects of pH, K^+ and Na^+ ions were studied by observing the mobility shift of CC and OC forms of pMTa4 (§ 2.26.2.). For monitoring the effect of pH on the mobility of the CC and OC forms, the pMTa4 isolates were prepared as described (§ 2.11.) in seven microfuge tubes, each starting with 1.5 ml AB1157 culture grown in the presence of 2000 µg AEBN per ml culture. The pMTa4 pellet in separate tubes were dissolved in 1 M Tris-Cl buffer adjusted to increasing pH, e.g., pH 5, 6, 7, 8, 9, 10 and 11. Similarly, for monitoring the effects of K^+ and Na^+ ions, the pMTa4 pellets in different tubes were dissolved in varying concentrations (5, 10, 15, 20, 25, 30 and 35 mM) of the ions. The tubes were left to stand at RT for 24 h after which the samples were subjected to AGE (§ 2.18.). The shift in mobilities were calculated (§ 2.26.2.) and results analyzed.

2.25. Restriction mapping of pMTa4

In order to study the effect of UV-C irradiation and exposure to AEBN of pMTa4 DNA on the restriction profile of the pMTa4 DNA, the pMTa4 DNA samples were digested as described below.

2.25.1. ***Restriction map of UV-C irradiated pMTa4 DNA:*** For the restriction mapping analysis of the effects of UV-C irradiation on pMTa4 DNA, unirradiated pMTa4 DNA or pMTa4 DNA irradiated with 4.8, 9.6, 19.2 and 38.4 $J.m^{-2}$ UV-C radiation were restriction digested with *DraI, SspI, AccI, NciI* and *HaeII* till the restriction digestion of the unirradiated control was complete (Humstoe *et al.*, 1998, 2003). The conditions of digestion were those recommended by the manufacturers.

2.25.2. ***Restriction map of pMTa4 DNA isolated from cells exposed to AEBN:*** For the restriction mapping of the pMTa4 DNA subjected to AEBN exposure, the pMTa4 DNA isolates were prepared (§ 2.11.) from AB1157 cultures grown as described (§ 2.5.2.) in the presence of 2000 µg AEBN per ml culture. The isolates were restriction digested with the different restriction endonucleases O/N.

The following day, AGE was performed and the results analyzed. The restriction digestion profile of the pMTa4 DNA was compared with the restriction digestion profile of an unirradiated or unexposed control pMTa4 DNA. The molecular sizes of the bands were analyzed by comparing the mobilities of the bands with the mobilities of the markers, Lambda DNA *HindIII* digest and Lambda DNA *HindIII EcoRI* double digest DNA markers.

2.26. Analysis of bands of pMTa4 DNA bands

Analysis of the different bands of plasmid DNA resolved on agarose gels was done with the help of KDS1D software. The software was used to quantify the bands as well as to calculate its mobilities on the gel by calculating its *Rf* values.

2.26.1. ***Quantification:*** The intensity of the band was measured as pixel density and was analyzed by comparing the band intensities of the irradiated or treated pMTa4 DNA with that of the untreated or unirradiated control bands.

2.26.2. ***Mobility calculation:*** The mobility of the bands was analyzed by comparing the *Rf* of the irradiated or treated pMTa4 DNA with that of the untreated or unirradiated control DNA. The molecular size of the restricted pMTa4 DNA was approximated by comparing the *Rf* of

the restriction digested fragments with the *Rf* of the DNA molecular weight markers using the same software.

2.27. Ethidium bromide (EB) intercalation assay

For monitoring the effect of UV-C radiation and conformational state of plasmid DNA on EB intercalation this assay was designed.

2.27.1. ***Buffers and solutions:*** The compositions of the buffers and solutions required are described below.

[a] ***TAE buffer:*** This was prepared as follows:

Tris-acetate, pH 8.0	40 mM
EDTA, pH 8.0	1 mM

[b] ***EB solution:*** A solution of concentration 0.4 $ng.\mu l^{-1}$ in sterile water was prepared from stock EB solution.

2.27.2. ***Methodology*:** In 100 ml of TAE buffer in a beaker, 1 g of agarose was added to prepare 1 % agarose gel. The agarose was dissolved by slowly heating the beaker to about 90 °C in a microwave with repeated swirling. The clear agarose solution was cooled to about 40 °C, slowly poured onto a clean glass slide. A template was inserted into the molten gel. After the gel had solidified, the template was removed leaving behind the wells on the gel.

In separate microfuge tubes, 2 µl (4 µg DNA) each of the pMTa4 isolate, purified CC form of the plasmid or purified OC form of the plasmid DNA were mixed well with 0.4 ng of EB (1 µl of EB solution). This mixture was loaded on the wells. The gel was allowed to stand at RT for 3 min and the fluorescence emancipating from the wells were captured and digitized (§ 2.26.).

2.28. Hyperchromicity assay

The pMTa4 isolates (2 µl containing 4 µg DNA) in separate tubes were exposed to 1.2, 2.4, 3.6, 4.8 and 6 $J.m^{-2}$ doses of UV-C radiation. Immediately afterwards their A_{260} were

recorded and compared with the A_{260} of the unirradiated control plasmid preparation. Similarly, the A_{260} of the unirradiated and irradiated purified CC form of pMTa4 DNA (§ 2.20.) was also recorded.

2.29. Absorption spectral analysis of AEBN interaction with pMTa4 DNA

The starting materials for this analysis were plasmid isolate (2 μg μl^{-1}) and AEBN (100 μg μl^{-1}). In different microfuge tubes 2 μl of pMTa4 DNA (4 μg DNA) each were aliquoted. The pMTa4 DNA was now subjected to increasing concentrations of AEBN (§ 2.17.1.). After gentle mixing, the tubes were incubated at 37 °C for different time intervals (30, 60 and 90 min). After this, the contents of the tubes were made up to 1 ml with sterile water. Absorbance spectra for each tube was recorded over a range of 235 to 320 nm using a spectrophotometer (Systronics, UV-Vis Spectrophotometer 119).

2.30. Effect of AEBN on mutation induction in microsatellite regions

Four microsatellite regions (table 4) of *E. coli* genome, namely ANTW, NCGT, TNT1 and INTG, were selected for studying induction of mutation upon exposure to AEBN. The selection of the sequences was based on the prevalence of AT- or GC- rich NT sequences and also on their susceptibility to damages (Metzgar *et al.*, 2001). The primers for amplifying the ANTW, NCGT, TNT1 and INTG microsatellites were designed by Metzgar *et al.* (2001). Prior to usage, the primers were checked for their annealing properties on the *E. coli* genome using the software NCBI Blast (http://www.ncbi.nlm.nih.gov/BLAST). The details of the primers used are given in table 4.

Table 4: Primer sequences of the selected microsatellite regions

Name of microsatellite	Genomic location	Primer sequence	Amplicon size (bp)	Annealing temperature (°C)
TNT1	522253 - 522533	Forward-GCGTTGAATGGATATTATCC Reverse-CGCCATACTGAGTCATATCTCC	280	43.2
ANTW	3903016-3903298	Forward-GACATCGGCCACATGGTTACC Reverse-GGATTGTTACCGCACTAAGCG	305	54.8
INTG	379108 - 379303	Forward-CGCACCTCATCATCTGCATGC Reverse-GGAAATTCTGATTCCTTCTGCC	192	52
NCGT	4083497 - 4083689	Forward-GCAAAGGTCCAGAATTGGCTC Reverse-GTGTTGTAAATCATCACGCCG	169	52

2.31. Polymerase chain reaction (PCR) based amplification

Standard protocol of PCR was followed as described in Sambrook and Russel (2001). Briefly, the methodology is described below.

2.31.1. Buffers and solutions: The compositions of the buffers and solutions required are described below.

[a] Buffer for a PCR reaction: This had the following composition:

KCl	50 mM
Tris-HCl	10 mM
Triton X-100	1%
$MgCl_2$	1.5 mM

[b] Deoxyribonucleotide mix: 0.2 mM

[c] Primers: 1 nM each of forward and reverse primers

[d] Taq DNA polymerase: 5U

2.31.1.1. Methodology: The PCR was performed in a Thermal Cycler (Techne, UK). The PCR reaction mix was constituted as per the manufacturer's instructions. The PCR reaction mix (25 µl), had the following compositions for each microsatellite:

Buffer:	2.5 µl
dNTPs:	1.5 µl
Primers:	1 µl each of forward and reverse primers

Taq DNA polymerase:	0.25 µl
Water:	17 µl
DNA template:	1 µl of 1 µg ml^{-1} genomic DNA

After mixing, the PCR reaction was carried out for 35 cycles as per the steps given below: Initial denaturation was carried out at 94 ° C for 5 min. Following this, 35 cycles of the following steps were performed.

Denaturation : 94 °C for 1 min

Annealing: Specified annealing temperature for 1 min (Table 4)

Extension: 72 °C for 1 min

After the 35 cycles were over, final extension was carried out at 72 °C for 10 min.

After amplification, AGE was performed (§ 2.11.) with 2 µl of the amplicon. Part of the amplicon was lyophilized and sent for sequencing along with its pair of primers.

2.32. Sequencing and alignment

The amplified sequences were sent for sequencing to Bangalore Genei, India, where the sequencing was done by the single pass analysis (SPA) technique and the sequencing results obtained. The results were then aligned using the Multalin software and the results analyzed.

2.33. Effect of UV-C radiation on AEBN interaction with pMTa4 DNA

The pMTa4 DNA (2 µl containing 4 µg DNA) was irradiated with UV-C and its effect on the binding characteristics of the AEBN on the DNA was studied as described (§ 2.21.).

2.33.1. ***Mobility shift analysis of UV-C irradiated pMTa4 DNA:*** pMTa4 (12 µl containing 24 µg DNA) was irradiated with UV-C for 150 s corresponding to a dose of 6 $J.m^{-2}$. Following this, the DNA was aliquoted into 6 different tubes. Each of the tubes containing 4 µg DNA, was subjected to increasing concentrations of AEBN (§ 2.17.1.), mixed well and incubated at 37 °C for 30 min. For the control, the DNA was incubated without AEBN. Following this, AGE was performed (§ 2.18.), the gel stained (§ 2.18.5.) and the mobility of the two bands of the DNA, the CC form and the OC forms were determined (§ 2.26.2.) from the gel.

2.33.2. ***Study of the effect of UV-C radiation on the molecular mass increase induced by AEBN on the linearized pMTa4 DNA:*** pMTa4 DNA, linearized with the restriction endonuclease *NcoI* (§ 2.25.), was irradiated with UV-C (6 $J.m^{-2}$) and incubated with increasing concentrations of AEBN (§ 2.17.1.). The samples were subjected to AGE (§ 2.18.) and the AEBN induced increase in the mass of the pMTa4 DNA was monitored from the induced change in the mobility of linear form of the pMTa4 DNA exposed to AEBN as compared to the untreated control.

2.34. Preparation of total protein samples

From an AB1157 culture grown as described (§ 2.5.2.), a 1.5 ml aliquot was taken and centrifuged. The cell pellet obtained was resuspended in 100 µl of sample buffer (§ 2.36.1.). The sample was then heated in a water bath which denatured the proteins and prepared samples for SDS- polyacrylamide gel electrophoresis (SDS-PAGE).

2.35. Estimation of proteins by Bradford's method

Estimation of total cellular proteins of *E. coli* was done using Bradford's method of protein estimation with BSA as a standard (Bradford, 1976). The materials needed and methodologies followed are briefly described below.

2.35.1. ***Buffers and solutions***: The reagents needed for the estimation of proteins are given below:

[a] *Stock Bradford reagent*: CBB G-250 (100 mg) was dissolved in 50 ml of 90 % ethanol. To this, 100 ml of 85 % (w/v) orthophosphoric acid was carefully added. The stock solution was stored refrigerated.

[b] *Working Bradford reagent*: Stock Bradford solution (15 ml) was slowly added to 85 ml of distilled water and filtered through Whatman #1 filter paper. The resulting solution was immediately used for estimation of proteins.

2.35.2. ***Methodology***: From the sample for protein estimation, 6 µl was taken and the volume was made up to 0.1 ml with distilled water. To this, 5 ml of the working Bradford reagent was

added and vortexed. The absorbance of the blue colored solution was read at 595 nm after 5 min. Each assay was performed in triplicate.

2.36. Sodium dodecyl sulphate - polyacrylamide gel electrophoresis (SDS-PAGE)

The SDS-PAGE analysis was carried out as described by Laemmeli (1970) with some modifications as adapted in the lab (Pariat *et al.,* 1997). It employed a 12 % resolving and a 3 % stacking gel. The methodology employed is briefly described below.

2.36.1. ***Buffers and solutions***: For the preparation of the gel, the following stock reagents were prepared. These were stored refrigerated and used for up to 1 year except some which are specified.

[a] *Gel making reagents*

(i) *Monomer solution*: This has the following composition:

Acrylamide:	30 %
Bis-acrylamide:	0.8 %

This solution was prepared in Millipore quality water and filtered through Whatman filter paper.

(ii)	Tris-Cl buffer, pH 8.8	1 M
(iii)	Tris-Cl buffer, pH 6.8	1 M
(iv)	SDS solution	10 %
(v)	APS	10 %.

This was freshly prepared before each use.

(vi) TEMED: This was used directly from the bottle as supplied.

Using these stock reagents, SDS-PAGE gel comprising 3 % stacking and 12 % separating gels were prepared by mixing the reagents in specified volume as described in table 5.

Table 5: Quantities of reagents used for the gel preparations

Stock reagent	Separating gel (12 %)	Stacking gel (3 %)
Monomer solution	4 ml	500 µl
Tris-Cl buffer, pH 8.8, 1 M	3.73 ml	-------
Tris-Cl buffer, pH 6.8, 1 M	--------	625 µl
Millipore water	2.21 ml	3.8 ml
SDS 10 %	100 µl	50 µl
APS 10 %	30 µl *	13 µl *
TEMED	10 µl *	12 µl *

* These solutions were added to the mixture after the solutions were degassed using a vacuum pump.

[b] *Sample loading buffer*: It consisted of the following:

SDS	12 %
DTT	0.6 M
Potassium phosphate buffer (pH 7)	60 mM
Glycerol	12 %
Bromophenol blue	0.36 %

To prepare sample for SDS-PAGE, the protein sample was mixed with $1/5^{th}$ volume of the sample lading buffer and heated in a boiling water bath for 3 min.

[c] *Electrophoresis buffer*: The buffer comprised the following:

Tris-Cl buffer, pH 8.8	25 mM
Glycine	192 mM
SDS	0.1 %

This buffer was prepared and stored refrigerated for use.

[d] *Staining solution*: This had the following composition:

Methanol	40 ml
Acetic acid	10 ml
CBB R-250	0.1 g
Water	50 ml

[e] *Destaining solution*: The solution was prepared by mixing methanol: glacial acetic acid: water in the ratio of 4:1:5.

2.36.2. ***Methodology***: Normally 15 µl (containing 6 µg proteins) of protein samples were loaded into the wells using long microtips. Electrophoresis was carried out at a constant voltage of 25 $V.cm^{-1}$ for 90 min at RT. After electrophoresis, the gel cassette was disassembled and the gel transferred to a staining tray. Staining was carried out on a rocker O/N in the staining solution. The stained gel was destained using by changing the destaining solution 3 times on the rocker till the background stain was totally removed. The gels were now photographed and analyzed.

2.37. Quantification an statistical analysis

On an average, the number of repeats performed for each experiment was at least five for the UV-C irradiation experiments, AEBN exposure experiments, restriction digestion experiments and three for the EB intercalation, gamma irradiation and induction of hyperchromicity experiments. Statistical analyses, i. e., the calculation of the mean, standard deviation, standard error of the mean and t-test were done with the help of MS Excel. The graphs were plotted using the MS Excel and Kaleidagraph softwares.

Results

3.1. Growth patterns of different strains of *E. coli*

Three different strains of *E. coli* used in this study were grown under optimal conditions as described in § 2.4.2. The increase in the number of *E. coli* cells, measured as OD at 600 nm every hour, was plotted as shown in Figure 3.1. A slight difference was observable in the growth curves of different strains of *E. coli*. The wild type strain, AB1157, and the *recF* mutant strain, JC9239, showed higher but nearly overlapping rates of growth as compared with the *recA* mutant strain, XL1-Blue. The AB1157 and JC9239 strains had identical lag phase of 4 h, while XL1-Blue showed a lag phase of about 5 h. Consequently, the former two entered the stationary phase in 13 h, while the XL1-Blue strain entered the stationary phase in 15 h. Overall, the *recA* mutant, XL1-Blue, grew slowly as compared to the wild type, AB1157 and the *recF*, JC9239 strains.

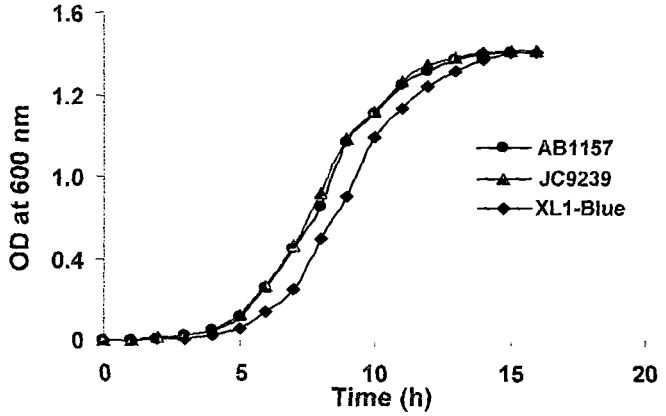

Figure 3.1: Growth curves of *E. coli* strains: The growth curves of three strains of *E. coli* used in this study, the wild type, AB1157 (—●—), the *recF* mutant, JC9239 (—▲—) and the *recA* mutant, XL1-Blue (—◆—), have been plotted.

3.2. Effect of UV-C radiation on survival of *E. coli* strains

This was done by clonogenic survival assay (§ 2.10.) following exposure to increasing doses of UV-C (§ 2.6.). Figure 3.2 shows the clonogenic survival of strains of *E. coli* used in the study. The survival of the *recA* mutant strain, XL1-Blue, was seen to be most compromised after UV-C exposure. At the maximum dose of UV-C radiation used (50 $J.m^{-2}$) the survival of the repair proficient, wild type strain (AB1157) was reduced marginally to 0.19 %. On the other hand, at this dose of UV-C radiation, *recF* (JC9239) and the *recA* (XL1-Blue) mutant strains showed no apparent survivals. The survival of *recF* (JC9239) mutant was < 0.1 % at 45 $J.m^{-2}$ UV-C

radiation. The *recA* (XL1-Blue) mutant showed highly compromised survival, with only 0.0001 % of the cells surviving after being irradiated with a dose of 5 $J.m^{-2}$ only.

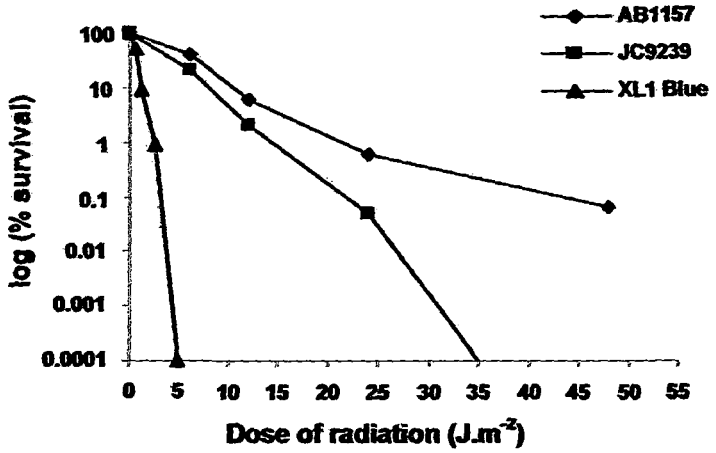

Figure 3.2: Clonogenic survival assay of *E. coli*: The clonogenic survival curves of the strains of *E. coli* used in the study as a function of dose of UV-C radiation; the wild type, AB1157 (—◆—), the *recF* mutant, JC9239 (—■—) and the *recA* mutant, XL1-Blue (—▲—).

3.3. Transformation efficiency of the pMTa4 plasmid DNA

In order to study the effect of the different mutagenic agents on the pMTa4 DNA, the plasmid was transformed into the different strains of *E. coli*, viz. AB1157, JC9239 and XL1-Blue. The pMTa4 DNA has Amp^r as a marker. Thus, when the transformation was successful the transformants turned Ampicillin resistant and were able to grow on LB-agar plates containing 100 $\mu g.ml^{-1}$ Ampicillin. Fig. 3.3 shows the colonies transformed with pMTa4 DNA that grew on

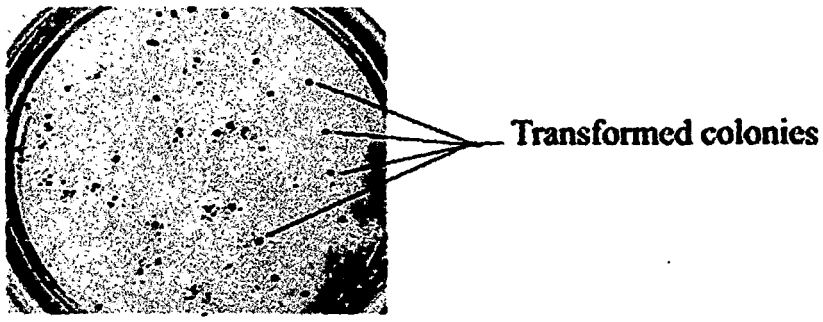

Figure 3.3: Growth of transformed colonies. *E. coli* cells transformed with the pMTa4 DNA appear as colonies on an Amp^+ LB-agar plate.

the Amp$^+$-LB-agar plate. The transformation efficiencies for the strains used in this study were found to be 1000 transformed colonies per ng pMTa4 DNA.

3.4. Effect of UV-C radiation on protein profile of *E. coli*

SDS-PAGE was performed (§ 2.36.) to monitor effects of increasing doses of UV-C radiation (4.8, 9.6 and 19.2 J.m^{-2}) on total protein profile of the *E. coli* strains AB1157 and JC9239 under repair non-permissive (R$^-$) and repair-permissive (R$^+$) conditions (§ 2.15.2.1. and 2.15.2.2., respectively). The protein profiles under R$^-$ and R$^+$ conditions were compared with the unirradiated control. From the gel photograph, as shown in figures 3.4 for AB1157 (A) and JC9239 (B), UV-C radiation did not induce any observable difference in the profile of cellular proteins at the doses of UV-C used.

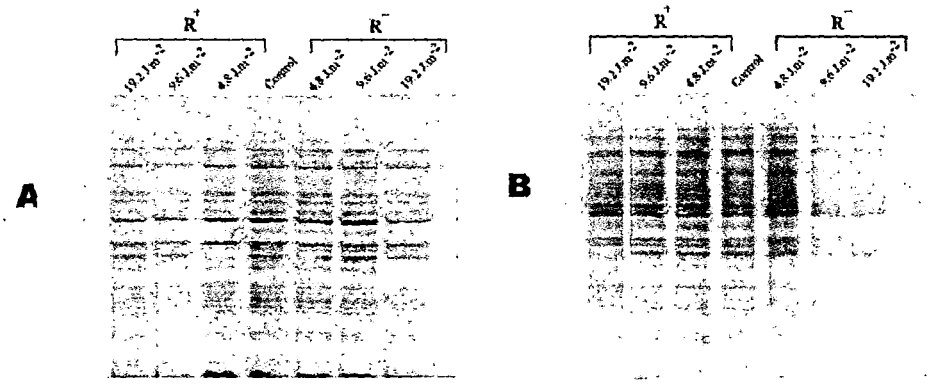

Figure 3.4: SDS-PAGE profile of total proteins of *E. coli*: Figure shows protein profiles of *E. coli* cells isolated immediately after exposing them to varying doses of UV-C irradiation as indicated in the figures under repair non-permisive (R$^-$) and permissive (R$^+$) conditions. Panel A shows the protein profiles of wild type strain, AB1157 and panel B that of *recF* mutant, JC9239.

3.5. Profile of pMTa4 DNA isolate of *E. coli*

The pMTa4 DNA isolated using the procedure detailed in § 2.11 from any strain used in the study showed, as expected, similar profiles after AGE, indicating that there was essentially no effect of the strain of *E. coli* being used as a host for the plasmid on its profile. Figure 3.5 shows a typical agarose gel electropherogram of pMTa4 DNA (lane A) and the pMTa4 linearized with *NcoI* (lane B). In the native form, all plasmids exist in the covalently closed circular (CC) form, a complex form where the plasmid is supercoiled, and hence the plasmid possesses a very

compact form. A nick in this complex relaxes the plasmid and it assumes open circular (OC) form.

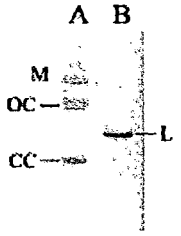

Figure 3.5: Profile of pMTa4 DNA: Gel photograph showing profile of pMTa4 (4 µg) immediately after isolation (lane A) and after linearization of the plasmid by *NcoI* (lane B). Different topological forms of pMTa4, marked on the gel, are covalently closed circular (CC), open circular (OC) and multimeric (M) forms. After the pMTa4 DNA was digested with *NcoI*, it converted all plasmid forms to its linear (L) form.

A single double stranded break (DSB), or two single stranded breaks (SSB) induced sufficiently close together in the plasmid, converts it to the linear (L) form. The plasmid isolates (Fig. 3.5; lane A) does not show any L form. Hence, pMTa4 DNA was digested with the restriction endonuclease *NcoI*, which has only one restriction site within the plasmid. It digested all topological forms of pMTa4 DNA into linear (L) form. Above the OC band of the plasmid, one or a few other bands were observed. These bands are the multimeric (M) forms of the plasmid, which are formed when multiple plasmid molecules are linked together during the process of isolation of the plasmid, which results in the increase in their molecular sizes and hence, these forms are seen to move slower than the other forms of the plasmid.

3.6. Effect of UV-C radiation on pMTa4 DNA *in vitro*

Isolated plasmid preparations were irradiated with 1.2, 2.4, 3.6, 4.8 and 6 $J.m^{-2}$ doses of UV-C radiation *in vitro* (§ 2.15.1), subjected to 1 % AGE (§ 2.18) and the gel analyzed to quantify different topological forms of pMTa4 (§ 2.26.1). Figure 3.6 shows the effect of UV-C irradiation on the resulting forms of pMTa4 DNA. The gel shows UV-C dose dependent increase in CC and OC forms of pMTa4 (Fig. 3.6 A). Upon quantification and plotting, the progressive increase in the band intensities of both the conformational forms was obvious (Fig. 3.6 B). The maximum increase in pixel density of CC and OC forms were 146.2 ± 3.0 and 123.8 ± 6.67 of the control, respectively. Also notable is the fact that the observed increase in band

intensity is more in the OC as compared to the CC form of pMTa4 DNA. No L form of the plasmid was produced by UV-C radiation.

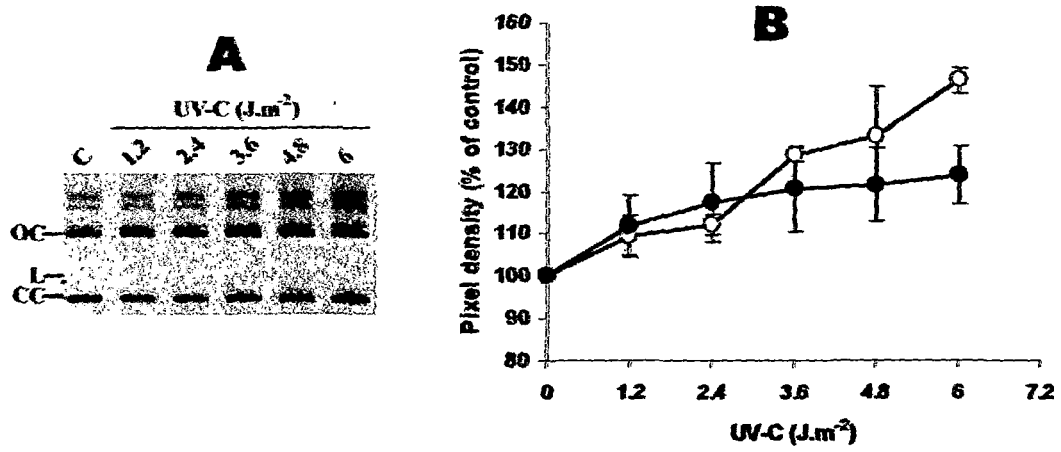

Figure 3.6: Effect of UV-C radiation on pMTa4 DNA *in vitro*: Panel A: Electropherogram showing CC and OC forms of pMTa4 DNA (4 µg) after being irradiated with increasing doses of UV-C (lane 1 (C) = unexposed pMTa4; lanes 2-6 = pMTa4 irradiated with 1.2, 2.4, 3.6, 4.8 and 6 $J.m^{-2}$). Panel B: Plot showing the percentage pixel densities of the CC (—●—) and OC (—○—) topological forms of the pMTa4 DNA as a function of UV-C dose. The data (mean ± SD) were obtained from the electropherograms.

3.7. Effect of UV-C radiation on pMTa4 DNA of AB1157 strain *in vivo*

Starting with a single colony of AB1157 strain from an agar plate (§ 2.5.3), an O/N culture was prepared (§ 2.5.2). The cultures were irradiated with different doses of UV-C radiation (§ 2.15.2). pMTa4 DNA was isolated from the tubes either immediately or after a repair incubations as described (§ 2.15.2).

3.7.1. ***Under repair-non-permissive conditions (R):*** Immediately after irradiation, plasmid DNA was isolated (§ 2.11), subjected to AGE (§ 2.18) and topological forms of the plasmid analysed (§ 2.26). Fig. 3.7 shows a typical electropherogram (panel A) and plot obtained from such an experiment (panel B). The gel visually showed a dose dependent increase in the band intensity of both CC and OC forms; the OC form depicted a greater increase in the band intensity as compared to the CC form of the plasmid (Fig. 3.7 A). The plot of pixel densities of CC and OC

bands (Fig. 3.7 B) shows that UV-C radiation induced increase in OC form was up to 146.0 ± 5.5 % of the control while it was relatively less for the CC form (123.07 ± 8.9 % of the control) at 6 $J.m^{-2}$.

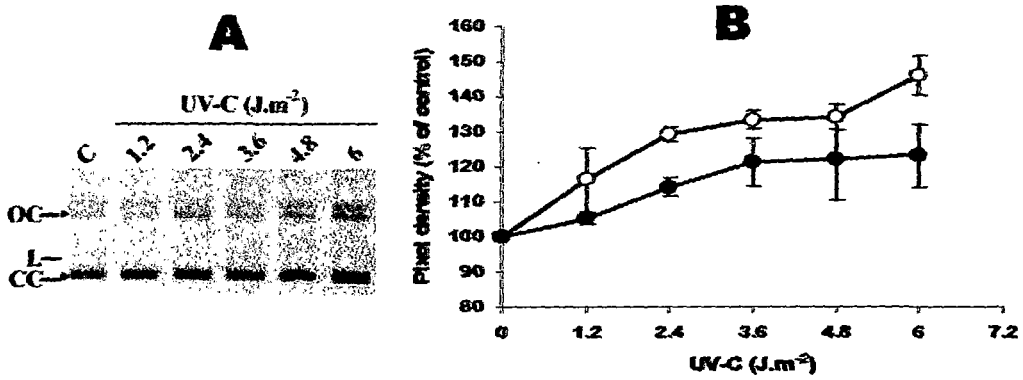

Figure 3.7: Effect of UV-C radiation on pMTa4 DNA of AB1157 strain *in vivo* under repair-non-permissive (R⁻) conditions: Panel A: Electropherogram showing CC and OC forms of pMTa4 DNA (4 µg) after being irradiated with increasing doses of UV-C *in vivo* under R^- conditions (lane 1 (C) = unexposed pMTa4; lanes 2-6 = pMTa4 after exposure of *E. coli* cells to 1.2, 2.4, 3.6, 4.8 and 6 $J.m^{-2}$). Panel B: Plot showing the percentage pixel densities of the CC (—●—) and OC (—○—) topological forms of the pMTa4 DNA as a function of UV-C dose. The data were obtained from the electropherograms.

3.7.2. ***Under repair-permissive conditions (R^+):*** The UV-C exposed cells were subjected to 60 min of post-irradiation repair incubation at 37 °C (§ 2.15.2.2) and then its plasmid DNA was

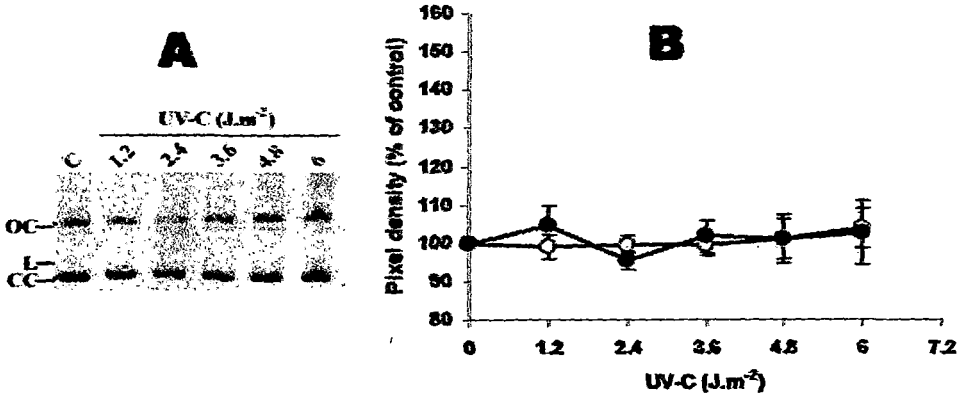

Figure 3.8: Effect of UV-C radiation on pMTa4 DNA of AB1157 strain *in vivo* under repair-permissive (R^+) conditions: Panel A: Electropherogram showing increase in the CC and OC forms of pMTa4 DNA (4 µg) after being irradiated with UV-C *in vivo* R^+ conditions (lane 1 (C) = unexposed pMTa4; lanes 2-6 = pMTa4 irradiated with 1.2, 2.4, 3.6, 4.8 and 6 $J.m^{-2}$). Panel B: Plot showing the percentage pixel densities of the CC (—●—) and OC (—○—) topological forms of the pMTa4 DNA as a function of UV-C dose. The data were obtained from the electropherogram.

isolated (§ 2.11), subjected to AGE (§ 2.18) and topological forms of the plasmid analyzed (§ 2.26). Figure 3.8 shows a typical electropherogram (panel A) and the plot obtained from the analyses (panel B). The results show that dose dependent increase in the band intensities of the CC and OC forms of pMTa4 DNA that was observed after the cells were irradiated with UV-C (Fig. 2.15.2) nearly completely disappeared after the cells were allowed repair incubation of 60 min (Fig. 3.8).

3.8. Effect of UV-C irradiation on pMTa4 DNA of JC9293 strain *in vivo*

Similarly, starting with a single colony of JC9293 strain from an agar plate (§ 2.5.3), an O/N culture was prepared (§ 2.5.2). The cultures were irradiated with different doses of UV-C radiation (§ 2.15.2). pMTa4 DNA was isolated from the tubes either immediately or after a repair incubations as described (§ 2.11).

3.8.1. ***Under repair-non-permissive conditions (R⁻):*** Immediately after irradiation, plasmid DNA was isolated (§ 2.11), subjected to AGE (§ 2.18) and topological forms of the plasmid analyzed

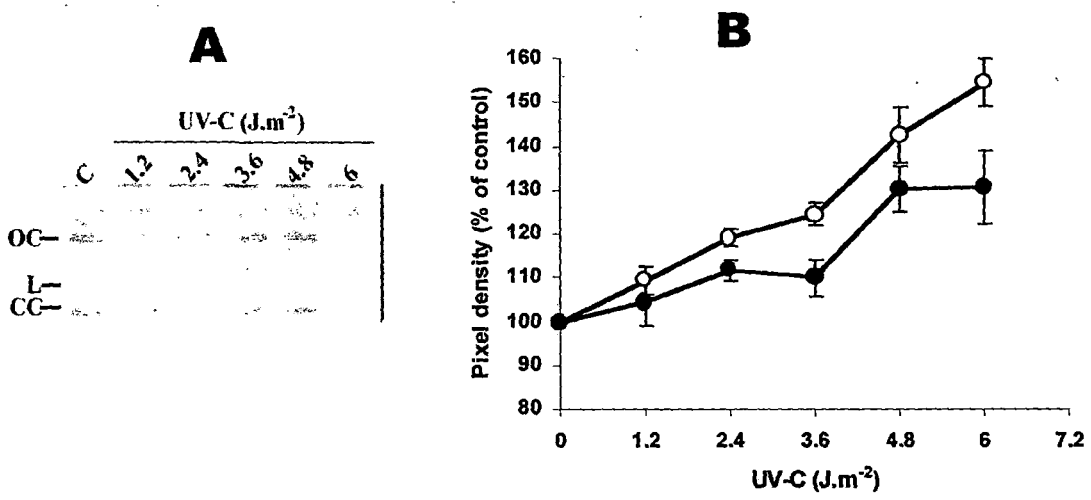

Figure 3.9: Effect of UV-C radiation on pMTa4 DNA of JC9239 strain under repair-non-permissive (R⁻) conditions: Panel A: Electropherogram showing pixel densities of the CC and OC forms of pMTa4 DNA (4 µg) after being irradiated with increasing doses of UV-C *in vivo* under R⁻ conditions (lane 1 (C) = unexposed pMTa4; lanes 2-6 = pMTa4 irradiated with 1.2, 2.4, 3.6, 4.8 and 6 J.m^{-2}). Panel B: Plot showing the percentage pixel densities of the CC (—■—) and OC (—○—) topological forms of the pMTa4 DNA as a function of UV-C irradiation. The data were obtained from the electropherogram.

(§ 2.26). Fig. 3.9 shows a typical electropherogram (panel A) and plot (panel B) obtained from such an experiment. The gel visually showed a dose dependent increase in the band intensity of both CC and OC forms; the OC form depicted a greater increase in the band intensity as compared to the CC form of the plasmid (Fig. 3.9 A). The plot of pixel densities of CC and OC bands (Fig. 3.9 B) shows that UV-C radiation induced increase in OC form was up to 153.2 ± 4.6 % of the control while it was relatively less for the CC form (128.07 ± 7.3 % of the control) at 6 $J.m^{-2}$.

3.8.2. ***Under repair permissive conditions (R^+):*** The JC9239 cells were irradiated with UV-C and then repair incubated as described (§ 2.15.2). Figure 3.10 shows a typical electropherogram and the plot obtained from the analyses. The results show that the increase in the band intensities of the CC and OC forms of the pMTa4 DNA that was observed after the cells were irradiated with UV-C (Fig. 3.10) persisted even after the cells were repair incubated.

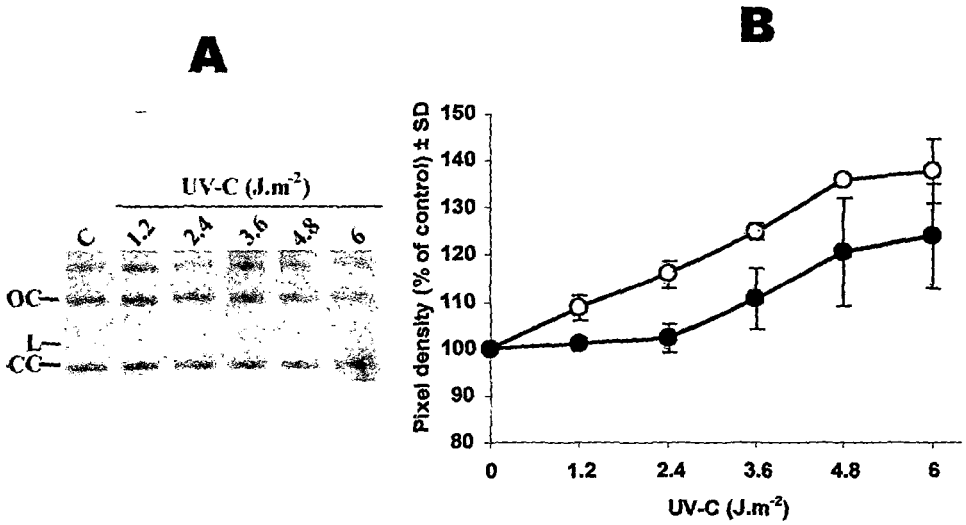

Figure 3.10: Effect of UV-C radiation on the pMTa4 DNA *in vivo* of JC9239 strain in repair-permissive (R^+) conditions: Panel A: Electropherogram showing the CC and OC forms of pMTa4 DNA (4 µg) after being irradiated with UV-C *in vivo* in R^+ conditions (lane 1 (C) = unexposed pMTa4; lanes 2-6 = pMTa4 irradiated with 1.2, 2.4, 3.6, 4.8 and 6 $J.m^{-2}$). Panel B: Plot showing the percentage pixel densities of the CC (—●—) and OC (—○—) topological forms of the pMTa4 DNA as a function of UV-C irradiation. The data were obtained from the electropherogram.

3.9. Effect of time of repair incubation on pMTa4 DNA profiles

The repair kinetics of pMTa4 DNA was studied by allowing the pMTa4 to undergo repair incubation *in vitro* and *in vivo* as described below:

3.9.1. ***Effect in vitro:*** The pMTa4 DNA was incubated at 37 °C in the presence of light for 0, 15 and 30 min, after being irradiated with 6 $J.m^{-2}$ UV-C radiation. As observed in figure 3.11, post-irradiation repair-incubation of 0, 15 and 30 min had no apparent effect on the UV-C induced increase in the band intensities of the two conformational forms, CC and OC of pMTa4 DNA.

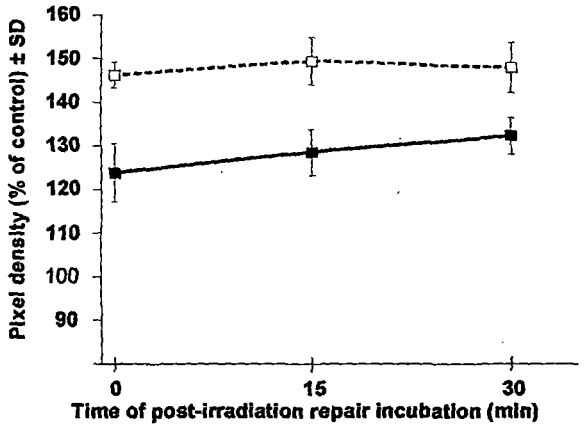

Figure 3.11: Effect of duration of UV-C irradiation on the pMTa4 *in vitro*. Panel shows a plot of the effect of UV-C radiation on the pixel densities of the CC (—■—) and OC (—□—) forms of the pMTa4 DNA after they were allowed to undergo repair incubation, for 0, 15 and 30 min following irradiation with 6 $J.m^{-2}$ UV-C.

Effect in vivo for AB1157 and JC9239 strains: Figure 3.12 shows the effect of time of post-irradiation repair incubation at 37 °C in presence of light for 0, 15 and 60 min on CC and OC forms of the pMTa4 DNA after they were exposed to 6 $J.m^{-2}$ of UV-C radiation *in vivo*.

As observed from the figure, the intensities of OC and CC forms of the pMTa4 DNA isolated from AB1157 strain decreased rapidly in the first 15 min which slowed down a bit beyond this point of repair incubation. In contrast, the pMTa4 DNA of JC9239 strain did not show significant difference in intensities of either topological forms of pMTa4 DNA at different post-irradiation incubation times.

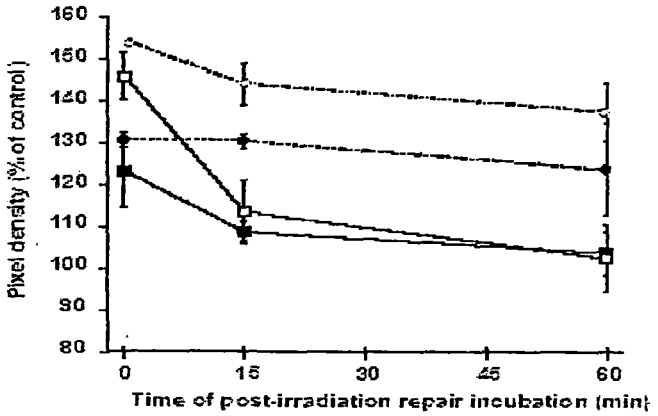

Figure 3.12: Effect of duration of UV-C irradiation on the pMTa4 *in vivo*: Panel shows a graph plotted to show the pixel densities of the CC (—■—) and OC (—□—)forms of the pMTa4 DNA isolated from AB1157 cells and the pixel densities of the CC (--●--) and OC (--○--) forms of the pMTa4 DNA isolated from the JC9239 strain after they were allowed to undergo repair incubation for 0, 15 and 60 min following irradiation with 6 $J.m^{-2}$ UV-C.

3.10. Effect of UV-C radiation on total RNA profile of AB1157 and JC9239 strains of *E. coli*

Total cellular RNA was isolated (§ 2.13) from unirradiated and UV-C irradiated AB1157 and JC9239 strains of *E. coli* under R^- and R^+ conditions (§ 2.15.3.) and analyzed by AGE (§ 2.18).

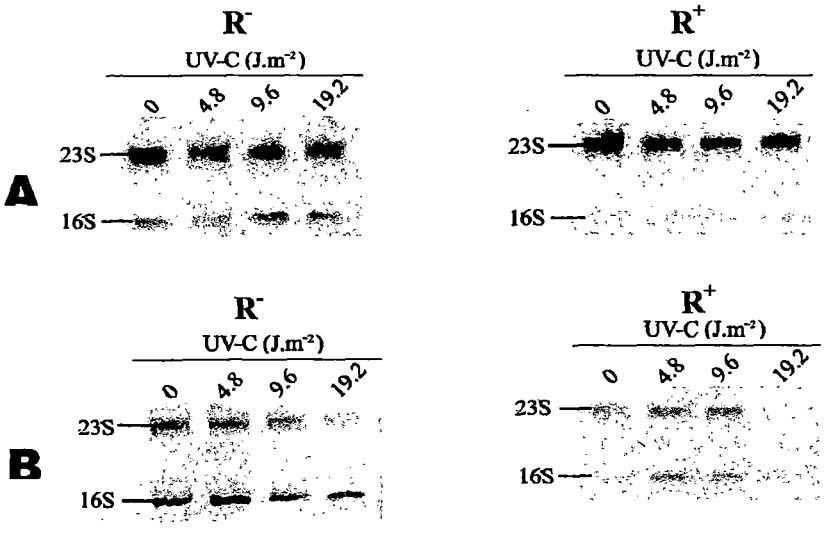

Figure 3.13: Total RNA profiles *E. coli*: AGE gels showing total RNA (4 µg) profiles of *E. coli* cells isolated after exposure to varying doses of UV-C radiation in R^- and R^+ conditions. (lane 1 (C) = unexposed control; lanes 2-4 = irradiated with 4.8, 9.6 and 19.2 $J.m^{-2}$). Panel A shows the total RNA profile obtained from AB1157 strain and panel B is from the JC9239 strain.

The results are shown in Figure 3.13. As expected, essentially only two species of RNA, the 23S and 16S rRNA were detectable on agarose gels (Heptinstall, 1993). The RNA profile of AB1157 essentially remained invariant. The JC9239 strain, on the other hand, exhibited a weak dose dependent down regulation of 23S and 16S rRNA, which were more pronounced under R^+ conditions (Fig. 3.12 B).

3.11. Ethidium bromide (EB) intercalation assay

An experiment was designed in the laboratory (§ 2.27) in order to observe the effect of UV-C irradiation on EB intercalation into total plasmid isolate and isolated CC and OC forms of pMTa4 (§ 2.20.). Figure 3.14 shows the effect of increasing doses of UV-C radiation on total plasmid isolate (A) and isolated CC (B) and OC (C) forms of pMTa4 DNA. A dose dependent increase in intercalation of EB was observable in all these cases.

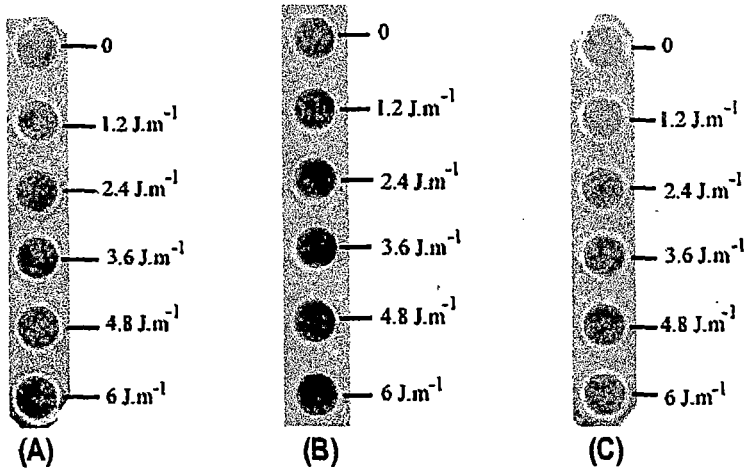

Figure 3.14: EB intercalation by pMTa4 DNA. Figures show the EB intercalation densities of the pMTa4 DNA (4 µg) irradiated with 0, 1.2, 2.4, 3.6, 4.8 and 6 $J.m^{-2}$ UV-C radiation. Panels show the EB intercalation densities of the total plasmids (panel A), CC form of the pMTa4 DNA (panel B) and OC form of the pMTa4 DNA (panel C).

The fluorescence emancipating from the EB were quantified as pixel density and plotted (Fig.3.15) confirming the dose dependent increase.

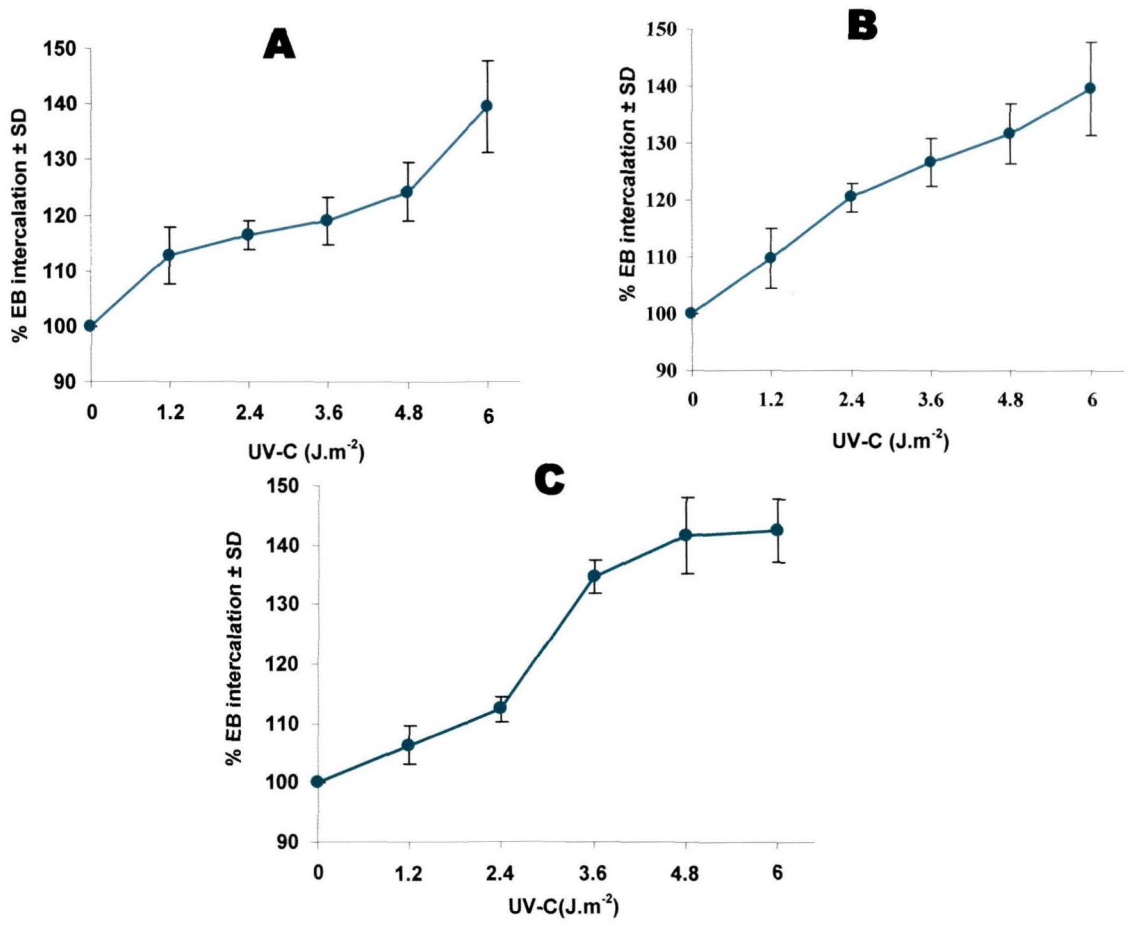

Figure 3.15: Effect of dose of UV-C radiation on EB intercalation: Figure shows graphs plotted to show the % EB intercalation densities of the total plasmids (panel A), CC (panel B) and OC (panel C) forms of the pMTa4 DNA after they were exposed to 0, 1.2, 2.4, 3.6, 4.8 and 6 $J.m^{-2}$ UV-C radiation.

3.12. Hyperchromicity assay

The effect of increasing doses of UV-C radiation (1.2, 2.4, 3.6, 4.8 and 6 $J.m^{-2}$) on the A_{260} of the total pMTa4 DNA and purified CC form were studied (§ 2.28.). The resulting hyperchromic shift was plotted against dose of UV-C for total (A) and purified CC form (B) of pMTa4. A dose dependent hyperchromicity increase was observed (Fig. 3.16). While the increase was progressive in case of total pMTa4 (Fig. 3.16 A), it reached a plateau beyond 2.4 $J.m^{-2}$ in case of CC form of pMTa4 (Fig. 3.16 B).

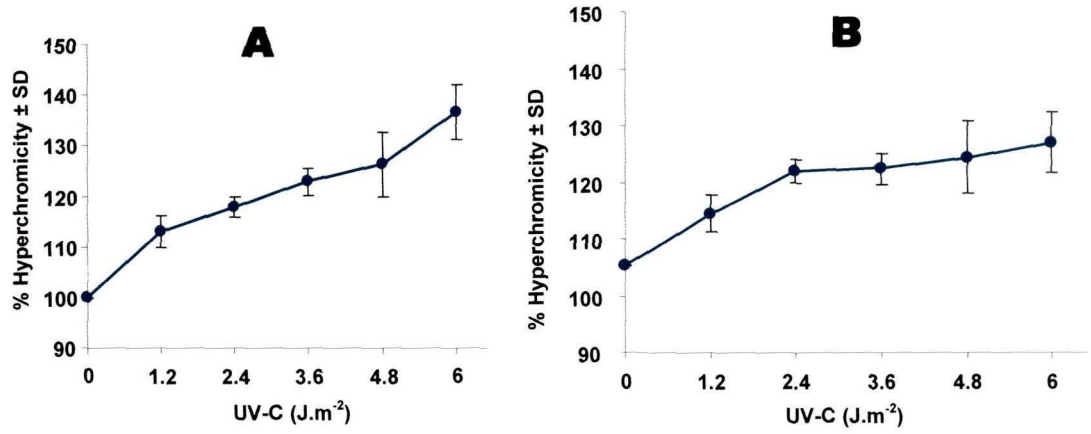

Figure 3.16: Effect of dose of UV-C radiation on hyperchromicity: Plots of the % hyperchromicity of the total plasmids (panel A) and CC form (panel B) of the pMTa4 DNA after they were exposed to 0, 1.2, 2.4, 3.6, 4.8 and 6 $J.m^{-2}$ UV-C radiation.

3.13. Correlation between EB intercalation and hyperchromicity effects induced by UV-C

*3.13.1. **In total plasmids**:*

Upon plotting the UV-C induced hyperchromicity increase against the EB intercalation increase for the total pMTa4 DNA, it was observed that both the increases followed very similar trends as observed in figure 3.17.

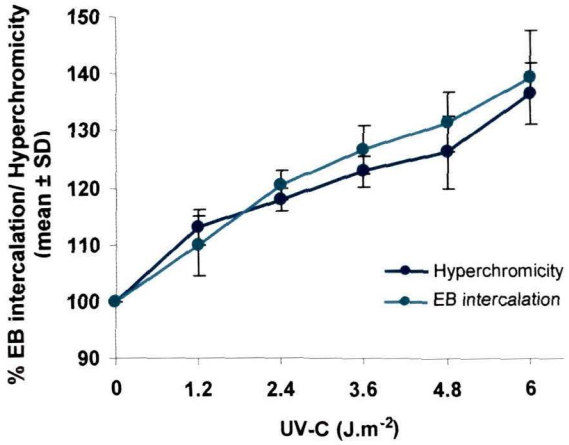

Figure 3.17: Comparison of the hyperchromicity and EB intercalation in total pMTa4 DNA: The figure shows comparative linear plots of the EB intercalation densities (—●—) and the hyperchromicity (—●—) observed for the total pMTa4 DNA obtained after irradiation of the DNA with varying doses of UV-C *in vitro*.

In order to better understand the way in which the hyperchromicity and EB intercalation correlated with each other, a correlation graph was plotted (Figure 3.18). From this graph, the slope of the line, and hence the correlation between the EB intercalation and induction of hyperchromicity was deduced. The correlation was found to be 0.98552, which is almost a linear correlation.

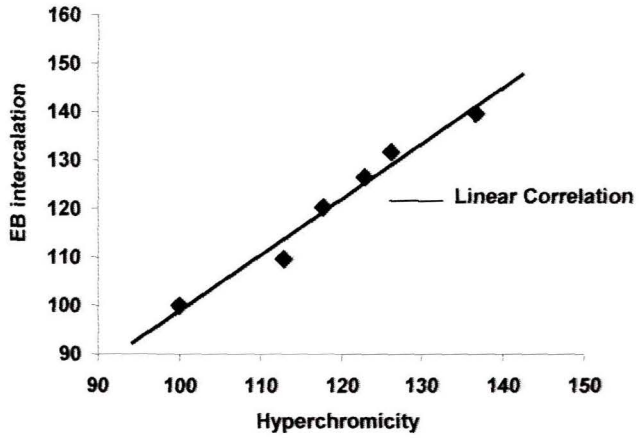

Figure 3.18: Correlation graph between the hyperchromicity and intensity due to EB intercalation: The figure shows a correlation plot obtained by plotting the EB intercalation densities and hyperchromicity of UV-C radiated total pMTa4 DNA.

3.13.2. In CC form of pMTa4 DNA:

Upon plotting the UV-C induced hyperchromicity increase against the EB intercalation increase

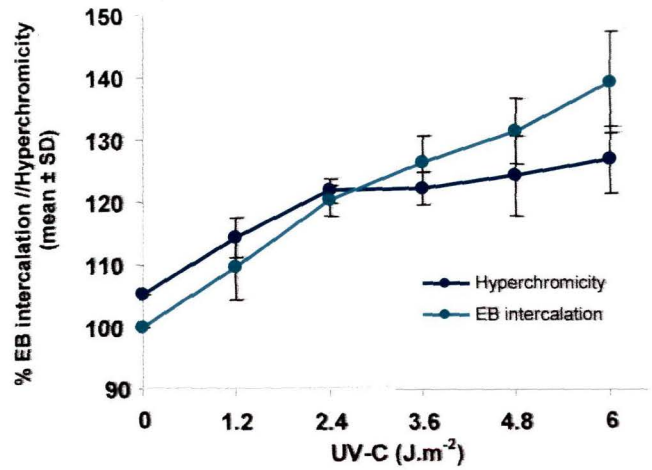

Figure 3.19: Comparison of the hyperchromicity and EB intercalation densities in the CC form of pMTa4 DNA: The figure shows comparative linear plots of the EB intercalation densities (—●—) and the hyperchromicity (—●—) observed for the total pMTa4 DNA obtained after irradiation of the DNA with varying doses of UV-C *in vitro*.

for the CC form of pMTa4 DNA, it was observed that both the increases followed very similar trends as observed in figure 3.19.

In order to better understand the way in which the hyperchromicity and EB intercalation correlated with each other, a correlation graph was plotted (Figure 3.20) From this graph, the slope of the line, and hence the correlation between the EB intercalation and induction of hyperchromicity was deduced. The correlation coefficient was found to be 0.96314, which is, again, almost a linear correlation.

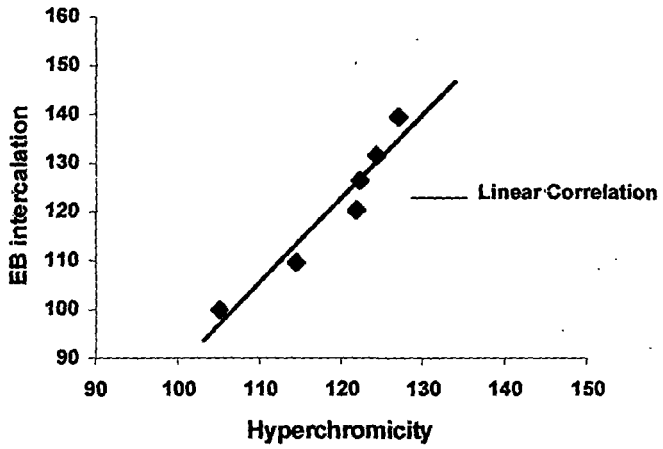

Figure 3.20: Correlation graph between the hyperchromicity and EB intercalation densities: The figure shows a correlation graph plotted between the hyperchromicity increase and the EB intercalation density increase observed after the CC form of the pMTa4 DNA was irradiated with UV-C radiation.

3.14. Restriction mapping of UV-C irradiated pMTa4 DNA

pMTa4 DNA was irradiated with 4.8, 9.6, 19.2 and 38.4 $J.m^{-2}$ UV-C radiation and restriction digested for the amount of time required to completely digest the unirradiated control pMTa4 DNA (§ 2.25.). These restriction maps were compared with the map of unirradiated control pMTa4 DNA.

3.14.1. ***Digestion with DraI:*** pMTa4 has four restriction sites for *DraI* (Fig. 3.21) generating four restriction fragments of sizes 2682, 2600, 696 and 19 bp.

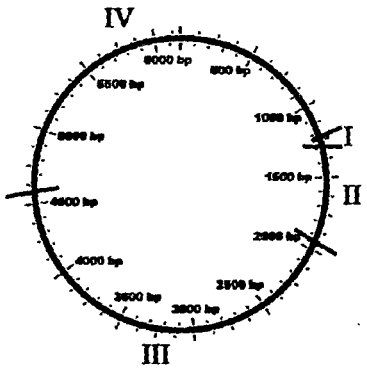

Figure 3.21: Schematic representation of the restriction sites of *DraI* on pMTa4 DNA: The restriction sites (—) of *DraI* on pMTa4 DNA are shown in the figure.

Figure 3.22. shows the restriction map of unirradiated (control) pMTa4 and pMTa4 DNA irradiated with UV-C as detailed in § 2.15.1.2.). The 19 bp fragment electrophoresed out of the gel due to its small size. Hence, the control lane showed only three bands (Fig. 3.22; lane 2). It was observed that upon irradiation with UV-C, pMTa4 DNA showed four additional slow migrating bands of sizes 3292, 3573, 5462 and 6173 bp (Fig. 3.22 ; lane 3-6), which were entirely absent in the unirradiated control. The intensity of the extra fragments was seen to increase with higher doses of UV-C irradiation. This indicates that the digestion of pMTa4 by *DraI* was influenced by UV-C radiation. The fragment sizes were determined using a DNA molecular size marker, lambda DNA *HindIII* digest (Fig. 3.22; lane 7).

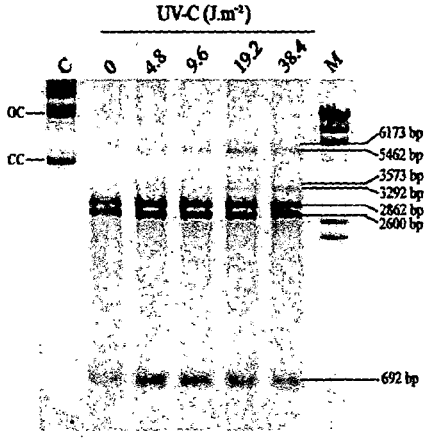

Figure 3.22: *DraI* restriction profile of UV-C irradiated pMTa4 DNA: The electropherogram shows unirradiated and UV-C irradiated pMTa4 DNA (4 µg) digested with *DraI*. Lane 1 (C) is the profile of the unirradiated, undigested pMTa4 DNA. Lane 2 (0) is the profile of the unirradiated pMTa4 DNA digested with *DraI*. Lanes 2-6 show the profiles of UV-C irradiated DNA digested with *DraI*. Lane 7 (M) indicates the molecular weight marker (lambda DNA *HindIII* digest). The fragment sizes (bp) of the bands are indicated in the figure.

Fig. 3.23 schematically explains the pMTa4 bands observed on agarose gel following restriction by *DraI*.

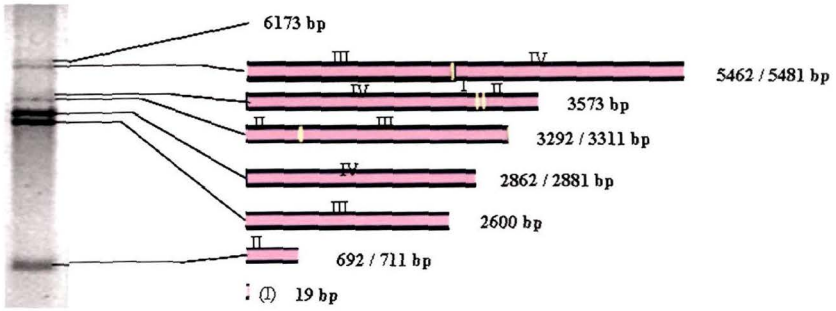

Figure 3.23: Schematic representation of the band sizes obtained after agarose gel electrophoresis of the digested pMTa4 DNA: The lines (▪) represent the restricted fragments. The yellow bands are indicative of the sites possibly showing resistance to restriction digestion.

The band intensities of different fragments were calculated using KDS 1D software. The plot of band intensities as pixel density of all bands against dose of UV-C radiation is shown in figure 3.24. The plot shows a dose dependent increase in intensities of extra fragments of 5462 and 3292 bp. The other two extra fragments, 6173 and 3573 bp, also show similar but weaker trend. A compensatory reduction in intensities of 2862, 2600 and 692 bp bands were noticeable in the plot.

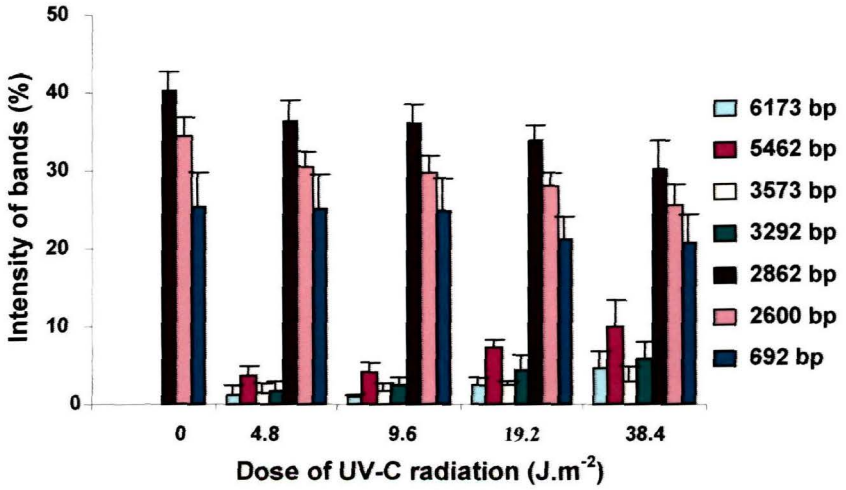

Figure 3.24: **Relative band intensities of the restricted fragments:** The figure represents the relative band intensities of the fragment sizes obtained after restriction digestion of UV-C irradiated pMTa4 DNA *in vitro*. The color coded fragment sizes are indicated in the legend.

3.14.2. ***Digestion with SspI:*** pMTa4 has two restriction sites for *SspI* (Fig. 3.25) generating two restriction fragments of sizes 6043 and 130 bp.

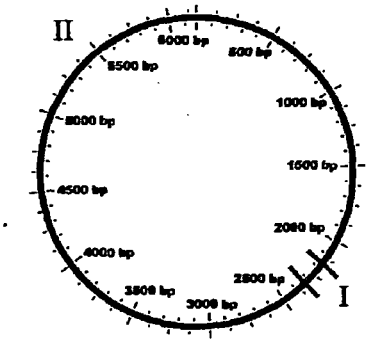

Figure 3.25: Schematic representation of the restriction sites of *SspI* on pMTa4 DNA: The restriction sites (—) of *SspI* on pMTa4 DNA are shown in the figure.

Figure 3.26 shows the restriction map of unirradiated control pMTa4 (lane 2) and pMTa4 DNA irradiated with UV-C (lanes 3-6) as detailed in § 2.15.1.2. The unirradiated control lane, therefore, showed only two bands (lane 2). It was observed that upon irradiation with UV-C, pMTa4 DNA showed one additional slow migrating band of size 6173 bp (Fig. 3.26; lanes 3-6) as determined by KDS 1D software with the help of lambda DNA *HindIII* digest as a marker (lane 7). The intensity of the UV-C induced extra band was invariant to increasing doses of UV-C radiation (Fig. 3.26). In addition, two bands, which corresponded with the CC and OC forms of the plasmid and not seen in the unirradiated control (Fig. 3.26; lane 2), made their appearances in the irradiated group (lanes 3-6). This indicates that the digestion by *SspI* was hindered due to UV-C irradiation. Depending upon hindrance to digestion at one or both restriction sites on the plasmid, results would be different. The former would generate fragment of 6173 bp size (Fig. 3.26). In the later condition, the topological form of the plasmid would remain intact. This explains reappearance of the CC and OC forms of pMTa4 in the irradiated group (lanes 3-6). It is to be noted that the hindrance to restriction by *SspI* was more prominent for OC form of the plasmid as it started showing its appearance from 4.8 $J.m^{-2}$ onwards. The reappearance of CC form was seen for the highest dose of UV-C, that is, 38.4 $J.m^{-2}$.

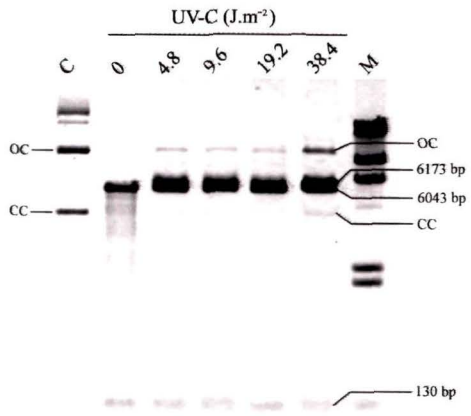

Figure 3.26: *SspI* restriction profile of UV-C irradiated pMTa4 DNA: The electropherogram shows unirradiated and UV-C irradiated pMTa4 DNA (4 µg) digested with *SspI*. Lane 1 (C) is the profile of the unirradiated, undigested pMTa4 DNA. Lane 2 (0) is the profile of the unirradiated pMTa4 DNA digested with *SspI*. Lanes 2-6 show the profiles of UV-C irradiated DNA digested with *SspI*. Lane 7 (M) indicates the molecular weight marker (lambda DNA *HindIII* digest). The fragment sizes (bp) of the bands are indicated in the figure.

Fig. 3.27 schematically explains the pMTa4 bands observed on agarose gel following restriction by *SspI*.

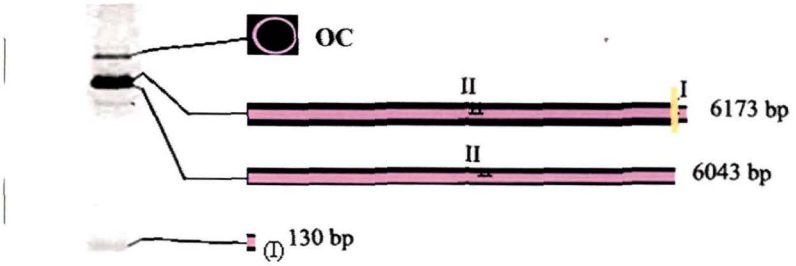

Figure 3.27: Schematic representation of the band sizes obtained after agarose gel electrophoresis of the digested pMTa4 DNA: The lines (■) represent the restricted fragments. The yellow bands are indicative of the sites possibly showing resistance to restriction digestion.

Quantification of all bands was done using the software KDS 1D and plotted in figure 3.28.

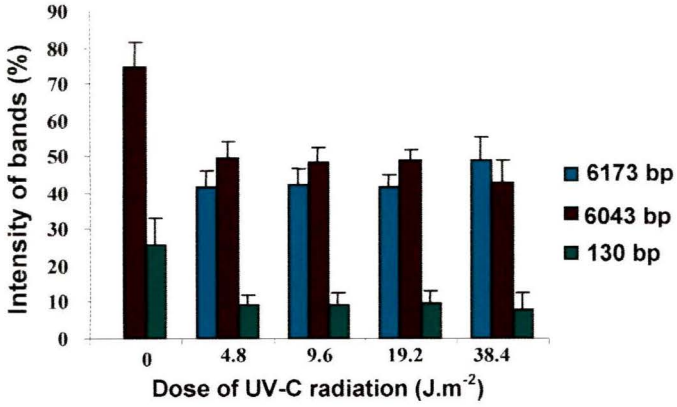

Figure 3.28: Relative band intensities of the restricted fragments: The figure represents the relative band intensities of the fragment sizes obtained after restriction digestion of UV-C irradiated pMTa4 DNA *in vitro*. The color coded fragment sizes are indicated in the legend.

3.14.3. ***Digestion with AccI:*** pMTa4 has three restriction sites for *AccI* (Fig. 3.29) generating three restriction fragments of sizes 3895, 1925 and 353 bp.

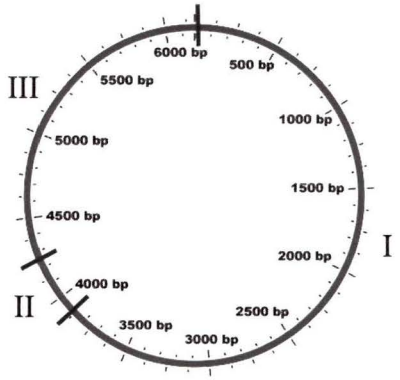

Figure 3.29: Schematic representation of the restriction sites of *AccI* on pMTa4 DNA: The restriction sites (—) of *AccI* on pMTa4 DNA are shown in the figure.

Figure 3.30 shows the restriction map of unirradiated (control) pMTa4 and pMTa4 DNA irradiated with UV-C as detailed in § 2.15.1.2. The unirradiated control lane 2, therefore, showed only three bands. It was observed that upon irradiation with UV-C, pMTa4 DNA showed an additional slow migrating band of size 5820 bp, which visually showed increase in intensity with increasing dose (Fig. 3.30; lanes 3-6). This indicates that the digestion by *AccI* was influenced by UV-C irradiation. The fragment sizes were determined using a DNA molecular size marker, lambda DNA *HindIII* digest (Fig. 3.30; lane 7).

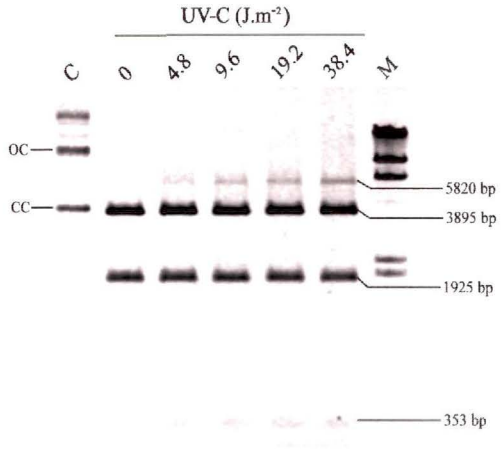

Figure 3.30: *AccI* restriction profile of UV-C irradiated pMTa4 DNA: The electropherogram shows unirradiated and UV-C irradiated pMTa4 DNA (4 µg) digested with *AccI*. Lane 1 (C) is the profile of the unirradiated, undigested pMTa4 DNA. Lane 2 (0) is the profile of the unirradiated pMTa4 DNA digested with *AccI*. Lanes 2-6 show the profiles of UV-C irradiated DNA digested with *AccI*. Lane 7 (M) indicates the molecular weight marker (lambda DNA *HindIII* digest). The fragment sizes (bp) of the bands are indicated in the figure.

Fig. 3.31 schematically explains the pMTa4 bands observed on agarose gel following restriction by *AccI*.

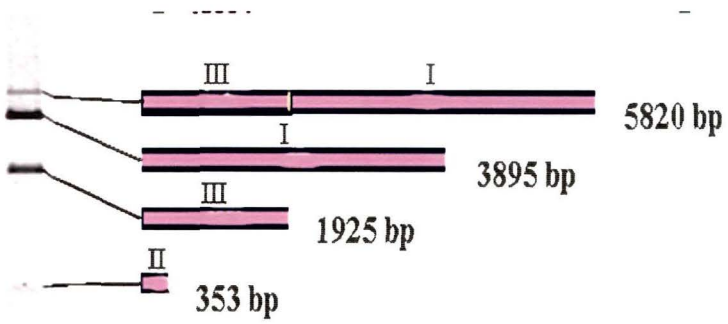

Figure 3.31: Schematic representation of the band sizes obtained after agarose gel electrophoresis of the digested pMTa4 DNA: The lines (■) represent the restricted fragments. The yellow bands are indicative of the sites possibly showing resistance to restriction digestion.

The band intensities of different fragments were calculated using KDS 1D software. The plot of band intensities as pixel density of all bands against dose of UV-C radiation is shown in figure 3.32. The plot shows that the intensity of the UV-C induced extra band exhibited a trend of marginal increase with increasing doses of UV-C radiation (Fig. 3.32).

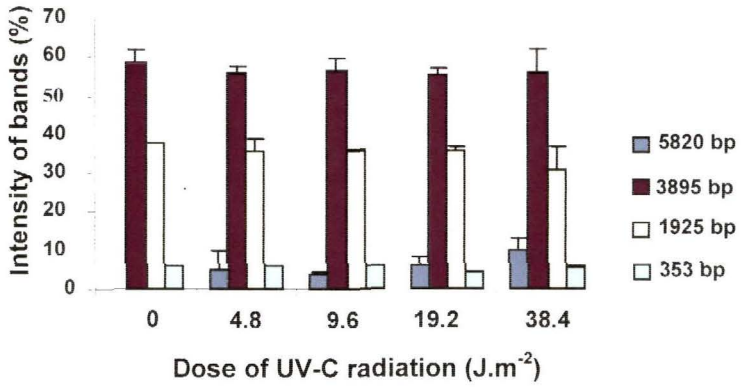

Figure 3.32: Relative band intensities of the restricted fragments: The figure represents the relative band intensities of the fragment sizes obtained after restriction digestion of UV-C irradiated pMTa4 DNA *in vitro*. The color coded fragment sizes are indicated in the legend.

3.14.4. ***Digestion with NciI:*** pMTa4 has six restriction sites for *NciI* (Fig. 3.33) generating six restriction fragments of sizes 2234, 1038, 1036, 818, 696 and 351 bp.

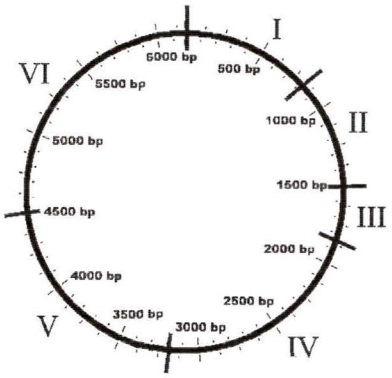

Figure 3.33: Schematic representation of the restriction sites of *NciI* on pMTa4 DNA: The restriction sites (—) of *NciI* on pMTa4 DNA are shown in the figure.

Figure 3.34 shows the restriction map of unirradiated (control) pMTa4 and pMTa4 DNA irradiated with UV-C as detailed in § 2.15.1.2. The 1038 and 1036 bp fragments, due to their very similar molecular sizes, are seen as the one band on the gel. Hence, the control lane showed only five bands (Fig. 3.34; lane 2). It was observed that upon irradiation with UV-C, pMTa4 DNA showed two very faint additional slow migrating bands of sizes 4318 and 3272 bp (Fig. 3.34). The fragment sizes were determined using a DNA molecular weight marker, lambda DNA *HindIII EcoRI* double digest (Fig. 3.34; lane 7).

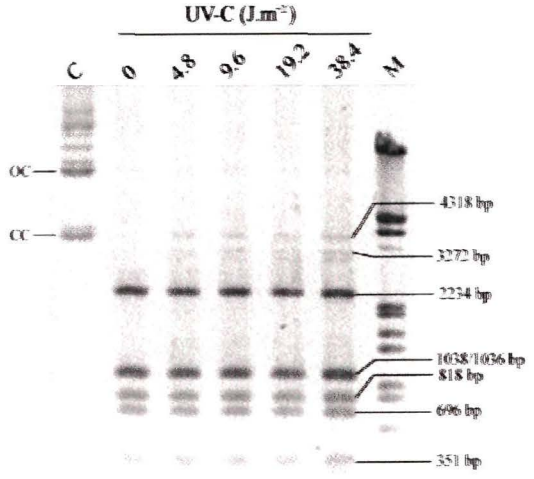

Figure 3.34: *NciI* restriction profile of UV-C irradiated pMTa4 DNA: The electropherogram shows unirradiated and UV-C irradiated pMTa4 DNA (4 µg) digested with *NciI*. Lane 1 (C) is the profile of the unirradiated, undigested pMTa4 DNA. Lane 2 (0) is the profile of the unirradiated pMTa4 DNA digested with *NciI*. Lanes 2-6 show the profiles of UV-C irradiated DNA digested with *NciI*. Lane 7 (M) indicates the molecular weight marker (lambda DNA *HindIII EcoRI double* digest). The fragment sizes (bp) of the bands are indicated in the figure.

Fig. 3.35 schematically explains the pMTa4 bands observed on agarose gel following restriction by *NciI*.

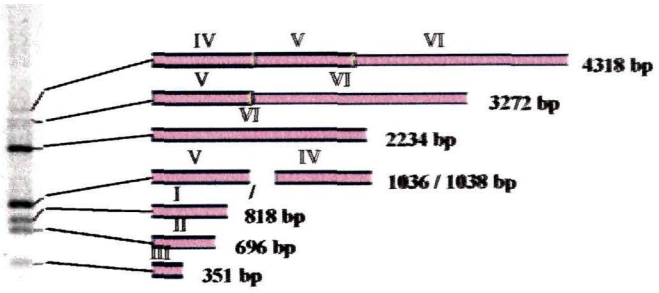

Figure 3.35: Schematic representation of the band sizes obtained after agarose gel electrophoresis of the digested pMTa4 DNA: The lines (▪) represent the restricted fragments. The yellow bands are indicative of the sites possibly showing resistance to restriction digestion.

The quantification of bands was done using KDS 1D software and plotted (Fig. 3.36). The band intensities of the extra fragments were essentially invariant following UV-C irradiation suggesting no influence of dose of UV-C radiation.

additional bands were observed after irradiation with UV-C (Fig. 3.38; lanes 3-6). This indicates that UV-C

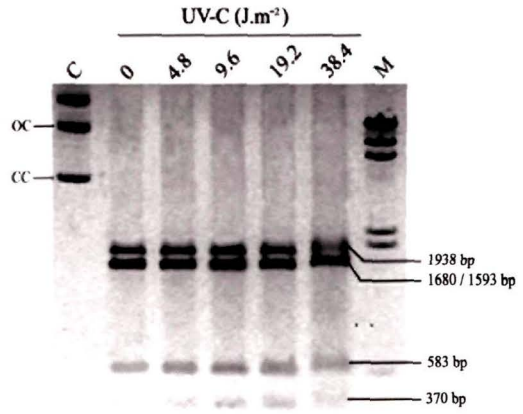

Figure 3.38: *HaeII* restriction profile of UV-C irradiated pMTa4 DNA: The electropherogram shows unirradiated and UV-C irradiated pMTa4 DNA (4 µg) digested with *HaeII*. Lane 1 (C) is the profile of the unirradiated, undigested pMTa4 DNA. Lane 2 (0) is the profile of the unirradiated pMTa4 DNA digested with DraI. Lanes 2-6 show the profiles of UV-C irradiated DNA digested with *HaeII*. Lane 7 (M) indicates the molecular weight marker (lambda DNA *HindIII* digest). The fragment sizes (bp) of the bands are indicated in the figure.

radiation did not influence pMTa4 restriction by *HaeII*. The fragment sizes were determined using a DNA molecular weight marker (Fig. 3.38; lane 7).

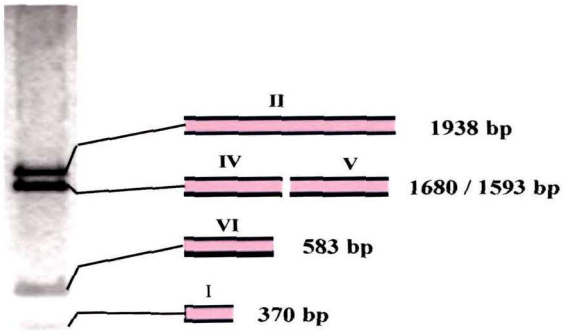

Figure 3.39: Schematic representation of the band sizes obtained after agarose gel electrophoresis of the digested pMTa4 DNA: The lines (■) represent the restricted fragments. The yellow bands are indicative of the sites possibly showing resistance to restriction digestion.

Fig. 3.39 schematically explains the pMTa4 bands observed on agarose gel following restriction by *HaeII*. The quantification of observed bands was done using KDS 1D software, which also supported the visual observation.

3.15. Effects of gamma radiation on pMTa4 DNA *in vivo*

E. coli O/N cultures were prepared (§ 2.5.2) and 1.5 ml of it irradiated with 100, 200 and 400 Gy gamma radiation *in vivo* (§ 2.17.1.2.). pMTa4 DNA was isolated either immediately (R^- condition) or after repair incubation (R^+ condition) as described § 2.15.3. The plasmid isolates were subjected to 1 % AGE (§ 2.18) and the results analyzed.

3.15.1. ***Effects in vivo for AB1157 strain:*** Figure 3.40 shows typical electropherograms of pMTa4 DNA isolates under R^- (panel A) and R^+ (panel B) conditions. Under R^- conditions an overall dose dependent degradation of CC and OC forms of pMTa4 DNA was observed which was pronounced at 200 and 400 Gy doses. Repair incubation (R^+), on the other hand, seemed to reverse the situation and the CC and OC forms of the plasmid exhibited no apparent effect of increasing doses of gamma radiation.

Figure 3.40: Effect of γ-irradiation on pMTa4 DNA isolated from *E. coli* strain AB1157: Panel A: Electropherogram showing effect of gamma irradiation under R^- conditions on pMTa4 DNA (4 µg). Panel B: Electropherogram showing effect of gamma irradiation under R^+ conditions on pMTa4 DNA (lane 1 (0) = unexposed pMTa4 lanes 2-4 = pMTa4 irradiated with 100, 200 and 400 Gy radiation).

3.15.2. ***Effects in vivo for XL1-Blue strain:*** Figure 3.41 shows typical electropherograms of pMTa4 DNA isolates under R^- (panel A) and R^+ (panel B) conditions. The overall dose dependent

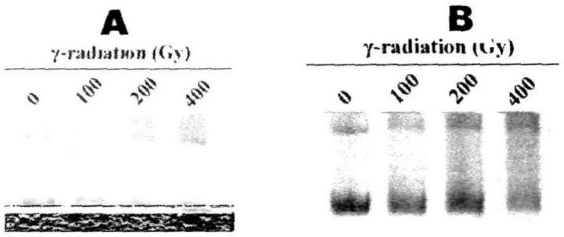

Figure 3.41: Effect of γ-irradiation on pMTa4 DNA isolated from *E. coli* strain XL1-Blue. Panel A: Electropherogram showing effect of gamma radiation under R^- conditions on pMTa4 DNA (4 µg). Panel B: Electropherogram showing effect of gamma irradiation under R^+ condition on pMTa4 DNA (lane 1 (0) = unexposed pMTa4 lanes 2-4 = pMTa4 irradiated with 100, 200 and 400 Gy gamma radiation).

degradation of CC and OC forms of pMTa4 DNA under R^- conditions was seen to persist specially for the OC form even after repair incubation (R^+).

3.15.3. ***pMTa4 DNA profile of XL1-Blue strain reconstituted with cell-free extract of AB1157 strain:*** Cell free extract (500 µl) isolated from 1 ml AB1157 culture (§ 2.5.2) was added to 1 ml O/N cultures of XL1-Blue and γ-irradiated (§ 2.16.1.).

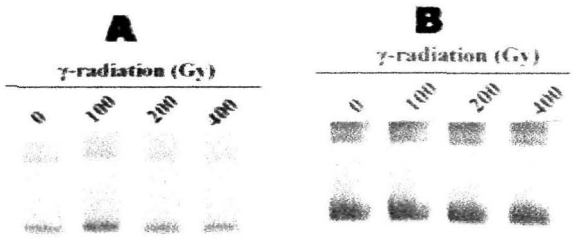

Figure 3.42: Effect of γ-irradiation on pMTa4 DNA isolated from *E. coli* XL1-Blue strain treated with cell free extract from AB1157. Panel A: Electropherogram showing effect of gamma irradiation under R^- conditions on pMTa4 DNA (4 µg). Panel B: Electropherogram showing effect of gamma irradiation under R^+ conditions on pMTa4 DNA (lane 1 (0) = unexposed pMTa4 (4µg) lanes 2-4 = pMTa4 irradiated with 100, 200 and 400 Gy gamma irradiation).

Figure 3.42 shows typical electropherograms obtained. The pMTa4 DNA isolated under R^- condition showed an overall degradation of the CC and OC forms. However, after repair incubation (R^+), the isolated pMTa4 DNA seemed to have undergone better repair and hence, damages induced by the γ-radiation seemed to be repaired better in XL1-Blue strain in the presence of cell-free extract of AB1157 strain.

3.16. Effect of aqueous extract of betel nut (AEBN) exposure on *E. coli*

The pMTa4 isolates *in vitro* or AB1157 cells *in vivo* were exposed to different doses of AEBN (§ 2.17.2.). Effects of the exposure were analyzed on different parameters described below.

3.16.1. ***On the morphology of AB1157 cells:*** Transmission electron micrography of *E. coli* cells grown in the absence or presence of 2000 µg AEBN revealed distinct differences in the morphology of the cells (Fig. 3.43). The AEBN exposed cells were larger in size and seen to have more electron dense cytoplasms (panels b & c) as compared to the controls (panel a). The cell walls showed invagination (panel c arrow) indicating damage.

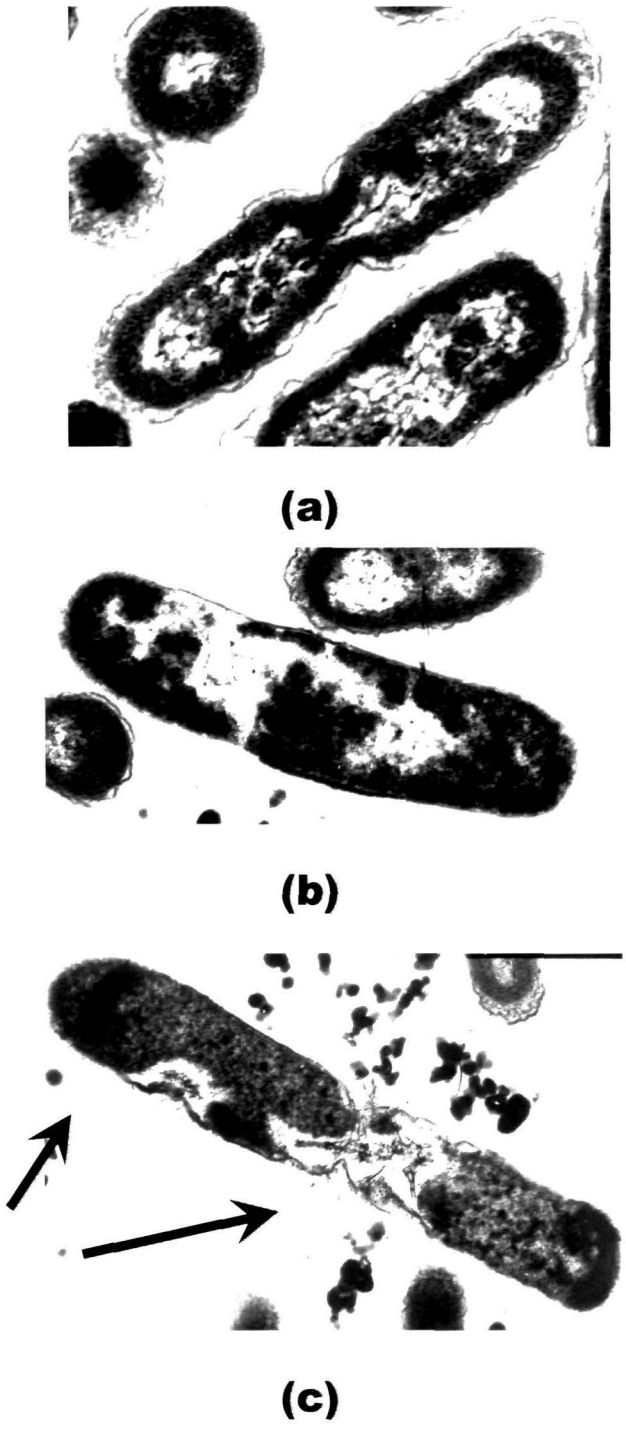

Figure 3.43: Transmission electron micrographs of *E. coli* AB1157 cells exposed to AEBN: (a) A dividing *E. coli* unexposed to AEBN (b), (c) AB1157 cells of *E. coli* exposed to AEBN. Magnification = 20,000X.

3.16.2. ***On spectrophotometric absorbance of pMTa4 DNA:*** pMTa4 DNA isolates (4 µg DNA) were exposed to increasing concentrations of AEBN at 37 °C for 30 min (panel A), 60 min (panel B) and 90 min (panel C) and their absorption spectra recorded. The results are shown in figure 3.44. As is apparent from the absorbance spectral plots (Fig. 3.44; A, B and C) both dose of AEBN and time of incubation affected absorption by pMTa4 DNA.

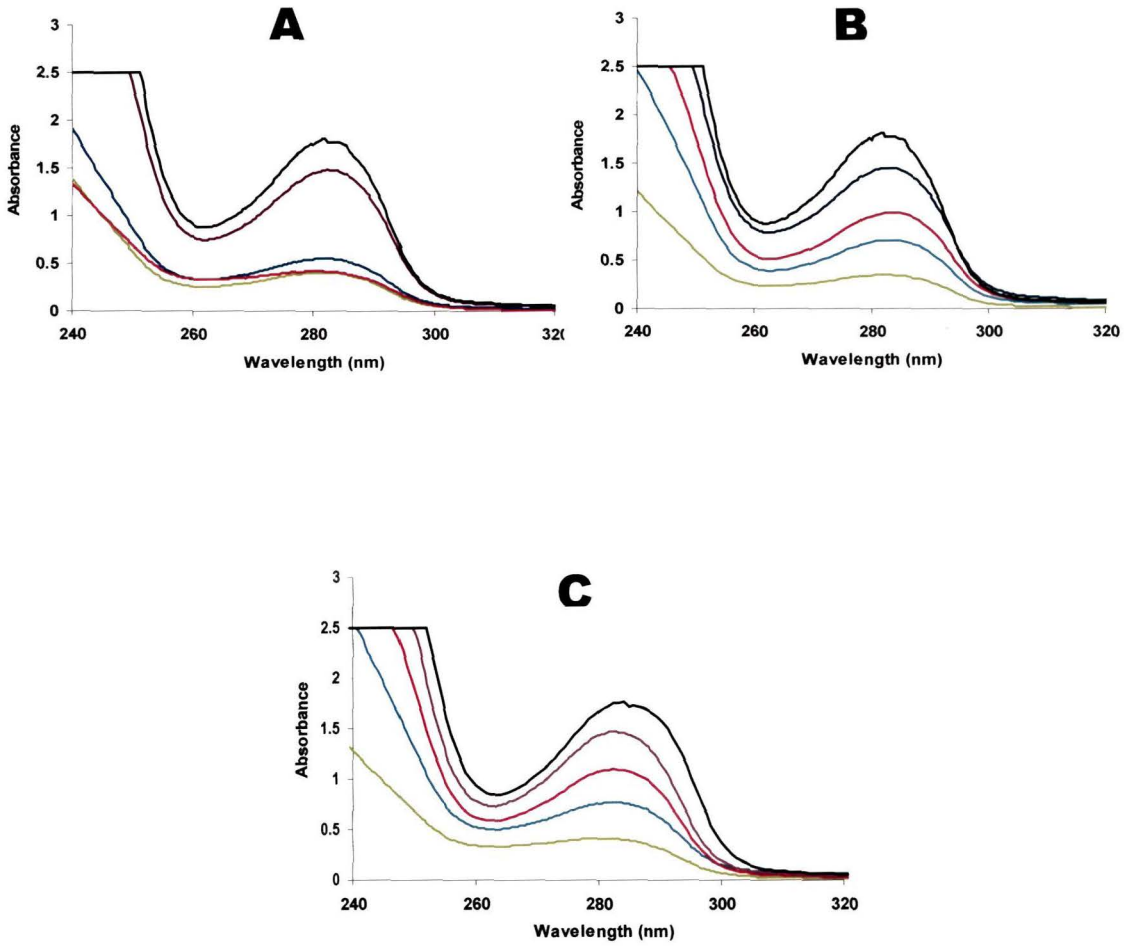

Figure 3.44: Absorption spectra analysis: Absorption spectra of pMTa4 DNA-AEBN mixture with 4 µg pMTa4 DNA and increasing concentrations of AEBN, viz., 50 µg (—), 100 µg (—), 150 µg (—), 200 µg (—) and 250 µg (—) when the incubation was allowed for 30 min (A), 60 min (B) and 90 min (C).

From these data, 4 µg pMTa4 DNA, 250 µg AEBN and 30 min incubation at 37 °C were chosen as 'saturating conditions' and were used for further studies. Under these conditions, the absorption spectra of pMTa4 DNA (4 µg), AEBN (250 µg) and 4 µg pMTa4 DNA exposed to 250 µg AEBN for 30 min at 37 °C were recorded (Fig. 3.45). The pMTa4 isolate absorbed maximally at a wavelength of 260.8 nm, as expected (arrow). The AEBN exposed pMTa4, on the other hand, was found to absorb maximally at 283.2 nm (open arrow). The AEBN exposed pMTa4 exhibited a trough at the original absorption maximum of DNA, i.e., 260.8 nm, indicating a significant shift in the absorption maximum of the DNA after its exposure to 250 µg AEBN for 30 min. The absorption maximum showed a red shift of 22.4 nm following exposure to AEBN indicating formation of AEBN adducts on pMTa4 DNA.

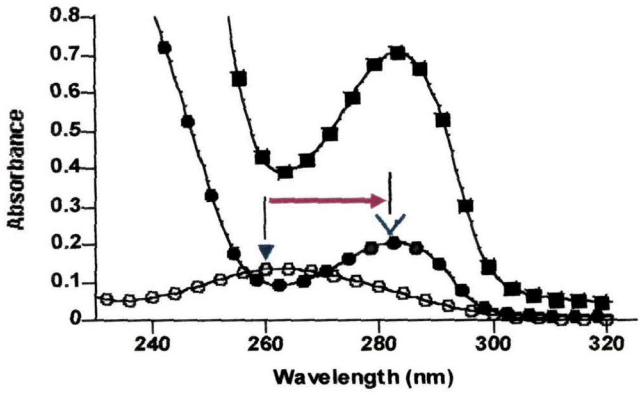

Figure 3.45: Spectrophotometric analyses of pMTa4 and AEBN interaction *in vitro*: Absorption spectra of 4 µg pMTa4 DNA (–○–), 250 µg AEBN (–■–) and 4 µg pMTa4 DNA exposed to 250 µg AEBN (–●–). Red arrow indicates the shift in the absorbance maximum of DNA following its exposure to AEBN for 30 min.

In another study the absorbance maxima at 283.2 nm of the pMTa4 incubated with varying concentrations of AEBN for different time periods (§ 2.17.1.) were recorded. The results were plotted in a graph as shown in figure 3.46. The results show that AEBN concentrations up to 100 µg exhibited no dependence on time of incubation. The dose of 150 µg AEBN, on the other hand, showed an increase in absorbance with time of incubation reaching a maximum at 60 min. The saturation effect was observed for 250 µg of AEBN in 30 min of incubation as absorbance maxima was lowered at 90 min incubation.

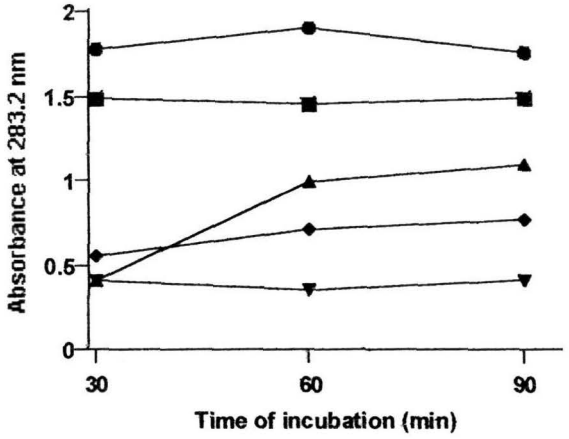

Figure 3.46: Analysis of the effect of pMTa4 DNA exposed to AEBN: Graph showing the absorption of the pMTa4 DNA-AEBN mixture at the absorption maximum, 283.2 nm when the pMTa4 DNA was incubated with 50 µg (▼), 100 µg (◆), 150 µg (▲), 200 µg (■) and 250 µg (●) AEBN for 30, 60 and 90 min.

3.16.3. On kinetics of association of AEBN with pMTa4 DNA as a function of concentration of AEBN in vitro: Figure 3.47 shows the effect of *in vitro* incubation (37 °C for 30 min) of varying concentrations of AEBN (50, 100, 150, 200 and 250 µg) on the mobility of pMTa4 DNA. The OC and CC bands of pMTa4 visually showed AEBN dose dependent retardation in mobility on agarose gel (panel A). From this, the Rf values of the OC and CC forms were calculated using

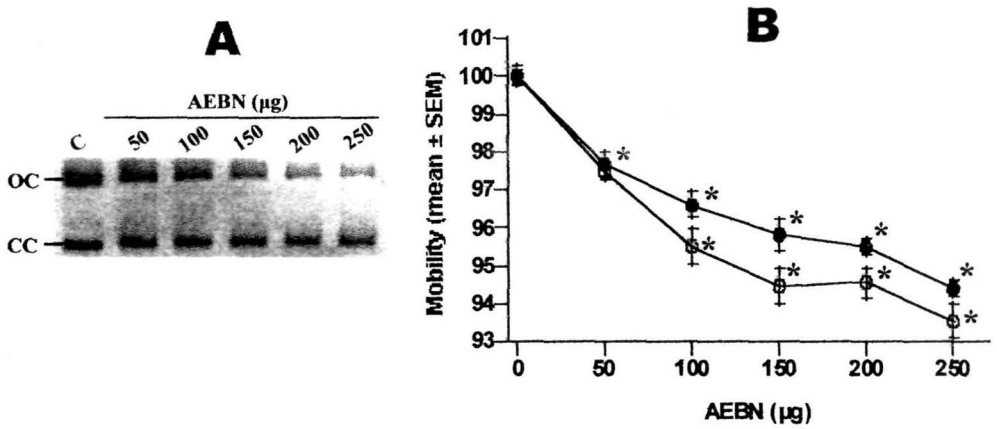

Figure 3.47: Effect of AEBN concentration on the mobilities of the CC and OC forms of the pMTa4 DNA *in vitro*: Panel A: Electropherogram showing retardation in the mobilities of the CC and OC forms of pMTa4 (4µg) DNA with increasing concentrations of AEBN (lane 1 (C) = unexposed pMTa4 lanes 2-6 = pMTa4 exposed to 50, 100, 150, 200 and 250 µg AEBN respectively at 37 °C for 30 min) Panel B: Plot of the percentage mobility changes for the CC (—●—) and OC (—⊖—) topological forms of pMTa4 DNA as a function of increasing doses of AEBN. Data (mean ± SD) were obtained from the electropherogram (panel A). * marked points are statistically significant ($p \leq 0.01$) compared to the controls.

KDS 1D software and plotted against dose of AEBN (panel B). The retardation was significant for both forms of pMTa4 but was more pronounced for OC form. The mobilities of the OC and CC forms of the pMTa4 DNA were seen to reach a minimum at 250 μg of AEBN (93.3 ± 0.9% and 94.5 ± 0.6 % of the control, respectively). Therefore, 250 μg AEBN was taken as the saturating concentration of AEBN required to produce maximum decrease in the mobilities of pMTa4 DNA.

3.16.4. ***On kinetics of association of AEBN with pMTa4 DNA as a function of concentration of AEBN in vivo:*** Figure 3.48 shows the effect of increasing concentrations of AEBN (500, 1000, 1500 and 2000 μg) on the mobility of pMTa4 DNA *in vivo* (§ 2.21.2.). The OC and CC bands of pMTa4 visually showed AEBN dose dependent retardation in mobility on the agarose gel (panel A). The Rf values of the OC and CC forms were calculated using KDS 1D software and plotted against dose of AEBN (panel B). The retardation was significant for both forms of pMTa4 but was more pronounced for OC form. The mobilities of the OC and CC forms of the pMTa4 DNA were seen to reach a minimum at 2000 μg dose of AEBN (94.5 ± 0.6 % and 93.3 ± 0.9 % of the control respectively). Therefore, 2000 μg AEBN was taken as the saturating

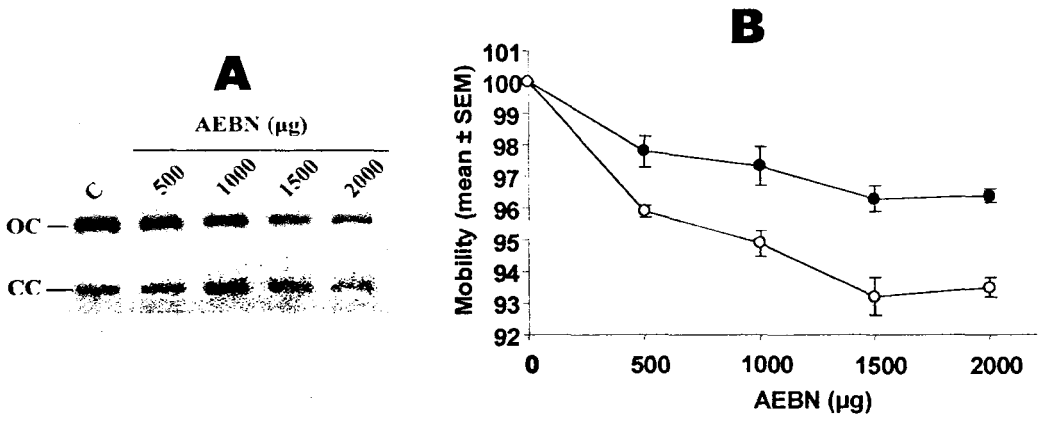

Figure 3.48: Effect of AEBN concentration on the mobilities of the CC and OC forms of the pMTa4 DNA *in vivo* in AB1157 cells: Panel A: Electropherogram showing retardation in the mobilities of the CC and OC forms of pMTa4 (4 μg) DNA with increasing concentrations of AEBN (lane 1 (C) = unexposed pMTa4 lanes 2-6 = pMTa4 exposed to 500, 1000, 1500 and 2000 μg AEBN respectively O/N at 37 °C). Panel B: Plot of the percentage mobility changes for the CC (—●—) and OC (—○—) topological forms of pMTa4 DNA as a function of increasing doses of AEBN. Data (mean ± SEM) were obtained from the electropherogram (panel A).

concentration of AEBN required to cause maximum decrease in the mobilities of the CC and OC forms of the pMTa4 DNA.

3.16.4.1. ***On kinetics of association of AEBN with pMTa4 DNA as a function of time of incubation of AEBN with DNA in vitro:*** Figure 3.49 shows the effect of the time of incubation of 4 μg pMTa4 DNA with 250 μg AEBN at 37 °C on the mobility of pMTa4 DNA. The OC and CC bands of pMTa4 visually showed a time dependent retardation in mobility on the agarose gel (panel A). From this, the Rf values of the OC and CC forms were calculated using KDS 1D software and plotted against time of incubation (panel B). The

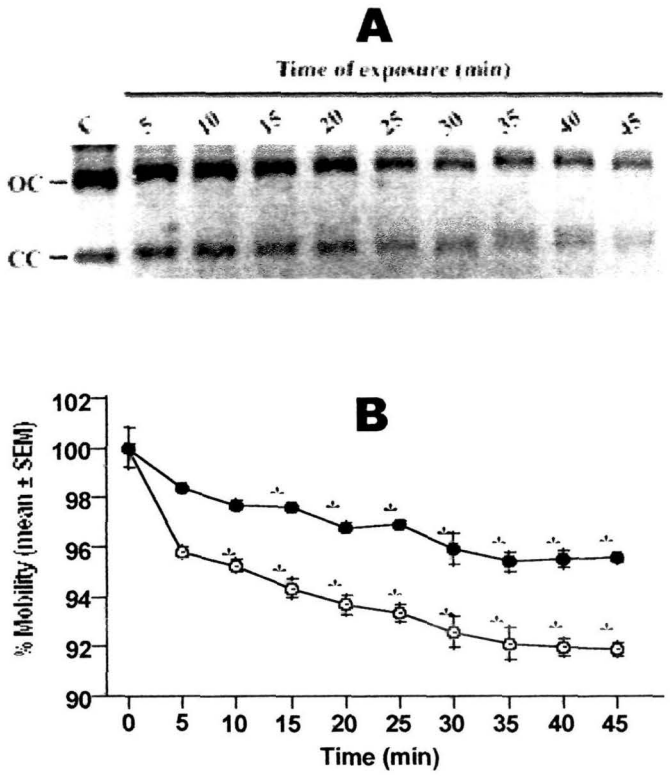

Figure 3.49: Effect of duration of AEBN exposure of plasmid pMTa4 *in vitro* on gel electrophoretic mobility: Panel A: Electropherogram showing retardation of the mobilities of CC and OC forms of the pMTa4 (4μg) DNA with increasing duration of exposure to AEBN (lane 1 (C) = unexposed pMTa4; lanes 2-10 = pMTa4 exposed to 250 μg of AEBN for 0, 5, 10, 15, 20, 25, 30, 35, 40 and 45 min respectively, at 37 °C). Plot B shows the percentage mobility changes for CC (—●—) and OC (—○—) topological forms of pMTa4 as a function of time of AEBN exposure. Data (mean ± SEM) were obtained from the electropherogram (panel A). * marked points are statistically significant ($p \leq 0.01$) compared to the controls.

retardation was significant for both forms, but more pronounced for the OC form. The mobilities of the OC and CC forms of the pMTa4 DNA were seen to reach a minimum (92 ± 0.3 % of the control and 95.8 ± 0.2 % of the control respectively) when the pMTa4 DNA was incubated with AEBN at 37 °C for 30 min. Therefore, 30 min of incubation at 37 °C was taken as the maximum time required for the formation of saturating amounts of adducts in the present experimental conditions.

3.16.5. ***Stability of the DNA as a result of the treatment with AEBN in vitro:*** The figure 3.50 shows the effect of withdrawal of the AEBN exposure regimen on mobility of pMTa4 DNA

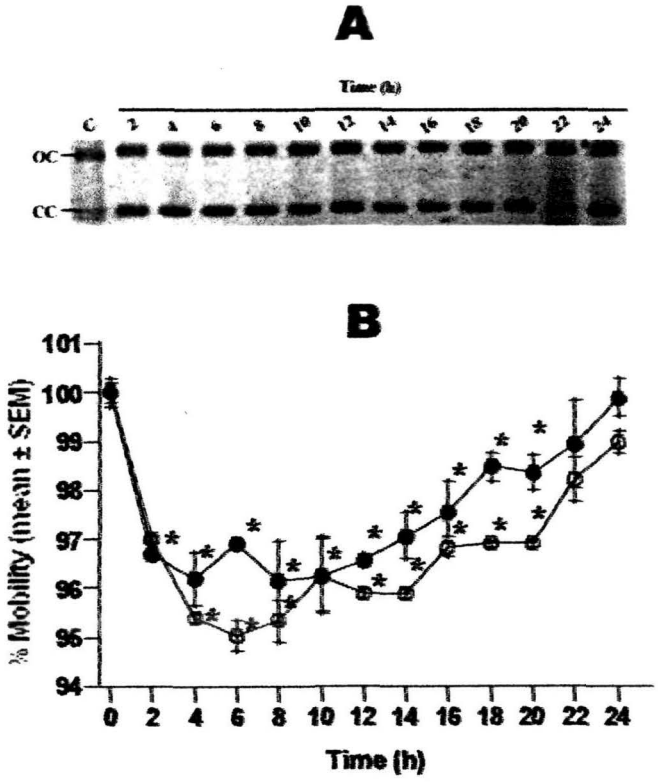

Figure 3.50: Time dependent restoration of mobilities of pMTa4 upon withdrawal of AEBN exposure regime: Panel A: Electropherogram showing the change in mobilities of CC and OC topological forms of pMTa4 (4 μg) isolated from AEBN exposed *E. coli in vivo* (2000 μg AEBN per ml culture) as a function of time of withdrawal of AEBN exposure (lane 1 (C) = unexposed pMTa4; lanes 2-13 = 2, 4, 6, 8, 10, 12, 14, 16, 18, 20, 22 and 24 h after the withdrawal of AEBN exposure regime, respectively). Panel B: Kinetics of restoration of mobilities of CC (—●—) and OC (—⊖—) forms of pMTa4 as a function of time after withdrawal of AEBN exposure. Data (mean ± SEM) were obtained from the electropherograms (panel A). * marked points are statistically significant ($p \leq 0.01$) compared to the control.

on agarose gel. With the withdrawal of the AEBN exposure regimen, the OC and CC bands visually showed a reversal in the retardation of the mobilities on the agarose gel (panel A). From this, the Rf values of the OC and CC forms were calculated using KDS 1D software and plotted against time of incubation (panel B). The mobilities of the CC and OC forms of DNA continued to be retarded up to 4-8 h after which the trend reversed. Normalcy was restored in about 24 h when the mobility of pMTa4 bands approached 100 % (Fig. 3.50). The retardation in the mobilities of the OC and CC forms of the pMTa4 DNA, which reached a minimum of 95.1 ± 0.8 % and 96.3 ± 1.2 % of the control, respectively, at 24 h due to the formation of AEBN adducts on pMTa4 DNA.

*3.16.6. **Effect of ions on the stability of the pMTa4 DNA-AEBN adduct:*** Figure 3.51 shows the effect of K^+ and Na^+ ions on the stability of the pMTa4 DNA-AEBN adducts (§ 2.24). The retardation in the mobilities of the CC and OC forms of the pMTa4 DNA induced by the exposure of pMTa4 DNA to AEBN (and thereby the formation of the AEBN-pMTa4 DNA adducts) persisted in K^+ (panel A) and Na^+ (panel B) ionic environments. This is in contrast to the earlier observation wherein the AEBN adducts on pMTa4 DNA completely dissociated in 24 h restoring mobilities to the control level in absence of ions (Fig. 3.51). Thus, the present results show that K^+ and Na^+ ions provided stability of AEBN adducts on pMTa4 DNA. The mobilities of CC and OC forms of the pMTa4 DNA were maintained at essentially the same

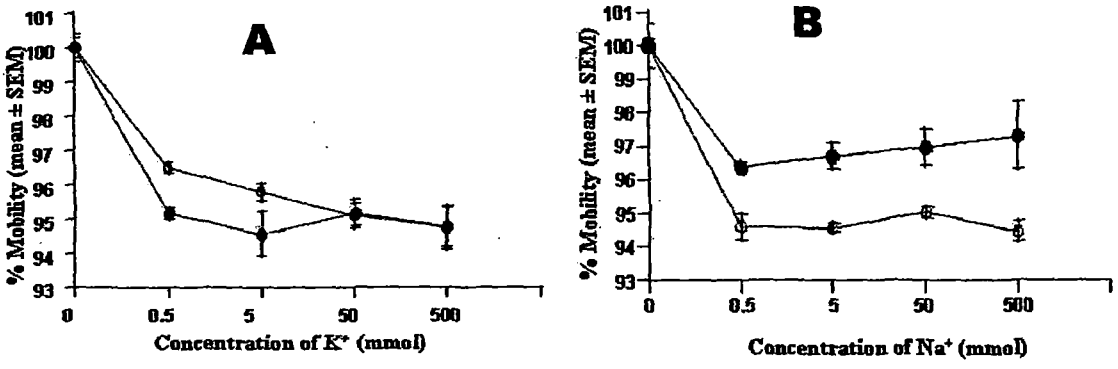

Figure 3.51: Study of the stability of the pMTa4 DNA-AEBN adducts in the presence of the cations K^+ and Na^+: Panel A: Plot showing the effect of K^+ ions (0.5, 5, 50 and 500 mmol) on the mobility shift of the CC (—●—) and OC (—⊖—) forms of pMTa4 DNA. Panel B: Plot showing the effect of Na^+ ions (0.5, 5, 50 and 500 mmol) on the mobility shift of the CC and OC forms of pMTa4 DNA.

level (94.8 ± 0.8 % and 94.7 ± 0.7 %, respectively for K^+ and 94.3 ± 0.5 % and 97.3 ± 1.8 %, respectively for Na^+) for different concentration of the ions. This also suggests that even 0.5 mmol of K^+ or Na^+ ions was enough to render the AEBN adducts stable on pMTa4 DNA.

3.16.7. ***Effect of pH on the stability of the pMTa4 DNA-ARBN adduct:*** Figure 3.52 shows the effect of varying the pH on the stability of the pMTa4 DNA-AEBN adduct (§ 2.24.). In contrast to effects of ions on the stability of AEBN adducts, different pH used in this investigation did not show any statistically significant influence on the mobilities of CC and OC forms of pMTa4 after incubation at 37 °C for 24 h. This indicates that pH in the range of 5 to 8 had no effect on the stability of AEBN adducts on pMTa4 DNA.

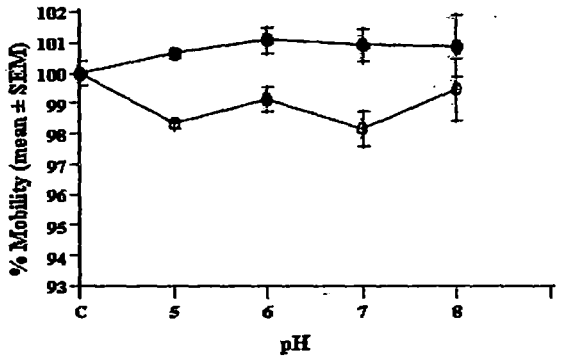

Figure 3.52: Study of the stability of the pMTa4 DNA-AEBN adducts in the presence of varying pH: Plot showing the effect of varying the pH on the mobility shift of the CC (—●—) and OC (—⊖—) forms of pMTa4 DNA due to the formation of pMTa4 DNA-AEBN adducts.

3.17. Effect of the formation of AEBN-pMTa4 DNA on the molecular weight of the linear form of the pMTa4 DNA

Figure 3.53 shows the effect of formation of adducts on the molecular size of the linear pMTa4 DNA (§ 2.22.). It can be observed from the electropherogram that there is a distinct dose dependent decrease in the Rf values of L form of the plasmid upon exposure to varying concentrations of AEBN (panel A). The Rf values of the bands were compared with a molecular weight marker, lambda DNA *HindIII* digest (lane 7), from which the molecular size of the band was determined. The plot (panel B) shows that there is a decrease in the mobility of the L form of the plasmid as a result of the formation of adduct, which corresponds to an increase in the

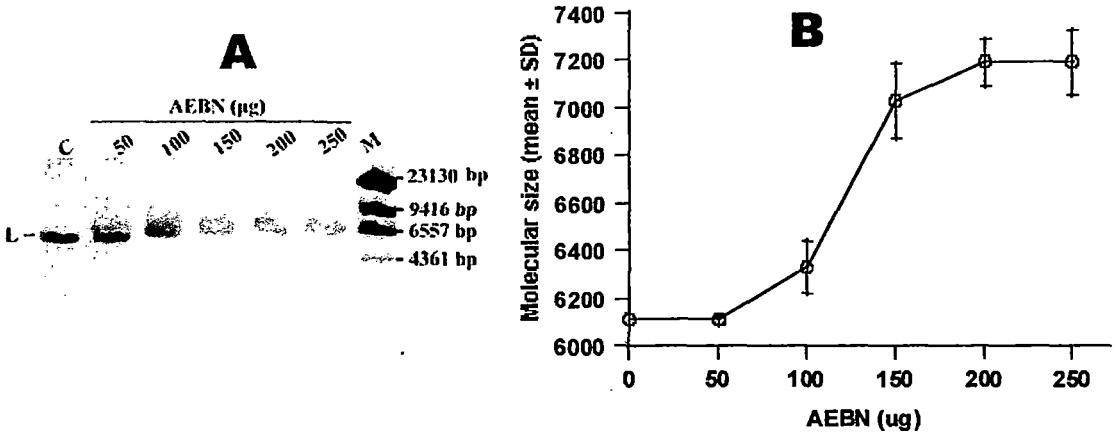

Figure 3.53: Increase in molecular size of pMTa4 DNA upon exposure to AEBN: Panel A: Electropherogram showing retardation of the mobility of linearized pMTa4 DNA (4 µg) exposed to increasing doses of AEBN (lane 1 (C) = unexposed pMTa4; lanes 2-6 = pMTa4 exposed to 50, 100, 150, 200 and 250 µg AEBN, respectively, at 37 °C for 30 min; lane 7 (M) = DNA marker (λ DNA *Hind III* digest) in bp. Panel B: Plot showing the increase in molecular size (bp) of pMTa4 DNA as a function of dose of AEBN. Data (mean ± SEM) were obtained from the electropherogram (panel A).

molecular size of the pMTa4 DNA. The increase in the molecular size of the pMTa4 DNA was ~7200 bp as a result of exposure to AEBN (Fig. 3.53 B).

3.18. Effect of the formation of AEBN-pMTa4 DNA adducts on the relative quantities of the CC, OC and L forms of the pMTa4 DNA

To determine the effects of AEBN treatment on the plasmid profiles, the pMTa4 DNA was exposed to increasing doses (50, 100, 150, 200 and 150 µg) of AEBN and subjected to AAGE (§ 2.19.). Under alkaline condition it is expected that some CC and/or OC form of pMTa4 DNA would be hydrolyzed to generate L form of the plasmid. Hence, the alkaline agarose gel should show all three forms of the plasmid. The results confirm this (Fig. 3.54; panel A). The plot of pixel densities of the CC, OC and L bands (Figure 3.54; panel B) shows AEBN dose dependent increase in the band intensities of OC and L forms with corresponding decrease in the CC band intensity. In comparison to the control, the band intensities of OC, L and CC forms of the plasmid at the highest dose of AEBN (250 µg) were 111.4 ± 6.6 %, 104.8 ± 6.3 % and 58.3 ± 8 %, respectively.

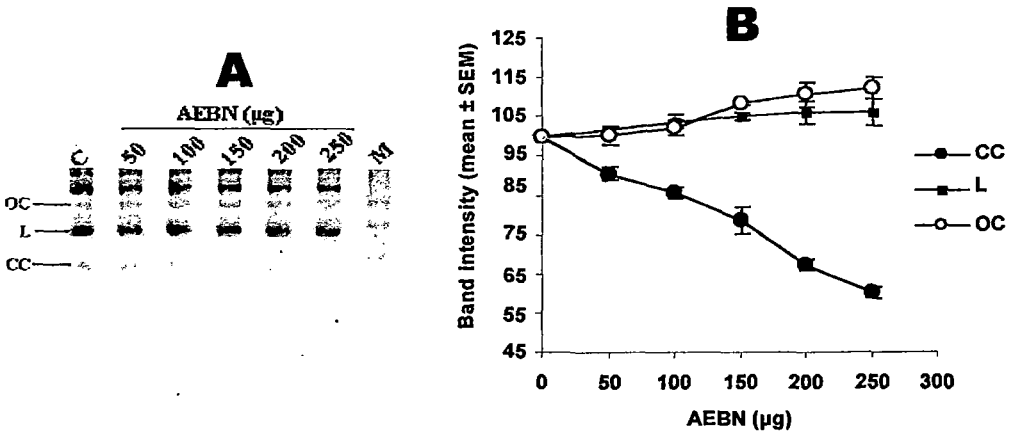

Figure 3.54: Relative degradation of the CC and OC forms of pMTa4 DNA upon exposure to AEBN: Panel A: Alkaline agarose gel electropherogram showing the relative degradation in the bands of the CC, OC and L forms of pMTa4 DNA(4 µg) after being exposed to increasing doses of AEBN (lane 1 (C) = unexposed pMTa4; lanes 2-6 = pMTa4 exposed to 0, 50, 100, 150, 200 and 250 µg AEBN, respectively, at 37 °C for 30 min; lane 7 (M) = DNA marker (λ DNA *Hind III* digest) in bp. Panel B: Plot showing the changes in the band intensities of the CC (—■—) and OC (—○—) and L (—▲—) forms of pMTa4 DNA as a function of doses of AEBN used. Data (mean ± SEM) were obtained from the electropherogram (panel A).

3.19. Induction of resistance to restriction digestion by exposure of pMTa4 DNA to AEBN *in vivo*

AB1157 cells were transformed with pMTa4 DNA (§ 2.8.) and exposed to 500, 1000, 1500 and 2000 µg AEBN. pMTa4 DNA was isolated from the exposed cells and digested with the restriction endonucleases *DraI, HaeII, NciI* and *AccI* O/N (§ 2.25.2.). The restriction patterns thus obtained were compared with the restriction patterns of unexposed control pMTa4 DNA. Some slow migrating bands were seen to appear in a number of the restriction digests. However, these bands were ignored in this section due to reasons to be discussed later.

3.19.1. ***Digestion with DraI:*** pMTa4 has four restriction sites for *DraI* (Fig. 3.21) generating 4 bands of sizes 2862, 2600, 692 and 19 bp. Figure 3.55 shows the restriction maps of unexposed control pMTa4 and that exposed to AEBN *in vivo* along with a molecular size marker, lambda DNA *HindIII EcoRI* double digest (lane 7). The 19 bp fragment electrophoresed out of the gel due to its small size. Hence, the control lane showed only three bands. (Fig. 3.55; lane 2). AEBN exposed pMTa4 DNA upon restriction digestion showed additional slow migrating bands which were absent in the unexposed control (Fig. 3.55). Concurrently with the

appearance of these slow migrating bands, the intensities of 2862, 2600 and 692 bp bands, products of restriction digestion, reduced in a dose dependent manner (Fig. 3.55; lanes 3-6).

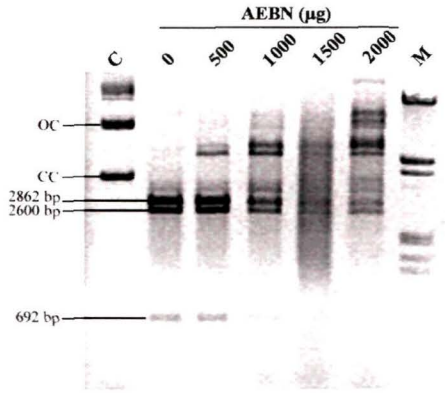

Figure 3.55: *DraI* restriction digestion profile of pMTa4 DNA which formed adducts with AEBN: The figure shows the electropherogram of pMTa4 DNA (4 µg) digested with *DraI*. Lane C is the profile of the unirradiated, undigested control pMTa4 DNA. Lane marked 0 is the *DraI* restriction profile of the unexposed pMTa4 DNA. Lanes 2-6 show the profiles of the pMTa4 DNA exposed to 500, 1000, 1500 and 2000 µg AEBN *in vivo* after digestion with *DraI*. Lane M indicates the molecular weight marker, lambda DNA *HindIII EcoRI* double digest.

For these three bands, the percentage digestion of the AEBN exposed pMTa4 DNA was calculated from the intensities of the AEBN exposed bands and the corresponding bands of unexposed control pMTa4 DNA and plotted (Fig. 3.56). The plot confirmed the visual observation.

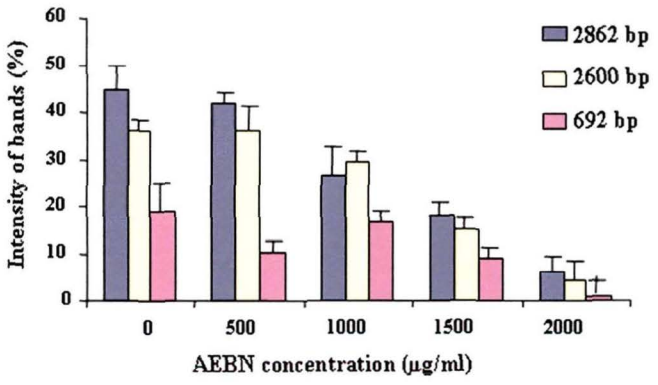

Figure 3.56: **Relative band intensities of the restricted fragments:** The figure represents the relative band intensities of the fragment sizes 2862, 2600 and 692 bp obtained after restriction digestion of UV-C irradiated pMTa4 DNA *in vitro*.

From these results, a cumulative percentage digestion graph was obtained (Fig. 3.57) which shows a dose dependent decrease in restriction by *DraI*.

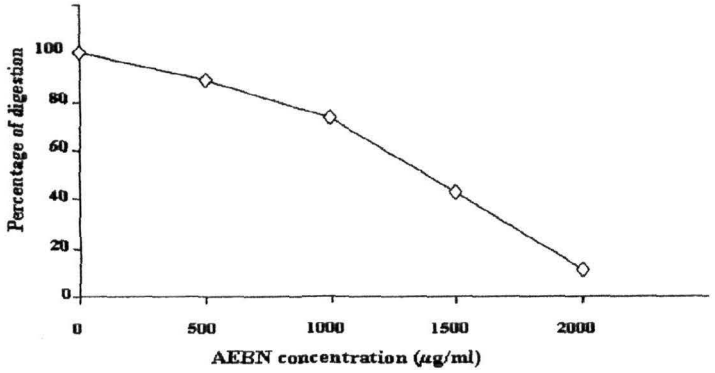

Figure 3.57: Percentage digestion of AEBN exposed pMTa4 DNA: Figure shows the relative digestion patterns as a result of being exposed to AEBN.

3.19.2. ***Digestion with NciI:*** pMTa4 has six restriction sites for *NciI* (Fig. 3.33) generating six bands of sizes 2234, 1038, 1036, 818, 696 and 351 bp. Figure 3.58 shows the restriction maps of unexposed control pMTa4 and that exposed to AEBN *in vivo* along with a molecular size marker, lambda DNA *HindIII EcoRI* double digest (lane 7). The 1038 and 1036 bp fragments, due to their similar sizes appear as a single band on the gel. Therefore, after complete digestion

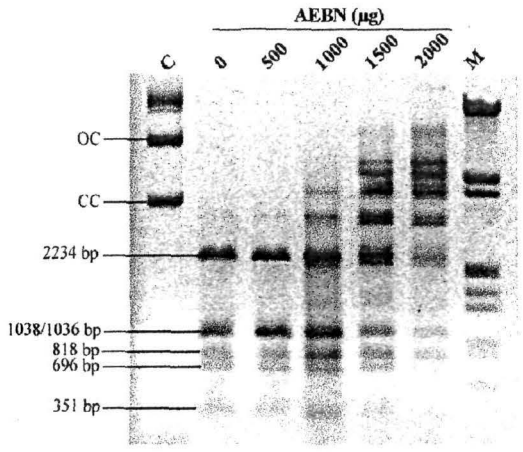

Figure 3.58: *NciI* restriction digestion profile of AEBN exposed pMTa4 DNA: The figure shows the electropherogram of pMTa4 DNA (4 µg) digested with *NciI*. Lane C is the profile of the unirradiated, undigested control pMTa4 DNA. Lane marked 0 is the *NciI* restriction profile of the unexposed pMTa4 DNA. Lanes 2-6 show the profiles of the pMTa4 DNA exposed to 500, 1000, 1500 and 2000 µg AEBN *in vivo* after digestion with *NciI*. Lane M indicates the molecular weight marker, lambda DNA *HindIII EcoRI* double digest.

with *NciI,* five bands are observed on the gel (Fig. 3.58; lane2). AEBN exposed pMTa4 DNA upon restriction digestion showed additional slow migrating bands which were absent in the unexposed control (Fig. 3.58). Concurrently with the appearance of these slow migrating bands, the intensities of 2234, 1038/1036, 818, 696 and 351 bp bands, products of restriction digestion, reduced in a dose dependent manner (Fig. 3.58; lanes 3-6). For these five bands, the percentage digestion of the AEBN exposed pMTa4 DNA was calculated from the intensities of the AEBN exposed bands and the corresponding bands of unexposed control pMTa4 DNA and plotted (Fig. 3.59). The plot confirmed the visual observation.

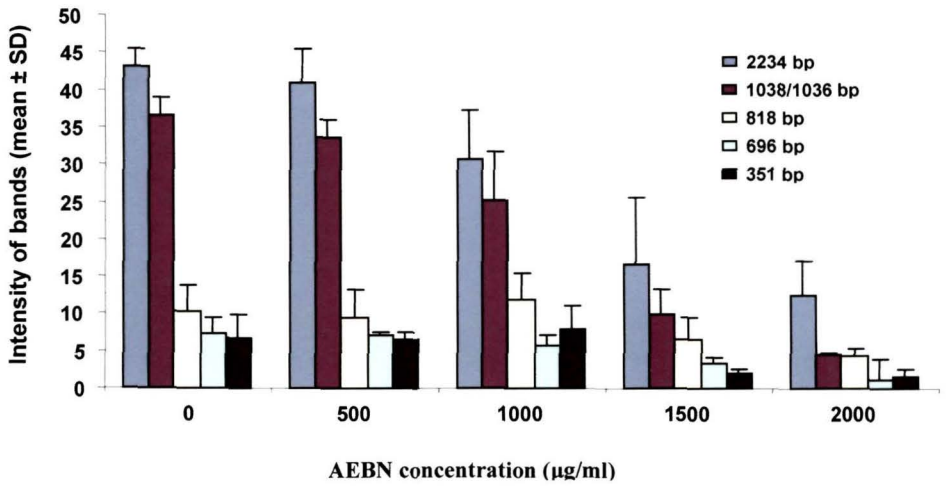

Figure 3.59: **Relative band intensities of the restricted fragments:** The figure represents the relative band intensities of the fragment sizes 2234, 1038/1036, 818, 696 and 351 bp obtained after restriction digestion of UV-C irradiated pMTa4 DNA *in vitro*.

From these results, a cumulative percentage digestion graph was obtained (Fig. 3.60) which shows a dose dependent decrease in restriction by *NciI*.

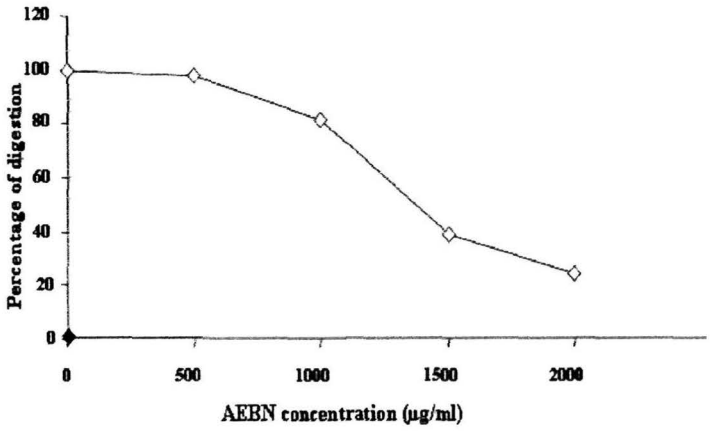

Figure 3.60: Percentage digestion of AEBN exposed pMTa4 DNA: Figure shows the relative digestion patterns as a result of being exposed to AEBN.

3.19.3. ***Digestion with HaeII:*** pMTa4 has six restriction sites on pMTa4 DNA for *HaeII* (Fig. 3.37) generating six bands of sizes 1938, 1680, 1593, 583, 370 and 8 bp. Figure 3.61 shows the restriction maps of unexposed control pMTa4 and that exposed to AEBN *in vivo* along with a molecular size marker, lambda DNA *HindIII EcoRI* double digest (lane 7). The 1680 and 1593 bp fragments, due to their similar sizes appear as a single band on the gel. The 8 bp band electrophoreses out of the gel due to their small size. Therefore, after complete digestion with *HaeII,* four bands were observed on the gel (Fig. 3.61; lane 2). AEBN exposed pMTa4 DNA upon restriction digestion showed additional slow migrating bands which were absent in the

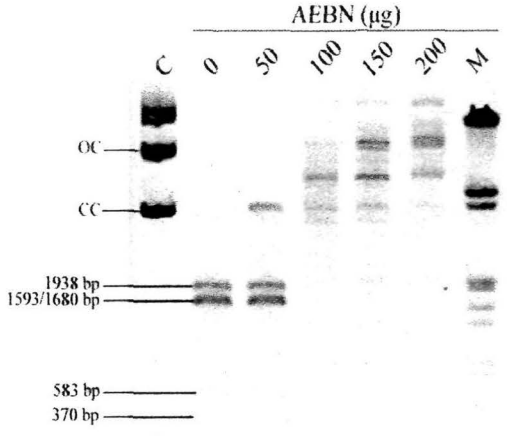

Figure 3.61: *HaeII* restriction digestion profile of AEBN exposed pMTa4 DNA: The figure shows the electropherogram of pMTa4 DNA (4 µg) digested with *HaeII*. Lane C is the profile of the unirradiated, undigested control pMTa4 DNA. Lane marked 0 is the *HaeII* restriction profile of the unexposed pMTa4 DNA. Lanes 2-6 show the profiles of the pMTa4 DNA exposed to 500, 1000, 1500 and 2000 µg AEBN *in vivo* after digestion with *HaeII*. Lane M indicates the molecular weight marker, lambda DNA *HindIII EcoRI* double digest.

unexposed control (Fig. 3.61). Concurrently with the appearance of these slow migrating bands, the intensities of 1938, 1680/1593, 583 and 370 bp bands, products of restriction digestion, reduced in a dose dependent manner (Fig. 3.61; lanes 3-6).

For these four bands, the percentage digestion of the AEBN exposed pMTa4 DNA was calculated from the intensities of the AEBN exposed bands and the corresponding bands of unexposed control pMTa4 DNA and plotted (Fig. 3.62). The plot confirmed the visual observation.

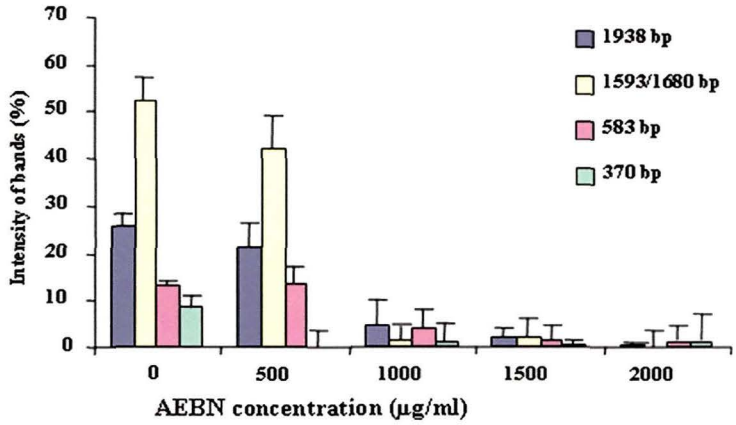

Figure 3.62: **Relative band intensities of the restricted fragments:** The figure represents the relative band intensities of the fragment sizes 1938, 1593/1680, 583 and 370 bp obtained after restriction digestion of UV-C irradiated pMTa4 DNA *in vitro*.

From these results, a cumulative percentage digestion graph was obtained (Fig. 3.63) which shows a dose dependent decrease in restriction by *HaeII*.

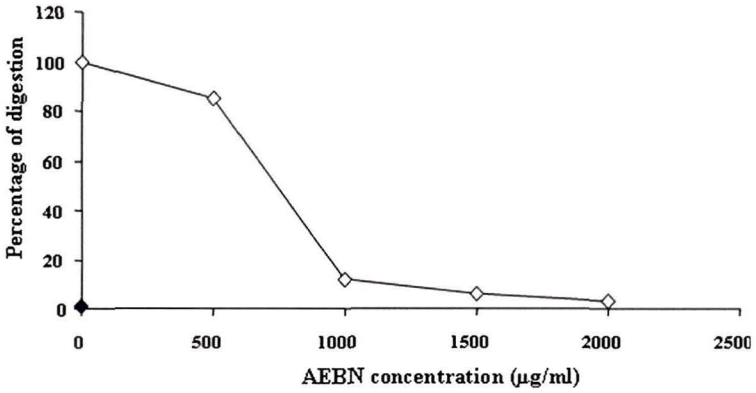

Figure 3.63: Percentage digestion of AEBN exposed pMTa4 DNA: Figure shows the relative digestion patterns as a result of being exposed to AEBN.

3.19.4. ***Digestion with AccI:*** pMTa4 has three restriction sites for *AccI* (Fig. 3.29) generating three bands of sizes 3895, 1925 and 353. Figure 3.64 shows the restriction maps of unexposed control pMTa4 and that exposed to AEBN *in vivo* as detailed in § 2.17.2 along with a molecular size marker, lambda DNA *HindIII EcoRI* double digest

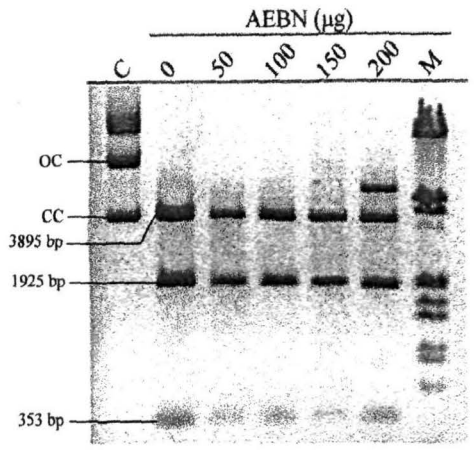

Figure 3.64: *AccI* restriction digestion profile of AEBN exposed pMTa4 DNA: The figure shows the electropherogram of pMTa4 DNA (4 µg) digested with *AccI*. Lane C is the profile of the unirradiated, undigested control pMTa4 DNA. Lane marked 0 is the *AccI* restriction profile of the unexposed pMTa4 DNA. Lanes 2-6 show the profiles of the pMTa4 DNA exposed to 500, 1000, 1500 and 2000 µg AEBN *in vivo* after digestion with *AccI*. Lane M indicates the molecular weight marker, lambda DNA *HindIII EcoRI* double digest.

(lane 7). After complete digestion with *AccI,* three bands are observed on the gel (Fig. 3.64; lane 2). It was observed that pMTa4 DNA isolated from AEBN exposed cultures, upon restriction digestion showed an additional slow migrating band after it was exposed to 2000 µg AEBN (Fig. 3.64). Concurrently with the appearance of the slow migrating band, the intensities of the 3895, 1925 and 353 bp bands reduced marginally at the highest dose (2000 µg AEBN) (lane 6). For these three bands, the percentage digestion of the AEBN exposed pMTa4 DNA was calculated from the intensities of the AEBN exposed bands and the corresponding bands of unexposed control pMTa4 DNA and plotted (Fig. 3.65).

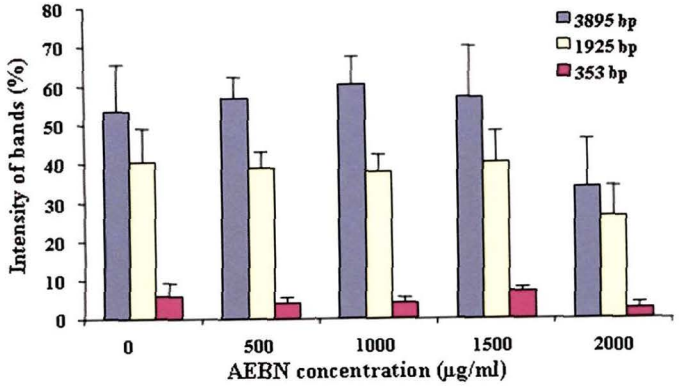

Figure 3.65: Relative band intensities of the restricted fragments: The figure represents the relative band intensities of the fragment sizes 3895, 1925 and 353 bp obtained after restriction digestion of UV-C irradiated pMTa4 DNA *in vitro*.

From these results, a cumulative percentage digestion graph was obtained (Fig. 3.66) which showed that the digestion was affected by the presence of AEBN only at a dose of 2000 µg AEBN.

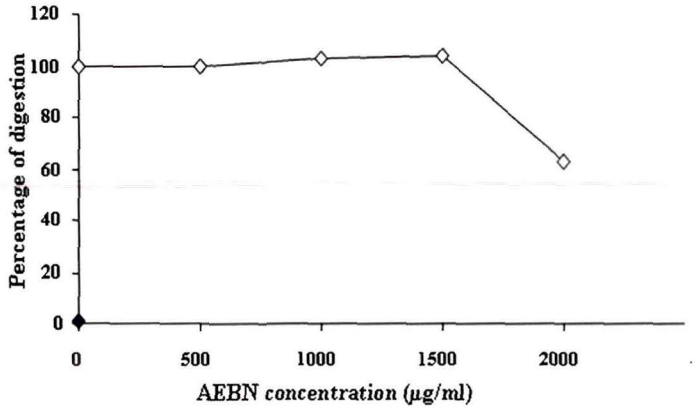

Figure 3.66: Percentage digestion of AEBN exposed pMTa4 DNA: Figure shows the relative digestion patterns as a result of being exposed to AEBN.

3.20. Effect of AEBN on the microsatellite regions of the *E. coli* genome

Four microsatellite regions were selected based on the repeating units of nucleotides in the microsatellite regions (Metzgar *et al.*, 1999). These regions were then amplified by PCR using recommended primers as detailed in Table 4. The amplicons for both strands were sequenced and analyzed (§ 2.34.).

3.20.1. ***Analysis of effect of AEBN treatment on the microsatellite region NCGT:*** Figure 3.67 shows the electropherogram of the amplified 169 bp fragment, NCGT, obtained from the unexposed control AB1157 cells and AB1157 cells exposed to 2000 µg AEBN *in vivo*.

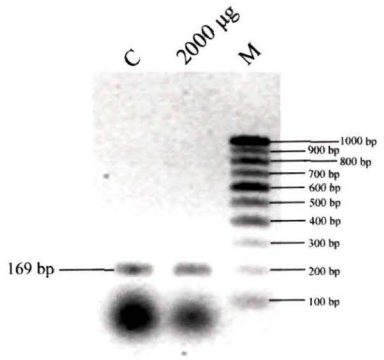

Figure 3.67: Electropherogram of the amplified fragments of the microsatellite DNA, NCGT. Lane 1(C) is the profile of the electropherogram of the unexposed control. Lane 2 is the profile of the electropherogram of the microsatellite region obtained from the AB1157 genome that has been exposed to 2000 µg AEBN. Lane M is the marker. The marker used is the 100 bp ladder.

From the electropherogram, no apparent difference was observed between the control and AEBN exposed amplicons. The amplified fragments were sequenced (sequence submitted to GenBank) and aligned using the software Multalin (§ 2.32.) to generate a consensus sequence for control and AEBN exposed amplicon (Fig. 3.68).

```
           1       10        20        30        40        50        60        70        80        90       100       110       120       130
           |--------+---------+---------+---------+---------+---------+---------+---------+---------+---------+---------+---------+---------|
Nconfor          ATTTCCTCATCAGGGGGGTTTGTACACAATACCATAATGTTGGTGTGTGTGTTCTTATCTGGTTAAGAGAAAGTGAAAAAAACACAGCGAAAAGAAATCGAAAATGTGACAAATATCACAGGTG
NChfor   ATCGGCATTTCCTCATCAGGAGGGTTTGT-AGAATACCATTTAGTTGGTGTGTGTGTTCAAATCTGGTTAAGAGAAAGTGAAAAAAACACAGCGAAAAGAAATCGAAAATGTGACAAATATCACAGGTG
Consensus ......ATTTCCTCATCAGGaGGGTTTGTa.AcAATACCATaaaGTTGGTGTGTGTGTTCaaATCTGGTTAAGAGAAAGTGAAAAAAACACAGCGAAAAGAAATCGAAAATGTGACAAATATCACAGGTG

           131     140       150       160       170 174
           |--------+---------+---------+---------+---|
Nconfor  TTCGTCAAATTGAGTTATGGCGGCGTGATGATTTACAACACACA
NChfor   TTCGTCAAATTGAGTTATGGCGGCGTGTTCATTTACAACACAA
Consensus TTCGTCAAATTGAGTTATGGCGGCGTGaTcATTTACAACACAaA

           1       10        20        30        40        50        60        70        80        90       100       110       120       130
           |--------+---------+---------+---------+---------+---------+---------+---------+---------+---------+---------+---------+---------|
Nconrev  TCGATAACTCT-TTTGACGATCCCTGTGATATCTGTCACATTTTCGATTTCTTTTCGCTGTGTTTTTTTCACTTTCTCTTAACCAGATAAGAACACACACACCAACATTATGGTATTCTGTTACAAACCC
NChrev   TCGATAACTCAGTTTGACGAACCCTGTGATATTTGTCACATTTTCGATTTCTTTTCGCTGTGTTTTTTTCACTTTCTCTTAACCAGATAAGAACACACACACCAACATTATGGTATTCTGTTACAAACCC
Consensus TCGATAACTCa.TTTGACGAaCCCTGTGATATcTGTCACATTTTCGATTTCTTTTCGCTGTGTTTTTTTCACTTTCTCTTAACCAGATAAGAACACACACACCAACATTATGGTATTCTGTTACAAACCC

           131     140       150       160       170173
           |--------+---------+---------+---------+---|
Nconrev  TTCCTGGATGGAGGGAAATTGAGCCAATTATGAACCTTTGCAA
NChrev   TTCCTGGATGGAGGGAAATTGAGCCAATTTTGGACCTTTGCA
Consensus TTCCTGGATGGAGGGAAATTGAGCCAATTaTGaACCTTTGCA.
```

Figure 3.68: Figure showing the consensus sequence obtained after the sequences were aligned.

This microsatellite region is particularly rich in A repeats. No significant NT sequence change was observable. Few changes in the NT sequences (in blue) were located towards the beginning and end of the amplicons and could be the result of errors of sequencing and hence, have not

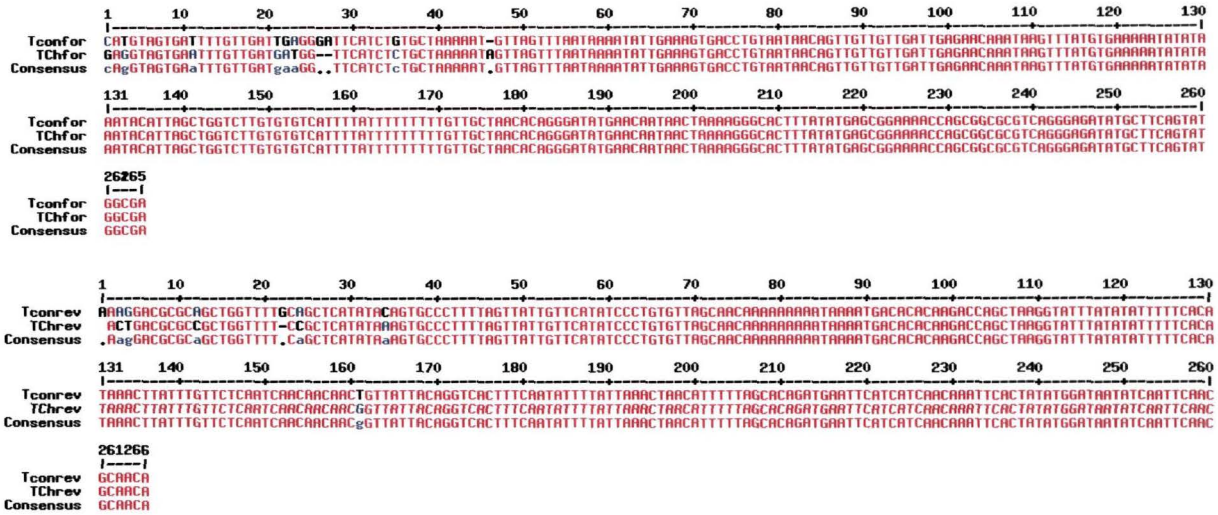

Figure 3.70: Figure showing the consensus sequence obtained after the sequences were aligned.

This microsatellite region is particularly rich in A, T and GT repeats. From the electropherogram, no apparent difference was observed between the two bands obtained. The amplified fragments were then sequenced and aligned using the software Multalin, as detailed in § 2.32. as shown in figure 3.70. In the figure 3.70, no significant changes were observed after the sequences were aligned. The few changes in the nucleotide sequences (indicated in blue) are located towards the beginning and end of the sequences and could be the result of errors during sequencing and hence, are not considered as significant changes. However, an insertion of an A nucleotide was observed after the 45th nucleotide in the forward strand. This change was, however, not corroborated by the sequence of the reverse strand. In the reverse strand, instead, a T was seen to change to G at the 161st nucleotide. Again, the change was not corroborated by the sequence of the forward strand. From these changes, it can be said that the changes observed were not mutations *per se*.

3.20.3. ***Analysis of effect of AEBN treatment on the microsatellite region INTG:*** Figure 3.71 shows the electropherogram of the amplified fragment, INTG, obtained from the unexposed control AB1157 cells and AB1157 cells exposed to 2000 µg AEBN *in vivo* using the required primers.

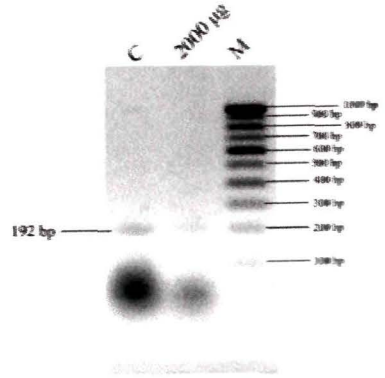

Figure 3.71: Electropherogram of the amplified fragments of the microsatellite DNA, INTG. Lane 1(C) is the profile of the electropherogram of the unexposed control. Lane 2 (2000 µg) is the profile of the electropherogram of the microsatellite region obtained from the AB1157 genome that has been exposed to 2000 µg AEBN. Lane M is the DNA molecular size marker (100 bp ladder).

From the electropherogram, no apparent difference was observed between the control and AEBN exposed amplicons. The amplified fragments were sequenced (sequence submitted; GenBank locus # bankit1015289; Sept 2007) and aligned using the software Multalin to generate a consensus sequence for control and AEBN exposed amplicon (Fig. 3.70).

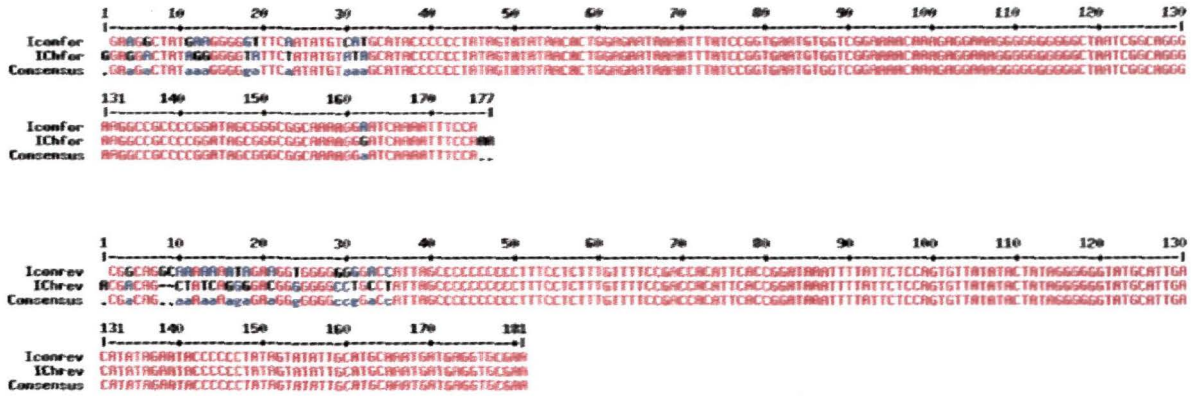

Figure 3.72: Figure showing the consensus sequence obtained after the sequences were aligned.

This microsatellite region is particularly rich in C, G and AT repeats. From the electropherogram, no apparent difference was observed between the two bands obtained. The amplified fragments were then sequenced and aligned using the software Multalin, as detailed in § 2.32. as shown in figure 3.72. In the figure, no significant changes were observable after the sequences were aligned except for a few changes (indicated in blue) in sequences located towards the beginning and end of the sequences which could be the result of errors during

sequencing. This shows that no NT change or mutation was induced by AEBN in this microsatellite region of the AB1157 genome by AEBN at 2000 ug used in the present investigation.

3.20.4. ***Analysis of effect of AEBN treatment on the microsatellite region ANTW:*** Figure 3.73 shows the electropherogram of the amplified fragment, INTG, obtained from the unexposed control AB1157 cells and AB1157 cells exposed to 2000 μg AEBN *in vivo* using the required primers.

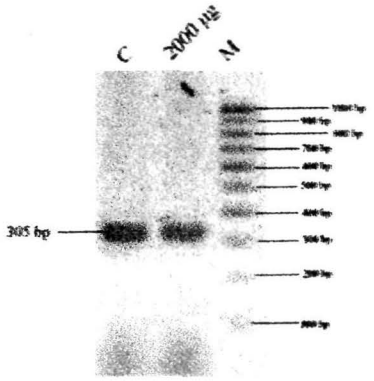

Figure 3.73: Electropherogram of the amplified fragments of the microsatellite DNA, ANTW. Lane 1(C) is the profile of the electropherogram of the unexposed control. Lane 2 is the profile of the electropherogram of the microsatellite region obtained from the AB1157 genome that has been exposed to 2000 μg AEBN. Lane M is the marker. The marker used is the 100 bp ladder.

From the electropherogram, no apparent difference was observed between the control and AEBN exposed amplicons. The amplified fragments were sequenced (sequence submitted; GenBank locus # bankit1015284; Sept, 2007) and aligned using the software Multalin to generate a consensus sequence for control and AEBN exposed amplicon (Fig. 3.70).

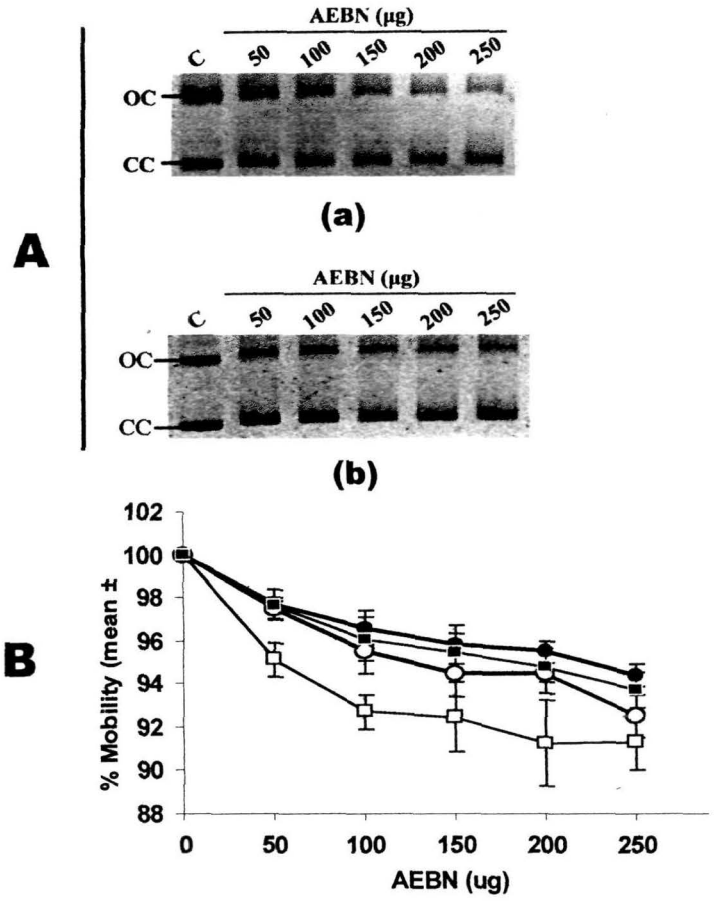

Figure 3.75: Effect of AEBN concentration on the mobilities of the CC and OC forms of the pMTa4 DNA *in vitro*: Panel A: Electropherograms showing retardation in the mobilities of the CC and OC forms of unirradiated (a) and UV-C irradiated (b) pMTa4 DNA with increasing concentrations of AEBN (lane 1 (C) = unexposed pMTa4 (4µg) lanes 2-6 = pMTa4 (4 µg) exposed to 50, 100, 150, 200 and 250 µg AEBN respectively for 30 min at 37 °C) Panel B: Plot of the percentage mobility changes for the CC (—●—) and OC (—○—) topological forms of unirradiated pMTa4 DNA and CC (—■—) and OC (—□—) topological forms of pMTa4 DNA irradiated with 6 $J.m^{-2}$ UV-C radiation as a function of increasing doses of AEBN. Data (mean ± SD) were obtained from the electropherogram (panel A).

condition (a) and that primed with UV-C radiation (b). The mobilities of the CC and OC forms of pMTa4 was plotted against dose of AEBN for UV-C unprimed and primed samples (panel B). The plot shows that adduct formation on pMTa4 DNA was dependent on both dose of AEBN and UV-C priming. UV-C irradiation resulted in a greater retardation in mobility as compared to the mobility shift observed for the unirradiated pMTa4 DNA. Though it was not significant for CC form of pMTa4, it was statistically significant ($p = <0.05$) for OC form, especially at 50, 100, 150, 200 and 250 µg doses of AEBN (Fig. 3.75B).

3.21.2. ***Linearized pMTa4***: Figure 3.76 (panel A) shows the electropherogram displaying the effect of varying concentrations of AEBN on the mobility of linearized pMTa4 DNA (4 μg) under control condition (a) and that primed with UV-C radiation (b). The decrease in the mobility of the linear form of the plasmid was again AEBN dose dependent. Being linear pMTa4, the molecular size of the bands could be calculated with the help of DNA molecular size marker

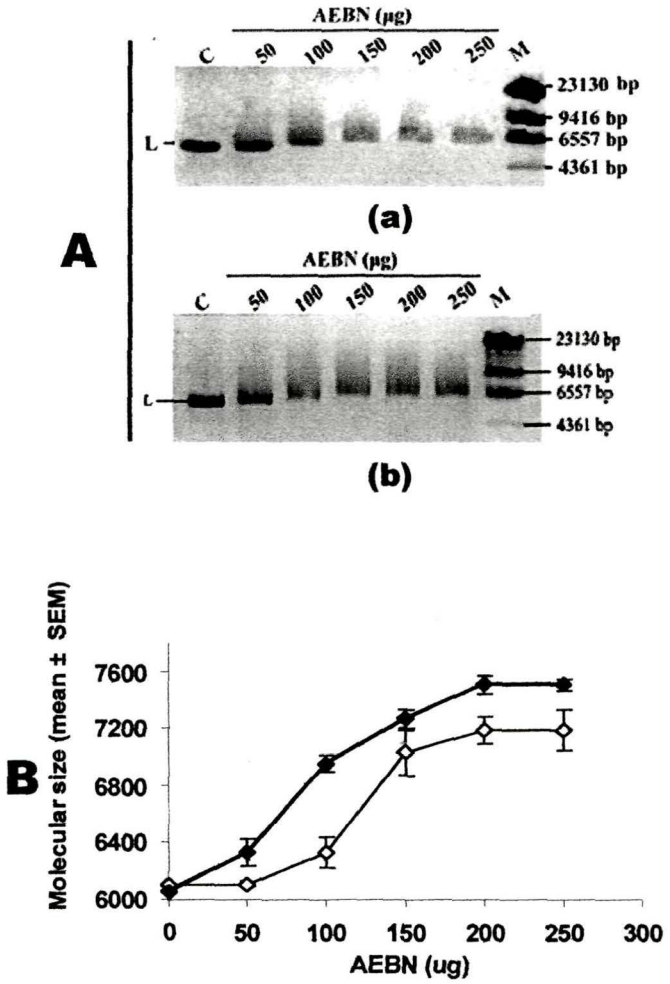

Figure 3.76: Effect of UV-C radiation on the increase in molecular size of pMTa4 DNA exposed to AEBN: Panel A: Electropherograms showing retardation of the mobility of linearized unirradiated (a) and UV-C irradiated (b) pMTa4 DNA exposed to increasing doses of AEBN (lane 1 (C) = unexposed pMTa4 (4 μg); lanes 2-6 = pMTa4 (4 μg) exposed to 50, 100, 150, 200 and 250 μg AEBN, respectively, at 37 °C for 30 min; lane 7 (M) = DNA marker (λ DNA *Hind III* digest) in bp. Panel B: Plot showing the increase in molecular size (bp) of the pMTa4 DNA as a function of dose of AEBN. Data (mean ± SEM) were obtained from the electropherogram (panel A).

(lane 7(M)). The adducts on linear form of pMTa4 would cause decrease in its mobility, which is indicative of an increase in the molecular size of the DNA. The molecular size of the unirradiated pMTa4 DNA was seen to progressively increase to ~7200 bp at 250 ug dose of AEBN. Upon UV-C irradiation, the molecular size of pMTa4 DNA increased to ~7500 bp at the same dose of AEBN. In both the cases, the molecular size seemed to reach a maximum at a dose of 200 µg AEBN per 4 µg pMTa4 DNA.

Discussion

Genomic instability has come under the limelight in recent years ever since its role in various diseases like Ataxia telangiectasia, Bloom's syndrome, Nijmegen breakage syndrome, Werner's syndrome, Fanconi anemia, and other diseases, which may ultimately lead to cancer, has been discovered. With a growing number of scientists now viewing genomic instability as a step that precedes the onset of cancer (Nowell, 1976), it is assumed that by identifying the underlying cause of genetic instability in these disorders, one can derive valuable information not only about the basis of particular genetic diseases, but also about the underlying causes of genomic instability in sporadic cancers in the general population. Many cancer biologists now believe that that genomic instability not only initiates carcinogenesis but also allows the tumor cell to become metastatic and evade drug toxicity (Tlsty, 1993). Loss of stability of the genome is becoming accepted as one of the most important aspects of carcinogenesis (Morgan, 1996). Scientists are slowly coming to a consensus on the fact that understanding genomic instability can be crucial in understanding the onset of cancer.

Genomic instability can be induced by a variety of agents including radiation and chemicals. *E. coli* serves as an excellent model to study the genomic instability because of its small size, ability to harbor plasmids and a generation time of ~30 min. Hence, this organism has been used for the study of genomic instability in the present investigation. The strains of *E. coli* used were kindly provided by Prof. K. Yamamoto (Tohoku University, Japan) and chosen on the basis of their ability or inability to repair damages induced by gamma and UV-C radiation. Three strains of *E. coli* were used in the study. They were AB1157, an *E. coli* K12 repair proficient strain, its repair deficient *recA* mutant, XL1 Blue, and *recF* mutant, JC9239 (§ 2.4.1.). AB1157, being wild with respect to both *recA* and *recF* genes was used as the wild type strain. XL1 Blue, being a *recA* mutant, was deficient in recombination repair (RR) and exhibited hypersensitivity to UV and gamma radiation. JC9239, being a *recF* mutant, was deficient in repair of DNA damage caused by UV-C radiation. In this study two qualitatively different genotoxins were used in order to get a holistic picture of biological response to the interventions. The genotoxins were UV-C radiation and aqueous extract of betel nut (AEBN). In contrast to UV-C radiation, which is essentially packets of photon energy, AEBN is a natural chemical entity that is known to

physically interact with DNA. Thus, the results of the investigations are likely to provide a more holistic view of genome instability because of the qualitative difference between the genotoxins being used for induction of genome instability.

When the growth characteristics of the *E. coli* strains were studied, it was observed that the wild type strain, AB1157, and the *recF* mutant, JC9239, have similar growth patterns while the *recA* mutant, XL1 Blue, showed a slightly slower rate of growth (Fig. 3.1). This was expected as XL1 Blue, being a *recA* mutant, lacks RecA protein which is crucial for normal recombination process as well as for RR of the DNA (Kuzminov, 2001). JC9239 is a *recF* mutant primarily concerned with repair of UV induced damages in the DNA (Courcelle *et al.*, 1997; Kuzminov *et al.*, 1999).

UV-C irradiation resulted in marginally compromised clonogenic survival of the AB1157 strain of *E. coli* (Fig. 3.2). The *recA* mutant showed the most compromised survival (~10^{-6} % survival) in comparison to the survival of the wild type strain. The *recF* mutant showed intermediate survival rates (~20 % survival) (Fig. 3.2). AB1157 strain is wild with respect to *recA* and *recF* genes that are involved with the repair of damages induced by ionizing and non-ionizing radiations (Kuzminov, 2001). Because RecF protein is responsible for repairing damages induced by UV radiation, assault of JC9239 with UV-C resulted in compromised survival of this strain. However, XL1 Blue strain showed more compromised survival as compared to the survival shown by JC9239. This result was expected as JC9239, despite being a *recF* mutant, has a functional *recA* gene. RecA protein is not only crucial for strand rejoining (Sharan *et al.*, 2007), it also takes part in an alternative pathway to repair damages caused by the UV-C radiation (Courcelle *et al.*, 1997; Kuzminov *et al.*, 1999). XL1 Blue, on the other hand, is a *recA* mutant. Hence, this mutant is unable to repair the damages induced by UV-C by RR. Thus, even if the RecF protein is functional, the mutation in the *recA* gene will indicate that damages induced cannot be repaired by the alternative mechanism, and hence, the survival is seen to be compromised (Fig. 3.2). RecA protein is also involved in the repair of damages induced by other agents. (Kuzminov, 1999; Lusetti and Cox, 2002; Sharan *et al.*, 2007).

For the present investigation, the effects of UV-C radiation, gamma radiation and AEBN on DNA were studied with the help of the plasmid pMTa4 construct as it has served as an excellent tool for the study of such damages (Humtsoe *et al.* 1998; Humtsoe and Sharan 2003; 2004; Odyuo and Sharan 2005), due to its small size (6173 bp), ease of propagation, and ease of its detection due to the presence of the Ampicillin resistance gene as a marker (§2.4.2.). Moreover, the results obtained are easily analyzed and, therefore, this tool was adopted for the study. The native conformation of plasmid DNA within a cell is the covalently closed circular (CC) form. However, the rigors that the plasmid endures during isolation invariably induce some SSB into them. As a result, the CC form of plasmid DNA relaxes into open circular (OC) form. If DSB is induced or if two proximal SSB are made on either strand of the plasmid DNA, the CC or OC form of plasmid gets converted into the linear (L) form. Our experiments, however, showed the appearance of only two conformational forms of the plasmid DNA, the CC and OC forms (Fig. 3.5; lane A). Typical plasmid isolates contained 60% of CC form and 40% of OC form. Few slow migrating bands of DNA were observed above the OC form which might be multimeric (M) plasmids produced due to the intra and/ or inter strand interactions between different plasmid molecules (Fig. 3.5; lane A). Such DNA structures have been observed by other investigators in plasmid (Washino and Schnabel, 1982; Herskind, 1987). The plasmid could be linearized with *NcoI,* which has one restriction site on pMTa4 (Fig. 2.1) to give the L form (Fig. 3.5; lane B). This showed the location of the L form (Fig. 3.5). Plasmid DNA is, thus, a convenient tool to study the induction of SSB and DSB induced by various genotoxins (Humstoe and Sharan, 2004).

The mechanism of induction of genomic instability by UV-C radiation, a non-ionizing radiation (NIR), is not known. A NIR type of radiation, which is a low energy radiation, essentially causes formation of cyclobutane pyrimidine dimers (CPD), 6,4-photoproducts (6-4 PP), interstrand and intrastrand dimers and so on in a DNA molecule. This is quite different from the effects of ionizing radiation (IR) like Gamma radiation, which being high energy photon, can potentially directly interact with DNA, cause ionization and lead to strand break type of damage. Due to relevance of UV-C radiation in human skin cancer, this

study was essentially focused on UV-C induced genome instability. However, Gamma radiation was also used in one set of experiments to serve as a standard.

UV-C (100 - 290 nm) is the most harmful fraction of UV radiation (Haseltine *et al.*, 1986, Matsunaga *et al.*, 1991, Ravanat *et al.*, 2001). Available information regarding the manner in which the UV-C radiation damages the DNA suggests that UV-C induces dimeric photoproducts (Douki *et al.*, 2003a), oxidized purine and pyrimidine nucleotides (Ravanat *et al.* 2001; Douki *et al.*, 2003b) and small number of SSB in DNA (Miguel and Tyrrell 1986; WHO 1994). Among the dimeric photoproducts, CPD (Matsunaga *et al.*, 1991) and 6-4 PP and their Dewar isomers, other nucleotide dimers and adenine dehydrodimer are documented (Haseltine, 1986; Ravanat *et al.*, 2001; Douki *et al.*, 2003b). A few or all of these damages induced in the DNA can cause the genome to become unstable and, hence, be potential mutagenic precursors if left unrepaired or misrepaired.

In order to study the effect of UV-C radiation on pMTa4 DNA, the plasmid was irradiated with UV-C radiation *in vitro*. The doses of radiation were chosen based on the biological significance of the radiation at that wavelength. The DNA was thus irradiated with 1.2, 2.4, 3.6, 4.8 and 6 $J.m^{-2}$ of UV-C radiation.

Upon electrophoresing pMTa4 DNA immediately after irradiation with UV-C *in vitro* and in dark, that is, in repair non-permissive (R^-) conditions, an increase was observed in the band intensities of the OC forms of the plasmid, when compared with the unirradiated control pMTa4 DNA (Fig. 3.6). This indicates that UV-C irradiation caused induction of SSB in the pMTa4 DNA. However, UV-C is a low energy source of radiation which cannot normally induce SSB by direct action. UV-C is known to cause formation of CPD and other kinds of distortions in the DNA. Therefore, it is likely that these changes induced in the DNA caused induction of SSB in pMTa4 DNA, which was seen as an increase in the band intensity of the OC form. It is also notable that no L form appeared. This is a clear indication that in the dose range selected for the study, UV-C was unable to induce DSB or that the SSB induced were sparsely placed. Otherwise, the two proximal SSB could potentially get converted to DSB causing the appearance of the L form of pMTa4 on the gel.

Under *in vitro* experimental condition in which aqueous solution of pMTa4 DNA was exposed to UV-C radiation, there existed no repair system. Therefore, even under repair permissive (R^+) conditions, no change in the status of UV-C induced damage to pMTa4 DNA is expected. This was experimentally verified by repair incubating UV-C exposed pMTa4 DNA at 37 °C for 60 min and observing change in the band intensity of CC and OC bands. As observed from the Fig. 3.11, the dose dependent increase persisted even under R^+ condition, indicating that repair incubation had no effect under *in vitro* condition on UV-C induced DNA strand breaks.

The effect of UV-C radiation on pMTa4 DNA was also studied *in vivo*. pMTa4 DNA was transformed into two strains of *E. coli*, viz. the wild type strain, AB1157 and *recF* mutant strain, JC9239 as described (§ 2.8.) (Fig. 3.3). Then, the cells were subjected to UV-C irradiation. It was observed that when the plasmids were isolated in R^- conditions (§ 2.15.3.1.) and subjected to AGE, UV-C irradiated pMTa4 DNA showed an increase in the band intensities of the OC form in both the wild and the *recF* mutant strains (Figs. 3.7 and 3.9). This result indicated that the cellular repair system was unable to repair damage induced by UV-C radiation. The cellular system is, however, known to repair damages, which are induced by UV-C radiation *in vivo* in R^+ conditions (Oguma *et al.* 2001; Burger *et al.* 2002). Therefore, the AB1157 and JC9239 cells were also subjected to post-irradiation repair incubation, kept at 37 °C in the presence of light, for 60 min (R^+). pMTa4 DNA was isolated afterwards and analyzed by AGE. In this case, the results obtained for two strains of *E. coli* were different. For the AB1157 strain, the band intensity increase observed after UV-C irradiation in R^- condition disappeared in R^+ condition (Fig. 3.8). However, the band intensity increase observed after UV-C irradiation persisted for the JC9239 strain even in R^+ condition (Fig. 3.10). Since the *recF* mutant is essentially an isogene of the wild type strain except for the *recF* gene, hence, it is an indication that the presence of this gene must have helped in the repair of the SSB caused by the UV-C radiation in the wild AB1157 strain.

The study was extended by performing a series of experiments to monitor the influence of duration of R^+ on repair of UV-C induced SSB *in vitro* as well as *in vivo* condition for wild

and *recF* strains for all dose points. For the *in vitro* investigation, aqueous solution of plasmid isolates were irradiated with UV-C, repair incubated (R^+) for 15 and 30 min and then analyzed by AGE. For *in vivo* experiments, wild and *recF* cultures harboring pMTa4 were irradiated and subjected to post-irradiation repair incubation (R^+) for 15 and 60 min before isolation of plasmid and analyzed by AGE as described. As expected, under *in vitro* exposure conditions, the band intensity increase observed in both the CC and OC forms as a result of UV-C irradiation remained invariant for increasing period of R^+ incubation indicating no repair of SSB (Fig. 3.12). Under *in vivo* exposure condition the wild strain showed a sharp decline in band intensity of OC and CC forms in 15 min of R^+. The decline remained constant up to 60 min (Fig. 3.12). The result suggests that the pace of repair of inflicted SSB was rather fast in the wild type and, perhaps, all SSB were completely repaired in 15 min of R^+. In *recF* mutant, on the other hand, the pixel density of OC declined only marginally after 15 min of R^+ and maintained the level for up to 60 min suggesting poor repair of SSB in *recF* mutant in line with the earlier observation (Fig. 3.12).

With the increase in band intensity of the OC form of pMTa4 DNA following UV-C irradiation, a corresponding decrease in the band intensity of CC form of pMTa4 DNA was expected, thereby indicating that induction of SSB in the CC form of pMTa4 DNA converted them to OC form. However, contrary to expectations, the CC form also showed, though smaller in magnitude, an increase in the band intensity induced by UV-C radiation in *in vitro* as well as repair non-permissive *in vivo* conditions, of both the wild and *recF* mutant strains (Fig. 3.6, 3.7 and 3.9), suggesting a common underlying mechanism inducing these changes. In the *in vitro* experiments, equal volumes of pMTa4 DNA were exposed to UV-C radiation, electrophoresed and analyzed as described. If we suggest the formation of SSB, then, one could expect induced SSB to convert the CC form of the pMTa4 DNA to the OC form. This would be seen on the electropherogram as an increase in the band intensities of OC form with a corresponding decrease in CC form of pMTa4 DNA. However, our results showed, although smaller in magnitude, simultaneous increase in the band intensities of CC form of pMTa4 DNA. The quantity of plasmid loaded in the wells was carefully monitored so that one is sure that equal quantities of pMTa4 DNA were loaded. Hence, the only explanation one could suggest to explain the observation is that pMTa4 DNA

intercalated more ethidium bromide (EB) after UV-C irradiation. Increased EB intercalation would increase the pixel density of the DNA being recorded for quantification even when the actual quantity of DNA in that band did not increase. EB intercalation in the relaxed forms, namely, the OC and L forms is 1.4 times more as compared with the compact form, eg. CC form of SV40 DNA (Jones *et al.*, 1993; Gulston *et al.*, 2002). This suggests that UV-C was inducing conformational relaxation in the CC form of pMTa4 DNA that caused an increase in the band intensity of the CC form of the pMTa4 DNA.

The conformational relaxation caused by the UV-C radiation is not a result of the strand breaks in pMTa4 DNA *in vitro*, as no conformational relaxation was seen following strand breaks induced by the γ-radiation (Humtsoe *et al.*, 1998), lithium swift ions (Humtsoe *et al.*, 2003) or radiomimetic chemicals like Fenton's reagent and Haber Weiss' reagent (Odyuo and Sharan, 2005). However, recent investigations into the effect of UV-C radiation on DNA has revealed that DNA can undergo tertiary structural changes as a result of exposure to UV-C radiation (Kurosaki *et al.*, 2003). Some studies have shown possible alternate DNA conformation that covalent damages and NT mismatch induces (Isaacs and Spielmann, 2004). Investigation into the direct influence of UV-C on the conformation of DNA have revealed that DNA double helix indeed unwinds by ~9° and the helical axis bends by ~30° due the formation of pyrimidine photoproducts (PP) induced by UV-C radiation (Park *et al.*, 2002). In addition to the formation of PP, it has also been observed that UV-C induces inter- and intra-strand crosslinkings in DNA (Douki *et al.*, 2003b). These changes may also contribute in the unwinding of the DNA. This kind of unwinding can take place in any conformational form of the DNA and hence the increase in band intensity of the OC form of the DNA was also observed.

It was now necessary to determine if the increase in the band intensity of the CC form of pMTa4 DNA was indeed a result of UV-C irradiation. In order to do this, we needed pure CC form of the plasmid DNA. From pMTa4 isolates, pure CC form of pMTa4 DNA was recovered as described (§ 2.20). That the CC form of pMTa4 DNA was 100 % pure was confirmed by AGE. To see if higher EB intercalation was taking place in relaxed form of the pMTa4 DNA, precisely measured (both by spectrophotometric and chemical

quantification (§ 2.14), equal quantities of the CC, OC and total pMTa4 isolates were irradiated with increasing doses of UV-C radiation, mixed with equal quantities of EB and loaded on wells punched on freshly cast agarose (§ 2.27). The results showed a dose dependent increase in the pixel density of DNA-intercalated EB (Fig. 3.14) by the CC, OC and total pMTa4 isolates (Fig. 3.15). This indicated that these three forms of pMTa4 DNA indeed exhibited a UV-C dose dependent increase in EB intercalation. It was, therefore, hypothesized that the increase in EB intercalation occurred due to the UV-C induced conformational relaxation of the DNA. Conformational relaxation of DNA can be confirmed by monitoring the hyperchromic shift in DNA under specified conditions (Berg *et al.*, 2002). The conformational relaxation was studied using the total pMTa4 DNA isolate and the purified CC form of the plasmid. The OC form of the DNA was not included in this study. This was because the OC form of the plasmid DNA has a free end. Because of this any torsional stress induced by UV-C in the plasmid form could get released.

The CC form of DNA, on the other hand, has no free ends. Hence, the UV-C induced transient strand relaxation or negative supercoiling introduces additional torsion in the backbone of the plasmid DNA. Irradiation of the CC form of pMTa4 DNA with UV-C was seen to cause dose dependent increase in A_{260} of the pMTa4 DNA (Fig. 3.16). This transient and localized relaxation or negatively supercoiling of pMTa4 DNA facilitates enhanced intercalation of EB. This would result in increase in the band intensity observed in the CC form of pMTa4 DNA with increasing doses of UV-C radiation.

Increase of hyperchromicity was also monitored for total plasmid isolate, that is, pMTa4 isolates containing all the conformational forms of pMTa4 DNA. In this case also increase in the hyperchromicity was observed in response to increasing doses of UV-C radiation (Fig. 3.16). This was expected because, as mentioned, the total plasmid isolate consists of the CC and OC forms of the plasmid in addition to the M forms of the plasmid. Hence, even if the other forms do not show any changes in A_{260}, post UV-C irradiation, the A_{260} increase in the CC form of the pMTa4 DNA would be seen. This resulted in the observed hyperchromic shift.

Attempt was now made to correlate the increase in intercalation of the EB in response to UV-C radiation with corresponding increase in the relaxation of pMTa4 DNA. Both the total and CC form of pMTa4 DNA showed similar trends in hyperchromicity and dot intensity increase (Figs. 3.17 and 3.19 respectively). Therefore, the UV-C dose dependent increase in pixel densities of CC and total plasmids was plotted against the corresponding hyperchromicity increase (Fig. 3.16). The correlation coefficient between the pixel density and hyperchromicity increase was calculated from the results. The plot obtained from the calculation showed an almost linear correlation for both the CC and total pMTa4 DNA. The correlation coefficient was found to be 0.98552 for the pMTa4 isolates and 0.96314 for the CC form (Fig. 3.18 and 3.20 respectively). This confirmed that the UV-C induced relaxation of pMTa4 DNA caused increase in EB intercalation.

In summation, we can say that UV-C irradiation relaxes the pMTa4 DNA due to the induction of the damages into the plasmid. This relaxation is responsible for increased intercalation of EB into the pMTa4 DNA.

As discussed before, the relaxation in the pMTa4 DNA is observable in the CC form of the plasmid DNA as this is the only conformational form of the plasmid that has no free ends. Hence, the torsion that is induced into the DNA backbone is probably responsible for the induction of SSB. This would convert the CC form into the OC form of the plasmid DNA. In addition to this possible process of induction of SSB, other processes might also be responsible for the induction of SSB. For example, oxidative damages to DNA bases or sugars are known to induce hydrolytic cleavage of phosphodiester bonds (Cowan 2001; Zeng and Sheppard 2004). The cleavage may also involve H· atom abstraction of the sugar moiety leading to partial decomposition of 2-deoxyribose unit and release of a base (Gurzadyan and Gorner, 1992). In addition, UV-C is known to make the N-glycosidic bonds of the nucleosides of the DNA to become labile and hence lose the base, hence, generating an abasic site, which would be prone to a phosphodiester break by β^2-elimination reaction. A few or all of these processes may be responsible for the generation of SSB, which is seen in the conversion of the CC form to the OC form of the pMTa4 DNA.

Sodium dodecyl sulfate polyacrylamide gel electrophoresis (SDS-PAGE) analysis was done to observe changes in the protein profiles of the wild strain AB1157 and the *recF* mutant strain JC9239 after UV-C irradiation under R^- and R^+ conditions. (Fig. 3.4). No significant changes were observed in the profiles of the cellular proteins of *E. coli*. Under the experimental condition, it appears that UV-C irradiation was unable to manifest its effect on the cellular proteins.

Total RNA was also isolated from the wild strain, AB1157, and the *recF* mutant, JC9239 under R^- and R^+ conditions and AGE performed. In all experiments only two bands were observed on agarose gels (Fig. 3.13). They are 16S and 5S rRNA bands as these two types of rRNA are present in *E. coli* in overwhelmingly large quantity (Heptinstall, 1998). Due to this, other types of RNA were not visible being relatively very small in quantity. Thus, under the experimental condition effects on total RNA could be monitored by monitoring only 16S and 5S rRNA. The RNA profiles did not show any significant changes as a result of UV-C irradiation in the wild type (Fig. 3.13; panel A). However, the *recF* mutant, JC9239, did exhibit a weak dose dependent down regulation of both 16S and 5S under R^- condition (Fig. 3.13; panel B). The results show that UV-C irradiation was able to down regulate total RNA in *recF* mutant but not in the wild type.

Use of restriction digestion has proved to be very useful for analysis of effect of NT sequence on manifestation of radiation induced damage to plasmid DNA (Humstoe and Sharan, 2004; Humstoe *et al.*, 1998). In this piece of work, restriction digestion of UV-C irradiated and unirradiated pMTa4 DNA was performed in order to observe if UV-C radiation was able to chemically alter some NT and if there was any dependence on the NT motif. If a NT was chemically altered, especially in a restriction site, it would affect the efficiency of restriction digestion. By choosing different RE, different types of NT sequence characteristics have been chosen in this study, that is, RE whose restriction site is GC or TA rich. pMTa4 DNA was irradiated with UV-C (4.8, 9.6, 19.2 and 38.4 J. m^{-2}), the dose at which maximal effects were observed on DNA *in vitro* and restriction digested for the exact time in which the RE was able to completely digest the unirradiated pMTa4 DNA. This time was empirically determined for each of the RE used and was strictly maintained to avoid

any forced or limit digestion so as to monitor even slightest resistance to restriction digestion. The RE used to study the effect of UV-C radiation on pMTa4 DNA were *DraI*, *SspI*, *NciI*, *AccI* and *HaeII*. While *DraI* and *SspI* have AT rich restriction sites, *AccI*, *NciI* and *HaeII* had their restriction sites that were GC-rich. The dose of UV-C to be used for the investigation was selected on the basis of the maximal effect that the UV-C was seen to have on the pMTa4 DNA.

Both *DraI* and *SspI* restricted the plasmid at AT rich sites. *DraI* digestion of unirradiated control pMTa4 DNA produced three bands on the electropherogram (Fig. 3.22). On the other hand, *SspI* digestion of unirradiated control pMTa4 DNA generates two bands on the electropherogram (Fig. 3.26). Upon UV-C irradiation of the pMTa4 DNA, it was observed that with increasing doses of UV-C radiation, some slow migrating bands appeared in the electropherogram with increasing band intensity in a dose dependent manner for *DraI*. Upon comparing the fragment sizes of the bands with the molecular size markers (Fig. 3.24 and 3.28 respectively), it was found that the fragment sizes corresponded with molecular sizes which would be generated if the digestion of the DNA did not take place between two (or more) adjacent fragments as indicated in the figure (3.23 and 3.27, respectively). For *SspI* digestion, irradiation of the pMTa4 DNA with UV-C causes the appearance of the slow migrating (linear) band at dose 2.4 $J.m^{-2}$ (Fig. 3.28). At higher doses, the reappearance of the OC and CC forms was observed with a prominent band of the CC form observed at the highest dose. This indicated that most of the pMTa4 molecules exhibited almost complete resistance to restriction digestion at these doses. The complete resistance to restriction digestion caused the pMTa4 to appear as completely uncut plasmid and hence, the appearance of the CC and OC forms of the pMTa4 DNA.

The resistance to restriction digestion by *DraI* and *SspI* was expected as these two RE have AT-rich restriction sites, which are most prone to damages by UV-C radiation (Matsunaga *et al.*, 1991). Thus, the damages induced by UV-C rays at these sites probably modified the restriction sites by the formation of CPD or 6-4 PP, such that the RE *DraI* and *SspI* were unable to recognize these sites and hence were unable to digest the DNA. Consequently, these uncut fragments appeared as new bands in the gel.

AccI restriction sites are CA-rich. *AccI* digestion of unirradiated pMTa4 DNA causes the appearance of three bands on the electropherogram (Fig. 3.30). Upon UV-C irradiation, an extra band appeared which showed a marginal dose dependent increase in band intensity (Fig. 3.32). This band was found to be of a fragment size that could be obtained if restriction digestion between two fragments of DNA was resisted as indicated in the figure 3.31, indicating that the restriction site was resisting digestion by *AccI* as a result of UV-C radiation. This could happen with *AccI* restriction site containing T residues, which are known to be modified upon UV-C irradiation. Thus, UV-C irradiation modified these NT, which caused resistance to digestion by *AccI* and hence, the appearance of the extra band. This was also expected as the restriction site contains pyrimidines, which might get converted to PP and, hence, induce resistance in restriction digestion.

The RE *HaeII* and *NciI* digest the DNA at restriction sites rich in GC NT. *HaeII* shows four bands in the electropherogram after complete digestion of unirradiated pMTa4 DNA. As expected, *HaeII* showed no resistance in digestion of the pMTa4 DNA upon being UV-C irradiated (Fig. 3.38) and hence no extra bands were obtained (Fig. 3.39). This is an indication that UV-C irradiation did not modify the restriction sites enough to cause changes in the restriction patterns. However, contrary to expectations, restriction with *NciI* seemed to have been resisted at least slightly as a result of UV-C irradiation as indicated by the appearance of two faint additional slow migrating bands on the electropherogram in the UV-C irradiated pMTa4 DNA (Fig. 3.34). The intensities of the slow migrating bands, however, remained almost invariant for the whole dose range used in the investigation. This indicated that the lowest dose (2.4 $J.m^{-2}$) itself caused maximal damages in the NT sequences of the restriction sites and hence, even at higher doses no significant increases in the slow migrating band intensities were observed (Figs. 3.30 and 3.34).

Resistance to restriction digestion as a result of UV-C radiation was expected with RE that recognized AT-rich sites (Sgura *et al.*, 1996). However, *NciI*, which has GC-rich restriction sites, also exhibited resistance, albeit marginal, in restriction digestion (Fig. 3.36) which corresponded with the band sizes as shown in Fig. 3.35. In order to understand the pattern of

digestion, a series of studies were done. First, the percentage of AT in the flanking regions on either side of the restriction sites was calculated to determine if the AT richness of the region had any effect on the observed resistance to restriction digestion. No influence of this was found under the experimental conditions used in this study. Next, the proximity of the TT residues (TT residues having a possibility of forming thymine dimers) to the restriction sites was studied in order to see if the proximity of the UV-C labile TT residues has any effect on UV-C induced alteration in restriction pattern. In this case as well, no direct correlation was observed between the proximity of the TT residues to the restriction sites and the resistance in restriction digestion.

Hence, in search of an alternative explanation, a motif search was done to determine the presence of any specific pattern of NT in the proximal region of the restriction site, which could be responsible for the observed pattern of resistance in digestion. The software AlignAce (AlignAce) was employed for the analysis. It was found that there does exist a motif, the presence of which caused resistance to restriction digestion in our investigation. The motif was found to be as follows:

CCGAGACGGGTCGTCCGCGGGAT

The presence of this motif ensured that the UV-C irradiated pMTa4 DNA was not going to be digested completely, while the absence ensured complete digestion. This motif is predominantly rich in GC residues. It has been found that adjacent C residues served as mutation hotspots in the p53 gene of the human non-melanoma skin cancers and murine tumours (Cadet *et al.,* 2002) upon exposure to solar radiation. Other studies indicate towards the lability of G residues to UV-C radiation. These results show that it is the possible effect of the UV-C radiation on these residues that render the restriction sites resistant to restriction digestion.

The effect of γ-radiation, another quality of radiation known to induce genome instability, on the pMTa4 DNA was also studied *in vivo*. γ-radiation, an IR, is known to produce SSB as well as DSB depending on dose (Sutherland *et al.*, 2000). pMTa4 DNA isolated from γ-

irradiated AB1157 (wild) and XL1 Blue (*recA*) mutant cells in R^- conditions showed a dose dependent break down of CC and OC forms of pMTa4 DNA (Figs. 3.40 and 3.41; panels A). Under R^+ conditions, however, the pMTa4 DNA isolated from AB1157 cells showed no smearing (Fig. 3.40; panel B), indicating that repair of the damage had taken place in this repair proficient strain of *E. coli*. In R^+ conditions in the *recA* mutant, however, the smearing was seen to persist (Fig. 3.41; panel B). This indicates that the *recA* mutant was unable to fully repair the γ-radiation induced damage within 60 min of post-irradiation repair incubation.

To further understand the effect of this quality if IR, the *recA* mutant cells were treated with the cell-free extract obtained from wild type cells (§ 2.7) and their repair patterns were studied in R^- and R^+ conditions (Fig. 3.42). Under R^+ conditions, the pMTa4 DNA was seen to completely abolish the smearing, indicating complete repair (3.42; panel B). This result shows that the presence of the cell-free extract obtained from the wild type cells was able to restore repair in recA mutant. Since the wild type cell is isogenic with the *recA* mutant barring the absence of a functional *recA* gene, therefore, the results indicate that the RecA protein is crucial in the repair of damage induced by γ-radiation. This is in agreement with previously obtained results (Peterson and Côtě, 2004; Sharan *et al.*, 2007).

Thus, studies on the effects of γ- and UV-C radiation on DNA have shown that whereas γ-radiation interacts with the DNA to form SSB and DSB, thereby causing the mutagenic effects, UV-C proceeds by the formation of PP on the DNA. Our studies have revealed that UV-C causes the induction of SSB also on the DNA backbone. It appeared that such SSB were formed by the relaxation of the plasmid backbone. Such relaxation was particularly visible on the CC form of the pMTa4 DNA. Also, restriction mapping of UV-C irradiated pMTa4 DNA have shown that UV-C irradiated pMTa4 DNA have shown that UV-C irradiation introduced some modifications in the restriction sites, which caused the pMTa4 DNA to exhibit resistance to restriction digestion. Such resistance was apparent where the RE *DraI* and *SspI* were used for the digestion. Also, though to a lesser degree, but restriction digestion was also resisted by the RE *NciI* and *AccI*. However, no such resistance was observed for the RE *HaeII*. Analysis of these results showed that presence or absence of

a particular motif was responsible for the observed pattern of resistance to restriction digestion.

Our studies have also shown that the strand break types of damages that were observed in the pMTa4 DNA isolated from the *recA* mutants immediately after γ-irradiation, disappeared upon incubation with the cell-free extract obtained from the wild strain (which contained active RecA protein. This indicated that the RecA protein is crucial in the repair of strand break types of damages.

As detailed earlier, AEBN is an entirely different quality of genotoxin that is also known to be strongly associated with carcinogenesis (IARC, 1985; 2004). Induction of carcinogenesis is ultimate expression of induced genome instability. A large human population across the globe uses betel nut (BN) as a social, traditional and habitual masticatory (IARC, 1985; 2004). Incidence of oropharyngeal cancer is reported to be high in this population suggesting that BN is a potent genome instabilizing agent. Study of AEBN induced genome instability, therefore, is quite relevant to human welfare. AEBN is also a genotoxin that is qualitatively different from UV-C radiation. Therefore, in order to get a more complete picture of genome instability, a detailed investigation into genome instabilizing effects of AEBN has also been carried out in this study.

Effects of AEBN exposure on gross morphology of *E. coli* were studied by transmission EM. In normal conditions, the average length and breadth of *E. coli* cells used in this study was 1.95 and 0.5 μm, respectively. The dimension of AEBN treated *E. coli* cells were significantly enhanced with average length and breadth reaching 3.37 and 0.7 μm, respectively. Even the dividing cells were larger in size (~ 6 and 0.7 μm) following AEBN exposure as compared to their normal counterparts (~2.85 x 0.5 μm) (Fig. 3.43). The cytoplasm of the *E. coli* cells appeared to be more electron dense after treatment with AEBN in comparison to the normal untreated *E. coli* cells (Fig. 3.43). Some of the treated *E. coli* cells showed extensive damage to the cell walls after AEBN treatment (Fig. 3.43; panel c). The cells also acquired a more elongated shape. These morphological changes indicate a stress on the cell as a result of exposure to AEBN. It has been reported that *E. coli*

undergoes an increase in the cell volume as a result of stress like heat (Neidhardt *et al.*, 1987). The stress that the cell had to undergo in the process of growing in the environment containing AEBN, which is quite acidic (pH ~5.0), could be one factor responsible for the induction of the observed changes (Fig. 3.43). It was also noted that the number of dividing cells was considerably low in AEBN treated cultures in comparison to the number of dividing cells found in the non-treated control cells. It is possible that many of the cells might have died under AEBN exposure stress.

AEBN comprises water extractable as well as soluble components of BN. The organic components of BN that gets extracted in AEBN can chemically interact with DNA. Such interaction can potentially produce DNA adducts. If chemical adducts are formed on pMTa4 DNA, the absorption characteristics of the plasmid should change. It has been observed that exposure to AEBN did lead to induction of a red shift, i.e., a rightward shift in the absorption maximum of the plasmid DNA after exposure to AEBN (Fig. 3.45). Changes in spectral characteristics of DNA was observed in terms of its fluorescence (Jiang *et al.*, 2004) and absorption spectra (Geacintov *et al.*, 1991). We observed that the absorption maximum of the DNA shifted from 260.8 nm to 283.20 nm, showing a red shift of 22.4 nm towards the absorption maximum of AEBN (Fig. 3.45). Further, in order to determine if adducts were being formed with AEBN, pure pMTa4 DNA was incubated with increasing concentrations of AEBN at 37 °C *in vitro*, for varying intervals of time (§ 2.17.1.) (Fig. 3.44). From the studies, it was found that 250 µg AEBN formed maximum number of adducts on 4 µg pMTa4 DNA at 37 °C in 30 min. These conditions are defined as saturating conditions.

When chemical groups (adducts) are added onto plasmid DNA either by non-covalent interactions or following covalent linkage logically the molecular size of the plasmid should show an equivalent increase. Consequently, the electrophoretic mobility of the plasmid would be retarded (Péréz-Cabré *et al.*, 2004). This should be observed as a decrease in the mobility of the plasmid DNA band following AGE. This shift is referred to as the mobility shift and has been widely used for the study of the formation of adducts on the DNA. In order to confirm if AEBN formed adducts with pMTa4 DNA under the experimental conditions, mobility shift assays were performed (§ 2.21). The results clearly showed that

the mobilities of both the CC and OC conformational forms of the pMTa4 DNA were retarded in an AEBN dose dependent manner reaching a maximum for both the conformational forms of the plasmid at a concentration of 250 μg AEBN for 4 μg of pMTa4 DNA (Fig. 3.47) for the *in vitro* studies. This confirms the formation of AEBN adducts on DNA. This study also confirmed the spectrophotometric observation that AEBN exposure lead to adduct formation on pMTa4 DNA (Fig. 3.44). For further studies, therefore, the concentration of AEBN chosen was 250 μg per 4 μg pMTa4 DNA in order to ensure that adequate amounts of AEBN was available for the formation of adducts. In the *in vivo* conditions, the mobilities of both the CC and OC forms of the plasmid reached a minimum when the wild type cells were incubated with 1500 μg AEBN per ml culture O/N. This indicates that the maximum number of adducts formed on DNA was at a concentration of 1500 μg AEBN per ml culture. However, in order to ensure that more than saturating concentrations of AEBN were present, 2000 μg AEBN was used as the standard amount of AEBN for the studies.

Some kinetic properties of this interaction were studied. When 4 μg pMTa4 DNA was incubated at 37 °C with 250 μg AEBN for varying intervals of time and the retardations in AGE mobility studied, it was found that adducts were maximally formed when the time of incubation at 37 °C was 30 min (Fig. 3.49). Incubation of the pMTa4 DNA with AEBN for a time period longer than this had very little effect on retardation of mobility of either conformational form of pMTa4 DNA (Fig. 3.49). This indicates that maximum AEBN induced adducts were already formed on available pMTa4 DNA in 30 min. From these results the optimized conditions for further studies were fixed at 250 μg AEBN, 4 μg pMTa4, 37 °C and 30 min incubation. This conditions were used for the study of the various aspects of the formation of adducts of AEBN on pMTa4 DNA.

Two conformational forms of pMTa4 DNA, CC and CC, showed differential AEBN induced adduct formation under identical exposure condition (Figs. 3.47, 3.48 and 3.49). In general the retardation in mobility of OC form of the pMTa4 DNA was more pronounced than the retardation of CC form. This suggests that a greater quantum of the AEBN induced adduct was forming on OC form than CC form under the same exposure condition. As the

OC form of the plasmid is relatively more relaxed or negatively supercoiled in comparison to the CC form (Humtsoe *et al.*, 1998; Humtsoe *et al.*, 2003; Odyuo *et al.*, 2005), AEBN has a higher probability of interaction with the DNA and, hence, more adducts were being formed on this topological form of pMTa4 DNA.

Among the components of AEBN, arecoline, upon nitrosation is known to be converted into several species of electrophilic betel-nut-specific-nitrosamines (BNSA), which interact with the DNA with the help of weak interactions or chemical bonds and hence readily interact and form adducts with the DNA (Sharan, 1996; Chen *et al.*, 1999; Liu *et al.* 2004). Moreover, this is the component of the DNA, which is known to be mutagenic (Balachandran *et al.*, 1995). Due to this reason, the main component of BN known to interact with DNA is considered to be arecoline as also widely reported in the literature (Jeng *et al.*, 1999).

To dwell further into the implications of formation of AEBN adducts on pMTa4 DNA, the same samples were subjected to alkaline agarose gel electrophoresis (AAGE). During AAGE run DNA is in its denatured form. In this condition, CC (native plasmid without any strand break), OC (plasmid DNA with SSB) and L (plasmid with DSB) forms of pMTa4 DNA would denature differently and also migrate differently on the gel. The DNA sample being subjected to alkaline separation condition during AAGE would also face alkaline hydrolysis of labile sites. The results showed an AEBN dose dependent prominent decrease in the CC form accompanied with almost similar increase in OC and L forms (Fig. 3.54). This indicates that AEBN dose dependent SSB as well as DSB were being induced in the plasmid DNA under the experimental conditions when analysed by AAGE. Thus, it can be interpreted that the formation of AEBN adducts on pMTa4 DNA lead to induction of strand breaks on DNA. Essentially only SSB induction was observed (Figs. 3.54). Though analysis of the damage by AGE essentially did not exhibit evidence of induction of DSB, it appears from the AAGE results that besides SSB there were labile sites that after alkaline hydrolysis generated DSB on the plasmid DNA.

With the knowledge about the formation of AEBN adducts on pMTa4 DNA, a study was made in order to find out the stoichiometry of the formation of the adducts. In this context it was necessary to quantify the AEBN adducts being formed on pMTa4 DNA. The electrophoretic mobility of circular plasmid DNA on AGE is a function of conformational as well as molecular size of the plasmid DNA (Herskind, 1996). Thus, it is not possible to correlate gel mobility with molecular size for circular DNA molecules. One needed to create a situation where the mobility of DNA band was dependent only on one factor, that is, the molecular size. This is evident from the fact that despite the CC and OC forms of pMTa4 being of the same size, their mobilities on AGE are distinctly different (Fig. 3.5). Hence, these circular forms of the plasmid are not suitable for calculating changes in the molecular size of the plasmid after adduct formation. However, if the same plasmid is linearized then its AGE mobility will entirely depend on its molecular size or quantum of adducts formed on the plasmid and can be measured with the help of a suitable DNA size marker. Thus, for the L form of pMTa4 DNA retardation in mobility on AGE would be directly proportional to increase in its molecular size due to AEBN induced adduct formation.

Such an approach was taken wherein the plasmid DNA was first linearized by *NcoI* having a single restriction site on pMTa4 DNA (Fig. 2.1). This L form of the plasmid was exposed to increasing concentrations of AEBN and subjected to AGE. The mobility of the L form of the pMTa4 DNA was, as expected, retarded progressively reaching a plateau at a concentration of 150 μg AEBN per 4 μg pMTa4 DNA, and remaining almost at that level for higher concentrations (Fig. 3.53). The total increase in the molecular size was found to be ~ 880 bp under the experimental conditions. The pMTa4 DNA molecule comprises 6173 bp (Table 2, Rakotomahanina *et al.*, 1994). Considering the average molecular weight of a NT as 330 Da and that of BNSA as 126.6 Da, it can be calculated that the increase in the molecular size is by 579,040 Da. This indicates that on an average, ~ 4573 adducts were formed on the DNA. Therefore, it can be calculated that on the 6173 bp long pMTa4 DNA, an adduct is formed every 3 NT approximately under the experimental conditions.

The stability of the AEBN induced adducts on DNA has important implications in the manifestation of possible damage to DNA. Continuing presence of adducts on DNA can

lead to increased rate of mutation and *vice versa*. Therefore, it was important to look into the stability of adducts induced on pMTa4 DNA under our experimental conditions. From our earlier *in vivo* studies it was found that saturating dose of AEBN *in vivo* was 1500 μg AEBN per ml *E. coli* culture (Fig. 3.48). To ensure continuance of the saturating condition in these *in vivo* experiments 2000 μg concentration of AEBN was used. Accordingly, pMTa4 DNA was isolated from the wild strain of *E. coli* harboring pMTa4 DNA from its O/N growth in LB medium supplemented with AEBN at a concentration of 2000 μg AEBN per ml medium. As described in § 2.23, the plasmid isolate was dissolved in water and equal amounts aliquoted out in separate microfuge tubes. The tubes were incubated at RT and the retardation in mobility of the plasmid was studied every 2 h for up to 24 h (Fig. 3.50). The results show maximum retardation in mobility at ~8 h of incubation. From this period onwards, the trend of retardation of mobility reversed and the mobility of plasmid DNA bands progressively regained its normal position, equivalent to unexposed control, after about 24 h. The results clearly show that the AEBN induced adducts on pMTa4 DNA was not stable under the experimental condition. As a result of this, they gradually dissociated from the plasmid DNA.

There can be only one possible explanation for the observed dissociation of AEBN induced adducts on pMTa4 DNA *in vitro*. The adduct would be unstable if it was associated with a NT on the plasmid DNA by non-covalent or weak interactions. Such weak interactions would break easily and progressively lead to dissociation as observed (Fig. 3.50). It is also possible that other components of the BN extract that were present in AEBN interfered with the adducts on pMTa4 DNA and induced or accelerated in sone unkown way leading to dissociation. These two factors might be contributing to the observed instability of AEBN induced adducts on pMTa4 DNA *in vitro*.

This result showing unstable nature of AEBN induced adducts on DNA does not fit into the ultimate effect of BN chewing, which is known to induce high degree of cancer, especially oropharyngeal cancers, in chewers. If the adducts dissociated so easily, there would be no adduct load on DNA. Therefore, there would be less mutation induced by AEBN. All this suggests that BN or AEBN should not be strongly associated with carcinogenesis. In reality,

however, it is known that BN, AEBN or its main alkaloid arecoline, have strong association with human cancer (IARC, 1985; 2004; Sharan, 1996). From this it is obvious that the BN or AEBN induced adduct on DNA might be getting stabilized under *in vivo* condition. It was, therefore, important to look into this aspect as identification of such factors which stabilize AEBN induced adducts on DNA would be useful for cancer therapy and control. Since the factor should be physiological in nature, we chose to study the effects of K^+ and Na^+ ionic concentrations, and pH on the stability of the induced adducts *in vivo* by gel mobility assay.

It was found that when the plasmid isolates were incubated at RT for 24 h in the presence of either K^+ or Na^+ (range: 0.5 to 500 mmol) the retardation in the mobility of the pMTa4 DNA reached its maximum at the lowest dose and persisted (Figs . 3.51; panels A and B). This indicates that the AEBN induced adducts on pMTa4 DNA acquired stability in the presence of as low as 0.5 mmol of either K^+ or Na^+ (Fig. 3.51). It is to be noted that the effective ionic concentration (0.5 mmol) of K^+ or Na^+ conferring stability to AEBN induced adducts was much smaller than the physiological concentration of these ions (1.5 mmol in physiological conditions) (Murray *et al.*, 2003). This brings to fore the fact that in the presence of physiological concentration of Na^+ or K^+ any AEBN induced adduct would become highly stable leading to persistent mutation and consequent carcinogenesis.

The effect of pH on the stability of the AEBN induced adducts on pMTa4 DNA was also studied. For this, plasmids were isolated as described (§ 2.11.) and re-established in Tris-Cl solutions at pH 5, 6, 7 and 8, for a period of 24 h (§ 2.24.). It was observed that the retardation in the mobility of CC and OC bands were completely abolished after 24 h for all pH values monitored in this experiment (Fig. 3.52). This indicates that the AEBN induced adducts on pMTa4 DNA remained unstable in acidic as well as alkaline pH and pH had no effect on conferring stability to the adducts.

In all *in vitro* experiments, it can be noticed that with the treatment of the pMTa4 DNA with AEBN, a decrease in the intensities of both the CC and OC forms of the plasmid were observed with increasing concentrations of AEBN. This decrease was seen to be always

more pronounced for OC form of the plasmid as compared with CC form. The OC form of the plasmid is a relaxed or negatively supercoiled form of plasmid. Due to this, AEBN components have a greater opportunity to interact with this conformational form as compared to the CC form, which is tight or positively supercoiled form. Therefore, OC conformational form of a plasmid shows higher response to any intervention than its CC counterpart. Our investigations consistently show this pattern.

The work was further extended to see if AEBN induced adduct formation on pMTa4 DNA had any preference to a specific NT sequence or motif. As was done in case of UV-C radiation, a set of RE were chosen and the restriction profile of the AEBN exposed pMTa4 was made for each one of them and compared with their respective unexposed controls. All attempts to use RE on pMTa4 isolate mixed with AEBN *in vitro* was unsuccessful due to the resulting pH of the plasmid isolate upon addition of AEBN. The pH of AEBN was highly acidic (approximately 5). Thus, AEBN treated plasmid isolate was highly acidic. At acidic pH neither the plasmid DNA nor any of the RE was stable. Both denatured and precipitated in acidic environment. Therefore, RE digestion study *in vitro* was not possible. Attempt to use DNase I under this experimental condition also did not succeed. Thus, this investigation was carried out under *in vivo* situation. Hence, pMTa4 DNA samples were isolated from AB1157 strain harboring the plasmid after its O/N growth in LB medium supplemented with different concentrations of AEBN. The plasmid isolates from different experimental groups were subjected to restriction digestion for 24 h, the time at which AEBN adducts almost completely dissociated from the plasmid DNA (Fig. 3.50). The pattern of digestion with the different RE was studied.

Upon exposure of pMTa4 DNA to AEBN *in vivo*, restriction digestion of the pMTa4 DNA was resisted in a dose dependent manner, as was apparent from the appearance of additional slow migrating bands in the AEBN exposed pMTa4 DNA. However, the analysis of these bands could not be done on the same lines as that done for the UV-C irradiated pMTa4 DNA. This was because the nature of the slow migrating bands in AEBN exposed pMTa4 DNA was distinctly different from the slow migrating bands in the UV-C exposed pMTa4 DNA. For the UV-C irradiated pMTa4 DNA the molecular size of the additional slow

migrating bands could be correlated with the molecular size of a band that would appear if some restriction sites resisted digestion by the specific RE. However, in case of AEBN treated pMTa4 DNA, the molecular size of the slow migrating bands could not be correlated with any such resitance in restriction digestion. Therefore, the analysis of these bands was not possible on similar lines.

Instead, attempts were made to study the resistance in digestion that was being displayed. Since complete digestion of the pMTa4 DNA yielded 3, 4 and 5 fragments upon digestion with either *AccI, DraI, HaeII* or *NciI* (Figs. 3.55, 3.58, 3.61 and 3.64, respectively), the percentage digestion was calculated from the relative decrease in the band intensities of these bands as a consequence of AEBN exposure. The cumulative band intensities of the completely digested pMTa4, obtained by the KDS 1D software was taken as 100 %. The relative decrease in the intensities of the individual bands was then studied. It was found that with RE *DraI, HaeII and NciI*, AEBN dose dependent decrease in band intensities were observed (Figs. 3.56, 3.59 and 3.62, respectively). The cumulative band intensities also shoed a dose dependent decrease (Figs. 3.57, 3.60 and 3.63, respectively). These results show that AEBN induces a dose dependent increase in resistance to restriction digestion.
The resistance in restriction digestion that was observed indicated that the exposure to AEBN probably induced changes in the restriction sites as a result of which the restriction sites were not recognized by the RE. Also, the increasing resistance in digestion that was observed is an indication that with increasing doses of AEBN, the numbers of changes increased, and consequently, the resistance in digestion.

In case of digestion with *AccI*, however, the resistance in restriction digestion was observed only when the DNA was exposed to the highest concentrations of AEBN used for the present investigation, viz., 2000 µg AEBN per ml culture (Fig. 3.65). A cumulative percentage digestion graph was plotted that indicated that the resistance in digestion was visible only at the concentration of 2000 µg AEBN per ml culture (Fig. 3.66). This indicates that AEBN is probably unable to alter this restriction site to an extent like the other restriction sites and hence complete digestion could take place at lower concentrations of AEBN. These results indicated that NT changes were being induced in the pMTa4 DNA by

exposure to AEBN. Attempts were made now to study the mutagenic effects of the AEBN induced changes on the *E. coli* genome.

With this in mind, genomic DNA was isolated from both treated as well as untreated samples of *E. coli*. Studying the effect of various mutagenic agents on the genome becomes a challenge due to the size of the genome. In order to overcome this problem, some microsatellite regions were chosen where the induction of damages by AEBN would be studied. Microsatellite regions have proved to be excellent regions to target for the study of such genomic instability (Leroy *et al.*, 2002). The microsatellite regions chosen in this study were based on the sequences of the microsatellite regions (Metzgar *et al.*, 2001). These regions in the genome are prone to being damaged by carcinogenic agents as a result of which they serve as ideal models for the study of damages to DNA. Four microsatellite regions were selected and the DNA from the genomic DNA amplified using PCR (Figs. 3.67, 3.69, 3.71 and 3.73). Both strands of the amplicons were sequenced and analysed (Fig. 3.68, 3.70, 3.72 and 3.74).

The NT sequence showed only a few in the earlier parts of the amplified region, which indicates that the differences in the terminal parts of the amplified region. The change was also not found consistently in both the strands. In general and due to technology employed for automated NT sequencing, such changes in NT sequence in the terminal parts of amplicons are taken as false signal or errors of sequencing. As no such consistent NT change on both strands in the central part of amplicons was observed, we interpret that no mutations were induced *per se*. Therefore, AEBN did not seem to induce any mutations in the selected microsatellite region NT studied for the present investigation.

Upon irradiation of the pMTa4 DNA with UV-C, it was found that the retardation in mobility of the CC and OC forms of the plasmid increased as compared to the retardation in the mobility of the unirradiated pMTa4 DNA (Fig. 3.75). This meant that there was an increase in the number of adducts formed in the plasmid in both CC and OC forms of the plasmid as a consequence of UV-C irradiation. Our studies have shown that UV-C induces conformational relaxation as a result of irradiation with UV-C. UV-C induces distortions in

the backbone of the DNA which relaxes the DNA and consequently, the plasmids were seen to intercalate more EB. In a similar manner, the distortions on the backbone of the pMTa4 DNA caused the DNA to interact with and form greater numbers of AEBN adducts on itself.

Our results thus indicated that UV-C irradiation apparently increased the numbers of adducts formed on the DNA. We then tried to determine the extent of increase in molecular size. For this purpose, the pMTa4 DNA was linearized and allowed to form adducts prior to and after irradiation with 6 $J.m^{-2}$ UV-C (§ 2.21). Upon UV-C irradiation, the increase in the molecular size of the L band observed was ~ 1300 bp as compared to ~ 880 bp increase in the unirradiated L form of the pMTa4 DNA (Fig. 3.76). This is indicative of an increase in molecular size by 855,400 Da. This indicates that on an average, 6756 adducts form on the DNA as compared to ~ 4573 adducts formed on the piece of DNA. Since the size of the DNA is 6173 bp, therefore, on an average, an adduct is formed every 2 NT. On unirradiated pMTa4 DNA, an adduct is formed every 3 NT approximately. Therefore, upon irradiation, as expected, the numbers of adducts formed on the pMTa4 DNA increases. On the basis of our findings, we can say that UV-C irradiation of the pMTa4 DNA induces conformational relaxation in the DNA backbone. Such relaxation exposes more of the DNA backbone and hence, the number of adducts formed increases.

CONCLUSION

From the studies the following conclusions can be drawn:

Features of the UV-C induced genomic instability:

1) UV-C was found to induce conformational relaxation in the pMTa4 DNA backbone in both the *in vitro* as well as *in vivo* conditions in the wild and *recF* mutant strains of *E. coli*.
2) The damages induced by UV-C were found to be repaired in the wild strain upon repair incubation. However, no repair was observed *in vitro* or in *recF* mutant strains.
3) Torsional strain was induced by UV-C which resulted in the formation of strand breaks in the backbone of the pMTa4 DNA.

4) The pMTa4 DNA showed a dose dependent resistance in restriction digestion by the restriction endonucleases *DraI* and *SspI* upon irradiation with UV-C.
5) UV-C irradiation of pMTa4 DNA was found to cause marginal resistance in restriction by the restriction endonucleases *AccI* and *NciI*. However, no dose dependence was observed. The resistance was found to reach saturation at the lowest dose, viz. 2.4 $J.m^{-2}$ and hence, no dose dependence was observed.
6) UV-C irradiation, however, was found to induce no resistance in restriction digestion of pMTa4 DNA by the restriction endonuclease *HaeII*.
7) Analysis of the results showed the presence of a motif CCGAGACGGGTCGTCCGCGGGAT at the restriction site to be decisive in determining if UV-C irradiation would introduce resistance in restriction digestion at that site.

Features of AEBN induced genomic instability:

1) AEBN was found to form adducts on the DNA.
2) The number of adducts formed on the OC form of pMTa4 DNA was higher than that formed on the CC form of pMTa4 DNA.
3) The adducts were formed by non-covalent interaction(s) with DNA.
4) The adducts were unstable in nature.
5) The presence of Na^+ and K^+ ions was found to stabilize the adducts.
6) One adduct was formed approximately every 3 NT.
7) Interaction with AEBN was found to cause gross structural changes in the morphology of the *E. coli* cells.

Effect of UV-C priming on the formation of AEBN induced adducts:

1) UV-C priming increased AEBN induced adduct formation on DNA.
2) UV-C priming increased the frequency of adducts formed from approximately 3 NT to an adduct approximately every 2 NT on DNA.

References

Aaltonen, L. A., Peltomaki, P., Leach, F. L., Sistonen, P., Pylkkanen, L., Mecklin, J.-P., Jarvinen. H., Powell. S. M., Jen, J., Hamilton, S. R., Petersen, G., Kinzler, K. W., Vogelstein, B., and de la Chapelle. A. (1993) Clues to the pathogenesis of familial colorectal cancer, *Science*, **260**, 812-816.

Alam, M. Z. and Oligaki, S. (2002) Role of hydrogen peroxide and hydroxyl radical in producing the residual effect of ultraviolet radiation. *Water Environmental Research*, **74**, 248-255.

AlignAce: http://atlas.med.harvard.edu/cgi-bin/alignace.pl

Ames, B. N., Gold, L. S. & Willet, W. C. (1995) The causes and prevention of cancer, *Proceedings of the National Academy of Sciences, USA*, **92**, 5258–5265.

Auerbach A.D. (1992) Fanconi anaemia and leukaemia: tracking the genes. *Leukaemia*, **6**, 1-4.

Ausubel, F. M., Brent, Editor, R., Kingston, R. E., Moore, D. D., Seidman, J. G., Struhl, K. and Smith, J. A. (1995) **Short Protocols in Molecular Biology**, John Wiley & Sons, USA.

Balachandran, B. and Sharan, R. N. (1995) Induction of mutations by different extracts of betel nut and radiation: Their implication in Carcinogenesis. In, **Radiation Research 1895-1995.** Hagen, U., Jung, H. and Streffer, C. (eds.), , U. S, Strutz A. G., Wuizburg, vol.1, pp. 164.

Berg, J. M., Tymoczko, J. L. and Stryer, L. (2002) **Biochemistry** (5th edition), W. H. Freeman & Co., New York, USA.

Beukers, R. and Berends, W. (1960) Isolation and identification of the irradiation products of thymine. *Biochimica et Biophysica Acta*, **41**, 550-551.

Bhattacharjee, C. and Sharan, R. N. (2006) UV-C radiation induced conformational relaxation of pMTa4 DNA in Escherichia coli may be the cause of single strand breaks, *International Journal of Radiation Biology*, **81(12)**, 919-927.

Bhide, S. V., Shivapuraker, N. M., Gothoskar, S. V. and Ranadive, K. J. (1979) Carcinogenicity of betel quid ingredients: feeding mice with aqueous extract and the polyphenol fraction of betel nut. *British Journal of Cancer*, **40**, 922-926.

Bichara, M., Pinet, I., Lambert, I. B. and Fuchs, R. P. P. (2007) RecA-mediated excision repair: a novel mechanism for repairing DNA lesions at sites of arrested DNA synthesis. *Molecular Microbiology*, **65**, 218-229.

Birrell, G. W., Giaever, G., Chu, A. M., Davis, R. W. and Brown, J. M. (2001) A genome-wide screen in *Saccharomyces cerevisiae* for genes affecting UV radiation sensitivity. *Proceedings of the National Academy of Sciences, USA*, **98**, 12608-12613.

Blaisdell, J. O. and Wallace, S. S. (2001) Abortive base-excision repair of radiation-induced clustered DNA lesions in *Escherichia coli*, *Proceedings of the National Academy of Sciences, USA*, **98**, 7426–7430.

Blakely, E. A., and Kronenberg, A. (1998) Heavy-ion radiobiology: new approaches to delineate mechanisms underlying enhanced biological effectiveness. *Radiation Research*, **150**, 126-145.

Bohr, V. A. and Dianov, G. L. (1999) Oxidative DNA damage processing in nuclear and mitochondrial DNA. *Biochimie*, **81**, 155-160.

Boveri, T. (1929) In, **The Origin of Malignant Tumors**. Williams & Wilkins Publishing Co.

Bradford, M. (1976) A rapid and sensitive method for the quantitation of microgram quantities of protein utilizing the principle of protein-dye binding. *Annals in Biochemistry*, **72**, 248-254.

Brentnall, T. A., Crispin, D. A., Bronner, M. P., Cherian, S. P., Hueffed, M. Rabinovitch, P. S., Rubin, C. E., Haggitt, R. C. and Boland, C. R. (1996) Microsatellite Instability in Nonneoplastic Mucosa from Patients with Chronic Ulcerative Colitis. *Cancer Research*, **56**, 1237-1240.

Bridges B. A. (1969) Mechanisms of radiation mutagenesis in cellular and subcellular systems, *Annual Reviews of Nuclear Science*, **19**:139-178.

Britt A. B. (1995) Repair of DNA damage induced by ultraviolet radiation, *Plant Physiology*, **108**, 891–896.

Britt, A. B. (1996) DNA damage and repair in plants, *Annual Reviews in Plant Physiology Plant Molecular Biology*, **47**, 75–100.

Budworth, H., Dianova, I. I., Podust, V. N. and Dianov, G. L. (2002) Repair of clustered DNA lesions. Sequence-specific inhibition of long-patch base excision repair by 8-oxoguanine. *Journal of Biological Chemistry*, **277**, 21300–21305.

Bullock, W. O., Fernandez, J. M., and Short, J. M. (1987) XL1-Blue: A high efficiency plasmid transforming recA Escherichia coli strain with β-galactosidase selection, *Biotechniques*, **5**, 376-379.

Burger, A., Raymer, J. and Bockrath, R. (2002) DNA damage-processing in *E. coli*: Ongoing protein synthesis is required for fixation of UV-induced lethality and mutation. *DNA Repair*, **1**, 821-831.

Burton, K. (1968) Determination of DNA concentration with diphenylamine, *Methods in Enzymology*, **12**, 163-166.

Cadet, J., Anselmino, C, Douki, T. and Voituriez L. (1992) Photochemistry of nucleic acids in cells. *Journal of Photochemistry and Photobiology*, **15**, 277-298.

Cadet, J., Douki, T, Pouget, J-P, Ravanat, J-L and Sauvaigo, S. (2001) Effects of UV and Visible Radiations on Cellular DNA, *Current Problems in Dermatology (Basel)*, Thiele, J. and Elsner, P. (eds.), In, **Oxidants and Antioxidants in Cutaneous Biology**, Karger, vol. 29, pp. 62–73.

Chang, M. C., Wu, H. L., Lee, J. J., Lee, P. H., Chang, H. H., Hahn, L. J., Lin, B. R., Chen, Y. J. and Jeng, J. H. (2004) The induction of prostaglandin E2 production, interleukin-6 production, cell cycle arrest, and cytotoxicity in primary oral keratinocytes and KB cancer cells by areca nut ingredients is differentially regulated by MEK/ERK activation. *Journal of Biological Chemistry*, **279**, 50676-50683.

Chattopadhyay, I., Kapur, S., Purkayastha, J., Phukan, R., Kataki, A., Mahanta, J. and Saxena, S. (2007) Gene expression profile of esophageal cancer in North East India by cDNA microarray analysis, *World Journal of Gastroenterology*, **13**, 1438-1444.

Chen, C-L., Chi, C-W., Chang K-W. and Liu T-Y. (1999) Safrole-like DNA adducts in oral tissue from oral cancer patients with a betel quid chewing history. *Carcinogenesis*, **20**, 2331-2334.

Clark, A. J. (1991) rec genes and homologous recombination proteins in *Escherichia coli*. *Biochimie*, **73**, 523-532.

Clark, A. J. and Margulies, A. D. (1965) Isolation and characterization of recombination deficient mutants of *E.coli*. *Proceedings of the National Academy of Sciences, USA*, **53**, 451 – 459.

Clark, A. J., Volkert, M. R. and Margossian, L. J. (1979) A role for *recF* in repair of UV damage to DNA. *Cold Spring Harbor Symposium on Quantitative Biology*, **43**, 887–892.

Clutton, S. M., Townsend, K. M. S., Goodhead, D. T., Ansell, J. D. and Wright, E. G. (1995) Differentiation and delayed cell death in embryonal stem cells exposed to low doses of ionising radiation. *Cell Death Differentiation*, **3**, 141-148.

Courcelle J., Carswell-Crumpton C., and Hanawalt P. C. (1997) *recF* and *recR* are required for the resumption of replication at DNA replication forks in *Escherichia coli. Proceedings of the National Academy of Sciences, USA,* **94**, 3714–3719.

Courcelle, J. and Hanawalt, P. C. (2001) Participation of recombination proteins in rescue of arrested replication forks in UV-irradiated *Escherichia coli* need not involve recombination. *Proceedings of the National Academy of Sciences, USA,* 98, 8196–8202.

Courcelle, J., Carswell-Crumpton, C. and Hanawalt, P. C. (1997) *recF* and *recR* are required for the resumption of replication at DNA replication forks in *Escherichia coli. Proceedings of the National Academy of Sciences, USA,* **94**, 3714-3719.

Cowan, J. A. (2001) Chemical nucleases. *Current Opinions in Chemical Biology*, **5**, 634-642.

Cox, M. M. (1999) Recombinational DNA repair in bacteria and the RecA protein. *Progress in Nucleic Acid Research Molecular Biology*, **63**, 311-366.

Cox, M. M. (2007) Regulation of Bacterial RecA Protein Function, *Critical Reviews in Biochemistry and Molecular Biology*, **42**, 41-63.

Cox, M. M. (2007) Regulation of Bacterial RecA Protein Function. *Critical Reviews in Biochemistry and Molecular Biology*, **42**, 41-63.

Crabbe, L., Jauch, A., Naeger, C. M., Holtgreve-Grez, H. and Karlseder, J. (2007) Telomere dysfunction as a cause of genomic instability in Werner syndrome. *Proceedings of the National Academy of Sciences, USA*, **104**, 2205-2210.

Dave, B. T., Trivedi, A. H. and Adhvaryu, S. C. (1992) Role of areca nut consumption in the cause of oral cancers. *Cancer*, **70**, 10717-10723.

DeWitt, S. K. and Adelberg, E. A. (1962) The occurrence of a genetic transposition in a strain of *Escherichia coli. Genetics*, **47**, 577-585.

Douki, T., Renaud-Angelin, A., Cadet, J. and Sage, E. (2003a) Bipyrimidine photoproducts rather than oxidative lesions are the main type of DNA damage involved in the genotoxic effect of solar UVA radiation. *Biochemistry*, **42**, 9221-9226.

Douki, T., Laporte, G. and Cadet, J., (2003b) Inter-strand photoproducts are produced in high yield within A-DNA exposed to UV-C radiation. *Nucleic Acid Research*, **31**, 3134-3142.

Dronkert, M. L., and Kanaar, R. (2001) Repair of DNA interstrand cross-links. *Mutation Research*, 486, 217-247.

Duell, T., Lengfelder, E., Fink, R., Giesen, R. and Bauchinger, M. (1995) Effect of activated oxygen species in human lymphocytes. *Mutation Research*, **336**, 28-39.

Emerit, I. and Cerutti, P. A. (1981) Tumour promotor phorbol- 12-myristate- 13-acetate induces chromosomal damage via indirect action. *Nature*, **293**, 144-145.

Field, D. and Wills, C. (1998) Abundant microsatellite polymorphism in *Saccharomyces cerevisiae*, and the different distributions of microsatellites in eight prokaryotes and *S. cerevisiae*, result from strong mutation pressures and a variety of selective forces. *Proceedings of the National Academy of Sciences, USA*, **95**, 1647-1652.

Friedberg, E. C., Walker, G. C. and Siede, W. (1995) **DNA repair and mutagenesis**, ASM Press, Washington DC.

Gaisor, S. L., Olivares, H., Ear, U., Hari, D. M. and Weichselbaum, R. and Bishop, D. K. (2001) Assembly of Rec-A like recombinases: Distinct roles for mediator proteins in mitosis and meiosis. *Proceedings of the National Academy of Sciences, USA*, **98**, 8411-8418.

Gaskell, M. (2004) Comparison of the mutagenic activity of the benzene metabolites, hydroquinone and para-benzoquinone in the *supF* forward mutation assay: A role for minor DNA adducts formed from hydroquinone in benzene mutagenicity, *Mutation Research*, **554**, 387-398.

Geacintov, N. E., Cosman, M., Mao, B., Alfano, A., Ibanez V. and. Harvey R. G. (1991) Spectroscopic characteristics and site I/ site II classification of *cis* and *trans* benzo[a]pyrene diolepoxide enantiomer-guanosine adducts in oligonucleotides and polynucleotides. *Carcinogenesis*, **12**, 2099-2108.

Giorno, R and Sauerbier, W. A (1976) Radiological analysis of the transcription units for heterogeneous nuclear RNA in cultured murine cells, *Cell.* **9**, 775–783.

Goodhead, D. T. (1994) Initial events in the cellular effects of ionizing radiations: Clustered damage in DNA. *International Journal of Radiation Biology*, **65**, 7-17.

Gorgojo, L. and Little, J.B. (1989) Expression of lethal mutations in the progeny of irradiated mammalian cells. *International Journal of Radiation Biology*, **55**, 619-630.

Grady, W. M. (2006) In, **Genomic instability and colorectal cancer**, Vol. 2, Number 2, Current Colorectal Cancer Reports, pp. 66-71.

Gulston, M., Fulford, J., Jenner, T., Delara, C. and O'Neill, P. (2002) Clustered DNA damage by γ-irradiation in human fibroblasts (HF19), hamster (V79-4) cells and plasmid DNA is revealed as Fpg and Nth sensitive. *Nucleic Acid Research*, **30**, 3464-3472.

Gurzadyan, G. G. and Gorner, H. (1992) Base release from DNA and polynuceotide upon 193 nm laser excitation. *Photochemistry and Photobiology*, **56**, 371-378.

Hancock, J.M. (1995) The contribution of slippage-like processes to genome evolution. *Journal of Molecular Evolution*, **41**, 1038-1047.

Harm, W. (1980) **Biological Effects of Ultraviolet Radiation**, IUPAB Biophysics Series I, Cambridge University Press, Cambridge.

Hartman, P. S., Hevelone, J., Dwarakanath, V. N. and Mitchell, D. L. (1989) Excision repair of UV radiation-induced DNA damage in *Caenorhabditis elegans*. *Genetics* **122**, 379-385.

Haseltine, W. A. (1986) UV light repair and mutagenesis revisited, *Cell*, **33**, 13-17.

Hayat, M. A. (1985) In, **Basic techniques for transmission electron microscopy**, Academic Press, Inc., USA.

He, Y. Y. and Hader, D. (2002) Reactive oxygen species and UV-B: effect on cyanobacteria. *Photochemical and Photobiological Sciences*, **1**, 729-736.

Heptinstall, J. (1998) RNA isolation and characterization protocols, In, **Methods in Molecular Biology**, vol. 86, Rapley, R. and Manning, J. (eds.) pp. 47-51.

Herskind, C. (1987) Single-strand breaks can lead to complex configurations of plasmid DNA *in vitro*. *International Journal of Radiation Biology*, **52**, 565-575.

Hoeijmakers, J. H. (2001) Genome maintenance mechanisms for preventing cancer. *Nature*, **411**, 366-374.

Holley, W. R., Chatterjee, A., Mian, I. S. and Rydberg, B. (1998) Theoretical modeling of radiation effects. In, **Trends in Radiation and Cancer Biology**, Sharan, R. N. (ed.), International Co-operation Bilateral Seminars Series, **29**, pp. 12-21, Forchungszentrum Juelich, GmbH, Germany.

Horii, T., Ogawa, T. and Ogawa, H. (1980) Organization of the *recA* gene of *E. coli*. *Proceedings of the National Academy of Sciences, USA*, **77**, 313-317.

Horii, Z., and Clark A. J. (1973) Genetic analysis of the RecF pathway of genetic recombination in *Escherichia coli* K-12: isolation and characterization of mutants. *Journal of Molecular Biology*, **80**, 327–344.

Humtsoe, J. O. and Sharan, R. N. (2004) Molecular radiobiology: Plasmid pMTa4 as a tool for studying effects of γ-radiation *in vitro* and *in vivo*. In **Radiobiology and Bio-Medical Research**, edited by Mishra, K. P. (, Narosa Publishing House, New Delhi, 51-61.

Humtsoe, J. O., Schneeweiss, F. H. A., Srivastava, A., Sarma, A. and Sharan, R. N. (2003) Biological effects induced by swift heavy ions of Lithium on aqueous solution of plasmid pMTa4. *Radiation Effects and Defects in Solids*, **158**, 603-607.

Humtsoe, J. O., Schroeder, C. H. and Sharan, R. N. (1998) Is there a relationship between nucleotide sequence and radiation induced DNA damage? In, **Trends in Radiation and Cancer Biology**, edited by R. N. Sharan (Juelich, Forschungszentrum Juelich GmbH), International Co-operation Bilateral Seminars series, **29**, 29-32.

IARC (1982) On the evaluation of the carcinogenic risk and industries associated with cancer in humans. In, **International Agency for Research on cancer**. Supplement 4. Lyon, France.

IARC (1985) IARC Monographs on the evaluation of carcinogenic risk of chemicals to Humans. Vol. 37. Tobacco habits other than smoking; Betel quid and areca nut chewing; and some related Nitrosamines. In, **International Agency for Research on Cancer**, Lyon, France. 5-269.

IARC (1987). Overall evaluation of Carninogenicity: An updating of IARC Monographs; in Monographs of evaluation of carcinogenic risk of chemicals to humans. Supplement 7. Volumes 1 to 42. In, **International Agency for Research on Cancer**, Lyon, France.

IARC (2004) Betel-quid and areca-nut chewing and some areca nut related nitrosamines, Vol 85, In, **International Agency for Research on Cancer,** Lyon, France.

Ionov, Y., Peinado, M. A., Malkhosyan, S., Shibata, D. and Perucho, M. (1993) Ubiquitous somatic mutations in simple repeated sequences reveal a new mechanism for colonic carcinogenesis. *Nature*, **363**, 558–561.

Isaacs, R. and Spielmann, H. P. (2004) A model for initial DNA lesion recognition by NER and MMR based on local conformational flexibility, *DNA Repair*, **3**, 455- 464.

Jackson, A. L., Chen, R. and Loeb, L. A. (1998). Induction of microsatellite instability by oxidative DNA damage. *Proceedings of the National Academy of Sciences, USA*, **95**, 12468-12473.

Jeng, J. H., Hahn, L. J., Lin, B. R., Hsieh, C. C., Chan, C. P. and Chang, M. C. (1999) Effects of areca nut, inflorescence piper betle extracts and arecoline on cytotoxicity, total and unscheduled DNA synthesis in cultured gingival keratinocytes. *Journal of Oral Pathology and Medicine*, **28**, 64-71.

Jeng, J. H., Kuo, M. L and Kuo, M. Y. P. (1994) Genotoxic effects of betel quid ingredients on oral mucosa fibroblast *in vitro*. *Journal of Dentology Research*, **73**, 1043-1049.

Jiang, G., Jankowiak, R., Grubor, N., Banasiewicz, M., Small, G. J., Skorvaga, M., Houten, B. V., and States, C. J. (2004) Supercoiling DNA promotes formation of intercalated *cis*-N2-deoxyguanine adduct and base-stacked *trans*-N2-deoxyguanine adduct by (+)-7R,8S-dihydrodiol-9S,10R-epoxy-7,8,9,10-tetra-hydrobenzo[a]pyrene. *Chemical Research in Toxicology*, **17**, 330-339.

Jiricny, J. (1998). Eukaryotic mismatch repair: an update, *Mutation Research*, **409**, 107-121.

Jones, G. D. D., Milligan, J. R., Ward, J. F., Calabro-Jones, P. M. and Aguilera, J. A. (1993) Yield of strand breaks as a function of scavenger concentration and LET for SV40 irradiated with ^{4}He ions. *Radiation Research*, **136**, 190-196.

Kadhim, M. A., MacDonald, D. A., Goodhead, D. T., Marsden, S. and Wright, E. G. (1992) Transmission of chromosomal instability after plutonium a-particle irradiation. *Nature,* **355**, 738-740.

Kelner, A. (1949) Effect of visible light on the recovery of *Streptomyces griseus* conidia from ultraviolet irradiation injury, *Proceedings of the National Academy of Sciences, USA,* **35**, 73-79.

Kiefer, J. (1990) **Biological Radiation Effects**, Springer-Verlag, Germany.

Klungland A., Rosewell, I., Hollenbach, S., Larsen, E., Daly, G., Epe, B., Seeberg, E., Lindahl, T. and Barnes, D.E. (1999) Accumulation of premutagenic DNA lesions in mice defective in removal of oxidative base damage. *Proceedings of the National Academy of Sciences, USA*, **96,** 13300–13305.

Kolodner, R., Fishel, R. A. and Howard, M. (1985) Genetic recombination of bacterial plasmid DNA: effect of RecF pathway mutations on plasmid recombination in *Escherichia coli. Journal of Bacteriology*, **163,** 1060–1066.

Kondo, S. (1973) Evidence that mutations are induced by errors in repair and replication, *Genetics*, **73**, 109-122.

Kowalczykowski, S. and Eggelston, A. (1994) Homologous pairing and DNA strand exchange proteins. *Annual Reviews in Biochemistry*, **63**, 991-1043.

Kronenberg, A. (1994) Radiation-induced genomic instability. *International Journal of Radiation Biology*, **66**, 603-609.

Kumpawat, K., Deb, S., Roy A. and Chatterjee, A. (2003) Genotoxic effects of raw betel-nut extract in relation to endogenous glutathione levels and its mechanism of action in mammalian cells, *Mutation Research*, **538**, 1-12.

Kurosaki, Y., Abe, H., Morioka, H., Hirayama, J., Ikebuchi, K., Kamo, N., Nikaido, O., Azuma, H. and Ikeda, H. (2003) Pyrimidine dimer formation and oxidative damages in M13 bacteriophage inactivation by ultraviolet C irradiation. *Photochemistry and Photobiology*, **78**, 349-354.

Kuzminov, A. (1999) Recombinational Repair of DNA Damage in *Escherichia coli* and Bacteriophage λ, *Microbiology and Molecular Biology Reviews*, **63 (4)**, 751–813.

Laemmli, U. K. (1970) Cleavage of structural proteins during the assembly of the head of bacteriophage T4. *Nature*, **227**, 680-385.

Lee, C. H., Lee, J. M., Wu, D. C., Hsu, H. K., Kao, E. L., Huang, H. L., Wang, T. N., Huang, M. C. and Wu, M. T. (2005) Independent and combined effects of alcohol intake, tobacco smoking and betel quid chewing on the risk of esophageal cancer in Taiwan. *International Journal of Cancer*, **113**, 475-482.

Lehmann, A. R. (1982) **Cancer Surveys** 1, University Press, Oxford, pp. 93-118.

Lehmann, A. R. (1995) Nucleotide excision repair and the link with transcription. *Trends in Biochemical Sciences*, **20**, 402–405.

Lengauer, C., Kinzler, K. W. and Vogelstein, B. (1998) Genetic instabilities in human cancers. *Nature*, **396**, 643–649.

Leroy, X. J., Leon, K., Hily, J. M. Chaumeil, P. and Branchard, M. (2001) Detection of stability of fingerprinting patterns through in vitro culture by Inter Simple Sequence Repeats. *Theoretical and Applied Genetics*, **102**, 885-891.

Levinson, G., and Gutman, G.A. (1987) Slipped-strand mispairing: a major mechanism for DNA sequence evolution. *Molecular Biology and Evolution*, **4**, 203-221.

Li, C. Y., Little, J. B., Hu, K., Zhang, W., Zhang, L, Dewhirst, M. W. and Huang, Q. (2001) Persistent genetic instability in cancer cells induced by non-DNA-damaging stress exposures. *Cancer Research*, **61**, 428–432.

Lindahl, T. and Wood, R. D. (1999) Quality control by DNA repair, *Science*, **286**, 1897–1905.

Little, J. W. and Mount, D. W. (1982) The SOS regulatory system of *Escherichia coli*, *Cell*, **29**, 11-22.

Loeb, K. R. and Loeb, L. A. (2000) Significance of multiple mutations in cancer. *Carcinogenesis*, **21**, 379-385.

Loeb, L. A. (1991) Mutator phenotype may be required for multistage carcinogenesis. *Cancer Research*, **51**, 3075-3079.

Loeb, L. A. (1994) Microsatellite instability: marker of a mutator phenotype in cancer. *Cancer Research*, **54**, 5059-5063.

Loeb, L. A. (2001). A mutator phenotype in cancer. *Cancer Research*, **61**, 3230-3239.

Longerich, S., Galloway, A. M., Harris, R. S., Wong, C., and Rosenberg, S. M. (1995) Adaptive mutation sequences reproduced by mismatch repair deficiency. *Proceedings of the National Academy of Sciences, USA*, **92**, 12017-12020.

Lui, J. M., Auerbach, A. D., Anderson, S.M. and Green, S. W. (1993) A trial of recombinant human superoxide dismutase in patients with Fanconi anaemia. *British Journal of Haematology*, 85, 406-408.

Lusetti, S.L. and Cox, M.M. (2002) The bacterial RecA protein and the recombinational DNA repair of stalled replication forks. In, **Annual Review of Biochemistry**. Richardson C. (ed.) Annual Reviews, Palo Alto, CA, Vol. 71, pp. 71-100.

Madiraju, M. V. V. S., and Clark, A. J. (1991) Effect of RecF protein on reactions catalyzed by RecA protein. *Nucleic Acids Research*, **19**, 6295–6300.

Madiraju, M. V. V. S., and Clark, A. J. (1992) Evidence for ATP binding and double-stranded DNA binding by *Escherichia coli* RecF protein. *Journal of Bacteriology*, **174**, 7705–7710.

Makrigorgas, G., Adelstein, S. J. and Kassis, A. I. (1990) Auger electron emitters: insights gained from *in vitro* experiments. *Radiation and Environmental Biophysics*, **29**, 75-91.

Matsunaga, T., Hatakeyama, Y., Ohta, M., Mori, T. and Nikaido, O. (1993) Establishment and characterization of a monoclonal-antibody recognising the Dewar isomers of (6-4) photoproducts, *Photochemistry and Photobiology*, **57**, 934–940.

Matsunaga, T., Hieda, K. and Nikaido, O. (1991) Wavelength dependent formation of thymine dimmers and (6-4) photoproducts in DNA by monochromatic UV light ranging from 150-365 nm. *Photochemistry and Photobiology*, **54**, 403-410.

McEntee, K., Weinstock, G. M. and Lehman, I. R. (1979) Initiation of general recombination catalyzed *in vitro* by the recA protein of *Escherichia coli*. *Proceedings of the National Academy of Sciences, USA*, **76**, 1638-1642.

Metzgar, D., Thomas, E., Davis, C., Field, D. and Wills, C. (2001) The microsatellites of Escherichia coli: rapidly evolving repetitive DNAs in a non-pathogenic prokaryote. *Molecular Microbiology*, **39**, 183-190.

Miguel, A. G. and Tyrrell, R. M. (1986) Repair of near-ultraviolet (365 nm) induced strand breaks in *Escherichia coli* DNA. The role of polA and recA gene products. *Biophysical Journal*, **49**, 485-491.

Mitchell, D. L. and Rosenstein, B. S. (1987) The use of specific radioimmunoassays to determine action spectra for the photolysis of (6-4) photoproducts. *Photochemistry and Photobiology*, **45**, 781–786.

Mitchell, D. L., Jen J. and Cleaver, J. E. (1991) Relative induction of cyclobutane dimers and cytosine photohydrates in DNA irradiated in vitro and *in vivo* with ultraviolet-C and ultraviolet-B light. *Photochemistry and Photobiology*, **54**, 741-746.

Mitchell, D. L., Vaughan, J. E. and Nairn, R. S. (1989) Inhibition of transient gene expression in Chinese hamster ovary cells by cyclobutane dimers and (6-4) photoproducts in transfected ultraviolet-irradiated plasmid DNA. *Plasmid*, **21**, 21–30.

Mol, C. D., Parikh, S. S., Putnam, C. D., Lo, T. P. and Tainer, J. A. (1999) DNA repair mechanisms for the recognition and removal of damaged DNA bases. *Annual Review of Biophysics and Biomolecular Structure*, **28**, 101-128.

Morgan, W. F., Day, J. P., Kaplan, M. I., McGhee, E. M. and Limoli, C. L. (1996) Genomic instability induced by ionizing radiation. *Radiation Research,* **146,** 247–258.

Muela, A., García-Bringas, J. M., Seco, C., Arana, I. and Barcina, I. (2002) Participation of oxygen and role of exogenous and endogenous sensitizers in the photoinactivation of Escherichia coli by photosynthetically active radiation, UV-A and UV-B. *Microbial Ecology*, **44**, 354-64.

Murray, R. K., Granner, D. K., Mayes, P. A., Rodwell, V. W. (eds.) (2003) **Harper's Illustrated Biochemistry**, 26th Edition, McGraw-Hill.

NCBI BLAST: http://www.ncbi.nlm.nih.gov.library.vu.edu.au/BLAST/

Neidhardt, F.C, and Van Bogelen, R.A. (1987) In ***Escherichia coli* and *Salmonella typhimurium*: *Cellular and Molecular Biology***. Neidhardt , F.C. (ed.).: American Society for Microbiology, Washington. D.C, pp. 680-691.

Nicoletti, G., De Giovanni, C., Landuzzi, L., Simone, C., Rocchi, P. and Nanni, P. (1992) Induction of myogenic differentiation in human rhabdomyosarcoma cells by ionising radiation, N.W.-dimethylfomamide, and their combination. *British Journal of Cancer,* **65**, 519-522.

Nowell, P. C (1976) The Clonal Evolution of Tumor Cell Populations, *Science* 1976, **194**, 23-28.

O'Neill, P. and Fielden, E. M. (1993) Primary free radical processes in DNA. *Advance in Radiation Biology,* **70**, 421-427.

Odyuo, M. M. and Sharan, R. N. (2005) Differential DNA strand breaking abilities of °OH and ROS generating radiomimetic chemicals and γ-rays: Study of plasmid, pMTa4, *in vitro*. *Free Radical Research*, **39**, 499-505.

Ogawa, T., Wabiko, H., Tsujimoto, T., Horii, T., Masukata, H. and Ogawa, H. (1978) DNA: Replication and Recombination. *Cold Spring Harbor Symposium on Quantitative Biology*, **43**, 909-915.

Oguma, K., Katayama, H., Mitani, H., Morita, S., Hirata, T. and Ohgaki, S. (2001) Determination of pyrimidine dimers in *Escherichia coli* and *Cryptosporidium parvum* during UV light inactivation, photoreactivation and dark repair, *Applied and Environmental Microbiology*, **67**, 4630-4637.

Pacelli, R., Wink, D. A., Cook, J. A., Krishna, M. C., DeGraff, W., Friedman, N., Tsokos, M., Samuni, A. and Mitchell, J. B. (1995) Nitric oxide potentiates hydrogen peroxide-induced killing of *Escherichia coli*. *Journal of Experimental Medicine*, **182**, 1469-1479.

Painter, R. B. (1979) The role of DNA damage and repair in cell killing induced by ionizing radiation. In, **Radiation Biology and Cancer Research**, Meyn, R. E. and Withers, H. R. (eds.), pp. 59-68, Raven press, USA.

Panigrahi, G. B. and Rao, A. R. (1984) Induction of *in vivo* sister chromatid exchanges by arecaidine, a betel nut alkaloid, in mouse bone marrow cells. *Cancer Letters*, **23**, 189-192.

Pariat, T. and Sharan, R. N. (1995) Low dose exposure of diethylnitrosamine affects mice liver Thymidine kinase. *Life Sciences*, **57**, 2431-2437.

Park, H., Zhang, K., Ren, Y., Nadji, S., Sinha, N., Taylor, J-S. and Kang, C. (2002) Crystal structure of a DNA decamer containing a cis-syn thymine dimer. *Proceedings of the National Academy of Science*, **99**, 15965-15970.

Pastink, A., Eeken, J. C. and Lohman, P. H. (2001) Genomic integrity and the repair of double-strand DNA breaks. *Mutation Research,* 480-481: 37-50.

Peinado, M. A., Malkhosyan, S., Velazquez, A. and Perucho, M. (1992) *Proceedings of the National Academy of Sciences, USA*, **89**, 10065–10069.

Peltomaki P., Lothe R. A., Aaltonen L. A., Pylkkanen L., Nystrom-Lahti M., Seruca R., David L., Holm R., Ryberg D., Haugen A., Brogger A., Borresen A. L. and de la Chapelle A. (1993) Microsatellite instability is associated with tumors that characterize the hereditary non-polyposis colorectal carcinoma syndrome *Cancer Research*, **53**, 5853–5855.

Peltomaki, P. (2001) DNA mismatch repair and cancer. *Mutation Research*, **488**, 77-85.

Perdiz, D., Grof, P., Mezzina, M., Nikaido, O., Moustacchi, E. and Sage, E. (2000) Distribution and repair of bipyrimidine photoproducts in solar UV-irradiated mammalian cells. Possible role of Dewar photoproducts in solar mutagenesis. *Journal of Biological Chemistry*, **275**, 26732-26742.

Péréz-Cabré, M., Cervantes G., Moreno, V., Prieto M. J., Pérez, J. M., Font-Bardia, M., and Solans, X. (2004) Pd (II) and Pt (II) complexes with aromatic diamines: study of their interaction with DNA. *Journal of Inorganic Chemistry*, **98**, 510-521.

Perucho M., (1996) Cancer of the microsatellite mutator phenotype, *Journal of Biological Chemistry*, **377**, 675-684.

Peterson C. L. and Côté J. (2004) Cellular machineries for chromosomal DNA repair. *Genes and Development*, **18**, 602-616.

Phukan, R. K., Ali, M. S., Chetia, C. K. and Mahanta, J. (2001) Betel nut and tobacco chewing; potential risk factors of cancer of oesophagus in Assam, India. *British Journal of Cancer*, **85**, 661-667.

Protic-Sabljic M. and Kraemer K. H. (1986) One pyrimidine dimer inactivates expression of a transfected gene in Xeroderma pigmentosum cells, *Proceedings of the National Academy of Sciences, USA*, **82**, 6622–6626.

Pupko, T., and Graur, D. (1999) Evolution of microsatellites in the yeast *Saccharomyces cerevisiae*: role of length and number of repeated units. *Journal of Molecular Evolution*, **48**, 313-316.

Radman, M. (1974) Phenomenology of an inducible mutagenic DNA repair pathway in *E. coli.* SOS repair hypothesis, Prakas, L., Sherman, F., Miller, M., Lawrence, C. and Tabor H. W. (eds.), In, **Molecular and environmental aspects of mutagenesis.** Charles C Thomas, Publisher, Springfield, III. pp. 129-142.

Rakotomahanina, C. K., Hilger, C., Fink, T., Zentgraf, H. and Schroeder, C. (1994) Biological activities of a putative truncated hepatitis B virus X gene product fused to a polylysin stretch, *Oncogenes*, **9**, 2613-2621.

Ravanat, J-C., Douki, T. and Cadet, J. (2001) Direct and indirect effects of UV radiation on DNA and its components. *Journal of Photochemistry and Photobiology B: Biology*, **63**, 88-102.

Roots, R., Kraft, G. and Gosschalk, E. (1985) The formation of radiation induced DNA breaks: The ratio of double-strand breaks to single-strand breaks. *International Journal of Oncology and Biological Physics*, **11**, 259-265.

Rupert, C. S. (1975) Enzymatic photoreactivation: overview,. In P. Hanawalt and R. B. Setlow (ed.), In, **Molecular mechanisms for repair of DNA, part A**. Plenum Press, New York. pp. 73-87.

Rupert, C. S., Harm, H. and To K. (1973) The anatomy of direct repair. *Anais da Academia Brasileira de Ciências*, **45(Suppl.)**, 151-159.

Saikia, J. R., Schneeweiss, F. H. A. and Sharan, R. N. (1995) Poly-ADP-ribosylation and its role in induced carcinogenesis. In, **Radiation Research 1895-1995**. Hagen, U., Jung, H. and Streffer, C. (eds.), U. S., Strutz A. G. Wurzburg, Vol. 1. pp. 317.

Saikia, J. R., Schneeweiss, F. H. and Sharan, R. N. (1999) Arecoline-induced changes of poly-ADP-ribosylation of cellular proteins and its influence on chromatin organization. *Cancer Letters*, **139**, 59-65.

Sambrook, J. and Russell, D. W. (2001) In, **Molecular cloning: A laboratory manual**. New York, Cold Spring Harbor Laboratory Press.

Sancar, A. (1996) DNA excision repair, *Annual Reviews in Biochemistry*, **65**, 43- 81.

Sancar, A., Stachelek, C., Konigsberg, W. and Rupp, D. (1980) Sequences of the *recA* gene and protein. *Proceedings of the National Academy of Sciences, USA*, **77**, 2611-2615.

Schaaper, R.M., and Dunn, R.L. (1987) Spectra of spontaneous mutations in *Escherichia coli* strains defective in mismatch correction: the nature of in vivo DNA replication errors. *Proceedings of the National Academy of Sciences, USA*, **84**, 6220-6224.

Schlotterer, C., and Tautz, D. (1992) Slippage synthesis of simple sequence DNA. *Nucleic Acids Research*, **20**, 211-215.

Scholes, G., Wilson, R. L. and Ebert, M. (1969) Pulse radiolysis of aqueous solutions of deoxyribonucleotides and of DNA: Reactions with hydroxy-radicals. *Journal of Chemical Society and Chemical Communication*, **35**, 17-18.

Seymour, C. B., Mothersill, C. and Alper, T. (1986) High yields of lethal mutations in somatic mammalian cells that survive ionising radiation. *International Journal of Radiation Biology*, **50**, 167-179.

Sgura, A., Meschini, R. J., Antoccia, A., Palitti, F., Obe, G. and TanzareUa C. (1996) DNA damage induced by UV light affects restriction endonuclease recognition sites: correlation between effects at chromosomal level and naked DNA. *Mutagenesis*, **11**, 463-466.

Sharan R. N., Ryo H. and Nomura T. (2007) Critical role of *RecA* and *RecF* proteins in strand break rejoining and maintenance of fidelity of rejoining following γ-radiation-induced damage to pMTa4 DNA in *E. coli*. *International Journal of Radiation Biology*, **83**, 89-97.

Sharan, R. N. (1996) Association of Betel nut with carcinogenesis. *The Cancer Journal*, **9**, 13-19.

Sharan, R. N. (1998) **Trends in Radiation and Cancer Biology**, International Cooperation Bilateral Seminars Series, Forschungszentrum, Juelich, GmbH, Germany, vol. 29.

Sharan, R. N. and Wary, K. K (1992) Study of unscheduled DNA synthesis following exposure of human cell to arecoline and extracts of betel nut *in vitro*. *Mutation Research*, **278**, 271-276.

Sharan, R. N., Ryo, H. and Nomura, T. (2007) Critical role of *RecA* and *RecF* proteins in strand break rejoining and maintenance of fidelity of rejoining following γ-radiation-induced damage to pMTa4 DNA in *E. coli*. *International Journal of Radiation Biology*, **83**, 89-97.

Shibata, T., DasGupta, C., Cunnigham, R. P. and Radding, C. M. (1979) Purified *Escherichia coli* recA protein catalzes homologous pairing of super helical DNA and single stranded fragments, *Proceedings of the National Academy of Sciences, USA*, **76**, 1638-1642.

Shugar, D. (1960) In, **The Nucleic Acids**. Academic Press, Inc., New York. 3.

Slater, T. F. (1987) Free radicals and tissue injury: fact and fiction. *British Journal of Cancer*, **55**, 5-10.

Snellman, E., Strozyk, M., Sefervack, D., Klimenko, T. and Hemminki K. (2003) Effect of the spectral range of a UV lamp on the production of cyclobutane pyrimidine dimers in human skin *in situ*. *Phorodermatology, Photoimmunology and Photomedicine,* **19**, 281-286.

Stoner, G. D., Gupta, A. (2001) Etiology and chemoprevention of esophageal squamous cell carcinoma. *Carcinogenesis*, **22**, 1737-1746.

Sundqvist, K. and Grafstrom, R. C. (1992) Effects of areca nut on growth, differentiation and formation of DNA damage in cultured human buccal epithelial cells. *International Journal of Cancer,* **52**, 305-310.

Sundqvist, K., Liu, Y., Erhardt, P., Nair, J., Bartsch, H. and Grafstrom, R. C. (1991) Areca nut toxicity in cultured human buccal epithelial cells; in relevance to human cancers of N-Nitroso compounds, Tobacco smoke and Mycotoxins. In, **IARC Science Publications**. O'Neill, I. K., Chen, J. and Bartsch, H. ed., Lyon France, **105**, 281-285.

Sundqvist, K., Liu, Y., Nair, J., Bartsch, H., Arvidson, K. and Grafstrom, R. C. (1989) Cytotoxic and genotoxic effects of areca nut-related compounds in cultured human buccal epithelial cells. *Cancer Research*, **49**, 5294-5298.

Sutherland, B. M., Bennet, P. V., Sidorkina, O. and Laval, J. (2000) Clustered DNA damages induced isolated DNA in human cells by low doses of ionizing radiation. *Proceedings of the National Academy of Sciences, USA*, **97**, 103-108.

Sy, D., Savoye, C., Begusova, M., Michalik, V., Charlier, M. and Spotheim-Maurizot, M. (1997) Sequence dependent variations os DNA structure modulate radiation-induced strand breakage. *International Journal of Radiation Biology*, **72**, 174-155.

Takahashi, N. and Kobayashi, I. (1990) Evidence for the double-strand break repair model of bacteriophage lambda recombination. *Proceedings of the National Academy of Sciences, U S A.*, **87**, 2790–2794.

Taylor, J. –S. (1994) Unraveling the molecular pathway from sunlight to skin cancer. *Accounts of Chemical Research*, **27**, 76-82.

Taylor, J. –S. and Cohrs, M. P. (1987) DNA, light and Dewar pyrimidones: the structure and biological significance of TpT3. *Journal of American Chemical Society*, **109**, 2834-2835.

Terzakis, J. A. (1968) Uranyl acetate, a stain and a fixative. *Journal of Ultrastructural Research*, **22**, 168.

Thibodeau, S. N., Bren, G. and Scaid, D. (1993) Microsatellite instability in cancer of the proximal colon. *Science*, **260**, 816-819.

Thoma, F. (1999) Light, dark in chromatin repair: repair of UV-induced DNA lesions by photolyase and nucleotide excision repair, *EMBO Journals*, **18**, 6585–6598.

Thomas, S. J., Bain, C. J., Battistutta, D., Ness, A. R., Paissat, D. and Maclennan, R. (2006) Betel quid not containing tobacco and oral cancer: A report on a case-control study in Papua New Guinea and a meta-analysis of current evidence. *International Journal of Cancer*, **120**, 1318–1323.

Thomas, S. M. and MacPhee, D. G. (1986) Rec-A independent mutagenesis in *Escherichia coli*: effects of *umuC* and *nucB* mutations. *Mutagenesis*, **1**, 191-194.

Thompson, L. and Schild, D. (2002) Recombinational DNA repair and human disease, *Mutation Research/Genetic Toxicology and Environmental Mutagenesis*, **519**, 15-24.

Thoms, B., and Wackernagel, W. (1987) Regulatory role of *recF* in the SOS response of *Escherichia coli*: impaired induction of SOS genes by UV irradiation and nalidixic acid in a *recF* mutant. *Journal of Bacteriology*, **169**, 1731–1736.

Tlsty, T. D., Jonczyk, P., White, A., Sage, M., Hall, I., Schaefer, D., Briot, A., Livanos, E., Roelofs, H. and Poulose, B. (1993) Loss of chromosomal integrity in neoplasia. *Cold Spring Harbor Symposium on Quantitative Biology*; **58**, 645-54.

Trivedi, A. H., Roy, S. K., Patel, R. K., Adhvaryu, S. G. and Balar, D. B (1995) Urine of tobacco/ areca nut chewers causes damage in chinese hamster ovary cells, *Carcinogenesis*, **16**, 205-208.
Trivedi, C. R., Craig, G. and Warnakulasuriya, S. (2002) The oral health consequences of chewing areca nut, *Addiction Biology*, 7, 115-125.

Umezu, K., Chi N. W., and Kolodner, R. D. (1993) Biochemical interaction of the *Escherichia coli* RecF, RecO, and RecR proteins with RecA protein and single-stranded DNA binding protein. *Proceedings of the National Academy of Sciences, USA*, **90**, 3875–3879.

Venema, J., Mullenders, L. H., Natarajan, A. T., van Zeeland, A. A. and Mayne, L. V. (1990) The genetic defect in Cockayne syndrome is associated with a defect in repair of UV-induced DNA damage in transcriptionally active DNA, *Proceedings of the National Academy of Sciences, USA*, **87**, 4707–4711.

Volff, J. N. and Altenbuchner, J. (1997) Influence of disruption of the *recA* gene on genetic instability and genome rearrangement in *Streptomyces lividans*. *Journal of Bacteriology*, **79**, 2440-5.

Wacker, A. (1963) In, **Progress in Nucleic Acid Research**, Academic Press, Inc., New York. 1.

Walker, G. C. (1985) Inducible DNA repair systems, *Annual Reviews in Biochemistry*, **54**, 425-457.

Ward J. F. (1985) Biochemistry of DNA session. *Radiation Research*, **104**, S103-S111.

Ward J. F. (1994) The complexity of DNA damage: Relevance to biological consequences. *International Journal of Radiation Biology*, **66**, 427-432.

Ward, J. F. (1988) DNA damage produced by ionizing radiation in mammalian cells: identities, mechanisms of formation and reparability. *Progress in Nucleic Acid Research and Molecular Biology*, **5**, 95-125.

Wary, K. K. and Sharan, R. N. (1988) Effect of the Radioprotector 2-Mercaptoprionylglycine (MPG) on the Radiation Inactivation of Catalase *in vitro*. *Journal of Radiation Research*, **29**, 104-109.

Wary, K. K. and Sharan, R. N. (1988)Aqueous extract of betel-nut of North-East India induces DNA strand breaks and enhances cell proliferation *in vitro*. *Journal of Cancer Research and Clinical Oncology*, **114**, 579-582.

Wary, K. K. and Sharan, R. N. (1991) Cytotoxic and cytostatic effects of arecoline and sodium nitrite on human cells *in vitro*. *International Journal of Cancer*, **47**, 396-400.

Washino, K. and Scnabel, W. (1982) Radiation induced molecular size changes in native and denatured deoxyribonucleic acid under anoxic conditions. A pulse radiolysis study. *Die Makromolecular Chemie*, **183**, 967-709.

Weinstock, G. M., McEntee, K. and Lehman, I. R. (1979) ATP-dependent renaturation of DNA catalyzed by the recA protein of *Escherichia coli*. *Proceedings of the National Academy of Sciences, USA*, **76**, 126-130.

Weirzchowski, K. L. and Shugar, D. (1961) Photochemistry of cytosine nucleosides and nucleotides, II. *Acta Biochimica Polonica*, **8**, 219-234.

Weissenbach, J., Gyapay, G., Dib, C., Vignal, A., Morissette, J., Millasseau, P., Vaysseix, G. and Lathrop, M. (1992) A second-generation linkage map of the human genome. *Nature*, **359**, 794–801.

Wenke, G., Brunnemann, K. D., Hoffmann, D. and Bhide, S. V. (1984) A study of betel quid carcinogenesis. IV. Analysis of saliva of betel chewers. A preliminary report. *Journal of Cancer Research Clinical Oncology*, **108**, 110-113.

Whitby, M. C., and Lloyd, R. G. (1995) Altered SOS induction associated with mutations in *recF*, *recO*, and *recR*. *Molecular and General Genetics*, **246**, 174–179.

WHO, 1994, Ultraviolet Radiation, 2nd edition; In, **Environmental Health Criteria**: 160 (Geneva, World Health Organization).

Witkin, E. M. (1969) Ultraviolet-induced mutation and DNA repair. *Annual Reviews in Microbiology*, **23**, 487-514.

Yasui, A. & Eker, A.P.M. 1998 DNA photolyases. In, **DNA Damage and Repair, Vol. II**, Nickoloff, J.A. & Hoekstra, M.F. (eds.) Humana Press, Totowa, pp. 932.

Zeng, Y. and Sheppard, T. L. (2004) Half-life and DNA scission products of 2-deoxyribolactone oxidative DNA damage lesion. *Chemical Research and Technology*, **17**, 197-207.

Zhou, L. and Streffer, H. (2003) Distinct pathways mediate UV-induced apoptosis in *Drosophila* embryo. *Developmental Cell*, **4**, 599-605.

Publication

Int. J. Radiat. Biol., Vol. 81, No. 12, December 2005, pp. 919–927

UV-C radiation induced conformational relaxation of pMTa4 DNA in *Escherichia coli* may be the cause of single strand breaks

CHAITALI BHATTACHARJEE & R. N. SHARAN

Radiation & Molecular Biology Unit, Department of Biochemistry, North-Eastern Hill University, Shillong, India

(Received 5 August 2004; accepted 8 January 2005)

Abstract

Purpose: The biological consequences of initial physicochemical events following exposure of DNA to germicidal (254 nm) ultraviolet C (UV-C) radiation are not fully understood despite progress that has been made. In particular the cause of UV-C induced single strand breaks is not known. This question has been addressed in the present investigation.

Materials and methods: A plasmid construct, pMTa4, was exposed to UV-C *in vitro* as well as *in vivo* after transforming the plasmid into a *repair* proficient wild type and *repair* deficient, *recF*, mutant of *E. coli*. Following UV exposure *in vivo*, the plasmid was isolated under repair non-permissive and permissive conditions. The plasmid isolate and the pure super-coiled closed circular (CC) topological form of the plasmid were analyzed by agarose gel electrophoresis. The dependence of UV-C induced damage and conformational changes on the dose of radiation as well as on the duration of post-irradiation repair incubations was observed. The influence of UV-C on hyperchromic change and intercalation of ethidium bromide into plasmid DNA were also recorded.

Results: UV-C exposure of pMTa4 DNA *in vitro* and *in vivo* induced dose dependent, but sparsely placed, single strand breaks (SSB). While the wild type (AB1157) *E. coli* was able to repair SSB nearly completely under repair permissive condition, the *recF* (JC9239) mutant failed to do so. A dose-dependent relaxation of super-structure of CC form of pMTa4 DNA concomitant with enhanced ethidium bromide intercalation into the plasmid DNA was observed.

Conclusion: It is proposed that the conformational relaxation generated negative super-coiling strain on the DNA backbone of CC form of plasmid as well as exposed chemical bonds for hydrolytic cleavage. This might be the cause of the production of sparsely placed single strand breaks in pMTa4 upon exposure to low doses of UV-C.

Keywords: *UV-C, pMTa4, E. coli, conformational relaxation, single strand breaks in DNA*

Introduction

The understanding of DNA damage induced by germicidal (254 nm) ultraviolet C (UV-C) radiation is biologically relevant as its wavelength coincides with the absorption maxima of purine and pyrimidine nucleotides (NT) (reviewed by the World Health Organization [WHO] 1994, Ravanat et al. 2001). The DNA damaging potential of UV-C has been attributed to its ability to induce dimeric photoproducts (Douki et al. 2003a), oxidized pyrimidine and purine NT (Ravanat et al. 2001, Douki et al. 2003b) and single strand breaks (SSB) in DNA (Miguel & Tyrrell 1986, WHO 1994). The major lesions induced by germicidal UV-C are reported to be cyclobutane pyrimidine dimers (CPD) (Matsunaga et al. 1991) as well as varying amounts of pyrimidine (6–4) pyrimidone photoproducts ((6-4)PP), their Dewar isomers, other dimeric NT and adenine dehydrodimer (Haseltine 1986, Ravanat et al. 2001, Douki et al. 2003b). Relatively few SSB are reported to be induced by UV-C radiation (WHO 1994). Nonetheless, even a low level of strand breakage in DNA can potentially become a source of mutations, if misrepaired or left unrepaired. *E. coli* is capable of recovering from UV induced damage primarily utilizing the nucleotide excision repair (NER) system (Kurosaki et al. 2003). In visible or near-UV (310–480 nm) light, the pyrimidine NT dimers are also repaired utilizing DNA photolyase (Oguma et al. 2001, Burger et al. 2002, Schul et al. 2002). However, in repair deficient situations the unrepaired or misrepaired SSB, even at a low level, can cause significant metabolic problems. Furthermore, compared to ionizing radiation, the absorbed UV-C energy is unlikely to cause DNA strand breaks

Correspondence: R. N. Sharan, Radiation & Molecular Biology Unit, Department of Biochemistry, North-Eastern Hill University, Shillong 793 022, India. Tel: (0364) 272 2121. Fax: (0364) 255 0108. E-mail: rnsharan@nehu.ac.in

ISSN 0955-3002 print/ISSN 1362-3095 online © 2005 Taylor & Francis
DOI: 10.1080/09553000600566048

directly. Therefore, it becomes important to understand how strand breaks are induced by UV-C radiation. To the best of our knowledge this has not been elucidated.

Plasmid DNA is a convenient tool to study the molecular mechanism of radiation-induced damage and its repair (Humtsoe & Sharan 2004). Using pMTa4, a plasmid construct of 6,173 base pairs (bp), we have earlier studied the effects of either low and high linear energy transfer (LET) radiation on induction and processing of DNA damage *in vitro* and *in vivo* (Humtsoe et al. 1998, 2003, Humtsoe & Sharan 2004) or radiomimetic chemicals (Odyuo & Sharan 2005). In the present investigation, we have used the plasmid after transforming it into repair proficient wild type and repair deficient *recF* mutant of *E. coli* to study the low-dose UV-C induced damage to pMTa4 DNA and its repair *in vivo*. The aim was elucidation of the cause of induced strand breaks. After exposure of *E. coli* to UV-C *in vivo*, the plasmid DNA was isolated under repair non-permissive and permissive conditions, and analyzed. For comparison, an aqueous solution of pMTa4 was exposed to UV-C radiation *in vitro* and analyzed. The initial events following UV-C exposure *in vitro* and *in vivo* appear to introduce conformational relaxation in DNA super-structure with concomitant increase in SSB. While the wild type *E. coli* could repair the damage, the *recF* mutant failed to do so.

Materials and methods

Chemicals

High purity biochemicals obtained from different sources, as indicated below, were used in the study: Ampicillin (Duchefa, Haarlem, The Netherlands); Agarose (Genei, Bangalore, India); Ethidium bromide (EB) and sodium hydroxide (Merck, Darmstadt, FRG); Acetic acid, ethylenediaminetetraacetic acid (EDTA), sodium chloride (NaCl), acetic acid, sulfuric acid, glucose and sucrose (Qualigens, Mumbai, India); Tris (Boehringer, Manheim, FRG); sodium dodecyl sulphate (SDS) (Sigma, St. Louis, Missouri, USA); Luria-Bertani (LB) broth and LB-agar (Himedia, Mumbai, India); diphenylamine (Glaxo, Mumbai, India) and trichloroacetic acid (TCA) (SRL, Mumbai, India).

E. coli *strains and culture condition*

A repair proficient, wild type *E. coli* K12 strain, AB1157, and a repair deficient *recF* mutant, JC9239, were used in the study (Humtsoe & Sharan 2004). The *recF* gene product is involved in repair of UV-induced DNA damage. The *recF* mutant lacks the functional *recF* gene product and, thus, is deficient in repair of UV-induced damage. Single colonies picked up from Ampicillin$^+$-agar plates were grown overnight at 37°C in LB medium supplemented with 100 μg ml^{-1} Ampicillin. The cells were harvested in mid-log phase for experiment.

Plasmid pMTa4 and its isolation

The plasmid pMTa4 has been described earlier (Humtsoe et al. 1998, 2003, Humtsoe & Sharan 2004, Odyuo & Sharan 2005). It was isolated from the overnight culture of *E. coli* by the alkaline lysis method with minor modification (Sambrook & Russel 2001). The plasmid isolate was dissolved in sterile water to avoid any influence of chemical constituents of buffer, such as counterions, and stored refrigerated.

Transformation of E. coli *with pMTa4*

A standard transformation protocol (Sambrook & Russel, 2001) was used with some modifications. Briefly, to 200 μl of freshly prepared competent cells in a pre-cooled tube, ≈75 μl (300 ng DNA) of pMTa4 was added, gently mixed and kept on ice for 20 min. The tube was then incubated, in sequence, at 42°C for 30 s and on ice for 180 s. LB medium (500 μl, pre-warmed to 37°C) was added into the tube, gently mixed and incubated at 37°C for 60 min. The content (200 μl) was then plated on LB agar plates (with 100 μg ml^{-1} Ampicillin) at 10^{-3} and 10^{-5} dilutions and incubated overnight at 37°C. The control was LB-agar plates without Ampicillin.

UV source, dose and experimental design

UV-C germicidal tube (Philips Eindhoven, The Netherlands) fitted in a glass chamber in a dark room was used for the study. The source was approximately 46 cm above the irradiation table delivering 0.04 J·m^{-2}·s^{-1} as measured by UV 340 dosimeter (Biostep, Johnsdorf, Germany). Samples for exposure were placed in open sterile Petri plates and irradiated in the dark for varying time (0–150 s) to accumulate UV-C doses of 0, 1.2, 2.4, 3.6, 4.8 and 6 J·m^{-2}.

(a) Dose and time kinetic studies *in vivo*. The overnight cultures of *E. coli* (1.5 ml; 8×10^8 cells ml^{-1}) harboring pMTa4 were pre-cooled on ice and exposed to different doses of UV rays on ice in the dark. Plasmid was isolated from the UV exposed *E. coli* either immediately after exposure (repair non-permissive, R$^-$) or after a post-exposure repair incubation of 60 min at 37°C under fluorescent light (repair permissive, R$^+$). In a 3-point time kinetic study,

the plasmid was also isolated after 15 and 60 min of post-irradiation repair incubation (R^+). The plasmid isolates were subjected to agarose gel electrophoresis.

(b) Dose and time kinetic studies *in vitro*. Aqueous solution of pMTa4 (5 μl containing 8.5 μg DNA) was irradiated to different doses of UV rays at room temperature. They were subjected to agarose gel electrophoresis immediately or after 15 and 30 min of post-irradiation sham-repair incubation (R^+).

Agarose gel electrophoresis

Agarose (1%) gel electrophoresis was done using Tris-acetate-EDTA (TAE) buffer at 1.5 V cm^{-1} for 60 min. After electrophoresis, the gel was stained with EB at a concentration of 0.3 $\mu g\ ml^{-1}$ for 15 min, de-stained in water for 30 min and EB-intercalated DNA bands visualized on an UV trans-illuminator (Bio-Rad, California, USA).

Preparation of CC form of pMTa4 DNA from plasmid isolate

A preparative agarose gel (1%) electrophoresis was done to separate out the CC and open circle (OC) forms of the plasmid DNA isolate. After electrophoresis, small piece of the gel with CC band was carefully excised out. The gel slice was placed in a sterile tube over a bed of sterile glass wool and centrifuged (8000 × *g* for 45 s). From the eluent, CC form of pMTa4 was purified by phenol-chloroform extraction. The extract was lyophilized. Typically, from a 200 μg isolate, 30–40 μg of CC form of plasmid was recovered. The purity of isolation of CC form was checked by agarose gel electrophoresis.

Monitoring hyperchromic shift to measure conformational relaxation in pMTa4

To monitor the conformational alteration in pMTa4 DNA molecules, its photochromic property was exploited (Berg et al. 2002). It is known that DNA molecules show maximum absorption at 260 nm and record increasing absorption (hyperchromic shift) with progressive denaturation and *vice versa*. This property of DNA was used to monitor UV-C induced conformational relaxation in pMTa4. Purified CC forms of the plasmid isolates (5.1 μg DNA in 1 ml H_2O) were taken in different tubes and their $A_{260\,nm}$ recorded (DU 530, Beckman, California, USA, UV/Vis spectrophotometer). The samples were then exposed to increasing doses of UV-C in the dark. Immediately after irradiation, the $A_{260\,nm}$ was recorded for each tube again. The difference of the two gave the hyperchromic shift induced by UV-C in pMTa4 since the quantity of pMTa4 DNA remained the same for each pair of measurements.

Monitoring ethidium bromide (EB) intercalation in pMTa4

The fluorescence of EB is known to increase 20–30 fold upon its intercalation into DNA helix (Smith et al. 1992) and the steady state fluorescence of EB is routinely used in visualization, detection and quantification of DNA. This property has been exploited to monitor alterations in the conformational state of pMTa4 following exposure to UV-C. In a relaxed conformational state, the same quantity of pMTa4 DNA would bind more of EB molecules than its native conformation. Equal amounts of purified CC form of pMTa4 isolates (5 μl containing 8.5 μg DNA) were taken and exposed to increasing doses of UV-C. Immediately afterwards, 2 μl of EB (40 ng ml^{-1}) was added to each irradiated sample and incubated for 30 min at room temperature. The mix was carefully loaded in wells (dot spots) punctured on freshly cast 1% agarose gel on glass slides. After 3 min incubation at room temperature, the gel was transferred onto a UV transilluminator to capture the emitting fluorescence from the wells.

Quantification of pMTa4 DNA by diphenylamine assay

DNA was estimated according to Burton (1956) using diphenylamine with slight modifications. The absorbance was recorded at 540 nm ($A_{540\,nm}$). Calf thymus DNA served as a standard.

Analysis

The images of electrophoresed or dot-spotted agarose gels were digitized (Kodak, New York, USA) immediately. Pixel densities of bands of the OC and CC topological forms of pMTa4 on electropherograms were quantified using 1D Image Analysis software (Kodak, New York, USA). Similarly, the total florescence emancipating from pMTa4 DNA in dot-spots on gels were also quantified.

Results and discussion

Plasmid (pMTa4) DNA has been used in this investigation as it offers a direct measure of induced SSB and double strand breaks (DSB) by acquiring different topological forms (OC and linear (L), respectively) from its native CC form that are clearly resolved on an agarose gel (Humtsoe et al. 1998, 2003, Humtsoe & Sharan 2004, Odyuo & Sharan 2005). Under *in vivo* conditions, the plasmid DNA exists in CC form. However, during its isolation, the methodological interventions invariably induce SSB.

The plasmid isolate in this study contained both CC and OC forms (Figures 1–3, lanes C) typically comprising 60% of CC and 40% of OC. The *in vitro* exposure of pMTa4 to increasing doses of UV-C radiation ($0-6 J \cdot m^{-2}$) showed a progressive increase in SSB on pMTa4 DNA as the pixel density of the OC form of the plasmid increased correspondingly (Fig. 1). No L form band of pMTa4 was detected on the electropherogram (Figure 1A) showing the inability of UV-C to induce DSB in the dose range used in this investigation. Figure 1A further suggests that the SSB induced by UV-C in pMTa4 were sparsely placed; otherwise some of the proximal SSB could potentially get converted to DSB causing appearance of the L form of pMTa4 on the gel. It is known that UV-C exposure essentially induces NT photoproducts (Matsunaga et al. 1991, WHO 1994, Ravanat et al. 2001, Douki et al. 2003a, b). The energy being low, UV-C does not produce nicks or SSB by direct action. This is in contrast to low- and high-LET radiation (Humtsoe et al. 1998, 2003, Humtsoe & Sharan 2004) or free radical generating Fenton and Haber-Weiss radiomimetic chemical systems (Odyuo & Sharan, 2005), which have been shown to induce both SSB and DSB in pMTa4 DNA by direct as well as indirect means. This investigation was designed to look into the possible consequences of UV-C induced changes in DNA. No direct measure of the induced NT-photoproducts was made in the investigation as estimates are available in literature (WHO 1994, Ravanat et al. 2001). The action spectrum for induction of SSB in cultured cells was reported to be highest for UV-C. This sharply decreased with increasing wavelength and matched rather well with the action spectrum of CDP and (6-4)PP inductions by UV rays, especially in the germicidal wavelength (254 nm) and higher (WHO 1994).

Interestingly, the profile of UV-C dose dependent induction of SSB on pMTa4 *in vitro* (Figure 1A and B) was remarkably similar to those under *in vivo* exposure conditions in AB1157 (Figure 2A and B) as well as in JC9239 (Figure 3A and B) under repair non-permissive (R^-) condition. This was expected as both *in vitro* and repair non-permissive (R^-) *in vivo* conditions were quite similar. In both, due to different reasons, damage to DNA was not repaired. However, following post-exposure repair incubation (R^+), the profiles of SSB in AB1157 (Figure 2C and D) and JC9239 (Figure 3C and D) were significantly different. The repair proficient wild strain of *E. coli*, AB1157, nearly completely abolished at least the SSB type of pMTa4 damage (Figure 2D) while its *recF* mutant, JC9239, failed to do so (Figure 3D). The study was extended by performing a series of experiments to monitor the influence of duration of repair incubation (R^+) on repair of UV-C induced SSB *in vitro* as well as *in vivo* condition for wild and *recF* strains for all dose points. The *in vitro* samples being aqueous solution of pMTa4 did not have any repair system. Nonetheless, they were still sham-repair incubated to create identical conditions of repair incubation as *in vivo*. This ensured that any chemical changes taking place on pMTa4 DNA during repair incubation was equally applicable to the *in vitro* and *in vivo* systems used in the investigation. Accordingly, for *in vitro* investigation, plasmid isolates were exposed to UV rays, repair incubated (R^+) for 15 and 30 min and then analyzed by electrophoresis. For *in vivo* experiments, wild and *recF* cultures harboring pMTa4 were irradiated and subjected to post-irradiation repair incubation (R^+) for 15 and 60 min before isolation of plasmid. The plasmid isolate was analyzed by electrophoresis as described. A representative set of results of such experiments for $6 J \cdot m^{-2}$ dose of UV is shown in

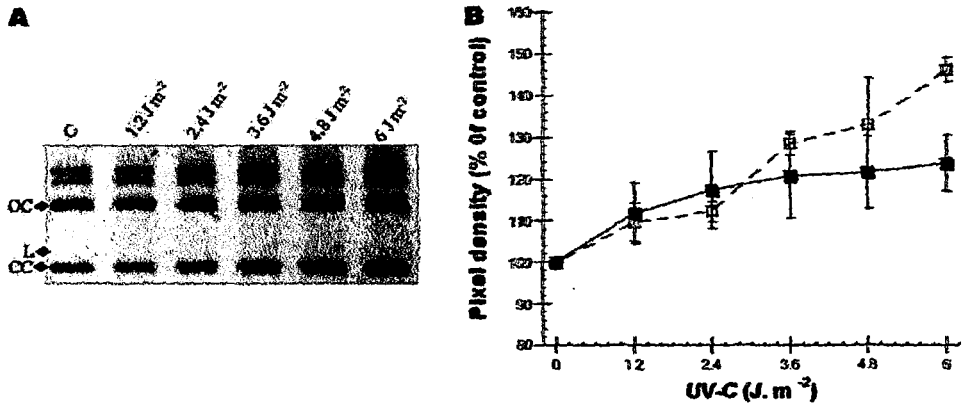

Figure 1. *In vitro* effect of UV-C radiation on pMTa4. The electropherogram (A) shows the resolved topological forms of pMTa4 as a function of increasing dose of UV-C. The pixel densities of CC (—■—) and OC (—□—) bands (mean ± SD) have been plotted (B) as a function of dose of UV-C ($n = 6$). L shows the expected position of linear band of pMTa4.

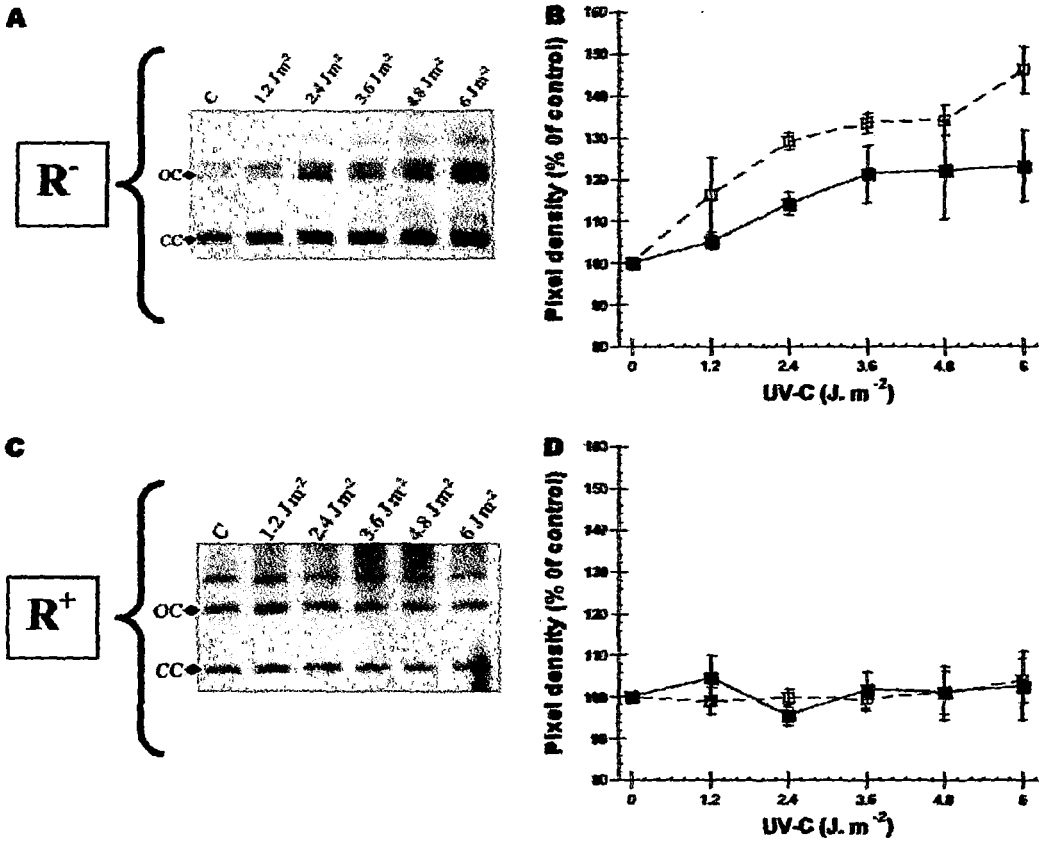

Figure 2. *In vivo* effect of UV-C radiation on AB1157 strain of *E. coli* harboring pMTa4. The electropherograms (A and C) show the resolved topological forms of pMTa4 isolated from AB1157 (wild) *E. coli* as a function of increasing dose of UV-C under repair non-permissive (R^-; top panel) and permissive (R^+; bottom panel) conditions. The corresponding pixel densities of the CC (—■—) and OC (---□---) bands (mean ± SD) have been plotted (B and D, respectively) as a function of dose of UV-C ($n = 5$).

Figure 4. As expected, under *in vitro* exposure condition (Figure 4A), both CC and OC forms remained invariant for increasing period of R^+ incubation indicating that no repair of SSB occurred. Under *in vivo* exposure condition, the wild type strain showed a sharp decline in pixel density of OC form in 15 min of R^+ incubation (Figure 4B). The results suggest that the pace of repair of inflicted SSB was rather fast in the wild type and, perhaps, all SSB were completely repaired in 15 min of R^+ only. In the *recF* mutant, on the other hand, the pixel density of OC declined only marginally after 15 min of R^+ and maintained the level for up to 60 min (Figure 4B) suggesting poor repair of SSB in *recF* mutant in line with the earlier observation (Figure 3). The trend was similar for all lower doses of UV-C for *in vitro* and for wild and *recF* mutant under *in vivo* condition (results not shown).

The UV hypersensitivity of JC9239 is known. We also observed clonogenic survival of AB1157 and JC9239 strains against UV-C wherein only JC9239 had a highly compromised survival (≈20 %) at the maximum dose. Repair of UV-C induced damage in *E. coli* is understandably complex, involving interplay of several repair pathways (Haseltine 1986, Miguel & Tyrrell 1986, Oguma et al. 2001, Burger et al. 2002, Schul et al. 2002, Kurosaki et al. 2003). Nonetheless, the nucleotide excision repair (NER) pathway is proposed to be the main machinery for repair of UV-C induced photoproducts (Kurosaki et al. 2003). Since the JC9239 mutant lacks *recF* protein and it showed persistence of SSB even under R^+ condition (Figure 3B, D), it is logical to assume that UV-C induced photoproducts were not repaired. The wild type, AB1157, which has all repair systems including *recF* protein mediated repair, showed total abolition of SSB under R^+ conditions. Therefore, it is apparent that in the presence of *recF* protein, AB1157 was able to completely repair UV-C induced damage on DNA manifesting as SSB under R^+ condition. In contrast, the JC9239 strain, lacking *recF* proteins, failed to do so and continued with SSB even after post-exposure repair incubation (Figure 3). These facts strongly indicate that persistence of UV-C NT-photoproducts in JC9239 might have been the cause of the observed SSB in pMTa4 DNA (Figures 3 and 4).

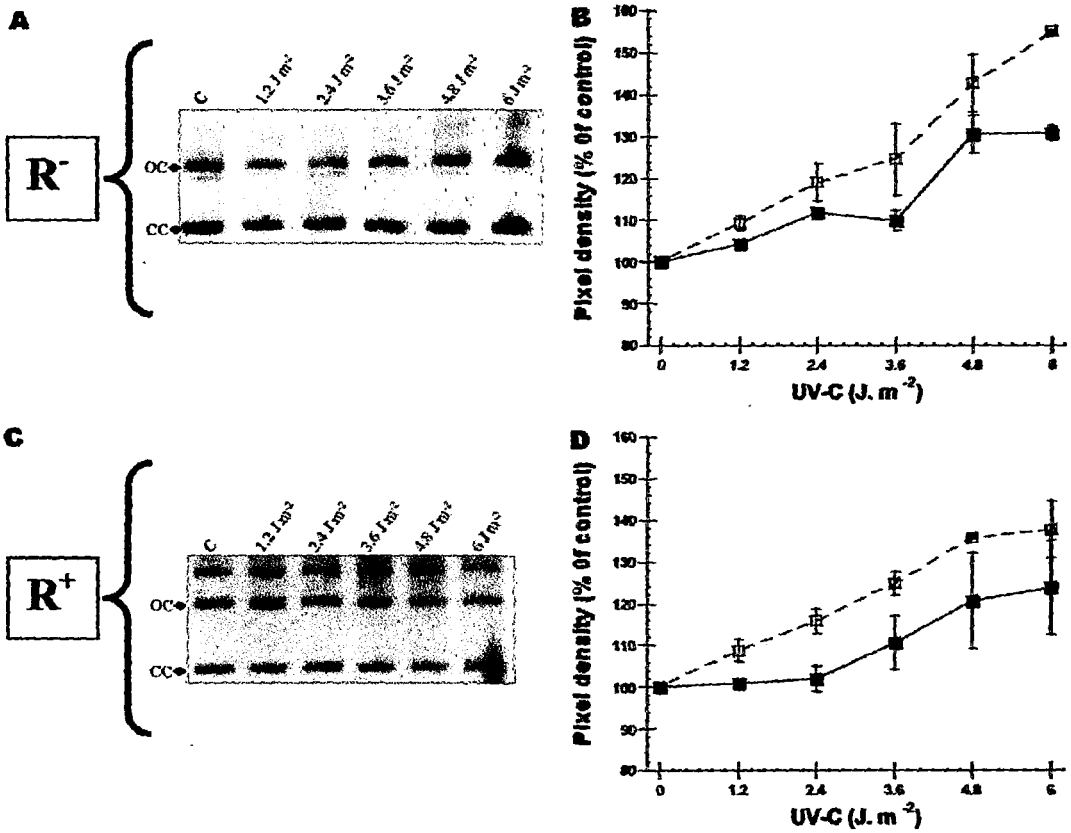

Figure 3. *In vivo* effect of UV-C radiation on JC9239 strain of *E. coli* harboring pMTa4. The electropherograms (A and C) show the resolved topological forms of pMTa4 isolated from JC9239 (*recF*) *E. coli* as a function of increasing dose of UV-C under repair non-permissive (R^-; top panel) and permissive (R^+; bottom panel) conditions. The corresponding pixel densities of the CC (—■—) and OC (—□—) bands (mean ± SD) have been plotted (B and D, respectively) as a function of dose of UV-C ($n=5$).

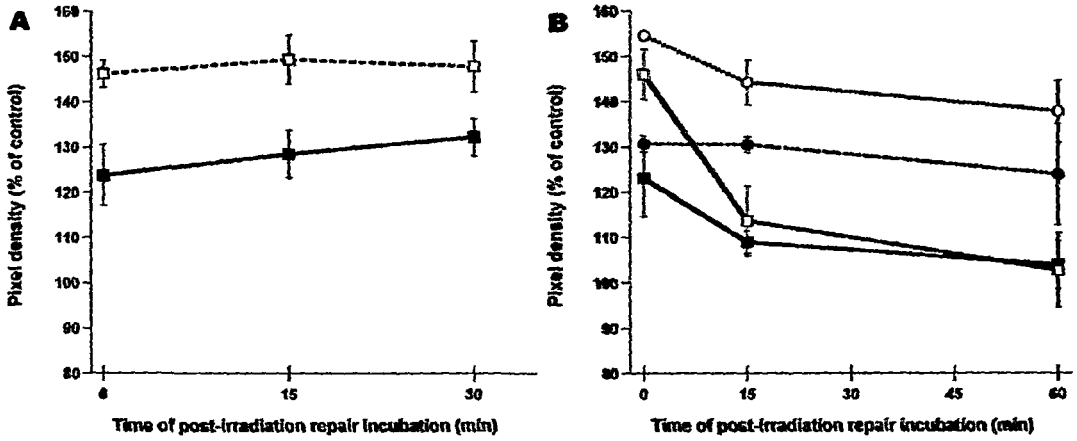

Figure 4. Effect of time of repair incubation on repair of induced SSB by 6 $J.m^{-2}$ dose of UV-C. *In vitro* (A) Plots of pixel densities of CC (—■—) and OC (—□—) bands (mean ± SD) of pMTa4 at 0 (control), 15 and 30 min of R^+. *In vivo* (B) Plots of pixel densities pMTa4 bands (mean ± SD) in wild (AB1157) strain [CC (—■—) and OC (—□—)] and *recF* mutant [CC (—●—) and OC (—○—)] at 0 (control), 15 and 60 min of R^+.

However, we also noticed a dose-dependent increase in the CC band of the plasmid exposed to UV-C *in vitro* (Figure 1) and *in vivo* in both AB1157 (Figure 2) and JC9239 (Figure 3) strains of *E. coli* under R^- condition. This is in contrast to γ-radiation induced or radiomimetic chemical strand breaks in

pMTa4 *in vitro* reported earlier wherein progressive increases in the pixel densities of OC and L bands on the agarose gel were accompanied by progressive decreases in CC form (Humtsoe et al. 1998, Humtsoe & Sharan 2004, Odyuo & Sharan 2005). Since UV-C induced increases in the pixel density of CC form of pMTa4 were remarkably similar under *in vitro* (Figure 1) and repair-non-permissive *in vivo* condition for wild type (Figure 2) and *recF* mutant (Figure 3) strains, it is logical to assume existence of a common cause for this. Under the *in vitro* conditions of our investigation, a fixed amount of pMTa4 preparations were exposed to UV-C and then analyzed by agarose gel electrophoresis (Figure 1). Part of the CC form of the plasmid DNA, upon sustaining SSB following UV-C exposure, should migrate with OC band on the gel (Figure 1). Therefore, with an increase in pixel density of the OC band, a corresponding decrease in CC band was expected. Since our results show otherwise, it can only be explained by hypothesizing that the observed increase in the pixel density of CC band on the gel was due to increased EB intercalation into the CC form of pMTa4 following UV exposure. In other words, the increase in observed pixel density of CC band following UV-C exposure was not due to an increase in the quantity of DNA in the CC band but due to an increase in intercalation of EB. EB binding affinity to relaxed forms (e.g., OC or L forms) is reported to increase up to 1.4 fold compared to the compact form (i.e., the CC form) of SV40 DNA (Jones et al. 1993, Gulston et al. 2002). Therefore, it appears that UV-C exposure was also inducing conformational relaxation in the CC form of pMTa4 DNA.

To verify whether or not UV-C exposure caused conformational relaxation in pMTa4 under our experimental conditions, we needed pMTa4 DNA only in the CC form. It was prepared (see above) and the product was confirmed as 100% pure CC form of pMTa4 isolate by agarose gel electrophoresis (result not shown). Hyperchromic shift in the CC form of plasmid DNA was monitored (see above) as a function of UV-C dose *in vitro* (Figure 5). The progressive increase in the absorption essentially suggests that UV-C induced a dose-dependent relaxation in the conformation of CC form of pMTa4 DNA by taking the positively super-coiled DNA into more negatively super-coiled or relaxed state. The negative super-coiling is likely to relax essentially the CC form of the plasmid as this is the only topological form of a plasmid, which has no free ends on the DNA backbone, to release torsional energy. For the OC forms, the situation was slightly different as it had free ends of the DNA backbone to release torsional energy. The same was true for the L form. Due to this, the negative super-coiling is unlikely to result in

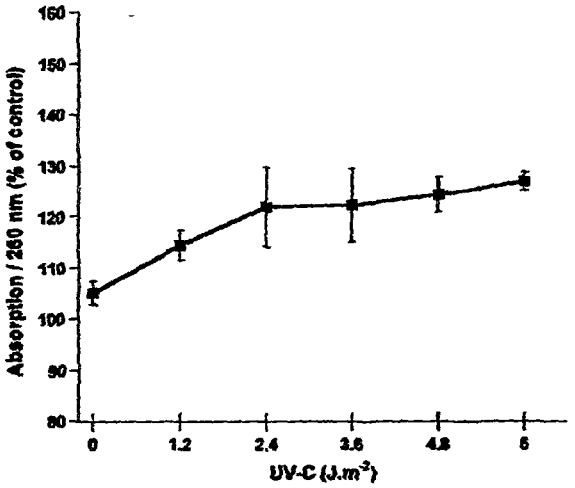

Figure 5. Effect of UV-C radiation on induction of hyperchromic shift in pMTa4. Absorbance (260 nm) of pMTa4 DNA has been plotted as a function of dose of UV-C ($n=4$) to monitor induced hyperchromic shift (see text for details).

conformational relaxation of OC form of pMTa4. Thus, the cause of the observed increase in pixel density of CC bands on gels as a function of UV-C dose (Figures 1, 2A and B, 3A and B) seems to be a UV-C induced negative super-coiling or relaxation of the CC form of pMTa4 DNA.

We assume UV-C induced photoproducts to be the main cause of the resulting negative super-coiling or relaxation of the CC form of pMTa4 DNA (Figure 5). This assumption derives support from the results of experiments dealing with the kinetics of repair of the plasmid DNA following UV-C exposure (Figure 4). We did not observe any significant modification in the proportions of OC and CC forms in JC9239 cells as a function of duration of repair incubation, but found a rapid decrease in the amount of OC form in AB1157 (Figure 4B). Interestingly, the pixel density of CC form in AB1157 did not increase as a function of repair time, as was expected, because the repair of the OC form leads to regeneration of the CC form of the plasmid. This observation is in agreement with our proposal of an increase in EB staining induced by the presence of photoproducts and consequent relaxation of plasmid DNA that would be lost in AB1157 during repair incubation because of efficient removal of base damage in the CC form.

To further verify whether or not the CC form of the plasmid in a relaxed conformational state intercalated more EB, precisely measured equal amounts of the purified CC fraction of pMTa4 isolate were exposed to increasing doses of UV-C radiation. After exposure, EB intercalation was monitored for a fixed amount of EB and intercalation time (see above). The results showed a dose-dependent increase in the pixel density of DNA-intercalated EB (Figure 6). Since the

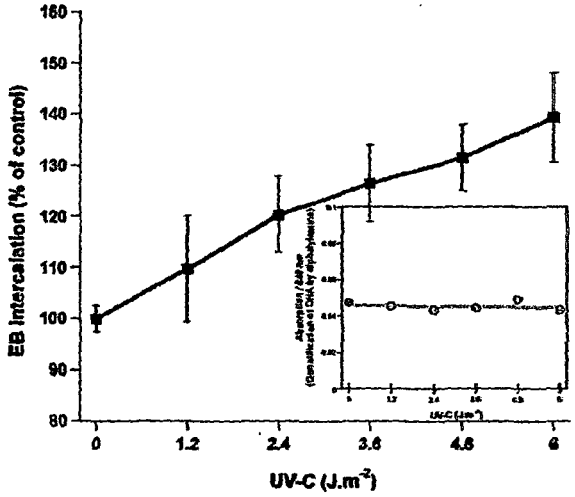

Figure 6. Effect of UV-C radiation on intercalation of ethidium bromide in pMTa4. The fluorescence of DNA-intercalated ethidium bromide in CC form of pMTa4 has been plotted as a function of dose of UV-C ($n=4$). The inset shows plot of DNA quantification by diphenylamine assay for the samples used for EB intercalation experiment. See text for details.

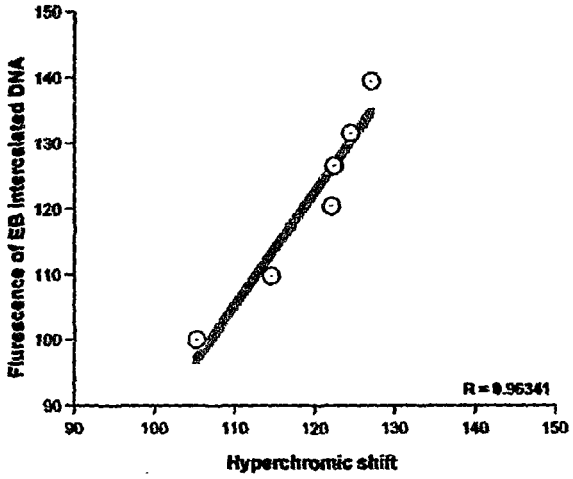

Figure 7. Correlation between hyperchromic shift and ethidium bromide intercalation in pMTa4. The data for hyperchromic shift and ethidium bromide intercalation for increasing doses of UV-C radiation were plotted to find correlation between the two. The correlation coefficient, R, of the slope of linear fit (solid bar) is 0.96341.

increase in pixel density of EB intercalated DNA also indicates a quantitative increase in DNA, it was important to reconfirm the equality of DNA samples in this experiment by an independent assay. Therefore, diphenylamine based chemical quantification of the amount of DNA in each sample was also done (Burton 1956). The result shows an invariant quantity of pMTa4 DNA (Figure 6: inset) in each sample used for the EB intercalation experiment. The chemical assay of DNA was preferred over possible assays using radiolabeling to avoid interference of another quality of radiation with UV-C radiation effects. The plot of EB fluorescence (Figure 6) versus hyperchromic shift in absorbance (Figure 5) shows a correlation coefficient of 0.96314 (Figure 7) – a near linear correlation for the dose range of UV-C used in this investigation. These results strongly suggest that (a) an UV-C induced conformational relaxation in the CC form of pMTa4 DNA occurred, and (b) in a relaxed conformation the CC form of plasmid DNA intercalated more EB.

Based on the results presented here it is hypothesized that the UV-C induced conformational relaxation of pMTa4 DNA might be the cause of induction of SSB. The conformational relaxation is not likely to be the effect of UV-C induced strand break as neither γ-rays (Humtsoe et al. 1998), lithium swift ion (Humtsoe et al. 2003) nor radiomimetic chemicals (Odyuo & Sharan 2005) induced any conformational relaxation in pMTa4 despite strand breaks. Furthermore, UV-C exposure *in vitro* (Figure 1) and *in vivo* (Figures 2 and 3) produced similar effects on the pMTa4 DNA. Lastly, we have directly measured UV-C induced conformational relaxation in CC form of pMTa4 DNA (Figures 5, 6). Kurosaki et al. (2003) have also observed tertiary structural changes in the genome of M13 virion after UV-C exposure. Isaacs and Spielmann (2004) have suggested possible induction of alternative DNA conformations by covalent damage and NT mismatch. DNA double helix unwinding by ≈9° and bending of the helical axis by ≈30° due to pyrimidine photodimerization have been directly measured in crystal structures (Park et al. 2002). UV-C induced inter- and intra-strand cross-links of NT (Douki et al. 2003b) are also likely to contribute to DNA unwinding. The conformational relaxation, negative supercoiling or unwinding is likely to generate significant torsional strain on the DNA backbone of the CC form of the plasmid pMTa4 as this form alone has no free end to release the generated torsional energy. This could lead to induction of sparsely placed SSB. However, a contribution of other chemical processes in the induction of SSB cannot be ruled out. For instance, oxidative damage to base or sugars moieties of DNA may induce hydrolytic cleavage of phosphodiester bonds (Cowan 2001, Zeng & Sheppard 2004). This may be achieved without degradation of the 2-deoxyribose moiety or loss of base. In contrast, cleavage may also involve H· atom abstraction of the sugar moiety leading to partial decomposition of 2-deoxyribose unit and release of a base (Gurzadyan & Gorner 1992). Additionally, UV-C induced modifications of nucleosides are also reported to exhibit labile N-glycosidic bonds. These, upon hydrolysis, might produce unstable abasic sites that through β-elimination result in breaks in phosphodiester bonds. Involvement or contribution of these processes in the

observed induction of strand breaks has not been ascertained in this work and should be studied further. Nonetheless, the results of the present investigation suggest that the immediate effect of UV-C exposure of pMTa4 DNA is a relaxation of the DNA super-structure. The resulting strain on the DNA backbone or consequent availability of vulnerable bonds for hydrolytic cleavage might be the cause of the induction of sparsely placed SSB on pMTa4 upon exposure to these low doses of UV-C radiation.

Acknowledgements

Authors gratefully acknowledge constructive suggestions from an anonymous referee on the manuscript. Partial financial support for the work came from CSIR by way of a research fellowship to CB.

References

Berg JM, Tymoczko JL, Stryer L. 2002. Biochemistry, 5th ed. New York: W. H. Freeman & Co.

Burger A, Raymer J, Bockrath R. 2002. DNA damage-processing in *E. coli*: Ongoing protein synthesis is required for fixation of UV-induced lethality and mutation. DNA Repair 1:821–831.

Burton K. 1956. A study of the conditions and mechanism of the diphenylamine reaction for the colorimetric estimation of deoxyribonucleic acid. Biochemical Journal 62:315–322.

Cowan JA. 2001. Chemical nucleases. Current Opinions in Chemical Biology, 5:634–642.

Douki T, Renaud-Angelin A, Cadet J, Sage E. 2003a. Bipyrimidine photoproducts rather than oxidative lesions are the main type of DNA damage involved in the genotoxic effect of solar UVA radiation. Biochemistry 42:9221–9226.

Douki T, Laporte G, Cadet J. 2003b. Inter-strand photoproducts are produced in high yield within A-DNA exposed to UV-C radiation. Nucleic Acid Research 31:3134–3142.

Gulston M, Fulford J, Jenner T, Delara C, O'Neill P. 2002. Clustered DNA damage by γ-irradiation in human fibroblasts (HF19), hamster (V79-4) cells and plasmid DNA is revealed as Fpg and Nth sensitive. Nucleic Acid Research 30:3464–3472.

Gurzadyan GG, Gorner H. 1992. Base release from DNA and polynuceotide upon 193 nm laser excitation. Photochemistry and Photobiology 56:371–378.

Haseltine WA. 1986. UV light repair and mutagenesis revisited. Cell 33:13–17.

Humtsoe JO, Sharan RN. 2004. Molecular radiobiology: Plasmid pMTa4 as a tool for studying effects of γ-radiation *in vitro* and *in vivo*. In Mishra KP, editor. Radiobiology and bio-medical research. New Delhi: Narosa Publishing House. pp 51–61.

Humtsoe JO, Schneeweiss FHA, Srivastava A, Sarma A, Sharan RN. 2003. Biological effects induced by swift heavy ions of lithium on aqueous solution of plasmid pMTa4. Radiation Effects & Defects in Solids 158:603–607.

Humtsoe JO, Schroeder CH, Sharan RN. 1998. Is there a relationship between nucleotide sequence and radiation induced DNA damage? In Sharan RN, editor. Trends in *radiation and cancer biology*. Juelich: Forschungszentrum Juelich GmbH, International Co-operation Bilateral Seminars series, vol. 29. pp 29–32.

Isaacs R, Spielmann HP. 2004. A model for initial DNA lesion recognition by NER and MMR based on local conformational flexibility. DNA Repair 3:455–464.

Jones GDD, Milligan JR, Ward JF, Calabro-Jones PM, Aguilera JA. 1993. Yield of strand breaks as a function of scavenger concentration and LET for SV40 irradiated with ^{4}He ions. Radiation Research 136:190–196.

Kurosaki Y, Abe H, Morioka H, Hirayama J, Ikebuchi K, Kamo N, Nikaido O, Azuma H, Ikeda H. 2003. Pyrimidine dimer formation and oxidative damages in M13 bacteriophage inactivation by ultraviolet C irradiation. Photochemistry and Photobiology 78:349–354.

Matsunaga T, Hieda K, Nikaido O. 1991. Wavelength dependent formation of thymine dimmers and (6-4) photoproducts in DNA by monochromatic UV light ranging from 150–365 nm. Photochemistry and Photobiology 54:403–410.

Miguel AG, Tyrrell RM. 1986. Repair of near-ultraviolet (365 nm) induced strand breaks in *Escherichia coli* DNA. The role of polA and recA gene products. Biophysical Journal 49:485–491.

Odiyuo MM, Sharan RN. 2005. Differential DNA strand breaking abilities of °OH and ROS generating radiomimetic chemicals and γ–rays: Study of plasmid DNA, pMTa4, *in vitro*. Free Radical Research 39:499–505.

Oguma K, Katayama H, Mitani H, Morita S, Hirata T, Ohgaki S. 2001. Determination of pyrimidine dimers in *Escherichia coli* and *Cryptosporidium parvum* during UV light inactivation, photoreactivation and dark repair. Applied and Environmental Microbiology 67:4630–4637.

Park H, Zhang K, Ren Y, Nadji S, Sinha N, Taylor J-S, Kang C. 2002. Crystal structure of a DNA decamer containing a cis-syn thymine dimer. Proceedings of the National Academy of Science 99:15965–15970.

Ravanat J-C, Douki T, Cadet J. 2001. Direct and indirect effects of UV radiation on DNA and its components. Journal of Photochemistry and Photobiology B. Biology 63:88–102.

Sambrook J, Russel DW. 2001. Molecular cloning: A laboratory manual. New York: Cold Spring Harbour Laboratory Press.

Schul W, Jans J, Rijksen YM, Klemann KH, Eker AP, De-Wit J, Nikaido O, Nakajima S, Yasu IA, Hoeijmakers JH, Van Der Horst GT. 2002. Enhanced repair of cyclobutane pyrimidine dimers and improved UV resistance in photolyase transgenic mice. EMBO Journal 21:4719–4729.

Smith SB, Finzi L, Bustamante C. 1992. Direct mechanical measurements of the elasticity of single DNA molecules by using magnetic beads. Science 258:1122–1126.

World Health Organization 1994. Ultraviolet radiation, 2nd ed. Environmental Health Criteria: 160. Geneva: WHO.

Zeng Y, Sheppard TL. 2004. Half-life and DNA scission products of 2-deoxyribolactone oxidative DNA damage lesion. Chemical Research and Technology 17:197–207.